



February 3, 2004

L-2004-029  
10 CFR 50.90

U. S. Nuclear Regulatory Commission  
ATTN: Document Control Desk  
Washington, D.C. 20555

RE: St. Lucie Units 1 and 2  
Docket Nos. 50-335 and 50-389  
Supplemental Information to  
Spent Fuel Pool Cask Pit Rack Amendments

On October 23, 2002, Florida Power & Light (FPL) submitted proposed license amendments to revise the Technical Specifications to include the design of a new cask pit rack for each St. Lucie unit, in order to increase each unit's spent fuel storage capacity. By subsequent letters dated August 28 and December 11, 2003, FPL provided responses to the U.S. Nuclear Regulatory Commission (NRC) requests for additional information (RAI) dated July 22 and November 4, 2003, respectively.

In October 2003, FPL determined that a design change to the proposed racks was necessary so that the stored fuel height would match the fuel height in the existing spent fuel pool storage racks. The change affects the height and weight of the racks and their associated platforms. The change was discussed with the NRC Project Manager in a December meeting at the St. Lucie plant, and it was agreed that FPL would submit a revision of the rack vendor's report attached to the original amendment request to reflect the change. The revised vendor report is submitted as Enclosure 1 to this letter.

Page R2 of Enclosure 1 identifies specific pages of the report that are affected by the height and weight changes. Other editorial changes to the report are also identified on page R2. Please note that only the non-proprietary version of the report is enclosed, because no proprietary information was revised. This enclosure in its entirety may be disclosed to the public.

The above change has been evaluated for impact on criticality, thermal-hydraulics, seismic, structural, and heavy loads considerations. The change does not adversely impact the conclusions of the evaluation for the amendment request, nor does it change the Determination of No Significant Hazards Consideration evaluation or the proposed Technical Specifications.

In addition to the enclosed revision to the vendor report, please note that the rack and platform design changes also affect height and weight numbers that appear on two pages of the original submittal's evaluation of proposed TS changes. Specifically:

- On page 23 of the evaluation under "Shallow Drop Scenario", the 36-inch distance between the top of the rack and the top of the active fuel region is reduced to 26 inches.
- On page 27 of the evaluation under "Handling of Heavy Loads", the platform weight of '(approximately 5 tons)' is increased to '(approximately 8 tons)'.

A001

St. Lucie Units 1 and 2  
Docket Nos. 50-335 and 50-389  
Supplemental Information to  
Spent Fuel Pool Cask Pit Rack Amendments

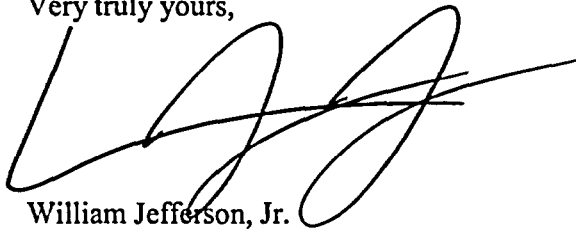
As stated previously, these changes do not adversely impact any conclusions of the amendment request evaluation.

Additionally, the NRC Staff requested that a description of the Boral™ poison material be included in the proposed St. Lucie Unit 2 spent fuel pool design features Technical Specification. A new Technical Specification mark-up and word-processed change for Technical Specification page 5-4 that incorporates the Boral™ description is provided in Enclosure 2. The Boral™ poison material is adequately described in the original submittal, and the proposed change has no adverse effect on the original No Significant Hazards determination.

In accordance with 10 CFR 50.91(b)(1), a copy of the RAI response is being forwarded to the State Designee for the State of Florida.

Please contact us if there are any questions about this supplemental information.

Very truly yours,

A handwritten signature in black ink, appearing to be 'W. Jefferson, Jr.', written over a horizontal line.

William Jefferson, Jr.  
Vice President  
St. Lucie Nuclear Plant

Enclosure

cc: Mr. W. A. Passetti, Florida Department of Health





Holtec Center, 555 Lincoln Drive West, Marlton, NJ 08053

Telephone (856) 797-0900

Fax (856) 797-0909

## **SPENT FUEL STORAGE EXPANSION**

at

**ST. LUCIE UNITS 1 AND 2**

for

***FLORIDA POWER & LIGHT***

**HOLTEC PROJECT NO. 1201**

**HOLTEC REPORT HI-2022882**

**REPORT CATEGORY: A**

**REPORT CLASS: SAFETY RELATED**

### **COMPANY PRIVATE**

This document version has all proprietary information removed and has replaced those sections, figures, and tables with highlighting and/or notes to designate the removal of such information. This document is to be used only in connection with the performance of work by Holtec International or its designated subcontractors. Reproduction, publication or presentation, in whole or in part, for any other purpose by any party other than the Client is expressly forbidden.

# HOLTEC INTERNATIONAL

## DOCUMENT ISSUANCE AND REVISION STATUS<sup>1</sup>

DOCUMENT NAME: St. Lucie Spent Fuel Storage Expansion License Amendment Report

DOCUMENT NO.: HI-2022882 CATEGORY:  GENERIC  
PROJECT NO.: 1201  PROJECT SPECIFIC

Rev. No. <sup>2</sup>	Date Approved	Author's Initials	VIR #	Rev. No.	Date Approved	Author's Initials	VIR #
0	8/9/02	SP	296874				
1	9/4/02	SP	368141				
2	1/5/04	SP	853952				

### DOCUMENT CATEGORIZATION

In accordance with the Holtec Quality Assurance Manual and associated Holtec Quality Procedures (HQP), this document is categorized as a:

- Calculation Package<sup>3</sup> (Per HQP 3.2)  Technical Report (Per HQP 3.2) (Such as a Licensing Report)
- Design Criterion Document (Per HQP 3.4)  Design Specification (Per HQP 3.4)
- Other (Specify):

### DOCUMENT FORMATTING

The formatting of the contents of this document is in accordance with the instructions of HQP 3.2 or 3.4 except as noted below:

Deviations as necessary for Project Plan

### DECLARATION OF PROPRIETARY STATUS

This document is labeled:

- Nonproprietary  Holtec Proprietary  TOP SECRET

Documents labeled TOP SECRET contain extremely valuable intellectual/commercial property of Holtec International. They cannot be released to external organizations or entities without explicit approval of a company corporate officer. The recipient of Holtec's proprietary or Top Secret document bears full and undivided responsibility to safeguard it against loss or duplication.

### Notes

- This document has been subjected to review, verification and approval process set forth in the Holtec Quality Assurance Procedures Manual. Password controlled signatures of Holtec personnel who participated in the preparation, review, and QA validation of this document are saved in the N-drive of the company's network. The Validation Identifier Record (VIR) number is a unique six-digit random number that is generated by the computer after the specific revision of this document has undergone the required review and approval process, and the appropriate Holtec personnel have recorded their password-controlled electronic concurrence to the document.
- A revision to this document will be ordered by the Project Manager and carried out if any of its contents is materially affected during evolution of this project. The determination as to the need for revision will be made by the Project Manager with input from others, as deemed necessary by him.
- Revisions to Calculation Packages may be made by adding supplements to the document and replacing the "Table of Contents", the "Review and Certification" page and the "Revision Log".

## SUMMARY OF REVISIONS

Revision 2 contains the following pages:	
COVER PAGE	1 page
DOCUMENT ISSUANCE AND REVISION STATUS	1 page
SUMMARY OF REVISIONS	1 page
TABLE OF CONTENTS	9 pages
1.0 INTRODUCTION	6 pages
2.0 CASK PIT STORAGE RACKS	27 pages
3.0 MATERIAL AND HEAVY LOADS CONSIDERATIONS	16 pages
4.0 CRITICALITY SAFETY ANALYSES	36 pages
-- APPENDIX 4A	26 pages
5.0 THERMAL-HYDRAULIC CONSIDERATIONS	36 pages
6.0 STRUCTURAL/SEISMIC CONSIDERATIONS	61 pages
7.0 FUEL HANDLING AND CONSTRUCTION ACCIDENTS	16 pages
8.0 FUEL POOL STRUCTURE INTEGRITY CONSIDERATIONS	30 pages
9.0 RADIOLOGICAL EVALUATION	4 pages
10.0 INSTALLATION	7 pages
11.0 ENVIRONMENTAL COST/BENEFIT ASSESSMENT	7 pages
TOTAL	284 pages

### Revision 1

Client editorial comments, provided in fax dated August 28, 2002, required changes to the following pages; 2-3, 3-10, 3-12, 4-9, 4-10, 4-24, 4-26, 4-27, 4-31, 5-1, 5-3, 5-4, 5-5, 5-12, 5-13, 5-15 thru 5-16, 5-18, and 5-22 thru 5-25. Faxed client comments are saved in Holtec network file G:\projects\1201\client. The following pages were revised to reflect the most recent summary results; 8-7, 8-8, and 8-18. The following pages were revised to denote proprietary information; 3-15, 4-4, 4-6, 4-7, 4-8, 4-28, 4-34, 4-36, 5-6, 5-7, 6-23, 6-24, 6-29, 7-3, and 7-4.

### Revision 2

Corrected reference numbers on the following pages 4-3, 4-4, 4-16, 4-17, 4-18, 6-35, 8-15. Adjusted fuel rod diameter tolerance for CE fuel in Table 4.1.4.1. Revised fuel weight discussion in Section 6.3.1. Removed proprietary designation from footer of Appendix 4A. Corrected baseplate hole diameter on pages 2-12, 2-15, and 2-16. Corrected cell inside dimension on page 2-15. Revised proprietary information highlighting designation on pages 6-23 and 6-24. Adjusted text on pages 2-14, 2-15, 2-16, 3-5, 5-22, 6-31, 6-32, 6-34, 7-1, 7-2, 7-5, 7-8, and 8-1 to address revised rack cell and platform heights and weights. Corrected Figure 2.1.3 to reflect revised rack platform lift point configuration.

## TABLE OF CONTENTS

---

1.0	INTRODUCTION .....	1-1
1.1	References .....	1-4
2.0	CASK PIT STORAGE RACKS .....	2-1
2.1	Introduction .....	2-1
2.2	Summary of Principal Design Criteria .....	2-2
2.3	Applicable Codes and Standards .....	2-3
2.4	Quality Assurance Program .....	2-9
2.5	Mechanical Design .....	2-10
2.6	Rack Fabrication .....	2-10
2.6.1	Rack Module for Region 1 .....	2-11
2.6.2	Rack Module for Region 2 .....	2-12
3.0	MATERIAL, HEAVY LOAD, AND CONSTRUCTION CONSIDERATIONS .....	3-1
3.1	Introduction .....	3-1
3.2	Structural Materials .....	3-1
3.3	Neutron Absorbing Material .....	3-1
3.3.1	Boral Material Characteristics .....	3-2
3.4	Compatibility with Environment .....	3-3
3.5	Heavy Load Considerations for the Proposed Rack Installations .....	3-3
3.6	References .....	3-8
4.0	CRITICALITY SAFETY ANALYSES .....	4-1
4.1	Unit 1 Cask Pit Rack .....	4-1
4.1.1	Introduction and Summary .....	4-1
4.1.2	Analysis and Criteria Assumptions .....	4-2
4.1.3	Acceptance Criteria .....	4-3
4.1.4	Design and Input Data .....	4-3
4.1.4.1	Fuel Assembly Design Specifications .....	4-3
4.1.4.2	Fuel Storage Cells .....	4-4
4.1.5	Methodology .....	4-4
4.1.6	Analysis Results .....	4-5
4.1.6.1	Reference Fuel Assembly .....	4-5
4.1.6.2	Evaluation of Uncertainties .....	4-6
4.1.6.2.1	Boron Loading Tolerance .....	4-6
4.1.6.2.2	Boral Width Tolerance .....	4-6
4.1.6.2.3	Tolerances in Water Gap Spacing, Cell Box Inner Dimension and Lattice Pitch .....	4-6
4.1.6.2.4	Stainless Steel Thickness Tolerances .....	4-7
4.1.6.2.5	Fuel Enrichment and Density Tolerances .....	4-7
4.1.6.2.6	Sheathing Thickness .....	4-8
4.1.6.2.7	Fuel Assembly Dimensional Tolerances .....	4-8
4.1.6.3	Eccentric Positioning of Fuel Assembly .....	4-8
4.1.6.4	Abnormal and Accident Conditions .....	4-9

## TABLE OF CONTENTS

4.1.6.4.1	Temperature and Void Effects .....	4-9
4.1.6.4.2	Dropped Fuel Assembly .....	4-9
4.1.6.4.3	Abnormal Location of a Fuel Assembly .....	4-10
4.1.6.5	Criticality Analysis Results .....	4-10
4.2	Unit 2 Cask Pit Rack .....	4-11
4.2.1	Objectives and General Description .....	4-11
4.2.1.2	Summary of Results .....	4-11
4.2.2	Analysis Criteria and Assumptions .....	4-12
4.2.3	Acceptance Criteria .....	4-13
4.2.4	Design and Input Data .....	4-14
4.2.4.1	Bounding Fuel Assembly .....	4-14
4.2.4.2	Storage Racks .....	4-14
4.2.4.3	Operating Parameters .....	4-14
4.2.5	Methodology .....	4-16
4.2.6	Evaluation of Uncertainties .....	4-17
4.2.6.1	Uncertainty in Manufacturing Tolerances .....	4-17
4.2.6.2	Uncertainty in Depletion Calculations .....	4-17
4.2.6.3	Eccentric Location of Fuel Assemblies .....	4-17
4.2.6.4	Temperature and Void Effects .....	4-18
4.2.6.5	Reactivity Effect of the Axial Burnup Distribution .....	4-18
4.2.7	Accident Conditions and Soluble Boron Requirements .....	4-18
4.2.8	Criticality Analyses Results and Conclusions .....	4-19
4.3	References .....	4-20
4.3.1	References for Section 4.1. ....	4-20
4.3.2	References for Section 4.2 .....	4-21
Appendix 4A	“Benchmark Calculations” .....	Total of 25 Pages including 6 figures
4A.1	Introduction and Summary .....	4A-1
4A.2	Effect of Enrichment .....	4A-3
4A.3	Effect of <sup>10</sup> B Loading .....	4A-4
4A.4	Miscellaneous and Minor Parameters .....	4A-5
4A.4.1	Reflector Material and Spacings .....	4A-5
4A.4.2	Fuel Pellet Diameter and Lattice Pitch .....	4A-5
4A.4.3	Soluble Boron Concentration Effects .....	4A-5
4A.5	MOX Fuel .....	4A-6
4A.6	References .....	4A-7
5.0	<b>THERMAL-HYDRAULIC CONSIDERATIONS</b> .....	5-1
5.1	Introduction .....	5-1
5.2	Cooling Systems Description .....	5-2
5.3	Offload/Cooling Alignment Scenarios .....	5-3
5.4	Maximum Pool Bulk Temperature .....	5-5
5.5	Minimum Time-to-Boil and Maximum Boiloff Rate .....	5-8
5.6	Maximum SFP Local Water Temperature .....	5-9
5.7	Fuel Rod Cladding Temperature .....	5-13

## TABLE OF CONTENTS

5.8	Results .....	5-14
5.8.1	Maximum Pool Bulk Temperatures .....	5-14
5.8.2	Minimum Time-to-Boil and Maximum Boiloff Rate .....	5-16
5.8.3	Local Water and Fuel Cladding Temperatures .....	5-16
5.9	References .....	5-17
6.0	STRUCTURAL/SEISMIC CONSIDERATIONS .....	6-1
6.1	Introduction .....	6-1
6.2	Overview of Rack Structural Analysis Methodology .....	6-1
6.2.1	Background of Analysis Methodology .....	6-2
6.3	Description of Racks .....	6-3
6.3.1	Fuel Weights .....	6-4
6.4	Synthetic Time-Histories .....	6-5
6.5	Modeling Methodology .....	6-6
6.5.1	Model Details for Spent Fuel Racks .....	6-6
6.5.1.1	Model Details and Assumptions .....	6-6
6.5.1.2	Element Details .....	6-8
6.5.2	Fluid Coupling Effect .....	6-10
6.5.3	Stiffness Element Details .....	6-11
6.5.4	Coefficients of Friction .....	6-12
6.5.5	Governing Equations of Motion .....	6-12
6.6	Structural Evaluation of Spent Fuel Rack Design .....	6-13
6.6.1	Kinematic and Stress Acceptance Criteria .....	6-13
6.6.2	Stress Limit Evaluations .....	6-14
6.6.3	Dimensionless Stress Factors .....	6-18
6.6.4	Loads and Loading Combinations for Spent Fuel Racks .....	6-19
6.7	Parametric Simulations .....	6-20
6.8	Time History Simulation Results .....	6-21
6.8.1	Rack Displacements .....	6-22
6.8.2	Pedestal Vertical Forces .....	6-22
6.8.3	Pedestal Friction Forces .....	6-23
6.8.4	Rack Impact Loads .....	6-23
6.8.4.1	Rack to Wall Impacts .....	6-23
6.8.4.2	Fuel to Cell Wall Impact Loads .....	6-23
6.9	Rack Structural Evaluation .....	6-24
6.9.1	Rack Stress Factors .....	6-24
6.9.2	Pedestal Thread Shear Stress .....	6-25
6.9.3	Local Stresses Due to Impacts .....	6-26
6.9.4	Assessment of Rack Fatigue Margin .....	6-26
6.9.5	Weld Stresses .....	6-29
6.10	Level A Evaluation .....	6-31
6.10.1	Unit 1 Cask Pit Rack .....	6-31
6.10.2	Unit 2 Cask Pit Rack .....	6-31
6.11	Hydrodynamic Loads on Pool Walls .....	6-32
6.12	Temperature Gradient Across Rack Cell Wall .....	6-32

## TABLE OF CONTENTS

6.12.1	Cell Wall Buckling .....	6-32
6.12.2	Cell-to-Cell Weld Stress Due to hot Cell Thermal Expansion .....	6-33
6.13	Rack Support Platform .....	6-34
6.14	References .....	6-36
7.0	MECHANICAL ACCIDENTS .....	7-1
7.1	Introduction .....	7-1
7.2	Description of Mechanical Accidents .....	7-1
7.3	Incident Impact Velocity .....	7-3
7.4	Mathematical Model .....	7-4
7.5	Results .....	7-5
7.5.1	Shallow Drop Event .....	7-5
7.5.2	Deep Drop Events .....	7-5
7.6	Conclusion .....	7-5
7.7	References .....	7-7
8.0	FUEL HANDLING BUILDING STRUCTURAL INTEGRITY EVALUATIONS .....	8-1
8.1	Unit 1 Evaluation .....	8-1
8.1.1	Introduction .....	8-1
8.1.2	Description of Cask Pit Structure and Exterior Building Walls .....	8-3
8.1.3	Analysis Procedures .....	8-3
8.1.4	Definition of Loads Included in Structural Evaluation .....	8-4
8.1.4.1	Static Loading .....	8-4
8.1.4.2	Seismic .....	8-4
8.1.4.3	Thermal Loading .....	8-5
8.1.4.4	Load Combinations and Acceptance Criteria .....	8-5
8.1.5	Results of Unit 1 Reinforced Concrete Analyses .....	8-7
8.1.5.1	Building East Wall Above Elevation 62' .....	8-7
8.1.5.2	North and East SFP Walls Below Elevation 62' .....	8-8
8.1.6	Pool Liner-Cask Pit Floor Bearing Evaluation .....	8-8
8.1.7	Conclusions for Unit 1 .....	8-9
8.2	Unit 2 Evaluation .....	8-10
8.2.1	Introduction .....	8-10
8.2.2	Description of Cask Pit Structure and Exterior Building Walls .....	8-11
8.2.3	Analysis Procedures .....	8-12
8.2.4	Definition of Loads Included in Structural Evaluation .....	8-13
8.2.4.1	Static Loading .....	8-13
8.2.4.2	Seismic .....	8-14
8.2.4.3	Thermal Loading .....	8-14
8.2.4.4	Static Loading .....	8-15
8.2.4.5	Seismic .....	8-15
8.2.4.3	Thermal Loading above Elevation 62' .....	8-15
8.2.4.4	Load Combinations .....	8-15
8.2.5	Results of Unit 2 Reinforced Concrete Analyses .....	8-17

## TABLE OF CONTENTS

---

8.2.5.1	Building East Wall Above Elevation 62' .....	8-17
8.2.5.2	Cask Pit .....	8-18
8.2.6	Pool Liner-Cask Pit Floor Bearing Evaluation .....	8-19
8.2.7	Conclusions for Unit 1 .....	8-19
8.3	References .....	8-20
9.0	<b>RADIOLOGICAL EVALUATION .....</b>	<b>9-1</b>
9.1	Fuel Handling Accident .....	9-1
9.2	Solid Radwaste .....	9-1
9.3	Gaseous Releases .....	9-1
9.4	Personnel Exposures .....	9-1
9.5	Anticipated Exposure During Rack Installation .....	9-2
9.6	Rack Removal and Storage During Cask Handling Operations .....	9-3
10.0	<b>INSTALLATION .....</b>	<b>10-1</b>
10.1	Introduction .....	10-1
10.2	Rack Arrangement .....	10-4
10.3	Rack Interferences .....	10-4
10.4	SFP Cooling .....	10-4
10.5	Installation of New Racks .....	10-5
10.6	Safety, Health Physics, and ALARA Methods .....	10-6
10.6.1	Safety .....	10-6
10.6.2	Health Physics .....	10-6
10.6.3	ALARA .....	10-6
10.7	Radwaste Material Control .....	10-7
11.0	<b>ENVIRONMENTAL COST/BENEFIT ASSESSMENT .....</b>	<b>11-1</b>
11.1	Introduction .....	11-1
11.2	Imperative for Additional Spent Fuel Storage Capacity .....	11-1
11.3	Appraisal of Alternative Options .....	11-1
11.3.1	Alternative Option Cost Summary .....	11-4
11.4	Cost Estimate .....	11-4
11.5	Resource Commitment .....	11-5
11.6	Environmental Considerations .....	11-5
11.7	References .....	11-7

## TABLE OF CONTENTS

### Tables

2.1.1	Geometric and Physical Data for Cask Pit Racks .....	2-14
2.5.1	Module Data for Unit 1 Region 1 Cask Pit Rack .....	2-15
2.5.2	Module Data for Unit 2 Region 2 Cask Pit Rack .....	2-16
3.3.1	Boral Experience List - PWRs .....	3-9 and 3-10
3.3.2	Boral Experience List - BWRs .....	3-11 and 3-12
3.3.3	1100 Alloy Aluminum Physical Characteristics .....	3-13
3.3.4	Chemical Composition - Aluminum (1100 Alloy) .....	3-14
3.3.5	Chemical Composition and Physical Properties of Boron Carbide .....	3-15
3.5.1	Heavy Load Handling Compliance Matrix (NUREG-0612) .....	3-16
4.1.4.1	Design Basis Fuel Assembly Specifications .....	4-22
4.1.6.1	Reactivity Effects of Manufacturing Tolerances in St. Lucie Unit 1 Nuclear Plant Cask Pit Storage Rack .....	4-23
4.1.6.2	Reactivity Effects of Temperature and Void for CE 14x14 Fuel in St. Lucie Unit 1 Cask Pit Rack .....	4-24
4.1.6.3	Reactivity Effects of Abnormal and Accident Conditions (Unit 1 CPR) .....	4-25
4.1.6.4	Summary of Criticality Safety Analyses for the Storage of Fresh Fuel Assemblies in St. Lucie Unit 1 Cask Pit Rack .....	4-26
4.2.4.1	Design Basis Fuel Assembly Specifications (Unit 2 CPR) .....	4-27
4.2.6.1	Reactivity Effects of Manufacturing Tolerances for CE 16x16 Fuel in St. Lucie Unit 2 Nuclear Plant Cask Pit Storage Rack .....	4-28
4.2.6.2	Reactivity Effects of Fuel Enrichment Tolerance in St. Lucie Unit 2 Cask Pit Storage Rack .....	4-29
4.2.6.3	Reactivity Effects of Temperature and Void in St. Lucie Unit 2 Cask Pit Storage Rack .....	4-30
4.2.6.4	Summary of the Criticality Safety Analyses for the Storage of Spent Fuel Assemblies in the St. Lucie Unit 2 Cask Pit Rack .....	4-31
4.2.6.5	Reactivity Effects of Abnormal and Accident Conditions in St. Lucie Unit 2 Cask Pit Rack .....	4-32
4.2.8.1	Enrichment - Minimum Burnup Correlation (Ref. Figure 4.2.1) Unit 2 CPR) .....	4-33
4A.1	Summary of Criticality Benchmark Calculations .....	4A-9 thru 4A-13
4A.2	Comparison of MCNP4a and Keno5a Calculated Reactivities for Various Enrichments .....	4A-14
4A.3	MCNP4a Calculated Reactivities for Critical Experiments with Neutron Absorbers .....	4A-15
4A.4	Comparison of MCNP4a and KENO5a Calculated Reactivities for Various <sup>10</sup> B Loadings .....	4A-16
4A.5	Calculations for Critical Experiments with Thick Lead and Steel Reflectors .....	4A-17

TABLE OF CONTENTS

---

4A.6	Calculations for Critical Experiments with Various Soluble Boron Concentrations .....	4A-18
4A.7	Calculations for Critical Experiments with MOX Fuel .....	4A-19
5.3.1	Historic and Projected Fuel Offload Schedule - Unit 1 .....	5-18
5.3.2	Historic and Projected Fuel Offload Schedule - Unit 2 .....	5-19
5.4.1	Key Input Data for Bulk Temperature Evaluation .....	5-20
5.5.1	Key Input Data for Time-to-Boil Evaluation .....	5-21
5.6.1	Key Input Data for Local Temperature Evaluation .....	5-22
5.8.1	Results of Transient Temperature Evaluations .....	5-23
5.8.2	Results of Loss-of-Forced Cooling Evaluations .....	5-24
5.8.3	Results of Maximum Local Water and Fuel Cladding Temperature Evaluations ....	5-25
6.2.1	Partial Listing of Fuel Rack Applications Using DYNARACK .....	6-38 through 6-40
6.3.1	Rack Material Data (200°F) (ASME - Section II, Part D) .....	6-41
6.4.1	Unit 1 Time-History Statistical Correlation Results .....	6-42
6.4.2	Unit 2 Time-History Statistical Correlation Results .....	6-43
6.5.1	Degrees-of-Freedom .....	6-44
6.9.1	Unit 1 Comparison of Bounding Calculated Loads/Stresses vs. Code Allowables at Impact Locations and at Welds .....	6-45
6.9.2	Unit 2 Comparison of Bounding Calculated Loads/Stresses vs. Code Allowables at Impact Locations and at Welds .....	6-46
7.4.1	Impact Event Data .....	7-8
7.4.2	Material Definition .....	7-9
8.1.1	Unit 1 Concrete and rebar Properties .....	8-21
8.2.1	Unit 2 Concrete and rebar Properties .....	8-22

## TABLE OF CONTENTS

---

### Figures

- 1.1.1 Unit 1 Cask Pit Rack Layout
- 1.1.2 Unit 2 Cask Pit Rack Layout
  
- 2.1.1 Schematic View of Typical Region 1 Rack Structure
- 2.1.2 Schematic of Typical Region 2 Rack Structure
- 2.1.3 Cask Pit Rack Platform
- 2.6.1 Seam Welded Precision Formed Channels
- 2.6.2 Tapered Region 1 Cell End
- 2.6.3 Composite Box Assembly
- 2.6.4 Assemblage of Region 1 Cells
- 2.6.5 Elevation View of Region 1 Rack
- 2.6.6 Support Pedestals for Holtec PWR Racks
- 2.6.7 Typical Array of Storage Cells (Non-Flux Trap Construction)
- 2.6.8 Elevation View of Storage Rack Module
  
- 3.5.1 Spent Fuel Pool Operating Deck Layout Plan
  
- 4.1.1 Unit 1 CPR Storage Cell Cross Section
- 4.2.1 Limiting Fuel Burnup-Enrichment Combinations
- 4.2.2 Unit 2 CPR Storage Cell Cross Section
  
- 4A.1 MCNP Calculated k-eff Values for Various Values of the Spectral Index
- 4A.2 KENO5a Calculated k-eff Values for Various Values of the Spectral Index
- 4A.3 MCNP Calculated k-eff Values at Various U-235 Enrichments
- 4A.4 KENO5a Calculated k-eff Values at Various U-235 Enrichments
- 4A.5 Comparison of MCNP and KENO5a Calculations for Various Fuel Enrichments
- 4A.5 Comparison of MCNP and KENO5a Calculations for Various Boron-10 Areal Densities
  
- 5.6.1 Unit 1 CFD Model Isometric View
- 5.6.2 Unit 2 CFD Model Isometric View
- 5.8.1 Unit 1 Scenario 1 - Partial Core Discharge with Coincident Single Active Failure
- 5.8.2 Unit 1 Scenario 2a - Full Core Discharge with Coincident Single Active Failure
- 5.8.3 Unit 1 Scenario 2b - Full Core Discharge without Coincident Single Active Failure
- 5.8.4 Unit 2 Scenario 1 - Partial Core Discharge with Coincident Single Active Failure
- 5.8.5 Unit 2 Scenario 2a - Full Core Discharge with Coincident Single Active Failure
- 5.8.6 Unit 2 Scenario 2b - Full Core Discharge without Coincident Single Active Failure
- 5.8.7 Unit 1 CFD Model with Converged Temperature Contours
- 5.8.8 Unit 2 CFD Model with Converged Temperature Contours
- 5.8.9 Unit 2 CFD Model with Converged Velocity Vectors

## TABLE OF CONTENTS

---

- 6.4.1 Unit 1 East-West Accelerogram (SSE)
- 6.4.2 Unit 1 North-South Accelerogram (SSE)
- 6.4.3 Unit 1 Vertical Accelerogram (SSE)
- 6.4.4 Unit 1 East-West Accelerogram (OBE)
- 6.4.5 Unit 1 North-South Accelerogram (OBE)
- 6.4.6 Unit 1 Vertical Accelerogram (OBE)
- 6.4.7 Unit 2 East-West Accelerogram (OBE)
- 6.4.8 Unit 2 North-South Accelerogram (OBE)
- 6.4.9 Unit 2 Vertical Accelerogram (OBE)
- 6.4.10 Unit 2 East-West Accelerogram (SSE)
- 6.4.11 Unit 2 North-South Accelerogram (SSE)
- 6.4.12 Unit 2 Vertical Accelerogram (SSE)
  
- 6.5.1 Schematic of the Dynamic Model of a Single Rack Module Used in DYNARACK
- 6.5.2 Fuel-to-Rack Gap/Impact Elements at Level of Rattling Mass
- 6.5.3 Two Dimensional View of the Spring-Mass Simulation
- 6.5.4 Rack Degrees-of-Freedom with Shear and Bending Springs
- 6.5.5 Rack Periphery Gap/Impact Elements
- 6.12.1 Loading on Rack Wall
- 6.12.2 Welded Joint in Rack
  
- 7.2.1 Schematic of the “Shallow” Drop Event
- 7.2.2 Schematic of the “Deep” Drop Scenario 1
- 7.2.3 Schematic of the “Deep” Drop Scenario 2
- 7.5.1 “Shallow” Drop: Maximum Plastic Strain
- 7.5.2 “Deep” Drop Scenario 1: Maximum Vertical Displacement
- 7.5.3 “Deep” Drop Scenario 2: Maximum Von Mises Stress - Liner
- 7.5.4 “Deep” Drop Scenario 2: Maximum Compressive Stress - Concrete
  
- 8.1.1 Plan View of Unit 1 FHB
- 8.1.2 Unit 1 Finite Element Mesh
- 8.1.3 Unit 1 Finite Element Boundary Conditions
- 8.2.1 Plan View of Unit 2 FHB
- 8.2.2 View Through Section A-A
- 8.2.3 View Through Section B-B
- 8.2.4 Unit 2 Cask Pit Finite Element Grid
- 8.2.5 East Wall Above El. 62' (between Column Lines 2FH2 and 2FH5) Finite Element Grid and Boundary Conditions

## 1.0 INTRODUCTION

St Lucie Plant is located on Hutchinson Island in St. Lucie County, Florida, south of the city of Fort Pierce. The plant consists of two Combustion Engineering Pressurized Water Reactor (PWR) nuclear units. Unit 1 has been in commercial operation since 1976 and Unit 2 since 1983.

St. Lucie Unit 1 is projected to lose full core reserve (FCR) in its Spent Fuel Pool (SFP) following Cycle 19, which ends in 2005. St. Lucie Unit 2 is projected to lose full core reserve in its Spent Fuel Pool following Cycle 17, which ends in 2007. Florida Power and Light intends to expand spent fuel storage capacity by adding a new rack within the Cask Pit of each Unit. This modification would increase the licensed storage capacity in Unit 1 from the current 1,706 storage cells to 1,849 storage cells and in Unit 2 from the current 1,360 storage cells to 1,585 storage cells. This report provides the design basis, analysis methodology, and results for the proposed spent fuel storage racks at St. Lucie to support the licensing process.

The storage expansion will add one 11 by 13 (143 total) cell Region 1 style storage rack to the Unit 1 Cask Pit and one 15 by 15 (225 total) cell Region 2 style storage rack to the Unit 2 Cask Pit. The physical descriptions of 'Region 1' and 'Region 2' racks are provided in Section 2 of this report. The functional fuel storage capabilities and safety margins are discussed in Section 4 of this report. The proposed fuel storage rack arrays for Units 1 and 2 are shown in the plan views provided by Figures 1.1.1 and 1.1.2, respectively.

The new Cask Pit storage racks are freestanding and self-supporting. The principal construction materials for the SFP racks are SA240-Type 304L stainless steel sheet and plate stock, and SA564-630 (precipitation hardened stainless steel) for the adjustable support spindles. The only non-stainless material utilized in the rack is the neutron absorber material, which is a boron carbide and aluminum-composite sandwich available under the patented product name Boral™.

The racks are designed to the stress limits of, and analyzed in accordance with, Section III, Division 1, Subsection NF of the ASME Boiler and Pressure Vessel (B&PV) Code [1]. The material procurement,

analysis, fabrication, and installation of the rack modules conform to 10CFR50 Appendix B requirements.

The rack design and analysis methodologies employed are a direct evolution of previous license applications. This report documents the design and analyses performed to demonstrate that the racks meet all governing requirements of the applicable codes and standards, in particular, "OT Position for Review and Acceptance of Spent Fuel Storage and Handling Applications", USNRC (1978) and 1979 Addendum thereto [2].

Sections 2 and 3 of this report provide an abstract of the design and material information on the racks.

Section 4 provides a summary of the methods and results of the criticality evaluations performed for the new and spent fuel storage racks. The criticality safety analysis requires that the neutron multiplication factor for the stored fuel array be bounded by the USNRC  $k_{eff}$  limit of 0.95 under assumptions of 95% probability and 95% confidence. The criticality safety analysis sets the requirements on the Boral panel length and the amount of  $B^{10}$  per unit area (i.e., loading density) of the Boral panel for the new racks.

Thermal-hydraulic consideration requires that fuel cladding will not fail due to excessive thermal stress, and that the steady state pool bulk temperature will remain within the 150°F limit prescribed in the UFSAR to satisfy the pool structural strength, operational, and regulatory requirements. The thermal-hydraulic analyses carried out in support of this storage expansion effort are described in Section 5.

Rack module structural analysis requires that the primary stresses in the rack module structure will remain below the ASME B&PV Code (Subsection NF) [1] allowables. Demonstrations of seismic and structural adequacy are presented in Section 6.0. The structural qualification also requires that the subcriticality of the stored fuel will be maintained under all postulated accident scenarios. The structural consequences of these postulated accidents are evaluated and presented in Section 7 of this report.

Section 8 discusses the evaluation of the Cask Pit structure to withstand the new rack loads. The radiological considerations are documented in Section 9.0. Sections 10, and 11, respectively, discuss the

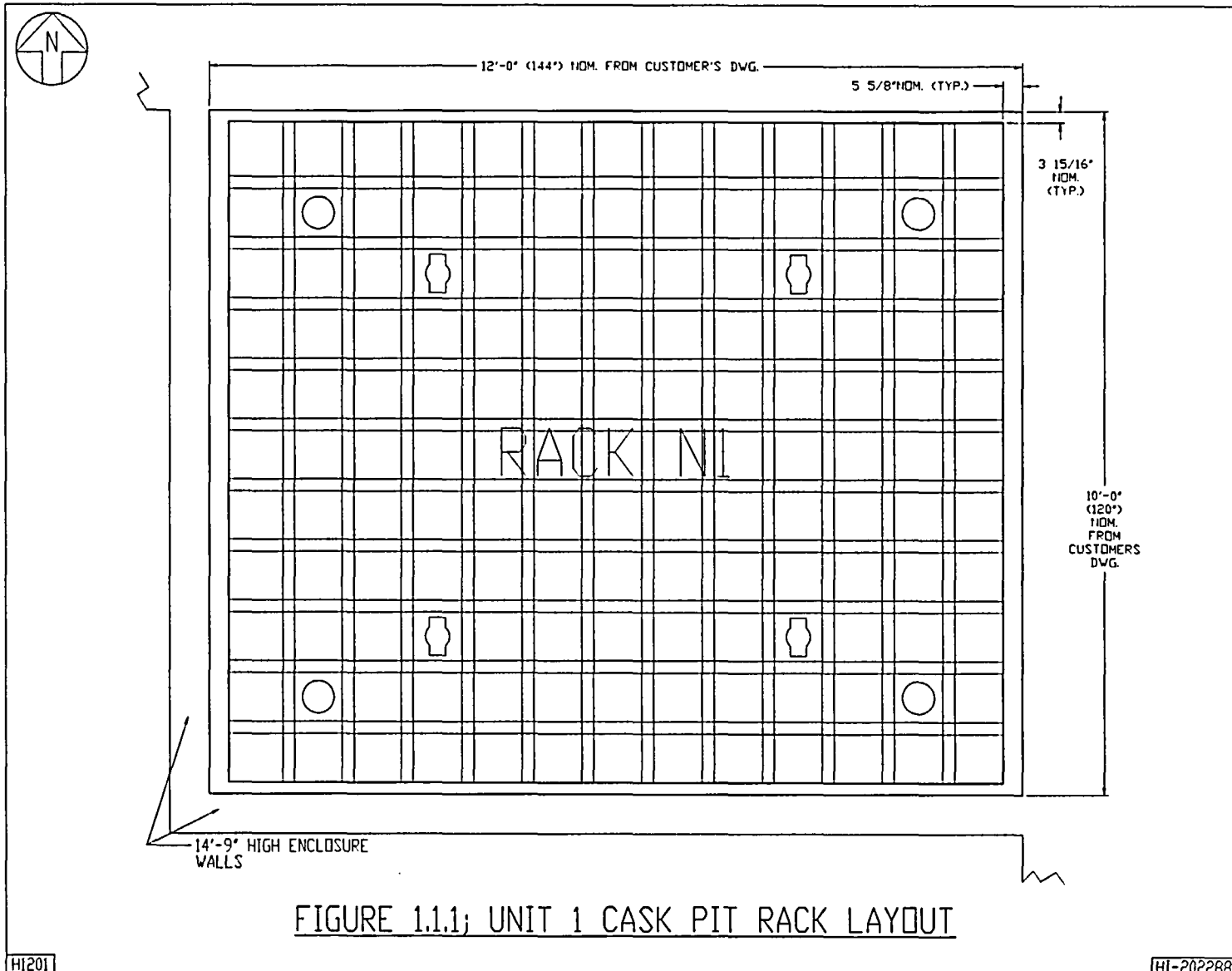
salient considerations in the installation of the new racks, and a cost/benefit and environmental assessment to establish the superiority of the wet storage expansion option.

All computer programs utilized to perform the analyses documented in this report are benchmarked and verified. These programs have been utilized by Holtec International in numerous license applications over the past decade.

The analyses presented herein clearly demonstrate that the rack module arrays possess wide margins of safety in respect to all considerations of safety specified in the OT Position Paper [2], namely, nuclear subcriticality, thermal-hydraulic safety, seismic and structural adequacy, radiological compliance, and mechanical integrity.

1.1 References

- [1] American Society of Mechanical Engineers (ASME), Boiler & Pressure Vessel Code, Section III, 1989 Edition, Subsection NF, and Appendices.
- [2] USNRC, "OT Position for Review and Acceptance of Spent Fuel Storage and Handling Applications, April 14, 1978, and Addendum dated January 18, 1979.



HI201

HI-2022882

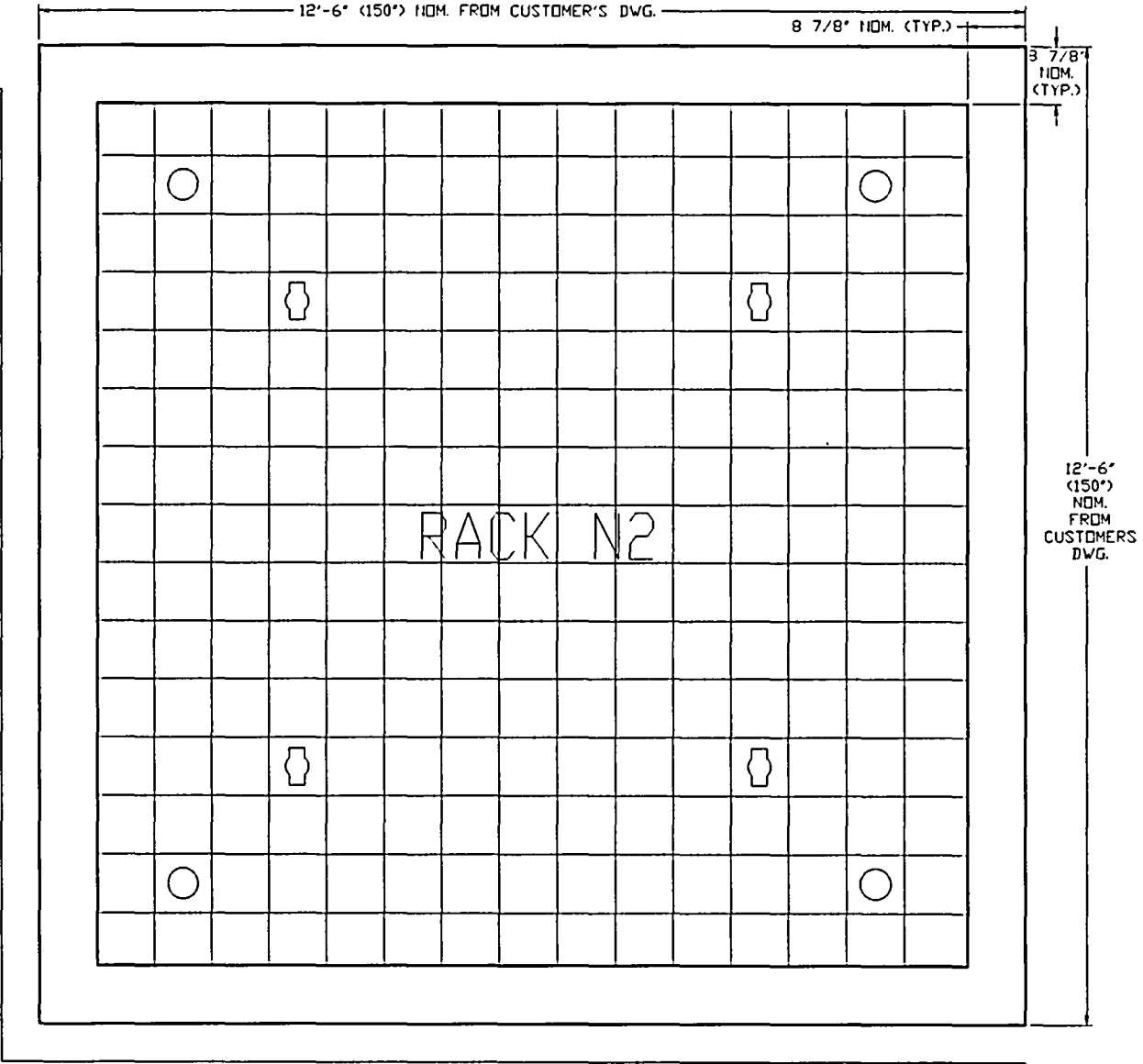
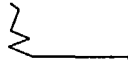


FIGURE 1.1.2; UNIT 2 CASK PIT RACK LAYOUT

## 2.0 CASK PIT STORAGE RACKS

### 2.1 Introduction

The Unit 1 St. Lucie Cask Pit fuel storage rack will be an 11 x 13 Region 1 storage rack with a storage capacity of 143 assemblies. The Unit 2 St. Lucie Cask Pit fuel storage rack will be a 15 x 15 Region 2 storage rack with a storage capacity of 225 assemblies. Each rack will be a freestanding module, made primarily from Type 304L austenitic stainless steel containing honeycomb storage cells interconnected through longitudinal welds. Boral cermet panels containing a high areal loading of the boron-10 (B-10) isotope provide appropriate neutron attenuation between adjacent storage cells.

Figures 2.1.1 and 2.1.2 provide isometric schematics of typical Region 1 and Region 2 storage rack modules, respectively. Data on the cross sectional dimensions, weight and cell count for each rack module is presented in Table 2.1.1. The spent fuel rack modules that do not utilize flux traps between storage cells are referred to as Region 2 style racks in wet storage technology terminology. Region 1 style racks contain a water gap (a.k.a flux trap) between storage cells to provide greater margin against reactivity, thereby allowing more reactive fuel to be stored within.

The baseplates on all spent fuel rack modules extend out beyond the rack module periphery wall such that the plate protrusions act to center the rack in the pit, and establish a required minimum separation between the rack and the walls. Each spent fuel rack module is supported by four pedestals, which are remotely height-adjustable. Thus, the racks can be made plumb and the top of the racks can easily be made co-planar with the racks in the adjacent pool. The rack module support pedestals are engineered to accommodate minor level adjustments.

The elevation of the Cask Pit floor liner in each Unit is approximately three feet lower than the floor liner in the adjacent spent fuel pool. Between the rack module pedestals and the Cask Pit floor liner is a rack platform, which serves to lift the new rack to the SFP rack height, and to diffuse the dead load of the loaded racks into the reinforced concrete structure of the pit slab. The height of the platform is designed to adjust the top of rack height to the same level as the racks in the adjacent spent fuel pool. A schematic view of one of these platforms is shown in Figure 2.1.3.

The overall design of the rack modules is similar to those presently in service in the spent fuel pools at many other nuclear plants, among them Davis-Besse, Callaway, and Byron-Braidwood. Altogether, over 50 thousand storage cells of this design have been provided by Holtec International to various nuclear plants around the world.

## 2.2 Summary of Principal Design Criteria

The key design criteria for the new Cask Pit racks are set forth in the USNRC memorandum entitled "OT Position for Review and Acceptance of Spent Fuel Storage and Handling Applications", dated April 14, 1978 as modified by amendment dated January 18, 1979. The individual sections of this report address the specific design bases derived from the above-mentioned "OT Position Paper". The design bases for the new racks are summarized in the following:

- a. Disposition: Both new rack modules are required to be free-standing.
- b. Kinematic Stability: Each freestanding module must be kinematically stable (against tipping or overturning) if a seismic event is imposed.
- c. Structural Compliance: All primary stresses in the rack modules must satisfy the limits postulated in Section III subsection NF of the ASME B & PV Code.
- d. Thermal-Hydraulic Compliance: The spatial average bulk pool temperature is required to remain below 150°F in the wake of a normal partial core offload (with a single failure) or a full core offload (without a single failure).
- e. Criticality Compliance: The Unit 1, Region 1 rack must be able to store fresh Zircaloy clad fuel of  $4.50 \pm 0.05$  weight percent (w/o) maximum enrichment while maintaining the reactivity ( $K_{eff}$ ) less than 0.95. The Unit 2, Region 2 rack must be able to store Zircaloy

clad fuel of  $4.50 \pm 0.05$  w/o maximum enrichment with a minimum burnup of 36,000 MWD/MTU while maintaining the reactivity ( $K_{eff}$ ) less than 0.95.

- f. Accident Events: In the event of postulated drop events (uncontrolled lowering of a fuel assembly, for instance), it is necessary to demonstrate that the subcritical geometry of the rack structure is not compromised.

The foregoing design bases are further articulated in Sections 4 through 7 of this licensing report.

### 2.3 Applicable Codes and Standards

The following codes, standards and practices are used as applicable for the design, construction, and assembly of the fuel storage racks. Additional specific references related to detailed analyses are given in each section.

a. Design Codes

- (1) American Institute of Steel Construction (AISC) Manual of Steel Construction, 9<sup>th</sup> Edition, 1989.
- (2) American National Standards Institute/ American Nuclear Society ANSI/ANS-57.2-1983, "Design Requirements for Light Water Reactor Spent Fuel Storage Facilities at Nuclear Power Plants" (contains guidelines for fuel rack design).
- (3) ASME B & PV Code Section III, 1989 Edition; ASME Section IX, 1989 Edition.
- (4) American Society for Nondestructive Testing SNT-TC-1A, June 1980, Recommended Practice for Personnel Qualifications and Certification in Non-destructive Testing.
- (5) American Concrete Institute Building Code Requirements for Reinforced Concrete (ACI 318-71).
- (6) Code Requirements for Nuclear Safety Related Concrete Structures, ACI 349-76/ACI 349R-76, and ACI 349.1R-80.
- (7) ASME Y14.5M, Dimensioning and Tolerancing
- (8) ASME B & PV Code, Section II-Parts A and C, 1989 Edition.

- (9) ASME B & PV Code NCA3800 - Metallic Material Organization's Quality System Program.

b. Standards of American Society for Testing and Materials (ASTM)

- (1) ASTM E165 - Standard Test Method for Liquid Penetrant Examination.
- (2) ASTM A240 - Standard Specification for Heat-Resisting Chromium and Chromium-Nickel Stainless Steel Plate, Sheet and Strip for Pressure Vessels.
- (3) ASTM A262 - Standard Practices for Detecting Susceptibility to Intergranular Attack in Austenitic Stainless Steel.
- (4) ASTM A276 - Standard Specification for Stainless Steel Bars and Shapes.
- (5) ASTM A479 - Standard Specification for Stainless Steel Bars and Shapes for use in Boilers and other Pressure Vessels.
- (6) ASTM A564 - Standard Specification for Hot-Rolled and Cold-Finished Age-Hardening Stainless Steel Bars and Shapes.
- (7) ASTM C750 - Standard Specification for Nuclear-Grade Boron Carbide Powder.
- (8) ASTM A380 - Standard Practice for Cleaning, Descaling, and Passivation of Stainless Steel Parts, Equipment and Systems.
- (9) ASTM C992 - Standard Specification for Boron-Based Neutron Absorbing Material Systems for Use in Nuclear Spent Fuel Storage Racks.
- (10) ASTM E3 - Standard Practice for Preparation of Metallographic Specimens.
- (11) ASTM E190 - Standard Test Method for Guided Bend Test for Ductility of Welds.

c. Welding Code:

ASME B & PV Code, Section IX - Welding and Brazing Qualifications, 1989.

d. Quality Assurance, Cleanliness, Packaging, Shipping, Receiving, Storage, and Handling

- (1) ANSI N45.2.1 - Cleaning of Fluid Systems and Associated Components during Construction Phase of Nuclear Power Plants - 1973 (R.G. 1.37).
- (2) ANSI N45.2.2 - Packaging, Shipping, Receiving, Storage and Handling of Items for Nuclear Power Plants - 1972 (R.G. 1.38).
- (3) ANSI N45.2.6 - Qualifications of Inspection, Examination, and Testing Personnel for the Construction Phase of Nuclear Power Plants - 1978. (R.G. 1.58).
- (4) ANSI N45.2.8 - Supplementary Quality Assurance Requirements for Installation, Inspection and Testing of Mechanical Equipment and Systems for the Construction Phase of Nuclear Plants - 1975 (R.G. 1.116).
- (5) ANSI N45.2.11 - Quality Assurance Requirements for the Design of Nuclear Power Plants - 1974 (R.G. 1.64).
- (6) ANSI N45.2.12 - Requirements for Auditing of Quality Assurance Programs for Nuclear Power Plants - 1977 (R.G. 1.144).
- (7) ANSI N45.2.13 - Quality Assurance Requirements for Control of Procurement of Items and Services for Nuclear Power Plants - 1976 (R. G. 1.123).
- (8) ANSI N45.2.23 - Qualification of Quality Assurance Program Audit Personnel for Nuclear Power Plants - 1978 (R.G. 1.146).
- (9) ASME B & PV Code, Section V, Nondestructive Examination, 1992 Edition.
- (10) ANSI N16.9-75 - Validation of Calculation Methods for Nuclear Criticality Safety.
- (11) ASME NQA-1 – Quality Assurance Program Requirements for Nuclear Facilities.
- (12) ASME NQA-2 – Quality Assurance Requirements for Nuclear Power Plants.

e. USNRC Documents

- (1) "OT Position for Review and Acceptance of Spent Fuel Storage and Handling Applications," dated April 14, 1978, and the modifications to this document of January 18, 1979.
- (2) NUREG 0612, "Control of Heavy Loads at Nuclear Power Plants", USNRC, Washington, D.C., July, 1980.

f. Other ANSI Standards (not listed in the preceding)

- (1) ANSI/ANS 8.1 - Nuclear Criticality Safety in Operations with Fissionable Materials Outside Reactors.
- (2) ANSI/ANS 8.17 - Criticality Safety Criteria for the Handling, Storage, and Transportation of LWR Fuel Outside Reactors.
- (3) ANSI N45.2 - Quality Assurance Program Requirements for Nuclear Power Plants - 1977.
- (4) ANSI N45.2.9 - Requirements for Collection, Storage and Maintenance of Quality Assurance Records for Nuclear Power Plants - 1974.
- (5) ANSI N45.2.10 - Quality Assurance Terms and Definitions - 1973.
- (6) ANSI N14.6 - American National Standard for Special Lifting Devices for Shipping Containers Weighing 10,000 pounds (4500 kg) or more for Nuclear Materials - 1993.
- (7) ANSI/ASME N626-3 - Qualification and Duties of Specialized Professional Engineers.
- (8) ANSI/ANS- 57.3 – Design Requirements for New Fuel Storage Facilities at Light Water Reactor Plants.

g. Code-of-Federal Regulations (CFR)

- (1) 10CFR20 - Standards for Protection Against Radiation.
- (2) 10CFR21 - Reporting of Defects and Non-compliance.
- (3) 10CFR50 Appendix A - General Design Criteria for Nuclear Power Plants.
- (4) 10CFR50 Appendix B - Quality Assurance Criteria for Nuclear Power Plants and Fuel Reprocessing Plants.

- (5) 10CFR61 - Licensing Requirements for Land Disposal of Radioactive Waste.
- (6) 10CFR71 - Packaging and Transportation of Radioactive Material.
- (7) 10CFR100 – Reactor Site Criteria

h. Regulatory Guides (RG)

- (1) RG 1.13 - Spent Fuel Storage Facility Design Basis (Revision 2 Proposed).
- (2) RG 1.25 - Assumptions Used for Evaluating the Potential Radiological Consequences of a Fuel Handling Accident in the Fuel Handling and Storage Facility for Boiling and Pressurized Water Reactors, Rev. 0 - March, 1972.
- (3) RG 1.28 - Quality Assurance Program Requirements - Design and Construction, Rev. 2 - February, 1979 (endorses ANSI N45.2).
- (4) RG 1.33 – Quality Assurance Program Requirements.
- (5) RG 1.29 - Seismic Design Classification, Rev. 2 - February, 1976.
- (6) RG 1.31 - Control of Ferrite Content in Stainless Steel Weld Metal.
- (7) RG 1.38 - Quality Assurance Requirements for Packaging, Shipping, Receiving, Storage and Handling of Items for Water-Cooled Nuclear Power Plants, Rev. 2 - May, 1977 (endorses ANSI N45.2.2).
- (8) RG 1.44 - Control of the Use of Sensitized Stainless Steel.
- (9) RG 1.58 - Qualification of Nuclear Power Plant Inspection, Examination, and Testing Personnel, Rev. 1 - September 1980 (endorses ANSI N45.2.6).
- (10) RG 1.60 – Design Response Spectra for Seismic Design of Nuclear Power Plants.
- (11) RG 1.61 - Damping Values for Seismic Design of Nuclear Power Plants, Rev. 0, 1973.
- (12) RG 1.64 - Quality Assurance Requirements for the Design of Nuclear Power Plants, Rev. 2 - June, 1976 (endorses ANSI N45.2.11).
- (13) RG 1.71 - Welder Qualifications for Areas of Limited Accessibility.
- (14) RG 1.74 - Quality Assurance Terms and Definitions, Rev. 2 - February, 1974 (endorses ANSI N45.2.10).

- (15) RG 1.85 - Materials Code Case Acceptability - ASME Section III, Division 1.
- (16) RG 1.88 - Collection, Storage and Maintenance of Nuclear Power Plant Quality Assurance Records, Rev. 2 - October, 1976 (endorses ANSI N45.2.9).
- (17) RG 1.92 - Combining Modal Responses and Spatial Components in Seismic Response Analysis, Rev. 1 - February, 1976.
- (18) RG 1.116 - Quality Assurance Requirements for Installation, Inspection and Testing of Mechanical Equipment and Systems, Rev. 0-R - May, 1977 (endorses ANSI N45.2.8-1975)
- (19) RG 1.123 - Quality Assurance Requirements for Control of Procurement of Items and Services for Nuclear Power Plants, Rev. 1 - July, 1977 (endorses ANSI N45.2.13).
- (20) RG 1.124 - Service Limits and Loading Combinations for Class 1 Linear-Type Component Supports, Revision 1, January, 1978.
- (21) RG 1.144 - Auditing of Quality Assurance Programs for Nuclear Power Plants, Rev.1 - September, 1980 (endorses ANSI N45.2.12-1977)
- (22) RG 3.4 - Nuclear Criticality Safety in Operations with Fissionable Materials at Fuels and Materials Facilities.
- (23) RG 8.8 - Information Relative to Ensuring that Occupational Radiation Exposures at Nuclear Power Stations will be as Low as Reasonably Achievable (ALARA).
- (24) IE Information Notice 83-29 - Fuel Binding Caused by Fuel Rack Deformation.
- (25) RG 8.38 - Control of Access to High and Very High Radiation Areas in Nuclear Power Plants, June, 1993.

i. Branch Technical Position

- (1) CPB 9.1-1 - Criticality in Fuel Storage Facilities.

j. American Welding Society (AWS) Standards

- (1) AWS D1.1 - Structural Welding Code - Steel.
- (2) AWS D1.3 - Structure Welding Code - Sheet Steel.
- (3) AWS D9.1 - Sheet Metal Welding Code.

- (4) AWS A2.4 - Standard Symbols for Welding, Brazing and Nondestructive Examination.
- (5) AWS A3.0 - Standard Welding Terms and Definitions.
- (6) AWS A5.12 - Specification for Tungsten and Tungsten Alloy Electrodes for Arc-Welding and Cutting
- (7) AWS QC1 - Standard for AWS Certification of Welding Inspectors.
- (8) AWS 5.4 – Specification for Stainless Steel Electrodes for Shielded Metal Arc Welding.
- (9) AWS 5.9 – Specification for Bare Stainless Steel Welding Electrodes and Rods.

#### 2.4 Quality Assurance Program

The governing quality assurance requirements for design and fabrication of the spent fuel racks are stated in 10CFR50 Appendix B. Holtec's Nuclear Quality Assurance program complies with this regulation and is designed to provide a system for the design, analysis and licensing of customized components in accordance with various codes, specifications, and regulatory requirements.

The manufacturing of the racks will be carried out by Holtec's designated manufacturer, U.S. Tool & Die, Inc. (UST&D). The Quality Assurance system enforced on the manufacturer's shop floor shall provide for all controls necessary to fulfill all quality assurance requirements. UST&D has manufactured high-density racks for over 60 nuclear plants around the world. UST&D has been audited by the nuclear industry group Nuclear Procurement Issues Committee (NUPIC), and the Quality Assurance branch of the USNRC Office of Nuclear Material Safety and Safeguards (NMSS) with satisfactory results.

The Quality Assurance System that will be used by Holtec to install the racks is also controlled by the Holtec Nuclear Quality Assurance Manual and by the St. Lucie site-specific requirements.

## 2.5 Mechanical Design

The St. Lucie rack modules are designed as cellular structures such that each fuel assembly has a square opening with conforming lateral support and a flat horizontal-bearing surface. All of the storage locations are constructed with multiple cooling flow holes to ensure that redundant flow paths for the coolant are available. The basic characteristics of the Cask Pit racks are summarized in Tables 2.5.1 and 2.5.2.

A central objective in the design of the new rack modules is to maximize structural strength while minimizing inertial mass and dynamic response. Accordingly, the rack modules have been designed to simulate multi-flange beam structures resulting in excellent de-tuning characteristics with respect to the applicable seismic events. The next subsection presents an item-by-item description of the rack modules in the context of the fabrication methodology.

## 2.6 Rack Fabrication

The object of this section is to provide a brief description of the rack module construction activities, which enable an independent appraisal of the adequacy of design. The pertinent methods used in manufacturing the Cask Pit racks may be stated as follows:

1. The rack modules are fabricated in such a manner that the storage cell surfaces, which would come in contact with the fuel assembly, will be free of harmful chemicals and projections (e.g., weld splatter).
2. The component connection sequence and welding processes are selected to reduce fabrication distortions.
3. The fabrication process involves operational sequences that permit immediate accessibility for verification by the inspection staff.

4. The racks are fabricated per the UST&D Appendix B Quality Assurance program, which ensures, and documents, that the fabricated rack modules meet all of the requirements of the design and fabrication documents.
5. The storage cells are connected to each other by austenitic stainless steel corner welds which leads to a honeycomb lattice construction. The extent of welding is selected to "detune" the racks from the seismic input motion

### 2.6.1 Rack Module for Region 1

This section describes the constituent elements of the St. Lucie Unit 1, Region 1 rack modules in the fabrication sequence. Figure 2.1.1 provides a schematic view of a typical Region 1 rack.

The rack module manufacturing begins with fabrication of the "box". The boxes are fabricated from two precision formed channels by seam welding in a machine equipped with copper chill bars and pneumatic clamps to minimize distortion due to welding heat input. Figure 2.6.1 shows the box. The minimum weld seam penetration is 80% of the box metal gage, which is 0.075 inch (14 gage).

A die is used to flare out one end of the box to provide the tapered lead-in (Figure 2.6.2). One-inch diameter holes are punched on at least two sides near the other end of the box to provide the requisite auxiliary flow holes.

Each box constitutes a storage location. Each external box side is equipped with a stainless steel sheathing, which holds one integral Boral sheet (poison material), except the boxes on the rack periphery, which only have Boral on the interior sides. The design objective calls for attaching Boral tightly on the box surface. This is accomplished by die forming the internal and external box sheathings, as shown in Figure 2.6.3. The flanges of the sheathing are attached to the box using skip welds and spot welds. The sheathings serve to locate and position the poison sheet accurately, and to preclude its movement under seismic conditions.

Having fabricated the required number of composite box assemblies, they are joined together in a fixture using connector elements in the manner shown in Figure 2.6.4. Figure 2.6.5 shows an elevation view of two storage cells of a Region 1 rack module. A representative connector element is also shown in the figure. Joining the cells by the connector elements results in a well-defined shear flow path, and essentially makes the box assemblage into a multi-flanged beam-type structure. The "baseplate" is

attached to the bottom edge of the boxes. The baseplate is a 0.75 inch thick austenitic stainless steel plate stock which has 5 inch diameter holes (except lift locations, which are rectangular) cut out in a pitch identical to the box pitch. The baseplate is attached to the cell assemblage by fillet welding the box edge to the plate.

In the final step, adjustable leg supports (shown in Figure 2.6.6) are welded to the underside of the baseplate. The adjustable legs provide a  $\pm 1/2$ -inch vertical height adjustment at each leg location.

Appropriate NDE (nondestructive examination) occurs on all welds including visual examination of sheathing welds, box longitudinal seam welds, box-to-baseplate welds, and box-to-box connection welds; and liquid penetrant examination of support leg welds, in accordance with the design drawings.

## 2.6.2 Rack Module for Region 2

Region 2 storage cell locations have a single poison panel between adjacent cell boxes on the wall surfaces separating them. The significant components (discussed below) of the Unit 2, Region 2 rack are: (1) the storage box subassembly (2) the baseplate, (3) the neutron absorber material, (4) the sheathing, and (5) the support legs.

1. Storage cell box subassembly: As described for Region 1, the boxes are fabricated from two precision formed channels by seam welding in a machine equipped with copper chill bars and pneumatic clamps to minimize distortion due to welding heat input. Figure 2.6.1 shows the box.

Each box has two lateral holes punched near its bottom edge to provide auxiliary flow holes. As shown in Figure 2.6.3, sheathing is attached to each side of the box with the poison material installed in the sheathing cavity. The edges of the sheathing and the box are welded together to form a smooth edge. The box, with integrally connected sheathing, is referred to as the "composite box".

The composite boxes are arranged in a checkerboard array to form an assemblage of storage cell locations (Figure 2.6.7). Filler panels and corner angles are welded to the edges of boxes at the outside boundary of the rack to make the peripheral formed cells. The inter-box welding and pitch adjustment are accomplished by small longitudinal connectors. This assemblage of box assemblies is welded edge-to-edge as shown in Figure 2.6.7, resulting in a honeycomb structure with axial, flexural and torsional rigidity depending on the extent of intercell welding provided. It can be seen from Figure 2.6.7 that two edges of each interior box are connected to the contiguous boxes resulting in a well-defined path for "shear flow".

2. Baseplate: The baseplate provides a continuous horizontal surface for supporting the fuel assemblies. The baseplate has a 5 inch diameter hole (except lift locations which are

rectangular) in each cell location as described in the preceding section. The baseplate is attached to the cell assemblage by fillet welds.

3. The neutron absorber material: As mentioned in the preceding section, Boral is used as the neutron absorber material.
4. Sheathing: As described earlier, the sheathing serves as the locator and retainer of the poison material.
5. Support legs: As stated earlier, all support legs are the adjustable type (Figure 2.6.6). The top (female threaded) portion is made of austenitic steel material. The bottom part is made of 17:4 Ph series stainless steel to avoid galling problems.

Each support leg is equipped with a readily accessible socket to enable remote leveling of the rack after its placement in the pool.

An elevation view of three contiguous Region 2 cells is shown in Figure 2.6.8.

TABLE 2.1.1: GEOMETRIC AND PHYSICAL DATA FOR CASK PIT RACKS

PSL Unit	MODULE I.D.	RACK TYPE	NO. OF CELLS		MODULE ENVELOPE SIZE		WEIGHT (lbs)	NO. OF CELLS PER RACK
			N-S Direction	E-W Direction	N-S	E-W		
2	N2	Region 2	15	15	132.305"	132.305"	29,000	225
1	N1	Region 1	11	13	112.105"	132.705"	32,870	143

Table 2.5.1

MODULE DATA FOR UNIT 1 REGION 1 CASK PIT RACK †

Storage cell inside nominal dimension	8.58in.
Cell pitch	10.3in.
Storage cell height (above the plate)	169.25 in.
Baseplate hole size (except for lift location)	5.0 in.
Baseplate thickness	0.75 in.
Support pedestal height	4.25 in.
Support pedestal type	Remotely adjustable pedestals
Number of support pedestals per rack	4
Number of cell walls containing 1" diameter flow holes at base of cell wall	All Four Cell Walls
Remote lifting and handling provisions	Yes
Poison material	Boral
Poison length	140 in.
Poison width	7.25 in.

† All dimensions indicate nominal values

Table 2.5.2

MODULE DATA FOR UNIT 2 REGION 2 CASK PIT RACK †

Storage cell inside nominal dimension	8.58 in.
Cell pitch	8.80 in.
Storage cell height (above the plate)	172.75 in.
Baseplate hole size (except for lift location)	5.0 in.
Baseplate thickness	0.75 in.
Support pedestal height	4.25 in.
Support pedestal type	Remotely adjustable pedestals
Number of support pedestals per rack	4
Minimum number of cell walls containing 1" diameter supplemental flow holes at base of each cell located away from pedestals	2
Number of cell walls containing 1" diameter flow holes at base of each cell located above a pedestal	4
Remote lifting and handling provisions	Yes
Poison material	Boral
Poison length	140 in.
Poison width	7.25 in.

† All dimensions indicate nominal values

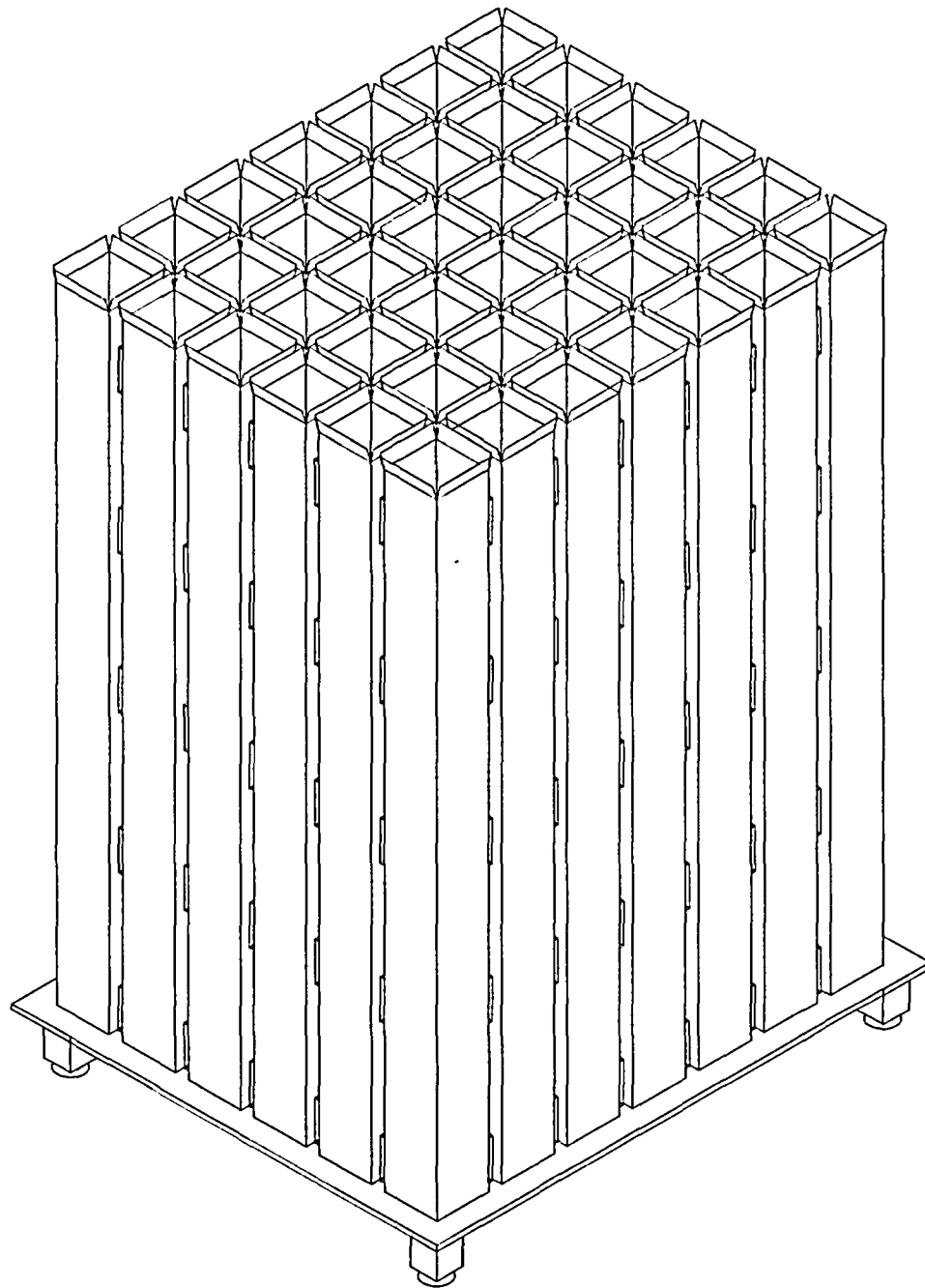


FIGURE 2.1.1; SCHEMATIC VIEW OF TYPICAL REGION 1 RACK STRUCTURE

HI201

HI-2022882

G:\DRAWINGS\1201\REPORT-HI-2022882\FIG2.1.1

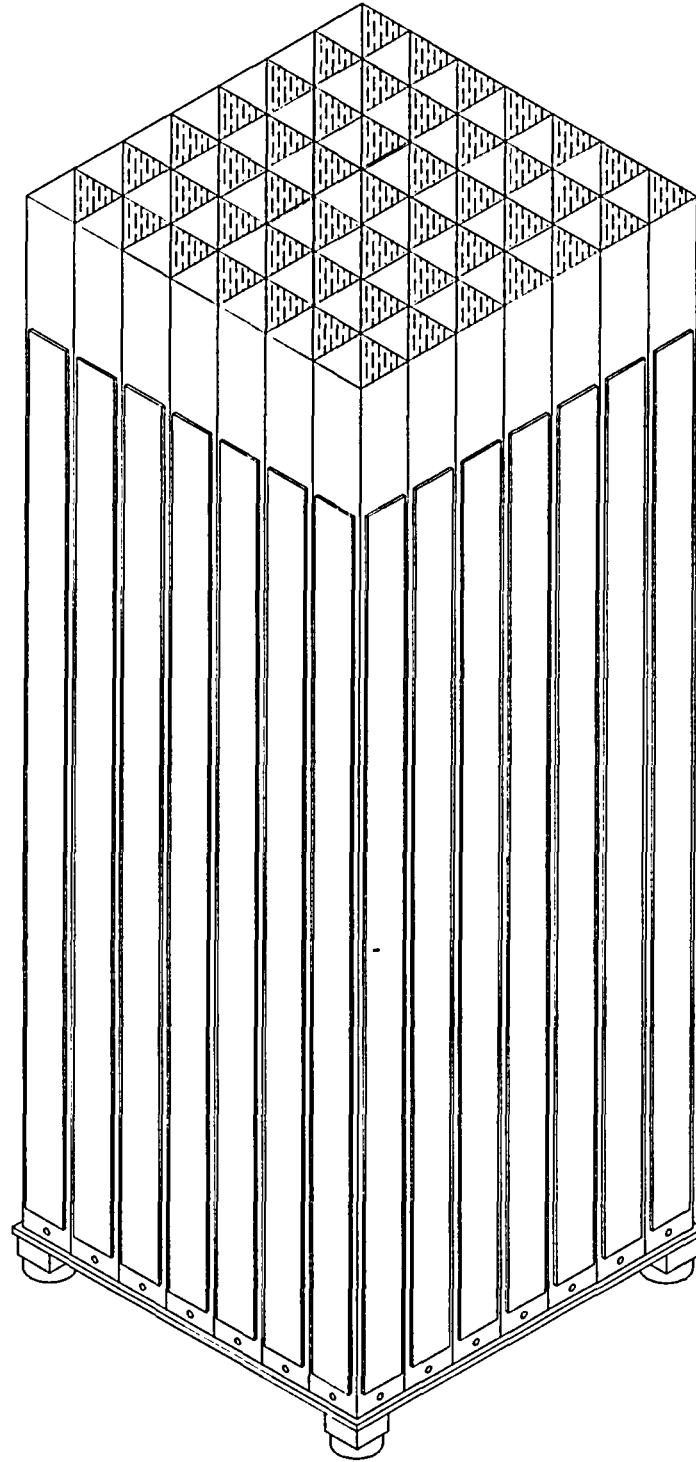
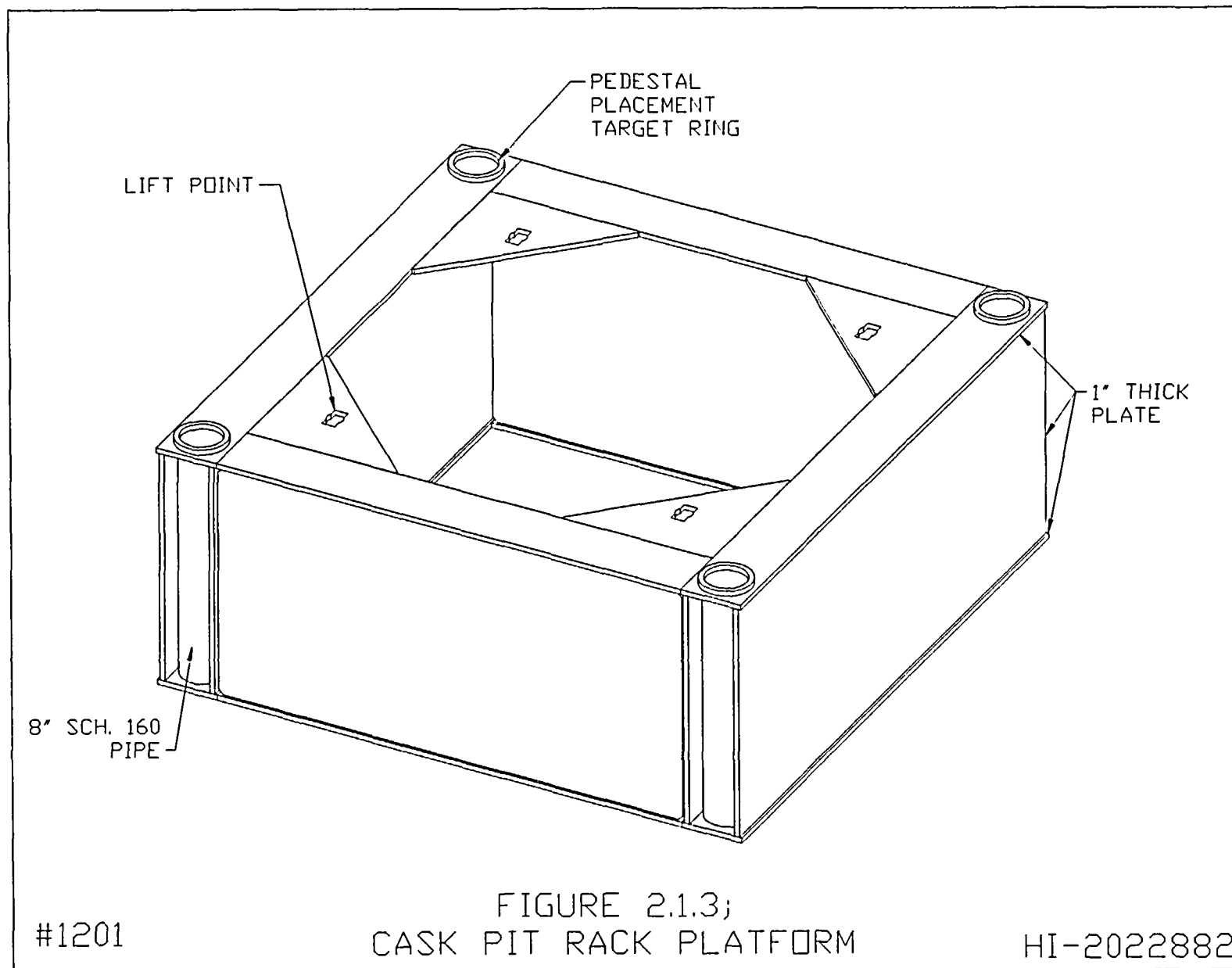


FIGURE 2.1.2; SCHEMATIC OF TYPICAL REGION 2 RACK STRUCTURE

H1201

HI-2022882



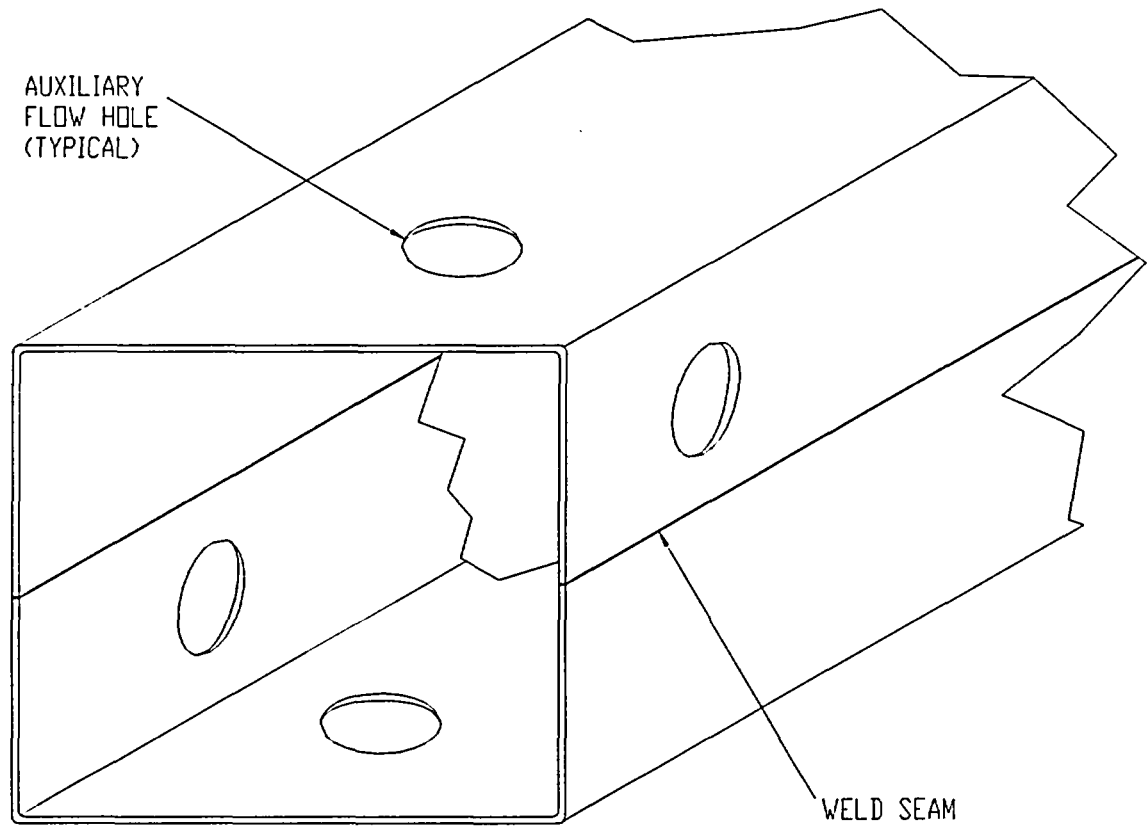


FIGURE 2.6.1; SEAM WELDED PRECISION FORMED CHANNELS

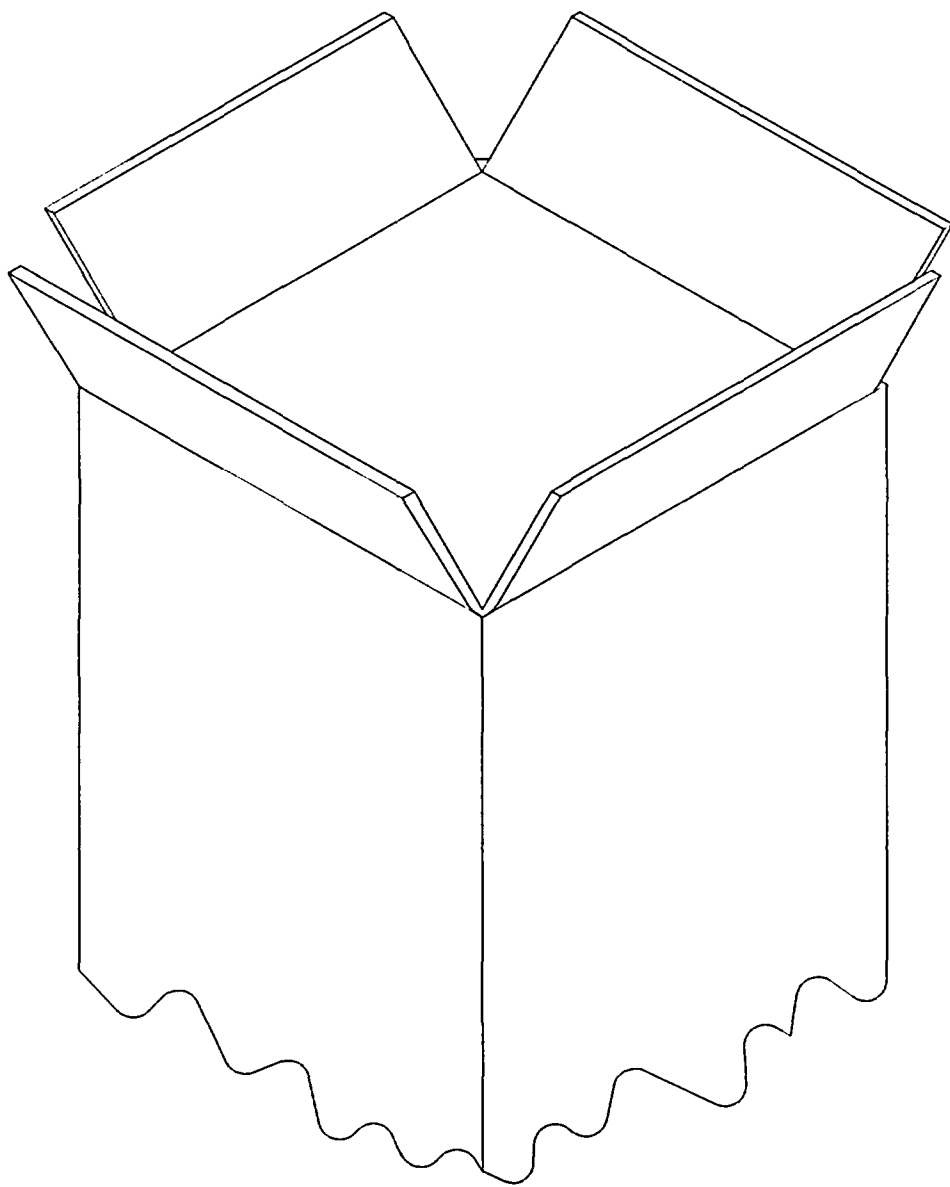


FIGURE 2.6.2; TAPERED REGION 1  
CELL END

H1201

HI-2022882

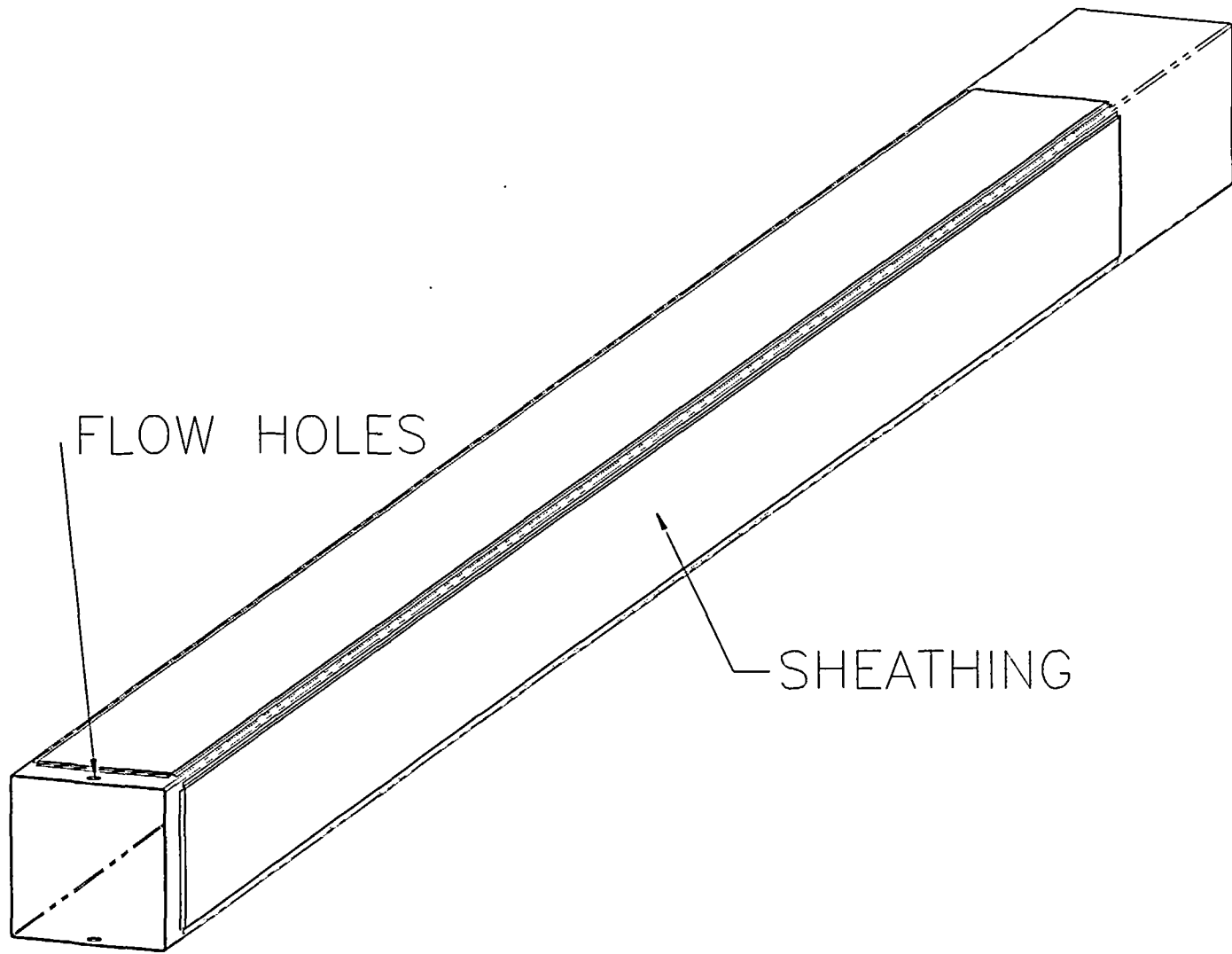


FIGURE 2.6.3; COMPOSITE BOX ASSEMBLY

H1201

HI-2022882

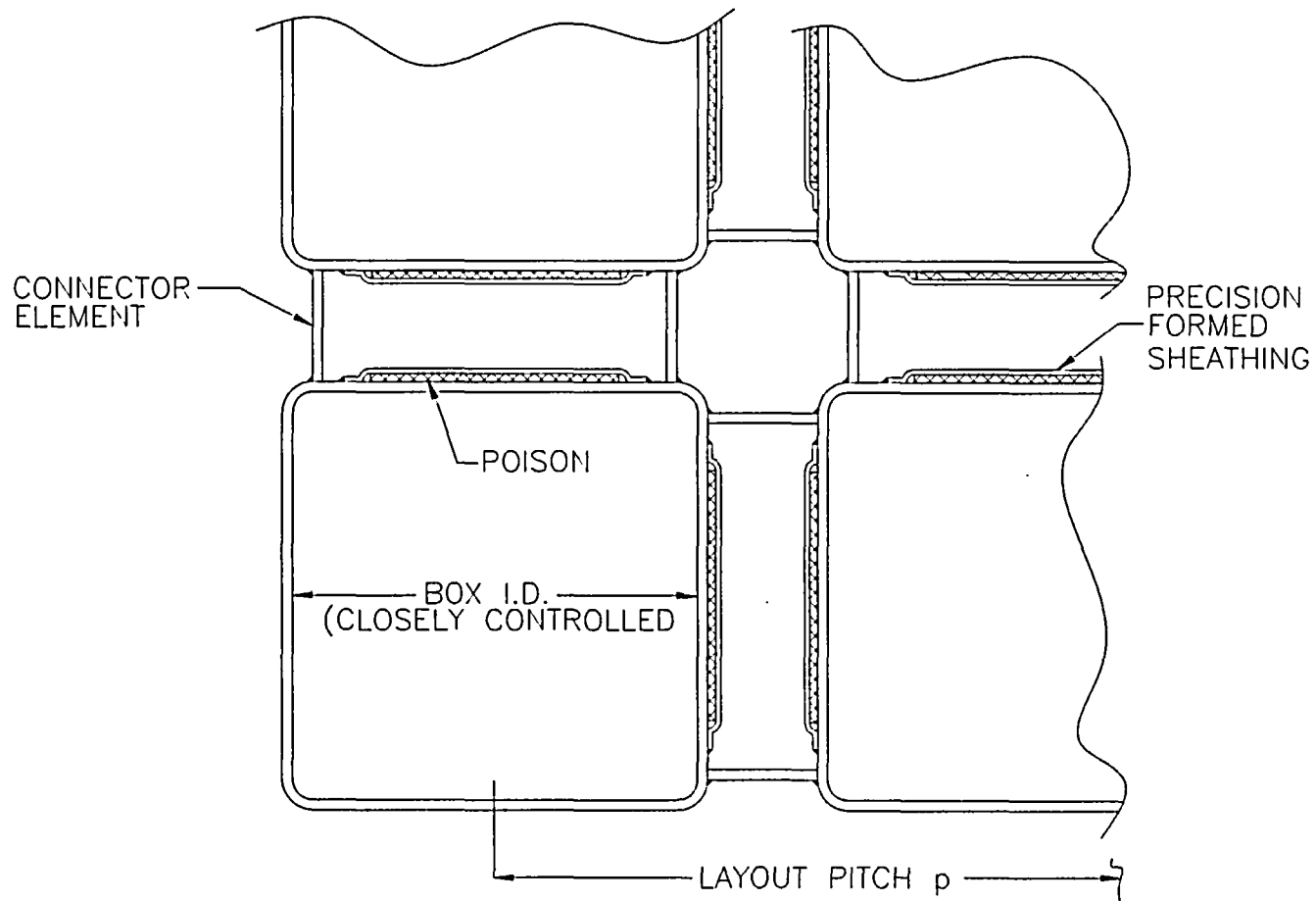


FIGURE 2.6.4; ASSEMBLAGE OF REGION 1 CELLS

H1201

HI-2022882

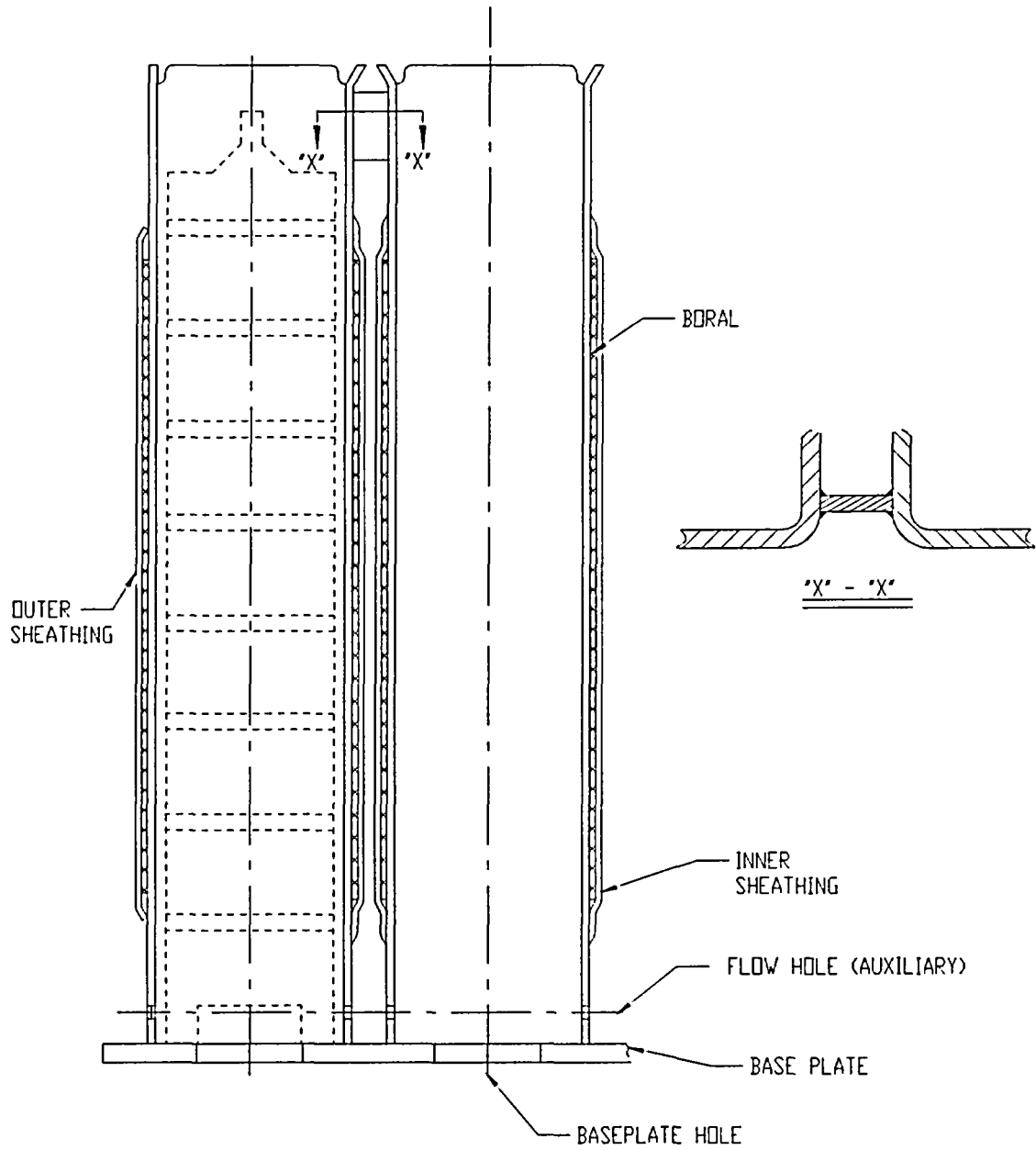
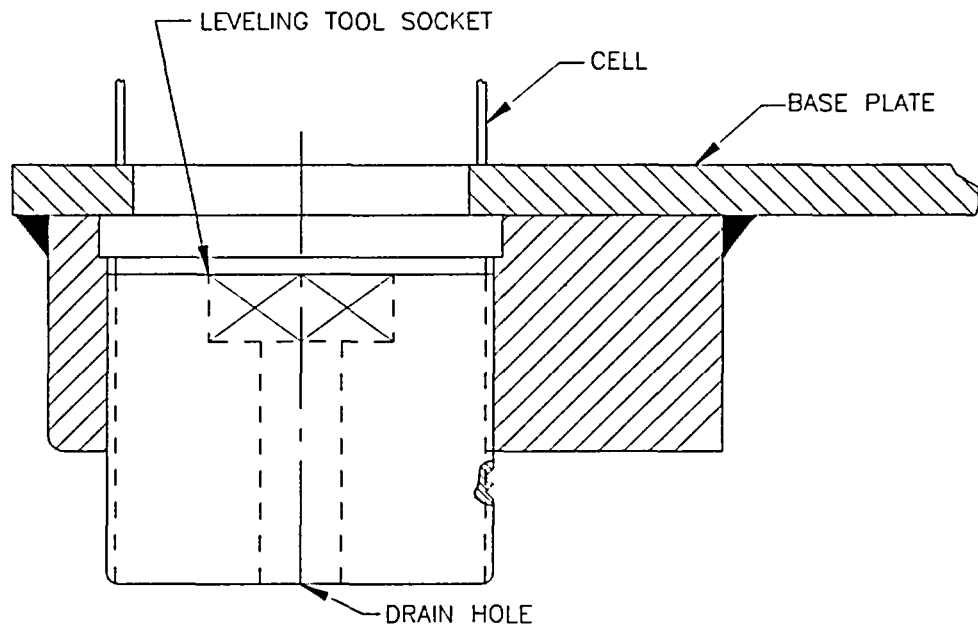
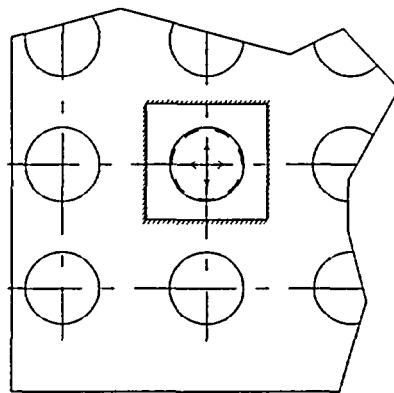


FIGURE 2.6.5: ELEVATION VIEW OF REGION 1 RACK

NOTE: DEPICTION OF STORED FUEL ASSEMBLY IS NOT INTENDED TO BE ACCURATE.



TYPICAL ELEVATION VIEW



TYPICAL PLAN VIEWS OF RACK BASEPLATE CORNER

FIGURE 2.6.6; SUPPORT PEDESTALS FOR HOLTEC PWR RACKS

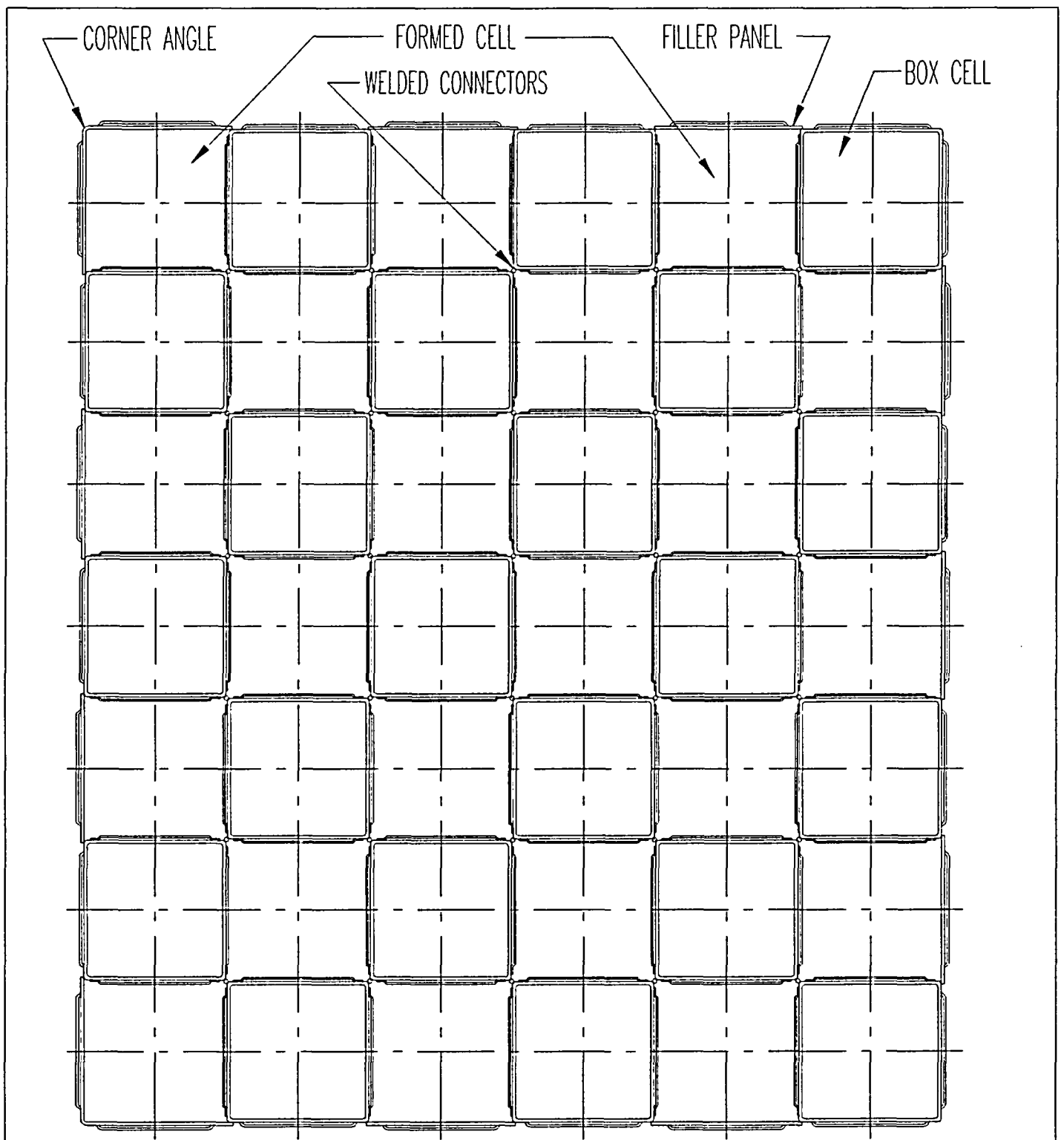


FIGURE 2.6.7; TYPICAL ARRAY OF STORAGE CELLS  
(NON-FLUX TRAP CONSTRUCTION)

H1201

HI-2022882

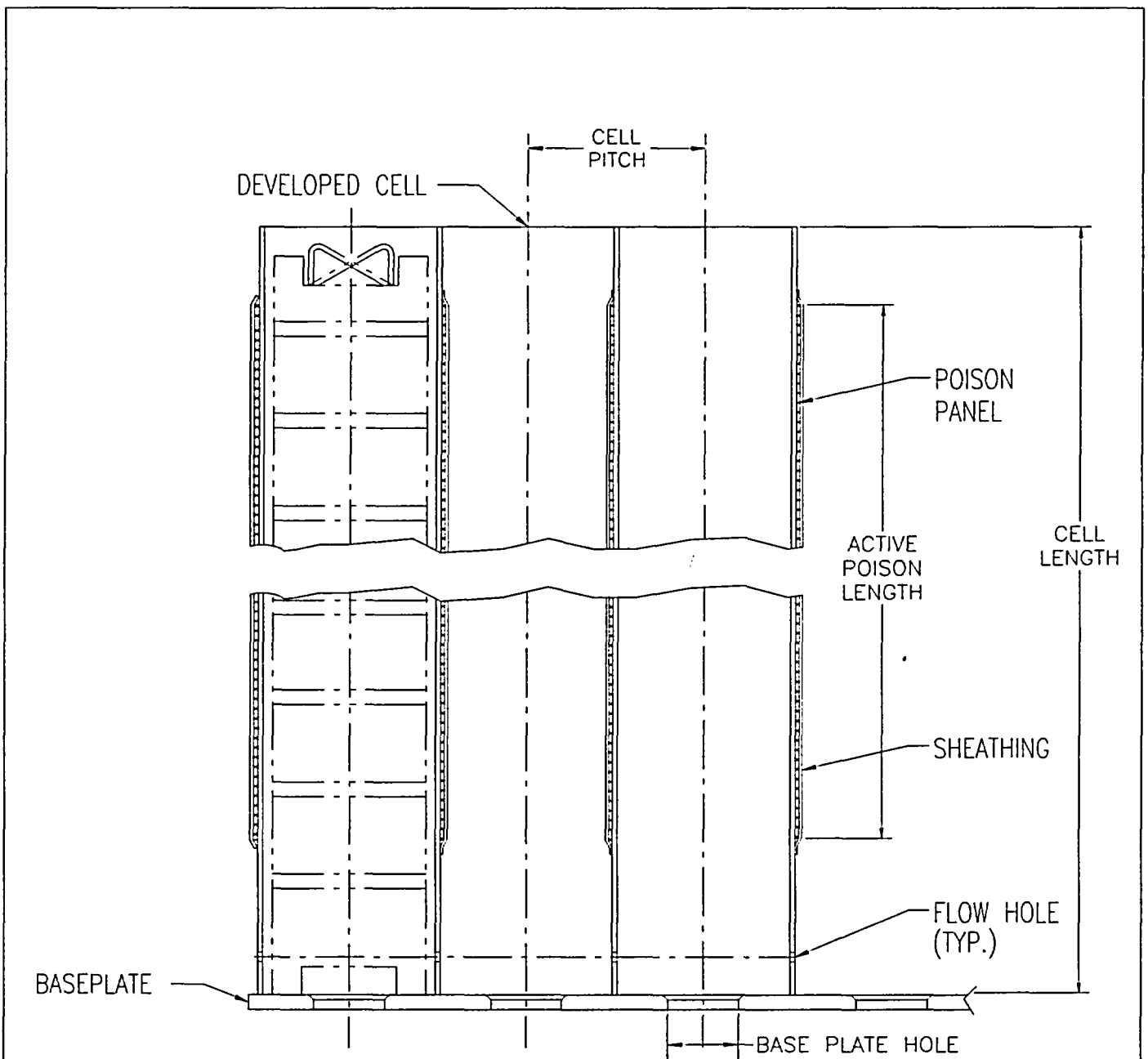


FIGURE 2.6.8; ELEVATION VIEW OF STORAGE RACK MODULE

NOTE: DEPICTION OF STORED FUEL ASSEMBLY IS NOT INTENDED TO BE ACCURATE.

## 3.0 MATERIAL AND HEAVY LOAD CONSIDERATIONS

### 3.1 Introduction

Safe storage of nuclear fuel in the pool requires that the materials utilized in the rack fabrication be of proven durability and compatible with the pool water environment. This section provides a synopsis of the considerations with regard to long-term design service life of 60 years.

### 3.2 Structural Materials

The following structural materials are utilized in the fabrication of the fuel racks:

- a. ASTM A240-304L for all sheet metal stock and baseplate
- b. Internally threaded support legs: ASTM A240-304L
- c. Externally threaded support spindle: ASTM A564-630 precipitation hardened stainless steel (heat treated to 1100°F)
- d. Weld material - ASTM Type 308

### 3.3 Neutron Absorbing Material

In addition to the structural and non-structural stainless material, the racks employ Boral<sup>TM</sup>, a patented product of AAR Manufacturing, as the neutron absorber material. A brief description of Boral, and its pool experience list follows.

Boral is a thermal neutron poison material composed of boron carbide and 1100 alloy aluminum. Boron carbide is a compound having a high boron content in a physically stable and chemically inert form. The 1100 alloy aluminum is a lightweight metal with high tensile strength, which is protected from corrosion by a highly resistant oxide film. The two materials, boron carbide and aluminum, are chemically compatible and ideally suited for long-term use in the radiation, thermal and chemical environment of a spent fuel pool. Boral has been shown [3.3.1] to be superior to alternative materials previously used as neutron absorbers in storage racks.

Boral has been exclusively used in fuel rack applications in recent years. Its use in spent fuel pools as the neutron absorbing material can be attributed to its proven performance (over 150 pool years of experience) and the following unique characteristics:

- i. The content and placement of boron carbide provides a very high removal cross-section for thermal neutrons.
- ii. Boron carbide, in the form of fine particles, is homogeneously dispersed throughout the central layer of the Boral panels.
- iii. The boron carbide and aluminum materials in Boral do not degrade as a result of long-term exposure to radiation.
- iv. The neutron absorbing central layer of Boral is clad with permanently bonded surfaces of aluminum.
- v. Boral is stable, strong, durable, and corrosion resistant.

Holtec International's Q.A. program ensures that Boral is manufactured by AAR Manufacturing under the control and surveillance of a Quality Assurance/Quality Control Program that conforms to the requirements of 10CFR50 Appendix B, "Quality Assurance Criteria for Nuclear Power Plants".

As indicated in Tables 3.3.1 and 3.3.2, Boral has been licensed by the USNRC for use in numerous BWR and PWR spent fuel storage racks and has been extensively used in international nuclear installations.

### 3.3.1 Boral Material Characteristics

**Aluminum:** Aluminum is a silvery-white, ductile metallic element. The 1100 alloy aluminum is used extensively in heat exchangers, pressure and storage tanks, chemical equipment, reflectors and sheet metal work.

It has high resistance to corrosion in industrial and marine atmospheres. Aluminum has atomic number of 13, atomic weight of 26.98, specific gravity of 2.69 and valence of 3. The physical, mechanical and chemical properties of the 1100 alloy aluminum are listed in Tables 3.3.3 and 3.3.4.

The excellent corrosion resistance of the 1100 alloy aluminum is provided by the protective oxide film that quickly develops on its surface from exposure to the atmosphere or water. This film prevents the loss of metal from general corrosion or pitting corrosion.

Boron Carbide: The boron carbide contained in Boral is a fine granulated powder that conforms to ASTM C-750-80 nuclear grade Type III. The material conforms to the chemical composition and properties listed in Table 3.3.5.

References [3.3.2], [3.3.3], and [3.3.4] provide further discussion as to the suitability of these materials for use in spent fuel storage module applications.

#### 3.4 Compatibility with Environment

All materials used in the construction of the Holtec racks have been determined to be compatible with the St. Lucie Spent Fuel Pool, and have an established history of in-pool usage. As evidenced in Tables 3.3.1 and 3.3.2, Boral has been successfully used in both PWR and BWR fuel pools. Austenitic stainless steel (304L) is a widely used stainless alloy in nuclear power plants.

#### 3.5 Heavy Load Considerations for the Proposed Rack Installations

The main hook of the Spent Fuel Cask Handling Crane for each Unit will be used for lifting the new rack and platforms into the respective Fuel Handling Building. Safe handling of heavy loads by the Spent Fuel Cask Handling Cranes will be ensured by following the defense in depth approach guidelines of NUREG 0612:

- Defined safe load paths in accordance with approved procedures
- Supervision of heavy load lifts by designated individuals
- Crane operator training and qualification that satisfies the requirements of ANSI/ASME B30.2-1976 [3.5.1]

- Use of lifting devices (slings) that are selected, inspected and maintained in accordance with ANSI B30.9-1971 [3.5.2]
- Inspection, testing and maintenance of cranes in accordance with ANSI/ASME B30.2-1976
- Ensuring the design of the Fuel Cask Cranes meets the requirements of CMAA-70 [3.5.3] and ANSI/ASME B30.2-1976
- Reliability of special lifting devices by application of design safety margins, and periodic inspection and examinations using approved procedures

The salient features of the lifting devices and associated procedures are described as follows:

a. **Safe Load Paths and Procedures**

Safe load paths will be defined for moving the new rack into the Fuel Handling Building (FHB). The rack will be lifted by the main hook of the Spent Fuel Cask Handling Crane and enter the FHB through the L-shaped door above the cask pit designed for ingress and egress of spent fuel casks. Therefore, the rack will enter the building at a location directly above the area of placement and need not be carried over portions of the Spent Fuel Pool. A staging area will be setup outside of the FHB as a laydown area for the new rack. The staging area location also will not require any heavy load to be lifted over the SFP or any safety-related equipment.

All phases of rack installation activities will be conducted in accordance with written procedures, which will be reviewed and approved by the owner.

b. **Supervision of Lifts**

Procedures used during the installation of the Cask Pit racks require supervision of heavy load lifts by a designated individual who is responsible for ensuring procedure compliance and safe lifting practices.

c. **Crane Operator Training**

All crew members involved in the use of the lifting and upending equipment will be given training by Holtec International using a videotape-aided instruction course which has been utilized in previous rack installation operations.

d. Lifting Devices Design and Reliability

The Spent Fuel Cask Handling Crane for each Unit is located outdoors, at the north end of its respective Fuel Handling Building, where it can access the L-shaped hatch, the adjacent laydown areas and the access road. The cranes, which are of the overhead bridge type, will be refurbished and upgraded to single failure proof capability before the rack installation commences. The rated capacities for each crane will also be increased to 150 tons (main hoist) and 25 tons (auxiliary hoist). Electrical interlocks and the physical design of the buildings prevent the cranes from carrying a load over the fuel storage area of the spent fuel pool. A temporary hoist with an appropriate capacity may be attached to the Cask Handling Crane hook to prevent submergence of the hook.

The following table determines the maximum lift weight during the installation of the new racks.

Item	Weight (lbs)
Rack	32,870 (max.)
Lift Rig	1,100
Rigging	500
Total Lift	34,470

It is clear, based on the heaviest rack weight to be lifted, that the heaviest load will be well below the 150 ton rating of the Spent Fuel Cask Handling Crane main hook. The hoist to be used in conjunction with the Cask Handling Crane will be selected to provide an adequate load capacity and comply with NUREG-0612.

Remotely engaging lift rigs, meeting all requirements of NUREG-0612, will be used to lift the new rack modules. The new rack lift rigs consist of four independently loaded traction rods in a lift configuration. The individual lift rods have a safety factor of greater than 10. If one of the rods break, the load will still be supported by at least two

rods, which will have a safety factor of more than 5 against ultimate strength. Therefore, the lift rigs comply with the duality feature called for in Section 5.1.6 (3) of NUREG 0612.

The lift rigs have the following attributes:

- The traction rod is designed to prevent loss of its engagement with the rig in the locked position. Moreover, the locked configuration can be directly verified from above the pool water without the aid of an underwater camera.
- The stress analysis of the rig is carried out and the primary stress limits postulated in ANSI N14.6 [3.5.4] are met.
- The rig is load tested with 300% of the maximum weight to be lifted. The test weight is maintained in the air for 10 minutes. All critical weld joints are liquid penetrant examined to establish the soundness of all critical joints.

e. Crane Maintenance

The Spent Fuel Cask Handling Cranes are maintained functional per the St. Lucie preventative maintenance procedures.

The proposed heavy loads compliance will be in accordance with the guidelines of NUREG-0612, which calls for measures to "provide an adequate defense-in-depth for handling of heavy loads near spent fuel...". The NUREG-0612 guidelines cite four major causes of load handling accidents, namely

- i. operator errors
- ii. rigging failure
- iii. lack of adequate inspection
- iv. inadequate procedures

The rack installation ensures maximum emphasis on mitigating the potential load drop accidents by implementing measures to eliminate shortcomings in all aspects of the operation including the four

aforementioned areas. A summary of the measures specifically planned to deal with the major causes is provided below.

**Operator errors:** As mentioned above, comprehensive training will be provided to the installation crew. All training shall be in compliance with ANSI B30.2.

**Rigging failure:** The lifting device designed for handling and installation of the new racks has redundancies in the lift legs and lift eyes such that there are four independent load members in the new rack lift rig, and three independent load members in the existing rack lifting rig. Failure of any one load bearing member would not lead to uncontrolled lowering of the load. The rig complies with all provisions of ANSI 14.6-1993, including compliance with the primary stress criteria, load testing at 300% of maximum lift load, and dye examination of critical welds.

The rig designs are similar to the rigs used in the initial racking or the rerack of numerous other plants, such as Hope Creek, Millstone Unit 1, Indian Point Unit Two, Ulchin II, Laguna Verde, J.A. FitzPatrick, and Three Mile Island Unit 1.

**Lack of adequate inspection:** The designer of the racks has developed a set of inspection points that have been proven to eliminate any incidence of rework or erroneous installation in numerous prior rerack projects. Surveys and measurements are performed on the storage racks prior to and subsequent to placement into the Cask Pit to ensure that the as-built dimensions and installed locations are acceptable. Measurements of the pool and floor elevations are also performed to determine actual pool configuration and to allow height adjustments of the pedestals prior to rack installation. These inspections minimize rack manipulation during placement into the pool.

**Inadequate procedures:** Procedures will be developed to address operations pertaining to the rack installation effort, including, but not limited to, mobilization, rack handling, upending, lifting, installation, verticality, alignment, dummy gage testing, site safety, and ALARA compliance. The procedures will be the successors of the procedures successfully implemented in previous projects.

Table 3.5.1 provides a synopsis of the requirements delineated in NUREG-0612, and its intended compliance.

3.6 References

- [3.3.1] "Nuclear Engineering International," July 1997 issue, pp 20-23.
- [3.3.2] "Spent Fuel Storage Module Corrosion Report," Brooks & Perkins Report 554, June 1, 1977.
- [3.3.3] "Suitability of Brooks & Perkins Spent Fuel Storage Module for Use in PWR Storage Pools," Brooks & Perkins Report 578, July 7, 1978.
- [3.3.4] "Boral Neutron Absorbing/Shielding Material - Product Performance Report," Brooks & Perkins Report 624, July 20, 1982.
- [3.5.1] ANSI/ASME B30.2, "Overhead and Gantry Cranes, (Top Running Bridge, Single or Multiple Girder, Top Running Trolley Hoist)," American Society of Mechanical Engineers, 1976.
- [3.5.2] ANSI B30.9, "Safety Standards for Slings," 1971.
- [3.5.3] CMMA Specification 70, "Electrical Overhead Traveling Cranes," Crane Manufacturers Association of America, Inc., 2000.
- [3.5.4] ANSI N14.6-1993, Standard for Special Lifting Devices for Shipping Containers Weighing 10000 Pounds or more for Nuclear Materials," American National Standard Institute, Inc., 1978.

Table 3.3.1			
BORAL EXPERIENCE LIST - PWRs			
Plant	Utility	Docket No.	Mfg. Year
Maine Yankee	Maine Yankee Atomic Power	50-309	1977
Donald C. Cook	Indiana & Michigan Electric	50-315/316	1979
Sequoyah 1,2	Tennessee Valley Authority	50-327/328	1979
Salem 1,2	Public Service Electric & Gas	50-272/311	1980
Zion 1,2	Commonwealth Edison	50-295/304L	1980
Bellefonte 1, 2	Tennessee Valley Authority	50-438/439	1981
Yankee Rowe	Yankee Atomic Power	50-29	1964/1983
Gosgen	Kernkraftwerk Gosgen-Daniken AG (Switzerland)		1984
Koeberg 1,2	ESCOM (South Africa)		1985
Beznau 1,2	Nordostschweizerische Kraftwerke AG (Switzerland)		1985
12 various Plants	Electricite de France (France)	--	1986
Indian Point 3	NY Power Authority	50-286	1987
Byron 1,2	Commonwealth Edison	50-454/455	1988
Braidwood 1,2	Commonwealth Edison	50-456/457	1988
Yankee Rowe	Yankee Atomic Power	50-29	1988
Three Mile Island I	GPU Nuclear	50-289	1990
Sequoyah (rerack)	Tennessee Valley Authority	50-327	1992
Donald C. Cook (rerack)	American Electric Power	50-315/316	1992
Beaver Valley Unit 1	Duquesne Light Company	50-334	1993
Fort Calhoun	Omaha Public Power District	50-285	1993

Table 3.3.1			
BORAL EXPERIENCE LIST - PWRs			
Plant	Utility	Docket No.	Mfg. Year
Zion 1 & 2 (rerack)	Commonwealth Edison	50-295/304L	1993
Salem Units 1 & 2 (rerack)	Public Gas and Electric Company	50-272/311	1995
Ulchin Unit 1	Korea Electric Power Company (Korea)	--	1995
Haddam Neck	Connecticut Yankee Atomic Power Company	50-213	1996
Ulchin Unit 2	Korea Electric Power Company (Korea)	--	1996
Kori-4	Korea Electric Power Company (Korea)	--	1996
Yonggwang 1,2	Korea Electric Power Company (Korea)	--	1996
Sizewell B	Nuclear Electric, plc (United Kingdom)	--	1997
Angra 1	Furnas Centrais-Elétricas SA (Brazil)	--	1997
Waterford 3	Entergy Operations	50-382	1997
Callaway	Union Electric	50-483	1998
Millstone 3	Northeast Utilities	50-423	1998
Davis-Besse	First Energy	50-346	1999
Wolf Creek	Wolf Creek Nuclear Operating	50-482	1999
Harris Pool 'C'	Carolina Power & Light	50-401	1999
Yonggwang 5/6	Korea Electric Power Company (Korea)	--	2001
Kewaunee	Wisconsin Public Service	50-305	2001

Table 3.3.2

## BORAL EXPERIENCE LIST - BWRs

Plant	Utility	Docket No.	Mfg. Year
Cooper	Nebraska Public Power	50-298	1979
J.A. FitzPatrick	NY Power Authority	50-333	1978
Duane Arnold	Iowa Electric Light & Power	50-331	1979
Browns Ferry 1,2,3	Tennessee Valley Authority	50-259/260/296	1980
Brunswick 1,2	Carolina Power & Light	50-324/325	1981
Clinton	Illinois Power	50-461/462	1981
Dresden 2,3	Commonwealth Edison	50-237/249	1981
E.I. Hatch 1,2	Georgia Power	50-321/366	1981
Hope Creek	Public Service Electric & Gas	50-354/355	1985
Humboldt Bay	Pacific Gas & Electric Company	50-133	1985
LaCrosse	Dairyland Power	50-409	1976
Limerick 1,2	Philadelphia Electric Company	50-352/353	1980
Monticello	Northern States Power	50-263	1978
Peachbottom 2,3	Philadelphia Electric	50-277/278	1980
Perry 1,2	Cleveland Electric Illuminating	50-440/441	1979
Pilgrim	Boston Edison Company	50-293	1978
Susquehanna 1,2	Pennsylvania Power & Light	50-387,388	1979
Vermont Yankee	Vermont Yankee Atomic Power	50-271	1978/1986
Hope Creek	Public Service Electric & Gas	50-354/355	1989
Harris Pool 'B' †	Carolina Power & Light	50-401	1991
Duane Arnold	Iowa Electric Light & Power	50-331	1993
Pilgrim	Boston Edison Company	50-293	1993

Table 3.3.2			
BORAL EXPERIENCE LIST - BWRs			
Plant	Utility	Docket No.	Mfg. Year
LaSalle 1	Commonwealth Edison	50-373	1992
Millstone Unit 1	Northeast Utilities	50-245	1989
James A. FitzPatrick	NY Power Authority	50-333	1990
Hope Creek	Public Service Electric & Gas Company	50-354	1991
Duane Arnold Energy Center	Iowa Electric Power Company	50-331	1994
Limerick Units 1,2	PECO Energy	50-352/50-353	1994
Harris Pool 'B' †	Carolina Power & Light Company	50-401	1996
Chinshan 1,2	Taiwan Power Company (Taiwan)	--	1986
Kuosheng 1,2	Taiwan Power Company (Taiwan)	--	1991
Laguna Verde 1,2	Comision Federal de Electricidad (Mexico)	--	1991
Harris Pool 'B' †	Carolina Power & Light Company	50-401	1996
James A. FitzPatrick	NY Power Authority	50-333	1998
Vermont Yankee	Vermont Yankee	50-271	1998
Plant Hatch	Southern Nuclear	50-321	1999
Harris Pool 'C' †	Carolina Power & Light Company	50-401	1999
Byron/Braidwood	Commonwealth Edison	50-401	1999
Enrico Fermi Unit 2	Detroit Edison	50-305	2000

† Fabricated racks for storage of spent fuel transhipped from Brunswick.

Table 3.3.3 1100 ALLOY ALUMINUM PHYSICAL CHARACTERISTICS	
Density	0.098 lb/in <sup>3</sup> 2.713 g/cm <sup>3</sup>
Melting Range	1190°F - 1215°F 643° - 657°C
Thermal Conductivity (77°F)	128 BTU/hr/ft <sup>2</sup> /F/ft 0.53 cal/sec/cm <sup>2</sup> /°C/cm
Coefficient of Thermal Expansion (68°F - 212°F)	13.1 x 10 <sup>-6</sup> in/in-°F 23.6 x 10 <sup>-6</sup> cm/cm-°C
Specific Heat (221°F)	0.22 BTU/lb-°F 0.23 cal/g-°C
Modulus of Elasticity	10 x 10 <sup>6</sup> psi
Tensile Strength (75°F)	13,000 psi (annealed) 18,000 psi (as rolled)
Yield Strength (75°F)	5,000 psi (annealed) 17,000 psi (as rolled)
Elongation (75°F)	35-45% (annealed) 9-20% (as rolled)
Hardness (Brinell)	23 (annealed) 32 (as rolled)
Annealing Temperature	650°F 343°C

Table 3.3.4 CHEMICAL COMPOSITION - ALUMINUM (1100 ALLOY)	
99.00% min.	Aluminum
1.00% max.	Silicone and Iron
0.05-0.20% max.	Copper
0.05% max.	Manganese
0.10% max.	Zinc
0.15% max.	Other

Table 3.3.5	
CHEMICAL COMPOSITION AND PHYSICAL PROPERTIES OF BORON CARBIDE	
CHEMICAL COMPOSITION (WEIGHT PERCENT)	
Total boron	70.0 min.
B <sup>10</sup> isotopic content in natural boron	18.0
Boric oxide	3.0 max.
Iron	2.0 max.
Total boron plus total carbon	94.0 min.
PHYSICAL PROPERTIES	
Chemical formula	B <sub>4</sub> C
Boron content (weight percent)	78.28%
Carbon content (weight percent)	21.72%
Crystal structure	rhombohedral
Density	0.0907 lb/in <sup>3</sup> 2.51 g/cm <sup>3</sup>
Melting Point	4442°F 2450°C
Boiling Point	6332°F 3500°C
Boral Loading (minimum grams B <sup>10</sup> per cm <sup>2</sup> )	

Table 3.5.1	
HEAVY LOAD HANDLING COMPLIANCE MATRIX (NUREG-0612)	
Criterion	Compliance
1. Are safe load paths defined for the movement of heavy loads to minimize the potential of impact, if dropped, on irradiated fuel?	Yes
2. Will procedures be developed to cover: identification of required equipment, inspection and acceptance criteria required before movement of load, steps and proper sequence for handling the load, defining the safe load paths, and special precautions?	Yes
3. Will crane operators be trained and qualified?	Yes
4. Will special lifting devices meet the guidelines of ANSI 14.6-1993?	Yes
5. Will non-custom lifting devices be installed and used in accordance with ANSI B30.20 [3.5.5], latest edition?	Yes
6. Will the cranes be inspected and tested prior to use in rack installation?	Yes
7. Does the crane meet the requirements of ANSI B30.2-1976 and CMMA-70?	Yes

## 4.0 Criticality Safety Analyses

The criticality analyses reported here include the new Cask Pit racks to be installed in both Unit 1 and Unit 2 of the St. Lucie Nuclear Power Plant.

### 4.1 Unit 1 Cask Pit Rack

#### 4.1.1 Introduction and Summary

The purpose of this evaluation is to document the criticality safety of the new fuel storage rack to be installed in the Cask Pit adjacent to the spent fuel pool of the FPL St. Lucie Unit 1 Nuclear Plant. The high density Region 1 rack is designed to assure that the effective neutron multiplication factor ( $k_{eff}$ ) is equal to or less than 0.95 with the rack fully loaded with most reactive fuel assemblies authorized to be stored and flooded with unborated water at the temperature within the operating range corresponding to the highest reactivity. The maximum calculated reactivity includes margins for uncertainty in reactivity calculations including mechanical tolerances. All independent uncertainties are statistically combined, such that the final  $k_{eff}$  will be equal to or less than 0.95 with a 95% probability at a 95% confidence level.

The analysis uses the MCNP4a Monte Carlo code developed by the Los Alamos National Laboratory as the primary methodology for the calculations. CASMO4 was used to determine the reactivity effects of manufacturing tolerances and, as necessary, to assess the effect of fuel burning. As permitted in the USNRC guidelines, parametric evaluations were performed for manufacturing tolerances and the associated reactivity uncertainties were combined statistically. All calculations were made using an explicit model of the fuel and storage cell geometry. Results of these calculations are then used to define the reference reactivity that assures safe storage of fuel assemblies in the Cask Pit rack.

Potential abnormal and accident conditions have also been considered in this study. The temperature and void coefficient of reactivity are negative and the maximum design reactivity occurs at 50 °F. No misloading event was evaluated for the Unit 1 Cask Pit rack.

The criticality analysis was performed assuming unborated water as the moderator. Although such a condition is not realistic in the cask pit, which shares borated water with the spent fuel pool, it bounds all possible boron dilution accidents and conforms to the requirements of 10CFR50.68. In practice, the presence of moderator soluble boron at the Technical Specification limit assures a significantly lower reactivity in the cask pit rack.

In summary, results of this analysis confirm that the Unit 1 Cask Pit fuel storage rack can safely accommodate fresh fuel with initial enrichments up to  $4.50 \pm 0.05$  wt%, with assurance that the maximum reactivity, including calculational and manufacturing uncertainties, will not exceed 0.95, with 95% probability at the 95% confidence level.

#### 4.1.2 Analysis and Criteria Assumptions

To assure that the true reactivity will always be less than the calculated reactivity, the following conservative analysis criteria and assumptions are used in the analysis of the Cask Pit rack.

1. An infinite radial array of storage cells was assumed.
2. Neutron absorption in minor structural members is neglected, i.e., spacer grids are analytically replaced by water.
3. Moderator is assumed to be un-borated water at a temperature that results in highest reactivity (50°F or 10° C)
4. No credit is taken for the presence of the Uranium-234 or Uranium-236 isotopes in the fuel.
5. The analyses used the most reactive fuel assemblies amongst CE 14x14 or Framatome 14x14 fuel.
6. Fuel assembly is centered in the cell.
7. The fuel assembly designs used in the evaluation do not contain any gadolinia and the results of the analysis yields a higher reactivity and therefore bounds any fuel with  $Gd_2O_3$  in the fuel.

### 4.1.3 Acceptance Criteria

The primary acceptance criterion for analysis of the Cask Pit rack is that, under a hypothetical condition of 0 ppm soluble boron in the cask pit, the maximum  $k_{eff}$  shall be less than or equal to 0.95, including calculational uncertainties and effects of mechanical tolerances. Applicable codes, standards, and regulations, or pertinent sections thereof, include the following:

- General Design Criterion 62, Prevention of Criticality in Fuel Storage and Handling.
- Code of Federal Regulation 10CFR50.68, Criticality Accident Requirements
- USNRC letter of April 14, 1978, to all Power Reactor Licensees - OT Position for Review and Acceptance of Spent Fuel Storage and Handling Applications
- ANSI-8.17-1984, Criticality Safety Criteria for the Handling, Storage and Transportation of LWR Fuel Outside Reactors.
- L. Kopp, "Guidance On The Regulatory Requirements For Criticality Analysis Of Fuel Storage At Light-Water Reactor Power Plants", USNRC Internal Memorandum, L. Kopp to Timothy Collins, August 19, 1998.

### 4.1.4 Design and Input Data

#### 4.1.4.1 Fuel Assembly Design Specifications

Two different fuel assembly designs were considered in the analyses; the CE 14x14 lattice and the Framatome 14x14 lattice. Table 4.1.4.1 provides the design details for the fuel assemblies.

#### 4.1.4.2 Fuel Storage Cells

The nominal Cask Pit rack storage cell used for the criticality analyses is shown in Figure 4.1.1. The cell is composed of each box face of an 8.58 inch square (inside dimension) stainless steel box that has a wall thickness of 0.075 inches with Boral absorber material mounted on the outside. The fuel assemblies are assumed to be centrally located in each storage cell on a nominal lattice spacing of 10.30 inches. This forms a water flux-trap between Boral absorber panels of adjacent cells of [REDACTED] inches. The Boral absorber has a thickness of [REDACTED] inches and a nominal B-10 areal density of [REDACTED] g/cm<sup>2</sup> ([REDACTED] g/cm<sup>2</sup> minimum). The outer stainless steel sheath is [REDACTED] inches thick.

#### 4.1.5 Methodology

The primary criticality analyses were performed with the three-dimensional MCNP Monte Carlo code [1] developed by the Los Alamos National Laboratory. Benchmark calculations, presented in Appendix A, indicate a bias of  $0.0009 \pm 0.0011$  (95%/95%) [2].

KENO5a [3], a 3-dimensional multi-group Monte Carlo code developed by the Oak Ridge National Laboratory, was used as an independent check and to determine the reactivity-effect of eccentric fuel assembly positioning. In these calculations, the 238-group SCALE cross-section library was used, together with the Norderm integral treatment for U-238 resonance shielding effects. Benchmark calculations (Appendix A) showed a calculational bias of  $0.0030 \pm 0.0012$ .

CASMO4, a two-dimensional deterministic code [4] using transmission probabilities, was used to evaluate the small (differential) reactivity effects of manufacturing tolerances. Validity of the CASMO4 code was established by comparison with results of the MCNP calculations for comparable cases.

In the geometric model used in the calculations, each fuel rod and each fuel assembly were explicitly described. Reflecting boundary conditions effectively defined an infinite radial array of storage cells. In the axial direction, a 30-cm water reflector was used to conservatively describe axial neutron leakage. Each stainless steel box and water within the box was explicitly described in the calculational model.

Monte Carlo calculations inherently include a statistical uncertainty due to the random nature of neutron tracking. To minimize the statistical uncertainty of the calculated reactivities, a minimum of 3 million neutron histories was accumulated in each calculation.

#### 4.1.6 Analysis Results

##### 4.1.6.1 Reference Fuel Assembly

Table 4.1.4.1 summarizes the two fresh fuel assembly designs expected to be stored in the Region 1 Cask Pit rack. Calculations were made to confirm the most reactive fuel assembly of those listed in Table 4.1.4.1 and the results are summarized below.

Fuel Assembly	$k_{inf}$ (CASMO @4.5 % Enrichment)
CE 14x14	0.8925
Framatome 14x14	0.8936

These data confirm that the Framatome 14x14 lattice fuel is more reactive and it is used in all the subsequent calculations.

#### 4.1.6.2 Evaluation of Uncertainties

Calculations were made to determine the uncertainties in reactivity associated with manufacturing tolerances. Tolerances that would increase reactivity were calculated; negative values are expected to be of equal magnitude but opposite in sign over the small tolerance variations. Results of these calculations are shown in Table 4.1.6.1. The reactivity effects were separately evaluated in a sensitivity study for each independent tolerance and the results were combined statistically. Tolerances considered include the following:

##### 4.1.6.2.1 Boron Loading Tolerance

The Boral absorber panels used in the storage cells are nominally [REDACTED] inch thick, [REDACTED] inch wide and 140-inch long, with a nominal B-10 areal density of [REDACTED] g/cm<sup>2</sup> ([REDACTED] g/cm<sup>2</sup> minimum). Differential CASMO-4 calculations indicate that the Boron loading tolerance limits result in incremental reactivity uncertainty shown in Table 4.1.6.1.

##### 4.1.6.2.2 Boral Width Tolerance

The reference storage cell design uses a Boral panel with a width of 7.25±[REDACTED] inches. For the maximum tolerance, the calculated reactivity uncertainty is shown in Table 4.1.6.1 as determined by differential CASMO-4 calculations.

##### 4.1.6.2.3 Tolerances in Water Gap Spacing, Cell Box Inner Dimension and Lattice Pitch

The design storage cell lattice spacing between fuel assemblies (10.3±[REDACTED] inches) results in a water-gap of 1.303±[REDACTED] inches. A decrease in lattice pitch or in water-gap (flux-trap) spacing or an increase in storage box I.D. increases reactivity. The inner stainless steel box dimension, 8.58±[REDACTED] inches, defines the storage box in which the fuel is stored. Tolerances on the three spacing dimensions are inter-related and all three tolerances are independently controlled. For example, the minimum lattice pitch tolerance of [REDACTED] inches can occur only for either (1) a decrease in water-gap thickness of [REDACTED] inches or (2) a decrease of [REDACTED] inches in box I.D. concurrent with a decrease of [REDACTED] inches in water gap

thickness. The bounding conditions for tolerances and the corresponding reactivity effect are listed below:

<b>TOLERANCES</b>			
<b>Cell Box I.D.</b>	<b>Water Gap Thickness</b>	<b>Lattice Pitch</b>	<b>Reactivity Effect, <math>\Delta k</math></b>
			+0.0017
			-0.0012
			+0.0087
			+0.0035
			+0.0095

The last case above represents the largest reactivity effect of the dimensional tolerances. This uncertainty value, 0.0095 is used in Table 4.1.6.1.

#### 4.1.6.2.4 Stainless Steel Thickness Tolerances

The nominal stainless steel thickness for the stainless steel box is 0.075 inches with a tolerance of  $\pm 0.001$  inches (standard ASME sheet metal tolerance). The maximum positive reactivity effect of the expected stainless steel box thickness tolerance is shown in Table 4.1.6.1.

#### 4.1.6.2.5 Fuel Enrichment and Density Tolerances

The nominal U-235 design enrichment for this analysis is  $4.50 \pm 0.05\%$ . Evaluation for the maximum enrichment of 4.55 wt% yielded an incremental reactivity effect for the enrichment tolerance as shown in Table 4.1.6.1. Calculations were also made with the fuel density increased by 5% to the maximum expected value of  $12.0$  g/cm<sup>3</sup> (stack density). Results are also given in Table 4.1.6.1 for the effect of this uncertainty in reactivity .

#### 4.1.6.2.6 Sheathing Thickness

The stainless steel sheath is nominally [REDACTED] inches thick with a standard ASME sheet metal tolerance of [REDACTED] inches. For this tolerance, the calculated reactivity uncertainty is listed in Table 4.1.6.1.

#### 4.1.6.2.7 Fuel Assembly Dimensional Tolerances

CASMO-4 calculations were made for various tolerances in the fuel assembly geometry. From these calculations, the incremental reactivity effects of each independent tolerance were determined. The tolerance effects calculated include the following:

- Tolerance in fuel rod pitch, statistically averaged for the 14x14 fuel rod array;  $k=0.8984$ ;  $\Delta k = 0.0048$
- Tolerance in fuel pellet OD ( $\pm$  [REDACTED] inch);  $k_{inf} = 0.8941$ ;  $\Delta k = 0.0005$
- Tolerance in fuel clad thickness (maximum thickness used)
- Tolerance in Guide Tube OD ( $\pm$  [REDACTED] inches);  $k_{inf} = 0.8935$ ;  $\Delta k = 0.0001$
- Tolerance in Guide Tube Wall Thickness ( $\pm$  [REDACTED] inches);  $k_{inf} = 0.8941$ ;  $\Delta k = 0.0005$

The statistical sum of these reactivity tolerances is shown in Table 4.1.6.1 and is combined with the other tolerances.

#### 4.1.6.3 Eccentric Positioning of Fuel Assembly

The fuel assembly is assumed to be normally located in the center of the storage rack cell. KENO5a calculations were also made with the fuel assemblies assumed to be in the corner of the storage rack cell (four eccentric assembly cluster at closest approach). These calculations indicated that the reactivity is slightly lower for the eccentric position and, therefore, the maximum reactivity occurs for the normal centered position of the fuel, as shown in Table 4.1.6.3.

#### 4.1.6.4 Abnormal and Accident Conditions

##### 4.1.6.4.1 Temperature and Void Effects

The moderator (bulk water) temperature coefficient of reactivity is negative; a minimum moderator temperature of 50 °F (10 °C) was assumed, which assures that the true reactivity will be lower for any value of water temperatures above 50 °F. Temperature effects on reactivity along with the effect of voids on reactivity are shown in Table 4.1.6.2. Introducing voids in the water (to simulate boiling) decreased reactivity, as shown in the table.

##### 4.1.6.4.2 Dropped Fuel Assembly

For a drop on top of the rack, the fuel assembly will come to rest horizontally on top of the rack with a minimum separation distance from the fuel in the rack of more than 12 inches, including the effect of any deformation resulting from seismic or accident conditions. At this separation distance, the effect on reactivity is insignificant. Furthermore, soluble boron in the pool water would substantially reduce the reactivity and assure that the true reactivity is always less than the limiting value for any conceivable dropped fuel accident.

If the dropped fuel assembly were to enter a storage cell vertically and impact the base plate, the base plate could experience a local deformation estimated at 2 inches or less. This magnitude of deformation causes no significant changes to reactivity despite the fact that the dropped assembly would have a small amount of fuel exposed below the Boral absorber. This exposed fuel occurs in a high neutron leakage area and hence, the positive reactivity effect is minimal as shown in Table 4.1.6.3. Conservative calculations, assuming that the 2 inch deformation occurred everywhere on the base plate, showed a very small increase in reactivity (+0.0001  $\Delta k$ ).

#### 4.1.6.4.3 Abnormal Location of a Fuel Assembly

The cask pit rack is designed for storage of fresh fuel assemblies with maximum initial enrichment of  $4.50\pm 0.05$  wt%. Hence, no internal fuel misloading accident is applicable. Due to the small clearance between the Cask Pit rack outer envelope and the Cask Pit liner, a fuel assembly cannot be positioned outside and adjacent to the cask pit rack. Thus, no accident scenario evaluation was performed.

#### 4.1.6.5 Criticality Analyses Results

A summary of the results of the criticality safety analysis for the storage of fresh fuel (initial enrichment of  $4.50\pm 0.05$  wt%) is given in Table 4.1.6.4. The table also contains the calculational biases and the uncertainties. The results indicate that the maximum calculated reactivity in the new CPR will be 0.9061, and therefore storage of fresh fuel with initial enrichment up to  $4.50\pm 0.05$  wt% meets the regulatory requirements.

## 4.2 Unit 2 Cask Pit Rack

### 4.2.1 Objectives and General Description

The objective of the criticality safety analysis presented in this section is to document the requirements for safe storage of spent fuel assemblies in the Region 2 St. Lucie Unit 2 cask pit storage rack. This rack uses Boral as the poison material. The presence of Gadolinium poison in the fuel assembly lattice has been considered but not credited in the present analysis. Postulated accident conditions, where a fresh fuel assembly is inadvertently placed outside the rack or into a cell intended to contain a spent fuel assembly, have also been evaluated. The design criteria are such that no soluble boron is required in the pool water to protect against a mis-loaded assembly accident.

The analysis uses the MCNP4a Monte Carlo code developed by the Los Alamos National Laboratory as the primary code for the calculations. CASMO4 was used for calculation of spent fuel composition as well as to determine reactivity-effects of manufacturing tolerances. As permitted in the USNRC guidelines, parametric evaluations were performed for manufacturing tolerances and the associated reactivity uncertainties were combined statistically. All calculations were made for an explicit modeling of the fuel and storage cell geometries to define the enrichment-burnup combinations for spent fuel assemblies that assure a safe storage of spent fuel assemblies in the Region 2 cask pit rack.

The criticality analysis was performed assuming unborated water as the moderator. Although such a condition is not realistic in the cask pit, which shares borated water with the spent fuel pool, it bounds all possible boron dilution accidents and conforms to the requirements of 10CFR50.68. In practice, the presence of moderator soluble boron at the Technical Specification limit assures a significantly lower reactivity in the cask pit rack.

#### 4.2.1.2 Summary of Results

The design specifications provide that the minimum burnup for the spent fuel (at an initial enrichment of  $4.50 \pm 0.05$  wt%) in the cask pit rack, a Region 2 style configuration, is 36,000 MWD/MTU. A summary of the calculation results for spent fuel with initial enrichment of  $4.50 \pm 0.05$  wt% is given in

Table 4.2.6.4. This table shows that the maximum  $k_{\text{eff}}$  under non-accident conditions is less than 0.916, which easily meets the acceptance criterion of  $\leq 0.95$ . The result for fuel assemblies with enrichments less than  $4.50 \pm 0.05$  wt% is illustrated in Figure 4.2.1, where the maximum reactivities on the curve are all the same.

Evaluation of postulated accident conditions demonstrate that, for the most significant fuel assembly mis-loading accident, the maximum reactivity ( $k_{\text{eff}}$  of 0.9417), including bias and uncertainties, remains below 0.95 and no soluble boron is required to mitigate the effect of this postulated accident in the cask pit rack.

#### 4.2.2 Analysis Criteria And Assumptions

To assure the true reactivity will always be less than the calculated reactivity, the following conservative analysis criteria or assumptions were used.

- Criticality safety analyses were based upon an infinite radial array of cells; i.e., no credit was taken for radial neutron leakage.
- Neutron absorption by minor structural materials was neglected; i.e., spacer grids were conservatively assumed to be replaced by water.
- Moderator is assumed to be un-borated water at a minimum temperature of 10°C (50°F).
- No axial blankets were assumed to be present in the fuel rods. The entire active fuel length was assumed to have the same enrichment.
- Credit for the reduction in reactivity with post-operation cooling time is not incorporated in the analysis.
- A conservative axial burnup distribution is used in evaluating the reactivity bias due to the burnup distribution (sometimes called the “end effect”).
- A 3-dimensional analysis with 10 axial zones is used in evaluating the end effect.
- The most reactive fuel assembly is assumed for the accident evaluation.

- The most reactive fuel assembly amongst the three fuel types to be stored in the Region 2 cask pit rack was used in the criticality safety analyses.
- Fuel assembly is centered in the cell.

#### 4.2.3 Acceptance Criteria

The primary acceptance criteria, in accordance with 10CFR50.68, is that (1) the storage racks remain sub critical, under the postulated accident of the loss of all soluble boron, including bias and uncertainties, and (2) that partial credit for the soluble boron present may be taken to maintain the maximum  $k_{eff}$  less than or equal to 0.95. The maximum  $k_{eff}$  includes calculation bias and uncertainties as well as the reactivity effects of mechanical tolerances, and was evaluated under the postulated accident of the loss of all soluble boron.

Applicable codes, standards, and regulations, or pertinent sections thereof, include the following:

- Code of Federal Regulations, 10CFR50, General Design Criterion 62, Prevention of Criticality in Fuel Storage and Handling.
- Code of Federal Regulation 10CFR50.68, "Criticality Accident Requirements"
- USNRC Standard Review Plan, NUREG-0800, Section 9.1.2, Spent Fuel Storage.
- USNRC letter of April 14, 1978, to all Power Reactor Licensees - OT Position for Review and Acceptance of Spent Fuel Storage and Handling Applications, including modification letter dated January 18, 1979.
- USNRC Regulatory Guide 1.13, Spent Fuel Storage Facility Design Basis, Rev. 2 (proposed), December, 1981.
- ANSI-8.17-1984, Criticality Safety Criteria for the Handling, Storage and Transportation of LWR Fuel Outside Reactors.
- L. Kopp, "Guidance On The Regulatory Requirements For Criticality Analysis Of Fuel Storage At Light-Water Reactor Power Plants", USNRC Internal Memorandum L. Kopp to Timothy Collins, August 19, 1998.

#### 4.2.4 Design And Input Data

##### 4.2.4.1 Bounding Fuel Assembly

Calculations were made, using CASMO4, to evaluate the reactivity of the fuel assemblies currently in use or anticipated for storage in a St. Lucie Unit 2 Cask Pit Rack. Calculations in the cask pit rack, based on the fuel design parameters given in Table 4.2.4.1, show that the CE 16x16 fuel assembly exhibits the highest reactivity at the burnups of interest in this analysis and it was used in all the subsequent calculations.

Burnup, GWD/MTU	CE 14x14	Framatome 14x14	CE 16x16
10	1.0607	1.0594	1.0614
20	0.9916	0.9900	0.9930
30	0.9276	0.9254	0.9304
36	0.8892	0.8865	0.8930
40	0.8649	0.8618	0.8694

##### 4.2.4.2 Storage Racks

A schematic of the cask pit fuel storage cell model, used in this analysis, is shown in Figure 4.2.2.

##### 4.2.4.3 Operating Parameters

The principal core operating parameters, used in this study, are summarized in the table below.

PARAMETER	VALUE
Average Fuel Pellet Temperature	1604 °F
Hot Leg Moderator Temperature	606 °F
Average Core Soluble Boron Concentration	750 ppm

The reactivity effects of the gadolinia present in the fresh fuel assemblies have also been evaluated in this analysis. Based on 20 Gadolinia bearing rods of 8% Gd<sub>2</sub>O<sub>3</sub> in each assembly, CASMO4 calculations were made with and without the gadolinia. These calculations are summarized below:

Burnup, GWD/MTU	k-inf with Gd <sub>2</sub> O <sub>3</sub>	k-inf without Gd <sub>2</sub> O <sub>3</sub>
1	0.9520	1.1295
10	0.9586	1.0614
20	0.9827	0.9930
30	0.9262	0.9304
36	0.8896	0.8930
45	0.8378	0.8406

Results of these calculations show that calculations without gadolinia are slightly more conservative (bounding) than with gadolinia present. Although gadolinia would be expected to harden the neutron spectrum (producing more plutonium), the poisoning effect of the residual gadolinia compensates for the higher plutonium production.

#### 4.2.5 Methodology

The primary criticality analyses were performed with the three-dimensional MCNP Monte Carlo code [1] developed by the Los Alamos National Laboratory. Benchmark calculations, presented in Appendix A, indicate a bias of  $0.0009 \pm 0.0011$  (95%/95%) [2].

CASMO4, a two-dimensional deterministic code [3] using transmission probabilities, was used to evaluate the small (differential) reactivity effects of manufacturing tolerances. Validity of the CASMO4 code was established by comparison with results of the MCNP calculations for comparable cases.

In the geometric model used in the calculations, each fuel rod and each fuel assembly were explicitly described. Reflecting boundary conditions effectively defined an infinite radial array of storage cells. In the axial direction, a 30-cm water reflector was used to conservatively describe axial neutron leakage. Each stainless steel box and water within the box was explicitly described in the calculational model.

Monte Carlo (MCNP) calculations inherently include a statistical uncertainty due to the random nature of neutron tracking. To minimize the statistical uncertainty of the calculated reactivities, a minimum of 3 million neutron histories was accumulated in each calculation. MCNP cannot perform depletion calculations, and depletion calculations were performed with CASMO4. Explicit description of the fission product nuclide concentrations in the spent fuel was determined from the CASMO4 calculations and used in the MCNP calculations. To compensate for those few fission product nuclides that cannot be described in MCNP, an equivalent amount of boron-10 in the fuel was determined which produced very nearly the same reactivity in MCNP as the CASMO4 result. This methodology explicitly incorporates approximately 40 of the most important fission products, accounting for all but about 1% in  $k$ . The remaining  $\sim 1$  % in  $k$  is included by the equivalent B-10 concentration in the fuel.

## 4.2.6 Evaluation of Uncertainties

### 4.2.6.1 Uncertainty in Manufacturing Tolerances

CASMO4 calculations were made to determine the uncertainties in reactivity associated with tolerances in the rack's dimensions, fuel density and fuel enrichments. The reactivity effects of each independent tolerance were combined statistically. The rack dimensions and tolerances are shown in Figure 4.2.2.

For estimating the reactivity uncertainties associated with tolerances in fuel enrichment and density, tolerances of  $\pm 0.05\%$  in enrichment and  $\pm 1\%$  in  $\text{UO}_2$  density were assumed. The reactivity associated with the fuel density tolerance is listed in Table 4.2.6.1. The reactivity effects of the tolerances in the rack dimensions are also listed in Table 4.2.6.1. The reactivity effects for the tolerance in fuel enrichment are listed in Table 4.2.6.2.

### 4.2.6.2 Uncertainty in Depletion Calculations

The uncertainty in depletion calculations is part of the methodology uncertainty and was taken as 5% of the reactivity decrement from beginning-of-life to the burnup of concern for the spent fuel [5]. This methodology uncertainty is included in the calculations of the final  $k_{\text{eff}}$  in Table 4.2.6.4.

### 4.2.6.3 Eccentric Location of Fuel Assemblies

The fuel assemblies are nominally stored in the center of the storage cells. Eccentric positioning of fuel assemblies in the cells normally results in a negligible effect or a reduction in reactivity for poisoned racks. Calculations have been made confirming negative reactivity effect of the eccentric positioning of four fuel assemblies at the position of closest approach. These calculations gave a small reduction in  $k_{\text{eff}}$  (-0.0013) confirming that eccentric positioning of fuel has a negligible effect.

#### 4.2.6.4 Temperature and Void Effects

Temperature effects were also evaluated, using CASMO4, in the temperature range from 10 °C to 120 °C and the results are listed in Table 4.2.6.3. These results show that the temperature coefficient of reactivity is negative. The void coefficient of reactivity (boiling conditions) was also found to be negative for the St. Lucie Unit 2 cask pit rack. The reference temperature is 20 °C. The reactivity effects of pool water temperatures below 20 °C to 10 °C are calculated using CASMO (Table 4.2.6.3). These data were interpolated for water temperature to 10 °C (50 °F) and the resulting reactivity increment is added to the calculated  $k_{eff}$  at 20 °C.

#### 4.2.6.5 Reactivity Effect of the Axial Burnup Distribution

Initially, fuel loaded into the reactor will burn with a slightly skewed cosine power distribution. As burnup progresses, the burnup distribution will tend to flatten, becoming more highly burned in the central regions than in the upper and lower ends. The more reactive fuel near the ends of the fuel assembly (less than average burnup) has reactivities slightly above that of the assembly average. Axial burnup penalty calculations based upon a conservative burnup distribution [4], gave a positive reactivity effect of the axial burnup distribution of  $0.0071\Delta k$  for spent fuel of 36 MWD/KgU. These calculations are based on 10 zone axial calculations, using specific (CASMO) concentrations of actinides and fission products in each zone. Calculations for 4% fuel at 30 MWD/KgU gave a correction of  $0.0007\Delta k$  and the correction becomes negative (neglected) below a burnup of  $\sim 29$  MWD/KgU.

#### 4.2.7 Accident Conditions And Soluble Boron Requirements

The accident scenarios considered in this analysis are summarized below:

- A dropped fuel assembly coming to rest horizontally across the top of the storage cell.
- A dropped fuel assembly, which enters the storage cell vertically and impacts the base plate.
- An extraneous assembly positioned outside and immediately adjacent to the storage rack

- The effects of a fresh fuel assembly mis-loaded into a cell intended to store a spent fuel assembly.

Among these, the most serious postulated accident condition is the misplacement of a fresh fuel assembly into a location intended for storage of a spent fuel assembly. Misplacement of a fuel assembly outside the periphery of a storage module is bounded by the more serious accident of a mis-placed assembly internal to the rack. This is due to the fact that the peripheral region between the rack and the wall is high neutron leakage area and Boral panels are present on the periphery of the cask pit rack. A dropped assembly lying on top of the rack would have a negligible reactivity effect because of the separation distance. If the dropped fuel assembly were to enter a storage cell vertically and impact the base plate, the base plate could experience a local deformation estimated at 2 inches or less. This magnitude of deformation causes no significant changes to reactivity despite the fact that the dropped assembly would have a small amount of fuel exposed below the Boral absorber. This exposed fuel occurs in a high neutron leakage area and hence, the positive reactivity effect is minimal as shown in Table 4.2.6.5. Conservative calculations, assuming that the 2 inch deformation occurred everywhere on the base plate, showed a negligible increase in reactivity (+0.0003  $\Delta k$ ).

The analysis shows that, for the most serious postulated accident condition with the internal misplacement of a fresh fuel assembly, the maximum reactivity (0.9417) remains well below 0.95 (including bias and uncertainties) and no soluble boron is required.

#### 4.2.8 Criticality Analyses Results And Conclusions

Storage of spent fuel assemblies in the Unit 2 Region 2 cask pit storage rack has been evaluated in this analysis. The results are summarized in Tables 4.2.6.4 for fuel of 4.5% initial enrichment. Minimum burnup requirements for fuel of lower enrichments are shown in Figure 4.2.1 and listed in Table 4.2.8.1. These burnup requirements give reactivity values equivalent to those for the design basis case of 4.5% enriched fuel burned to 36 MWD/kgU. All points on the curve in Figure 4.2.1 have the same maximum reactivity and were evaluated in the same way as the design basis case, including appropriate bias and uncertainties. Temperature correction and MCNP4a bias were conservatively assumed to be independent of the initial enrichment. A summary of the conclusions are given below:

- The criticality margin of spent fuel assemblies ( $4.50 \pm 0.05$  wt% initial enrichment) stored in the cask pit rack of St. Lucie Unit 2 is acceptable within NRC guidelines and regulations. Storage of fuel assemblies of lower enrichment, conforming to the minimum burnup-enrichment combination shown in Figure 4.2.1, is permitted.
- Accident analysis show that soluble boron is not required to compensate for the reactivity effects of the most serious postulated fuel misplacement in the cask pit rack and the  $k_{eff}$  remains below 0.95, including all uncertainties and biases.

### 4.3 References

#### 4.3.1 References for Section 4.1

1. J.F. Briesmeister, Ed., "MCNP - A General Monte Carlo N-Particle Transport Code, Version 4A", Los Alamos National Laboratory, LA-12625-M (1993).
2. M.G. Natrella, Experimental Statistics, National Bureau of Standards, Handbook 91, August 1963.
3. R.M. Westfall, et. al., "NITAWL-S: Scale System Module for Performing Resonance Shielding and Working Library Production" in SCALE: A Modular Code System for Performing Standardized Computer Analyses for Licensing Evaluation., NUREG/CR-0200, 1979.  
  
L.M. Petrie and N.F. Landers, "KENO Va. An improved Monte Carlo Criticality Program with Subgrouping" in SCALE: A Modular Code System for Performing Standardized Computer Analyses for Licensing Evaluation., NUREG/V-0200, 1979.
4. A. Ahlin, M. Edenius, H. Haggblom, "CASMO- A Fuel Assembly Burnup Program," AE-RF-76-4158, Studsvik report (proprietary).  
  
A. Ahlin and M. Edenius, "CASMO- A Fast Transport Theory Depletion Code for LWR Analysis," ANS Transactions, Vol. 26, p. 604, 1977.  
  
D. Knott, "CASMO4 Benchmark Against Critical Experiments", Studsvik Report SOA-94/13 (Proprietary).  
  
M. Edenius et al., "CASMO4, A Fuel Burnup Program, Users Manual" Studsvik Report SOA/95/1.

#### 4.3.2 References For Section 4.2

1. J.F. Briesmeister, Ed., "MCNP - A General Monte Carlo N-Particle Transport Code, Version 4A", Los Alamos National Laboratory, LA-12625-M (1993).
2. M. G. Natrella, "Experimental Statistics", National Bureau of Standards, Handbook 91, August 1961.
3. A. Ahlin, M. Edenius, H. Haggblom, "CASMO- A Fuel Assembly Burnup Program," AE-RF-76-4158, Studsvik report (proprietary).  
  
A. Ahlin and M. Edenius, "CASMO- A Fast Transport Theory Depletion Code for LWR Analysis," ANS Transactions, Vol. 26, p. 604, 1977.  
  
D. Knott, "CASMO4 Benchmark Against Critical Experiments", Studsvik Report SOA-94/13 (Proprietary).  
  
M. Edenius et al., "CASMO4, A Fuel Burnup Program, Users Manual" Studsvik Report SOA/95/1.
4. S. E. Turner, "Uncertainty Analysis – Burnup Distributions," Presented at the 1988 DOE/SANDIA Technical Meeting on Fuel Burnup Credit.
5. L. Kopp, "Guidance On The Regulatory Requirements For Criticality Analysis Of Fuel Storage At Light-Water Reactor Power Plants", USNRC Internal Memorandum, L. Kopp to Timothy Collins, August 19, 1998.

Table 4.1.4.1 Design Basis Fuel Assembly Specifications

PARAMETER	CE 14X14	Framatome 14X14
Rod Array Size	14x14	14x14
Rod Pitch (inches)	0.580±0.015	0.580±0.015
Active Fuel Length (inches)	136.7±0.50	136.7±0.50
Stack Density (gm/cm <sup>3</sup> )	10.05 ± 5%	10.30 ± 5%
Total Number of Fueled Rods	176	176
Fuel Rod Outer Diameter (inches)	0.440±0.0055	0.440±0.002
Cladding Thickness (inches)	0.026 - 0.028 ±0.002	0.028 - 0.031 ±0.003
Cladding Material	Zr-4	Zr-4
Pellet Diameter (inches)	0.3805±0.001	0.3770±0.001
Number of Guide/Instrument Tubes	5	5
Guide/Instrument Outer Diameter (inches)	1.115±0.003	1.115±0.003
Guide/Instrument Wall Thickness (inches)	0.040±0.004	0.040±0.004
Material	Zr-4	Zr-4

Table 4.1.6.1 Reactivity Effects of Manufacturing Tolerances in St. Lucie Unit 1 Nuclear Plant Cask Pit Storage Rack

PARAMETER	Value with Tolerance	$k_{inf}$ *	$\Delta k$
Reference $k_{inf}$	-	0.8936	-
Variation in Boral Panel B-10 Loading	0.028 g/cm <sup>2</sup>	0.8958	±0.0022
Boral Panel Width	7.1875 inches	0.8945	±0.0009
Maximum Tolerance Effect of Box I.D., Water-gap Thickness, and Lattice Pitch (See Section 4.1.6.2.3)	-	0.9031	±0.0095
SS Box Wall Thickness	0.082 inches	0.8945	±0.0009
SS Sheathing Thickness	0.0238 inches	0.8934	±0.0002
Uncertainty in Maximum Fuel Enrichment	4.55 wt%	0.8954	±0.0018
Uncertainty in Fuel Density	10.815 gm/cm <sup>3</sup>	0.8991	±0.0055
Fuel Assembly Dimensional Tolerance (Combined)	-	(See Section 4.1.6.2.7)	±0.0048
Statistical Sum	-	-	±0.0124

\* All of the  $k_{inf}$  presented for tolerance effects are single variable effects.

Table 4.1.6.2. Reactivity Effects of Temperature and Void for CE 14x14 Fuel in St. Lucie Unit 1 Cask Pit Rack

T=10°C ( 50°F)		T = 20 °C		T = 60 °C		T = 120 °C		T = 120 °C + VOID	
$k_{inf}$	$\Delta k^*$	$k_{inf}$	$\Delta k$	$k_{inf}$	$\Delta k^*$	$k_{inf}$	$\Delta k^*$	$k_{inf}$	$\Delta k$
0.8945	+0.0009	0.8936	0	0.8872	-0.0064	0.8723	-0.0213	0.8448	-0.0488

\* 20 °C is the reference temperature for calculations.

Table 4.1.6.3 Reactivity Effects of Abnormal And Accident Conditions (Unit 1 CPR)

Accident/Abnormal Conditions	Reactivity Effect
Temperature increase (above 50°F)	Negative
Void (boiling)	Negative (Table 6.2)
Assembly dropped on top of rack	Negligible (<0.0001 Δk)
Deep Drop of Fuel Assembly Through a Rack	Positive (0.0001 Δk)
Lateral rack module movement	NA
Mis-positioning of a fuel assembly within the Cask Pit Rack	NA
Eccentric Positioning of Fuel Assemblies	Negative

Table 4.1.6.4. Summary of the Criticality Safety Analyses for the Storage of Fresh Fuel Assemblies in St. Lucie Unit 1 Cask Pit Rack.

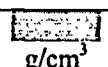
DESIGN BASIS ENRICHMENT	4.50±0.05 wt%
Reference $k_{eff}$ (MCNP4a calculation)	0.8918
Calculational Bias, $\Delta k$	0.0009
Temperature (50°F)	0.0009
<b><u>Uncertainties</u></b>	
MCNP Bias Statistics (one sided tolerance factor [2] x standard deviation)	±0.0011
MCNP Statistics (1.7 x $\sigma$ )	±0.0009
Manufacturing Tolerances	±0.0124
Eccentric Position	Negative
Statistical Combination of Uncertainties	±0.0125
Total	0.8936±0.0125
Maximum Reactivity ( $k_{inf}$ )	0.9061

Table 4.2.4.1 Design Basis Fuel Assembly Specifications (Unit 2 CPR)

PARAMETER	VALUE		
	CE 14X14	Framatome 14X14	CE 16X16
Initial Enrichment, wt% U <sup>235</sup>	4.50	4.50	4.50
Rod Array Size	14x14	14x14	16x16
Rod Pitch (inches)	0.580	0.580	0.506
Active Fuel Length (inches)	136.7	136.7	136.7
Uranium Stack Density*	96% of theoretical	96% of theoretical	96% of theoretical
Total Number of Fueled Rods	176	176	236
Fuel Rod Outer Diameter (inches)	0.440	0.440	0.382
Cladding Thickness (inches)	0.028	0.031	0.025
Cladding Material	Zr-4	Zr-4	Zr-4
Pellet Diameter (inches)	0.3805	0.3770	0.3255
Number of Guide/Instrument Tubes	5	5	5
Guide/Instrument Tube Outer Diameter (inches)	1.115	1.115	0.980
Guide/Instrument Tube Thickness (inches)	0.040	0.040	0.040
Material	Zr-4	Zr-4	Zr-4

\* Fuel pellet dishing and chamfering not included.

Table 4.2.6.1 Reactivity Effects of Manufacturing Tolerances for CE 16x16 Fuel in St. Lucie Unit 2 Nuclear Plant Cask Pit Storage Rack.

Parameter, MWD/KgU	Value w/Tolerance	Burnup, 0 MWD/KgU		Burnup, 10 MWD/KgU		Burnup, 20 MWD/KgU		Burnup, 30 MWD/KgU		Burnup, 36 MWD/KgU	
		$k_{inf}$	$\Delta k$	$k_{inf}$	$\Delta k$	$k_{inf}$	$\Delta k$	$k_{inf}$	$\Delta k$	$k_{inf}$	$\Delta k$
Reference	-	1.1438	—	1.0614	—	0.9930	—	0.9304	—	0.8930	—
Minimum B-10	 g/sq- cm	1.1478	0.004	1.0652	0.0038	0.9965	0.0035	0.9337	0.0033	0.8962	0.0032
Boral Width	 cm	1.1448	0.001	1.0624	0.001	0.9939	0.0009	0.9312	0.0008	0.8938	0.0008
Min. Box ID	 in.	1.1465	0.0027	1.0639	0.0025	0.9952	.0022	0.9323	0.0019	0.8948	0.0018
SS Thickness	 in.	1.1448	0.001	1.0624	0.001	0.9938	0.0008	0.9311	0.0007	0.8937	0.0007
Guide Tube	 in.	1.1442	0.0004	—	—	—	—	—	—	—	—
Fuel Density	 g/cm <sup>3</sup>	1.1446	0.0008	1.0621	0.0007	0.9938	0.0008	0.9314	0.001	0.8943	0.0013
Pellet OD	 in.	1.1442	0.0004	—	—	—	—	—	—	—	—
Statistical Sum*		0.0051		0.0048		0.0044		0.0041		0.0041	

\* The statistical sum is the root-mean-square of the individual tolerance effects.

Table 4.2.6.2 Reactivity Effects of Fuel Enrichment Tolerance in St. Lucie Unit 2 Cask Pit Storage Rack

Burnup, MWD/KgU	B20	B20e	B25	B25e	B30	B30e	B35	B35e	B40	B40e	B45	B45e
1	0.92623	0.93314	0.98730	0.99256	1.03459	1.03874	1.07243	1.07581	1.10345	1.10626	1.12949	—
$\Delta k$	0.0069		0.0053		0.0042		0.0034		0.0028		—	
10	0.85689	0.86302	0.91345	0.91855	0.96044	0.96468	0.99975	1.00332	1.03298	1.03603	1.06144	1.06406
$\Delta k$	0.0061		0.0051		0.0042		0.0036		0.0031		0.0026	
20	0.78819	0.79353	0.83979	0.84469	0.88623	0.89056	0.92689	0.93064	0.96220	0.96547	0.99299	0.99585
$\Delta k$	0.0053		0.0049		0.0043		0.0038		0.0033		0.0029	
30	0.73391	0.73818	0.77750	0.78189	0.82065	0.82483	0.86102	0.86486	0.89766	0.90110	0.93036	0.93343
$\Delta k$	0.0043		0.0044		0.0042		0.0038		0.0034		0.0031	
36	0.70764	0.71113	0.74461	0.74850	0.78403	0.78798	0.82292	0.82670	0.85949	0.86299	0.89301	0.89617
$\Delta k$	0.0035		0.0039		0.0040		0.0038		0.0035		0.0032	

Table 4.2.6.3 Reactivity Effects of Temperature and Void in St. Lucie Unit 2 Cask Pit Storage Rack.

BURNUP, GWD/MTU	T = 20 °C	T = 10 °C	T=40°C	T = 80 °C	T=100°C	T = 120 °C	T = 120 °C + VOID
	$k_{inf}$	$k_{inf}$	$k_{inf}$	$k_{inf}$	$k_{inf}$	$k_{inf}$	$k_{inf}$
0	1.1438	1.1451	1.1404	1.1320	1.1269	1.1213	1.0979
10	1.0614	1.0627	1.0582	1.0501	1.0453	1.0400	1.0172
20	0.9930	0.9941	0.9900	0.9824	0.9780	0.9731	0.9506
30	0.9304	0.9313	0.9277	0.9209	0.9170	0.9126	0.8909
36	0.8930	0.8939	0.8906	0.8844	0.8807	0.8767	0.8555

Table 4.2.6.4 Summary of the Criticality Safety Analyses for the Storage of Spent Fuel Assemblies in the St. Lucie Unit 2 Cask Pit Rack.

Required Burnup of the Spent Fuel Assemblies	36 GWD/MTU
Initial Enrichment of Spent Fuel Assembly	4.5
MCNP calculated $k_{eff}^3$	0.8929 (0.9192 <sup>(4)</sup> )
MCNP4a Bias	0.0009
Temperature Correction to 10 °C (50 °F)	0.0009
Axial Burnup Distribution Penalty	0.0071
<b>Uncertainties</b>	
MCNP4a Bias Uncertainty	± 0.0011
MCNP4a Statistics (95/95) Uncertainty <sup>(1)</sup>	± 0.0007
Manufacturing Tolerance Uncertainty	± 0.0052 <sup>(2)</sup>
Depletion Uncertainty (5% of 1.1438-0.8930)	± 0.0125
Fuel Eccentric Positioning Uncertainty	Negative
Statistical Combination of Uncertainties	± 0.0136
Nominal k-eff	0.9014±0.0136
Maximum $k_{eff}$	0.9154 <sup>(3)</sup> (0.9417 <sup>(4)</sup> )
Regulatory Limiting $k_{eff}$	0.9500

- (1)  $1.7 * \sigma$  ( $\sigma = 0.0004$  or less)  
(2) Statistical combination of tolerances from Table 4.2.6.1 and 4.2.6.2  
(3) Maximum  $k_{eff} = 0.9155$  by CASMO calculations.  
(4) For the postulated fuel assembly mis-loaded accident.

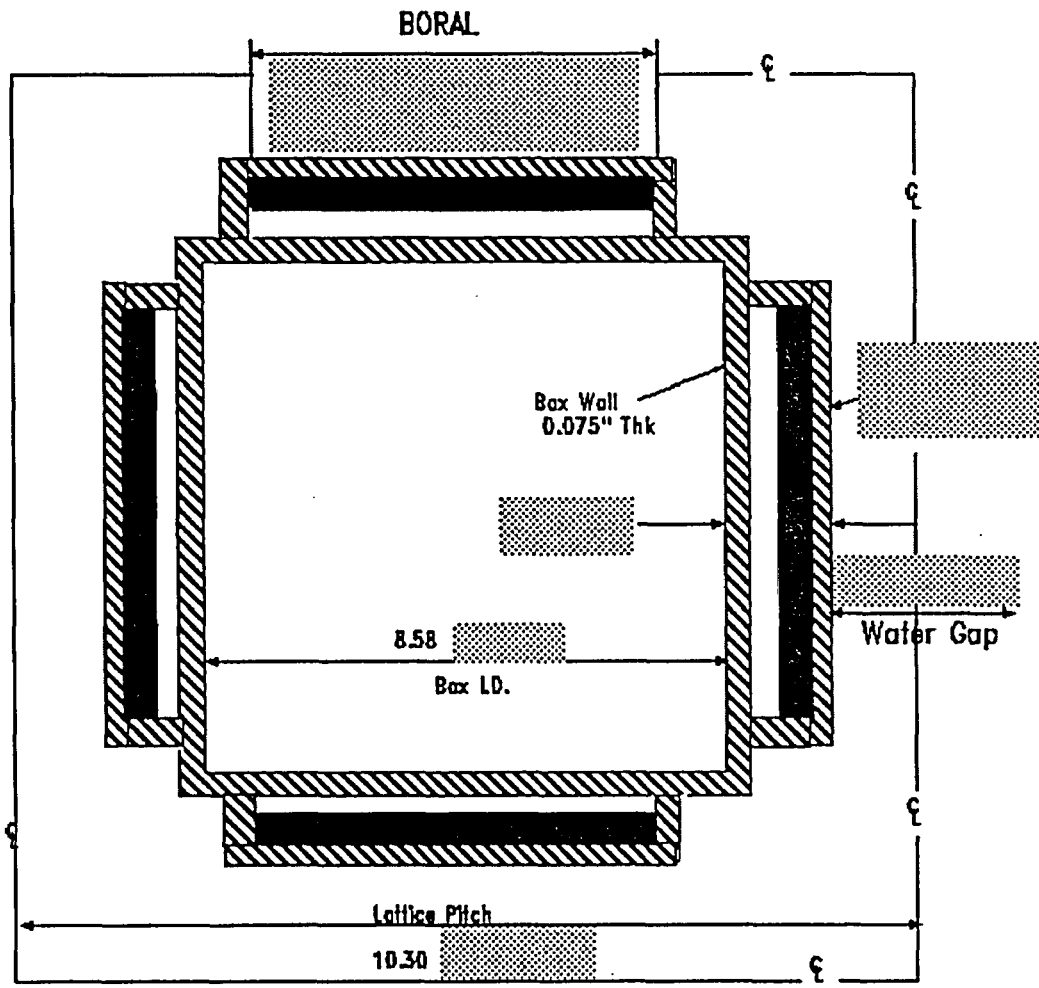
Table 4.2.6.5 Reactivity Effects of Abnormal and Accident Conditions in St. Lucie Unit 2 Cask Pit Rack.

<u>ACCIDENT/ABNORMAL CONDITIONS</u>	<u>REACTIVITY EFFECT</u>
Temperature increase (See Table 6.3)	Negative
Void (Boiling) (See Table 6.3)	Negative
Misplacement of a fresh fuel assembly	Positive: for the most serious misplacement accident the maximum reactivity remains below 0.95
Deep Drop of Fuel Assembly Through a Rack	Positive (0.0003 $\Delta k$ )
Eccentric Positioning of Fuel Assemblies	Negative

Table 4.2.8.1 Enrichment – Minimum Burnup Correlation (Ref. Figure 4.2.1). (Unit 2 CPR)

<b>Initial Enrichment wt% U235</b>	<b>Minimum Required Burnup, MWD/KgU</b>
2.0	5.80 (5.99)
2.5	11.80 (11.81)
3.0	17.61 (17.71)
3.5	23.67 (23.72)
4.0	29.47 (29.81)
4.5	36.00 (36.00)

Note: Values in the parenthesis are derived from the polynomial fit in Figure 1.



(Not to Scale)

Figure 4.1.1; Unit 1 CPR Storage Cell Cross Section

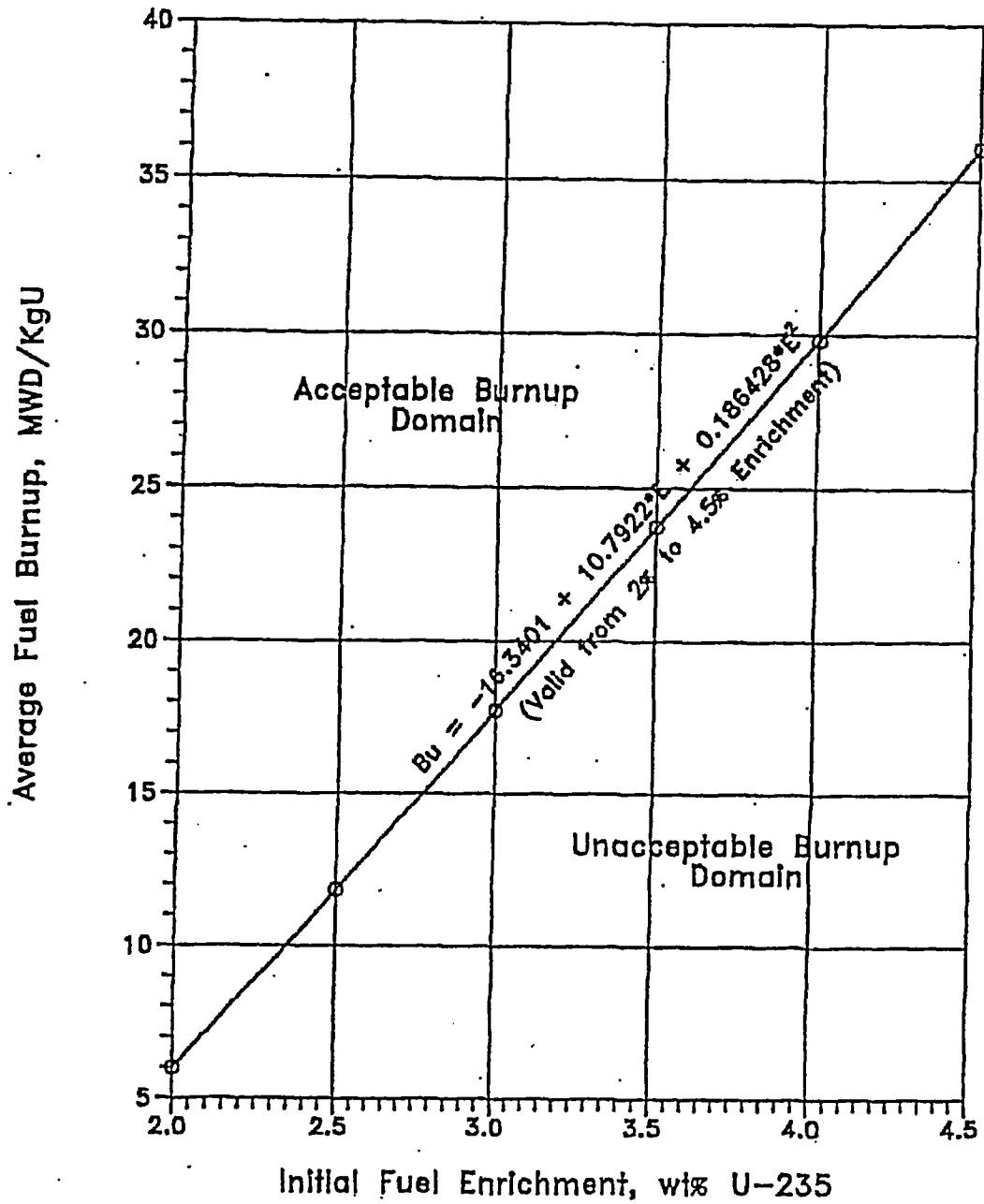


Figure 4.21; Limiting Fuel Burnup-Enrichment Combinations

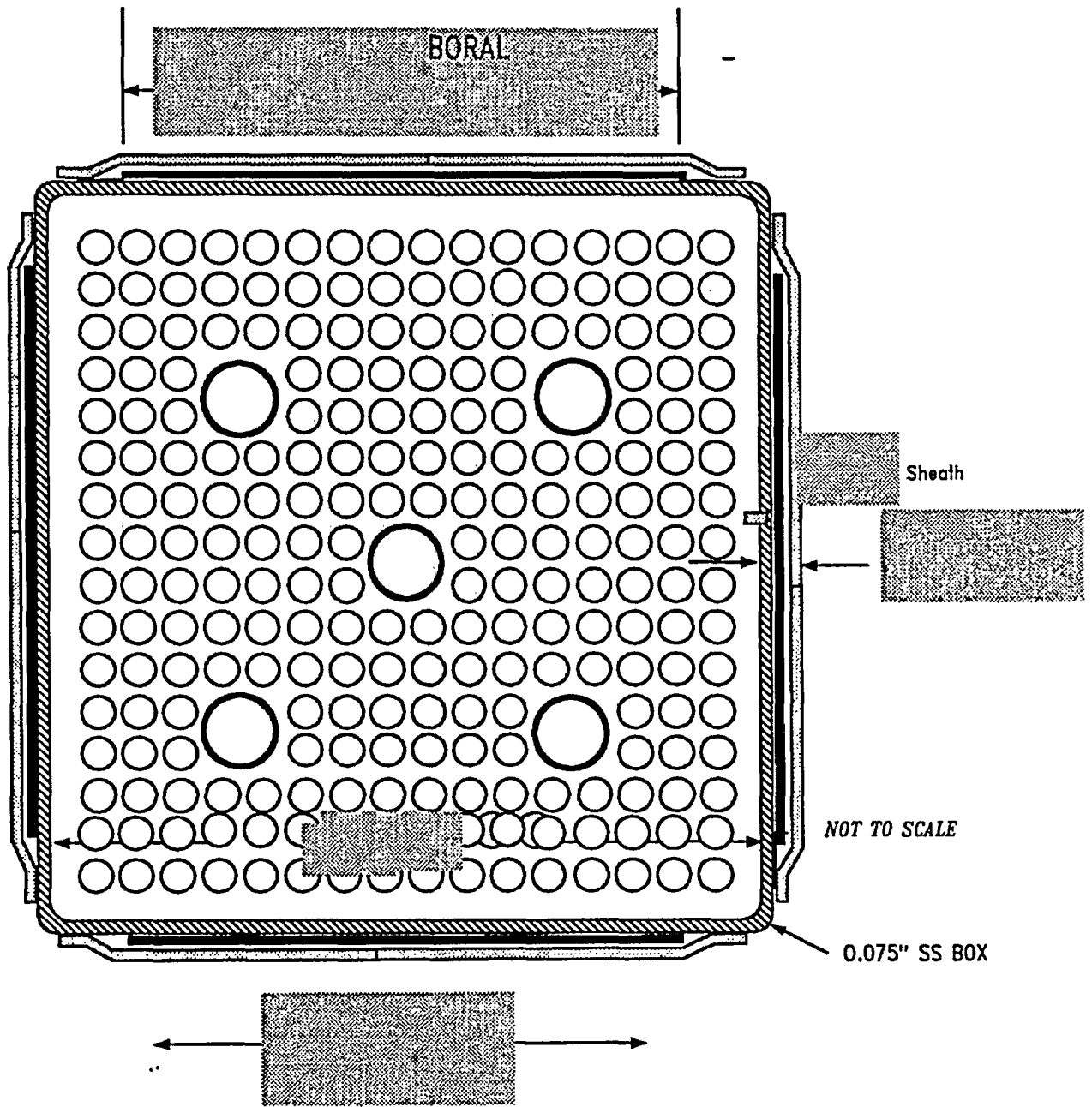


Figure 4.2.2 Unit 2 CPR STORAGE CELL Cross Section

**APPENDIX A: BENCHMARK CALCULATIONS**  
(Total of 26 Pages Including This Page)

Note: This appendix was taken from a different report. Hence, the next page is labeled  
"Appendix 4A, Page 1".

## APPENDIX 4A: BENCHMARK CALCULATIONS

### 4A.1 INTRODUCTION AND SUMMARY

Benchmark calculations have been made on selected critical experiments, chosen, in so far as possible, to bound the range of variables in the rack designs. Two independent methods of analysis were used, differing in cross section libraries and in the treatment of the cross sections. MCNP4a [4A.1] is a continuous energy Monte Carlo code and KENO5a [4A.2] uses group-dependent cross sections. For the KENO5a analyses reported here, the 238-group library was chosen, processed through the NITAWL-II [4A.2] program to create a working library and to account for resonance self-shielding in uranium-238 (Nordheim integral treatment). The 238 group library was chosen to avoid or minimize the errors<sup>†</sup> (trends) that have been reported (e.g., [4A.3 through 4A.5]) for calculations with collapsed cross section sets.

In rack designs, the three most significant parameters affecting criticality are (1) the fuel enrichment, (2) the <sup>10</sup>B loading in the neutron absorber, and (3) the lattice spacing (or water-gap thickness if a flux-trap design is used). Other parameters, within the normal range of rack and fuel designs, have a smaller effect, but are also included in the analyses.

Table 4A.1 summarizes results of the benchmark calculations for all cases selected and analyzed, as referenced in the table. The effect of the major variables are discussed in subsequent sections below. It is important to note that there is obviously considerable overlap in parameters since it is not possible to vary a single parameter and maintain criticality; some other parameter or parameters must be concurrently varied to maintain criticality.

One possible way of representing the data is through a spectrum index that incorporates all of the variations in parameters. KENO5a computes and prints the "energy of the average lethargy causing fission" (EALF). In MCNP4a, by utilizing the tally option with the identical 238-group energy structure as in KENO5a, the number of fissions in each group may be collected and the EALF determined (post-processing).

---

<sup>†</sup> Small but observable trends (errors) have been reported for calculations with the 27-group and 44-group collapsed libraries. These errors are probably due to the use of a single collapsing spectrum when the spectrum should be different for the various cases analyzed, as evidenced by the spectrum indices.

Figures 4A.1 and 4A.2 show the calculated  $k_{eff}$  for the benchmark critical experiments as a function of the EALF for MCNP4a and KENO5a, respectively (UO<sub>2</sub> fuel only). The scatter in the data (even for comparatively minor variation in critical parameters) represents experimental error<sup>†</sup> in performing the critical experiments within each laboratory, as well as between the various testing laboratories. The B&W critical experiments show a larger experimental error than the PNL criticals. This would be expected since the B&W criticals encompass a greater range of critical parameters than the PNL criticals.

Linear regression analysis of the data in Figures 4A.1 and 4A.2 show that there are no trends, as evidenced by very low values of the correlation coefficient (0.13 for MCNP4a and 0.21 for KENO5a). The total bias (systematic error, or mean of the deviation from a  $k_{eff}$  of exactly 1.000) for the two methods of analysis are shown in the table below.

Calculational Bias of MCNP4a and KENO5a	
MCNP4a	0.0009 ± 0.0011
KENO5a	0.0030 ± 0.0012

The bias and standard error of the bias were derived directly from the calculated  $k_{eff}$  values in Table 4A.1 using the following equations<sup>††</sup>, with the standard error multiplied by the one-sided K-factor for 95% probability at the 95% confidence level from NBS Handbook 91 [4A.18] (for the number of cases analyzed, the K-factor is ~2.05 or slightly more than 2).

$$\bar{k} = \frac{1}{n} \sum_i^n k_i \quad (4A.1)$$

---

<sup>†</sup> A classical example of experimental error is the corrected enrichment in the PNL experiments, first as an addendum to the initial report and, secondly, by revised values in subsequent reports for the same fuel rods.

<sup>††</sup> These equations may be found in any standard text on statistics, for example, reference [4A.6] (or the MCNP4a manual) and is the same methodology used in MCNP4a and in KENO5a.

$$\sigma_k^2 = \frac{\sum_{i=1}^n k_i^2 - (\sum_{i=1}^n k_i)^2 / n}{n(n-1)} \quad (4A.2)$$

$$Bias = (1 - \bar{k}) \pm K \sigma_{\bar{k}} \quad (4A.3)$$

where  $k_i$  are the calculated reactivities of  $n$  critical experiments;  $\sigma_k$  is the unbiased estimator of the standard deviation of the mean (also called the standard error of the bias (mean));  $K$  is the one-sided multiplier for 95% probability at the 95% confidence level (NBS Handbook 91 [4A.18]).

Formula 4.A.3 is based on the methodology of the National Bureau of Standards (now NIST) and is used to calculate the values presented on page 4.A-2. The first portion of the equation,  $(1 - \bar{k})$ , is the actual bias which is added to the MCNP4a and KENO5a results. The second term,  $K \sigma_{\bar{k}}$ , is the uncertainty or standard error associated with the bias. The  $K$  values used were obtained from the National Bureau of Standards Handbook 91 and are for one-sided statistical tolerance limits for 95% probability at the 95% confidence level. The actual  $K$  values for the 56 critical experiments evaluated with MCNP4a and the 53 critical experiments evaluated with KENO5a are 2.04 and 2.05, respectively.

The bias values are used to evaluate the maximum  $k_{eff}$  values for the rack designs. KENO5a has a slightly larger systematic error than MCNP4a, but both result in greater precision than published data [4A.3 through 4A.5] would indicate for collapsed cross section sets in KENO5a (SCALE) calculations.

#### 4A.2 Effect of Enrichment

The benchmark critical experiments include those with enrichments ranging from 2.46 w/o to 5.74 w/o and therefore span the enrichment range for rack designs. Figures 4A.3 and 4A.4 show the calculated  $k_{eff}$  values (Table 4A.1) as a function of the fuel enrichment reported for the critical experiments. Linear regression analyses for these data confirms that there are no trends, as indicated by low values of the correlation coefficients (0.03 for MCNP4a and 0.38 for KENO5a). Thus, there are no corrections to the bias for the various enrichments.

As further confirmation of the absence of any trends with enrichment, a typical configuration was calculated with both MCNP4a and KENO5a for various enrichments. The cross-comparison of calculations with codes of comparable sophistication is suggested in Reg. Guide 3.41. Results of this comparison, shown in Table 4A.2 and Figure 4A.5, confirm no significant difference in the calculated values of  $k_{eff}$  for the two independent codes as evidenced by the 45° slope of the curve. Since it is very unlikely that two independent methods of analysis would be subject to the same error, this comparison is considered confirmation of the absence of an enrichment effect (trend) in the bias.

#### 4A.3 Effect of $^{10}\text{B}$ Loading

Several laboratories have performed critical experiments with a variety of thin absorber panels similar to the Boral panels in the rack designs. Of these critical experiments, those performed by B&W are the most representative of the rack designs. PNL has also made some measurements with absorber plates, but, with one exception (a flux-trap experiment), the reactivity worth of the absorbers in the PNL tests is very low and any significant errors that might exist in the treatment of strong thin absorbers could not be revealed.

Table 4A.3 lists the subset of experiments using thin neutron absorbers (from Table 4A.1) and shows the reactivity worth ( $\Delta k$ ) of the absorber.<sup>†</sup>

No trends with reactivity worth of the absorber are evident, although based on the calculations shown in Table 4A.3, some of the B&W critical experiments seem to have unusually large experimental errors. B&W made an effort to report some of their experimental errors. Other laboratories did not evaluate their experimental errors.

To further confirm the absence of a significant trend with  $^{10}\text{B}$  concentration in the absorber, a cross-comparison was made with MCNP4a and KENO5a (as suggested in Reg. Guide 3.41). Results are shown in Figure 4A.6 and Table 4A.4 for a typical geometry. These data substantiate the absence of any error (trend) in either of the two codes for the conditions analyzed (data points fall on a 45° line, within an expected 95% probability limit).

---

<sup>†</sup> The reactivity worth of the absorber panels was determined by repeating the calculation with the absorber analytically removed and calculating the incremental ( $\Delta k$ ) change in reactivity due to the absorber.

#### 4A.4 Miscellaneous and Minor Parameters

##### 4A.4.1 Reflector Material and Spacings

PNL has performed a number of critical experiments with thick steel and lead reflectors.<sup>†</sup> Analysis of these critical experiments are listed in Table 4A.5 (subset of data in Table 4A.1). There appears to be a small tendency toward overprediction of  $k_{eff}$  at the lower spacing, although there are an insufficient number of data points in each series to allow a quantitative determination of any trends. The tendency toward overprediction at close spacing means that the rack calculations may be slightly more conservative than otherwise.

##### 4A.4.2 Fuel Pellet Diameter and Lattice Pitch

The critical experiments selected for analysis cover a range of fuel pellet diameters from 0.311 to 0.444 inches, and lattice spacings from 0.476 to 1.00 inches. In the rack designs, the fuel pellet diameters range from 0.303 to 0.3805 inches O.D. (0.496 to 0.580 inch lattice spacing) for PWR fuel and from 0.3224 to 0.494 inches O.D. (0.488 to 0.740 inch lattice spacing) for BWR fuel. Thus, the critical experiments analyzed provide a reasonable representation of power reactor fuel. Based on the data in Table 4A.1, there does not appear to be any observable trend with either fuel pellet diameter or lattice pitch, at least over the range of the critical experiments applicable to rack designs.

##### 4A.4.3 Soluble Boron Concentration Effects

Various soluble boron concentrations were used in the B&W series of critical experiments and in one PNL experiment, with boron concentrations ranging up to 2550 ppm. Results of MCNP4a (and one KENO5a) calculations are shown in Table 4A.6. Analyses of the very high boron concentration experiments (> 1300 ppm) show a tendency to slightly overpredict reactivity for the three experiments exceeding 1300 ppm. In turn, this would suggest that the evaluation of the racks with higher soluble boron concentrations could be slightly conservative.

---

<sup>†</sup> Parallel experiments with a depleted uranium reflector were also performed but not included in the present analysis since they are not pertinent to the Holtec rack design.

#### 4A.5 MOX Fuel

The number of critical experiments with PuO<sub>2</sub> bearing fuel (MOX) is more limited than for UO<sub>2</sub> fuel. However, a number of MOX critical experiments have been analyzed and the results are shown in Table 4A.7. Results of these analyses are generally above a  $k_{eff}$  of 1.00, indicating that when Pu is present, both MCNP4a and KENO5a overpredict the reactivity. This may indicate that calculation for MOX fuel will be expected to be conservative, especially with MCNP4a. It may be noted that for the larger lattice spacings, the KENO5a calculated reactivities are below 1.00, suggesting that a small trend may exist with KENO5a. It is also possible that the overprediction in  $k_{eff}$  for both codes may be due to a small inadequacy in the determination of the Pu-241 decay and Am-241 growth. This possibility is supported by the consistency in calculated  $k_{eff}$  over a wide range of the spectral index (energy of the average lethargy causing fission).

**References**

- [4A.1] J.F. Briesmeister, Ed., "MCNP4a - A General Monte Carlo N-Particle Transport Code, Version 4A; Los Alamos National Laboratory, LA-12625-M (1993).
- [4A.2] SCALE 4.3, "A Modular Code System for Performing Standardized Computer Analyses for Licensing Evaluation", NUREG-0200 (ORNL-NUREG-CSD-2/U2/R5, Revision 5, Oak Ridge National Laboratory, September 1995.
- [4A.3] M.D. DeHart and S.M. Bowman, "Validation of the SCALE Broad Structure 44-G Group ENDF/B-Y Cross-Section Library for Use in Criticality Safety Analyses", NUREG/CR-6102 (ORNL/TM-12460) Oak Ridge National Laboratory, September 1994.
- [4A.4] W.C. Jordan et al., "Validation of KENO.V.a", CSD/TM-238, Martin Marietta Energy Systems, Inc., Oak Ridge National Laboratory, December 1986.
- [4A.5] O.W. Hermann et al., "Validation of the Scale System for PWR Spent Fuel Isotopic Composition Analysis", ORNL-TM-12667, Oak Ridge National Laboratory, undated.
- [4A.6] R.J. Larsen and M.L. Marx, An Introduction to Mathematical Statistics and its Applications, Prentice-Hall, 1986.
- [4A.7] M.N. Baldwin et al., Critical Experiments Supporting Close Proximity Water Storage of Power Reactor Fuel, BAW-1484-7, Babcock and Wilcox Company, July 1979.
- [4A.8] G.S. Hoovier et al., Critical Experiments Supporting Underwater Storage of Tightly Packed Configurations of Spent Fuel Pins, BAW-1645-4, Babcock & Wilcox Company, November 1991.
- [4A.9] L.W. Newman et al., Urania Gadolinia: Nuclear Model Development and Critical Experiment Benchmark, BAW-1810, Babcock and Wilcox Company, April 1984.

- [4A.10] J.C. Manaranche et al., "Dissolution and Storage Experimental Program with 4.75 w/o Enriched Uranium-Oxide Rods," Trans. Am. Nucl. Soc. 33: 362-364 (1979).
- [4A.11] S.R. Bierman and E.D. Clayton, Criticality Experiments with Subcritical Clusters of 2.35 w/o and 4.31 w/o  $^{235}\text{U}$  Enriched  $\text{UO}_2$  Rods in Water with Steel Reflecting Walls, PNL-3602, Battelle Pacific Northwest Laboratory, April 1981.
- [4A.12] S.R. Bierman et al., Criticality Experiments with Subcritical Clusters of 2.35 w/o and 4.31 w/o  $^{235}\text{U}$  Enriched  $\text{UO}_2$  Rods in Water with Uranium or Lead Reflecting Walls, PNL-3926, Battelle Pacific Northwest Laboratory, December, 1981.
- [4A.13] S.R. Bierman et al., Critical Separation Between Subcritical Clusters of 4.31 w/o  $^{235}\text{U}$  Enriched  $\text{UO}_2$  Rods in Water with Fixed Neutron Poisons, PNL-2615, Battelle Pacific Northwest Laboratory, October 1977.
- [4A.14] S.R. Bierman, Criticality Experiments with Neutron Flux Traps Containing Voids, PNL-7167, Battelle Pacific Northwest Laboratory, April 1990.
- [4A.15] B.M. Durst et al., Critical Experiments with 4.31 wt %  $^{235}\text{U}$  Enriched  $\text{UO}_2$  Rods in Highly Borated Water Lattices, PNL-4267, Battelle Pacific Northwest Laboratory, August 1982.
- [4A.16] S.R. Bierman, Criticality Experiments with Fast Test Reactor Fuel Pins in Organic Moderator, PNL-5803, Battelle Pacific Northwest Laboratory, December 1981.
- [4A.17] E.G. Taylor et al., Saxton Plutonium Program Critical Experiments for the Saxton Partial Plutonium Core, WCAP-3385-54, Westinghouse Electric Corp., Atomic Power Division, December 1965.
- [4A.18] M.G. Natrella, Experimental Statistics, National Bureau of Standards, Handbook 91, August 1963.

Table 4A.1

Summary of Criticality Benchmark Calculations

Reference	Identification	Enrich.	Calculated $k_{eff}$		EALF <sup>†</sup> (eV)		
			MCNP4a	KENO5a	MCNP4a	KENO5a	
1	B&W-1484 (4A.7)	Core I	2.46	0.9964 ± 0.0010	0.9898 ± 0.0006	0.1759	0.1753
2	B&W-1484 (4A.7)	Core II	2.46	1.0008 ± 0.0011	1.0015 ± 0.0005	0.2553	0.2446
3	B&W-1484 (4A.7)	Core III	2.46	1.0010 ± 0.0012	1.0005 ± 0.0005	0.1999	0.1939
4	B&W-1484 (4A.7)	Core IX	2.46	0.9956 ± 0.0012	0.9901 ± 0.0006	0.1422	0.1426
5	B&W-1484 (4A.7)	Core X	2.46	0.9980 ± 0.0014	0.9922 ± 0.0006	0.1513	0.1499
6	B&W-1484 (4A.7)	Core XI	2.46	0.9978 ± 0.0012	1.0005 ± 0.0005	0.2031	0.1947
7	B&W-1484 (4A.7)	Core XII	2.46	0.9988 ± 0.0011	0.9978 ± 0.0006	0.1718	0.1662
8	B&W-1484 (4A.7)	Core XIII	2.46	1.0020 ± 0.0010	0.9952 ± 0.0006	0.1988	0.1965
9	B&W-1484 (4A.7)	Core XIV	2.46	0.9953 ± 0.0011	0.9928 ± 0.0006	0.2022	0.1986
10	B&W-1484 (4A.7)	Core XV <sup>††</sup>	2.46	0.9910 ± 0.0011	0.9909 ± 0.0006	0.2092	0.2014
11	B&W-1484 (4A.7)	Core XVI <sup>††</sup>	2.46	0.9935 ± 0.0010	0.9889 ± 0.0006	0.1757	0.1713
12	B&W-1484 (4A.7)	Core XVII	2.46	0.9962 ± 0.0012	0.9942 ± 0.0005	0.2083	0.2021
13	B&W-1484 (4A.7)	Core XVIII	2.46	1.0036 ± 0.0012	0.9931 ± 0.0006	0.1705	0.1708

Table 4A.1

Summary of Criticality Benchmark Calculations

Reference	Identification	Enrich.	Calculated $k_{eff}$		EALF <sup>†</sup> (eV)		
			MCNP4a	KENO5a	MCNP4a	KENO5a	
14	B&W-1484 (4A.7)	Core XIX	2.46	0.9961 ± 0.0012	0.9971 ± 0.0005	0.2103	0.2011
15	B&W-1484 (4A.7)	Core XX	2.46	1.0008 ± 0.0011	0.9932 ± 0.0006	0.1724	0.1701
16	B&W-1484 (4A.7)	Core XXI	2.46	0.9994 ± 0.0010	0.9918 ± 0.0006	0.1544	0.1536
17	B&W-1645 (4A.8)	S-type Fuel, w/886 ppm B	2.46	0.9970 ± 0.0010	0.9924 ± 0.0006	1.4475	1.4680
18	B&W-1645 (4A.8)	S-type Fuel, w/746 ppm B	2.46	0.9990 ± 0.0010	0.9913 ± 0.0006	1.5463	1.5660
19	B&W-1645 (4A.8)	SO-type Fuel, w/1156 ppm B	2.46	0.9972 ± 0.0009	0.9949 ± 0.0005	0.4241	0.4331
20	B&W-1810 (4A.9)	Case 1 1337 ppm B	2.46	1.0023 ± 0.0010	NC	0.1531	NC
21	B&W-1810 (4A.9)	Case 12 1899 ppm B	2.46/4.02	1.0060 ± 0.0009	NC	0.4493	NC
22	French (4A.10)	Water Moderator 0 gap	4.75	0.9966 ± 0.0013	NC	0.2172	NC
23	French (4A.10)	Water Moderator 2.5 cm gap	4.75	0.9952 ± 0.0012	NC	0.1778	NC
24	French (4A.10)	Water Moderator 5 cm gap	4.75	0.9943 ± 0.0010	NC	0.1677	NC
25	French (4A.10)	Water Moderator 10 cm gap	4.75	0.9979 ± 0.0010	NC	0.1736	NC
26	PNL-3602 (4A.11)	Steel Reflector, 0 separation	2.35	NC	1.0004 ± 0.0006	NC	0.1018

**Table 4A.1**  
**Summary of Criticality Benchmark Calculations**

Reference	Identification	Enrich.	Calculated $k_{eff}$		EALF <sup>†</sup> (eV)		
			MCNP4a	KENO5a	MCNP4a	KENO5a	
27	PNL-3602 (4A.11)	Steel Reflector, 1.321 cm sepn.	2.35	0.9980 ± 0.0009	0.9992 ± 0.0006	0.1000	0.0909
28	PNL-3602 (4A.11)	Steel Reflector, 2.616 cm sepn	2.35	0.9968 ± 0.0009	0.9964 ± 0.0006	0.0981	0.0975
29	PNL-3602 (4A.11)	Steel Reflector, 3.912 cm sepn.	2.35	0.9974 ± 0.0010	0.9980 ± 0.0006	0.0976	0.0970
30	PNL-3602 (4A.11)	Steel Reflector, infinite sepn.	2.35	0.9962 ± 0.0008	0.9939 ± 0.0006	0.0973	0.0968
31	PNL-3602 (4A.11)	Steel Reflector, 0 cm sepn.	4.306	NC	1.0003 ± 0.0007	NC	0.3282
32	PNL-3602 (4A.11)	Steel Reflector, 1.321 cm sepn.	4.306	0.9997 ± 0.0010	1.0012 ± 0.0007	0.3016	0.3039
33	PNL-3602 (4A.11)	Steel Reflector, 2.616 cm sepn.	4.306	0.9994 ± 0.0012	0.9974 ± 0.0007	0.2911	0.2927
34	PNL-3602 (4A.11)	Steel Reflector, 5.405 cm sepn.	4.306	0.9969 ± 0.0011	0.9951 ± 0.0007	0.2828	0.2860
35	PNL-3602 (4A.11)	Steel Reflector, Infinite sepn. **	4.306	0.9910 ± 0.0020	0.9947 ± 0.0007	0.2851	0.2864
36	PNL-3602 (4A.11)	Steel Reflector, with Boral Sheets	4.306	0.9941 ± 0.0011	0.9970 ± 0.0007	0.3135	0.3150
37	PNL-3926 (4A.12)	Lead Reflector, 0 cm sepn.	4.306	NC	1.0003 ± 0.0007	NC	0.3159
38	PNL-3926 (4A.12)	Lead Reflector, 0.55 cm sepn.	4.306	1.0025 ± 0.0011	0.9997 ± 0.0007	0.3030	0.3044
39	PNL-3926 (4A.12)	Lead Reflector, 1.956 cm sepn.	4.306	1.0000 ± 0.0012	0.9985 ± 0.0007	0.2883	0.2930

**Table 4A.1**  
**Summary of Criticality Benchmark Calculations**

Reference	Identification	Enrich.	Calculated $k_{eff}$		EALF <sup>†</sup> (eV)		
			MCNP4a	KENO5a	MCNP4a	KENO5a	
40	PNL-3926 (4A.12)	Lead Reflector, 5.405 cm sepn.	4.306	0.9971 ± 0.0012	0.9946 ± 0.0007	0.2831	0.2854
41	PNL-2615 (4A.13)	Experiment 004/032 - no absorber	4.306	0.9925 ± 0.0012	0.9950 ± 0.0007	0.1155	0.1159
42	PNL-2615 (4A.13)	Experiment 030 - Zr plates	4.306	NC	0.9971 ± 0.0007	NC	0.1154
43	PNL-2615 (4A.13)	Experiment 013 - Steel plates	4.306	NC	0.9965 ± 0.0007	NC	0.1164
44	PNL-2615 (4A.13)	Experiment 014 - Steel plates	4.306	NC	0.9972 ± 0.0007	NC	0.1164
45	PNL-2615 (4A.13)	Exp. 009 1.05% Boron-Steel plates	4.306	0.9982 ± 0.0010	0.9981 ± 0.0007	0.1172	0.1162
46	PNL-2615 (4A.13)	Exp. 012 1.62% Boron-Steel plates	4.306	0.9996 ± 0.0012	0.9982 ± 0.0007	0.1161	0.1173
47	PNL-2615 (4A.13)	Exp. 031 - Boral plates	4.306	0.9994 ± 0.0012	0.9969 ± 0.0007	0.1165	0.1171
48	PNL-7167 (4A.14)	Experiment 214R - with flux trap	4.306	0.9991 ± 0.0011	0.9956 ± 0.0007	0.3722	0.3812
49	PNL-7167 (4A.14)	Experiment 214V3 - with flux trap	4.306	0.9969 ± 0.0011	0.9963 ± 0.0007	0.3742	0.3826
50	PNL-4267 (4A.15)	Case 173 - 0 ppm B	4.306	0.9974 ± 0.0012	NC	0.2893	NC
51	PNL-4267 (4A.15)	Case 177 - 2550 ppm B	4.306	1.0057 ± 0.0010	NC	0.5509	NC
52	PNL-5803 (4A.16)	MOX Fuel - Type 3.2 Exp. 21	20% Pu	1.0041 ± 0.0011	1.0046 ± 0.0006	0.9171	0.8868

Table 4A.1

Summary of Criticality Benchmark Calculations

Reference	Identification	Enrich.	Calculated $k_{eff}$		EALF <sup>†</sup> (eV)		
			MCNP4a	KENO5a	MCNP4a	KENO5a	
53	PNL-5803 (4A.16)	MOX Fuel - Type 3.2 Exp. 43	20% Pu	1.0058 ± 0.0012	1.0036 ± 0.0006	0.2968	0.2944
54	PNL-5803 (4A.16)	MOX Fuel - Type 3.2 Exp. 13	20% Pu	1.0083 ± 0.0011	0.9989 ± 0.0006	0.1665	0.1706
55	PNL-5803 (4A.16)	MOX Fuel - Type 3.2 Exp. 32	20% Pu	1.0079 ± 0.0011	0.9966 ± 0.0006	0.1139	0.1165
56	WCAP-3385 (4A.17)	Saxton Case 52 PuO <sub>2</sub> 0.52" pitch	6.6% Pu	0.9996 ± 0.0011	1.0005 ± 0.0006	0.8665	0.8417
57	WCAP-3385 (4A.17)	Saxton Case 52 U 0.52" pitch	5.74	1.0000 ± 0.0010	0.9956 ± 0.0007	0.4476	0.4580
58	WCAP-3385 (4A.17)	Saxton Case 56 PuO <sub>2</sub> 0.56" pitch	6.6% Pu	1.0036 ± 0.0011	1.0047 ± 0.0006	0.5289	0.5197
59	WCAP-3385 (4A.17)	Saxton Case 56 borated PuO <sub>2</sub>	6.6% Pu	1.0008 ± 0.0010	NC	0.6389	NC
60	WCAP-3385 (4A.17)	Saxton Case 56 U 0.56" pitch	5.74	0.9994 ± 0.0011	0.9967 ± 0.0007	0.2923	0.2954
61	WCAP-3385 (4A.17)	Saxton Case 79 PuO <sub>2</sub> 0.79" pitch	6.6% Pu	1.0063 ± 0.0011	1.0133 ± 0.0006	0.1520	0.1555
62	WCAP-3385 (4A.17)	Saxton Case 79 U 0.79" pitch	5.74	1.0039 ± 0.0011	1.0008 ± 0.0006	0.1036	0.1047

Notes: NC stands for not calculated.

† EALF is the energy of the average lethargy causing fission.

†† These experimental results appear to be statistical outliers (>3σ) suggesting the possibility of unusually large experimental error. Although they could justifiably be excluded, for conservatism, they were retained in determining the calculational basis.

Table 4A.2

COMPARISON OF MCNP4a AND KENO5a CALCULATED REACTIVITIES<sup>†</sup>  
FOR VARIOUS ENRICHMENTS

Enrichment	Calculated $k_{eff} \pm 1\sigma$	
	MCNP4a	KENO5a
3.0	0.8465 $\pm$ 0.0011	0.8478 $\pm$ 0.0004
3.5	0.8820 $\pm$ 0.0011	0.8841 $\pm$ 0.0004
3.75	0.9019 $\pm$ 0.0011	0.8987 $\pm$ 0.0004
4.0	0.9132 $\pm$ 0.0010	0.9140 $\pm$ 0.0004
4.2	0.9276 $\pm$ 0.0011	0.9237 $\pm$ 0.0004
4.5	0.9400 $\pm$ 0.0011	0.9388 $\pm$ 0.0004

---

<sup>†</sup> Based on the GE 8x8R fuel assembly.

Table 4A.3

MCNP4a CALCULATED REACTIVITIES FOR  
CRITICAL EXPERIMENTS WITH NEUTRON ABSORBERS

Ref.	Experiment		$\Delta k$ Worth of Absorber	MCNP4a Calculated $k_{eff}$	EALF <sup>†</sup> (eV)
4A.13	PNL-2615	Boral Sheet	0.0139	0.9994±0.0012	0.1165
4A.7	B&W-1484	Core XX	0.0165	1.0008±0.0011	0.1724
4A.13	PNL-2615	1.62% Boron-steel	0.0165	0.9996±0.0012	0.1161
4A.7	B&W-1484	Core XIX	0.0202	0.9961±0.0012	0.2103
4A.7	B&W-1484	Core XXI	0.0243	0.9994±0.0010	0.1544
4A.7	B&W-1484	Core XVII	0.0519	0.9962±0.0012	0.2083
4A.11	PNL-3602	Boral Sheet	0.0708	0.9941±0.0011	0.3135
4A.7	B&W-1484	Core XV	0.0786	0.9910±0.0011	0.2092
4A.7	B&W-1484	Core XVI	0.0845	0.9935±0.0010	0.1757
4A.7	B&W-1484	Core XIV	0.1575	0.9953±0.0011	0.2022
4A.7	B&W-1484	Core XIII	0.1738	1.0020±0.0011	0.1988
4A.14	PNL-7167	Expt 214R flux trap	0.1931	0.9991±0.0011	0.3722

---

<sup>†</sup>EALF is the energy of the average lethargy causing fission.

Table 4A.4

COMPARISON OF MCNP4a AND KENO5a  
CALCULATED REACTIVITIES<sup>†</sup> FOR VARIOUS <sup>10</sup>B LOADINGS

<sup>10</sup> B, g/cm <sup>2</sup>	Calculated $k_{\text{eff}} \pm 1\sigma$	
	MCNP4a	KENO5a
0.005	1.0381 $\pm$ 0.0012	1.0340 $\pm$ 0.0004
0.010	0.9960 $\pm$ 0.0010	0.9941 $\pm$ 0.0004
0.015	0.9727 $\pm$ 0.0009	0.9713 $\pm$ 0.0004
0.020	0.9541 $\pm$ 0.0012	0.9560 $\pm$ 0.0004
0.025	0.9433 $\pm$ 0.0011	0.9428 $\pm$ 0.0004
0.03	0.9325 $\pm$ 0.0011	0.9338 $\pm$ 0.0004
0.035	0.9234 $\pm$ 0.0011	0.9251 $\pm$ 0.0004
0.04	0.9173 $\pm$ 0.0011	0.9179 $\pm$ 0.0004

---

<sup>†</sup> Based on a 4.5% enriched GE 8x8R fuel assembly.

Table 4A.5

**CALCULATIONS FOR CRITICAL EXPERIMENTS WITH  
THICK LEAD AND STEEL REFLECTORS<sup>†</sup>**

Ref.	Case	E, wt%	Separation, cm	MCNP4a $k_{eff}$	KENO5a $k_{eff}$
4A.11	Steel Reflector	2.35	1.321	$0.9980 \pm 0.0009$	$0.9992 \pm 0.0006$
		2.35	2.616	$0.9968 \pm 0.0009$	$0.9964 \pm 0.0006$
		2.35	3.912	$0.9974 \pm 0.0010$	$0.9980 \pm 0.0006$
		2.35	$\infty$	$0.9962 \pm 0.0008$	$0.9939 \pm 0.0006$
4A.11	Steel Reflector	4.306	1.321	$0.9997 \pm 0.0010$	$1.0012 \pm 0.0007$
		4.306	2.616	$0.9994 \pm 0.0012$	$0.9974 \pm 0.0007$
		4.306	3.405	$0.9969 \pm 0.0011$	$0.9951 \pm 0.0007$
		4.306	$\infty$	$0.9910 \pm 0.0020$	$0.9947 \pm 0.0007$
4A.12	Lead Reflector	4.306	0.55	$1.0025 \pm 0.0011$	$0.9997 \pm 0.0007$
		4.306	1.956	$1.0000 \pm 0.0012$	$0.9985 \pm 0.0007$
		4.306	5.405	$0.9971 \pm 0.0012$	$0.9946 \pm 0.0007$

<sup>†</sup> Arranged in order of increasing reflector-fuel spacing.

Table 4A.6

CALCULATIONS FOR CRITICAL EXPERIMENTS WITH VARIOUS SOLUBLE BORON CONCENTRATIONS

Reference	Experiment	Boron Concentration, ppm	Calculated $k_{eff}$	
			MCNP4a	KENO5a
4A.15	PNL-4267	0	$0.9974 \pm 0.0012$	-
4A.8	B&W-1645	886	$0.9970 \pm 0.0010$	$0.9924 \pm 0.0006$
4A.9	B&W-1810	1337	$1.0023 \pm 0.0010$	-
4A.9	B&W-1810	1899	$1.0060 \pm 0.0009$	-
4A.15	PNL-4267	2550	$1.0057 \pm 0.0010$	-

Table 4A.7

CALCULATIONS FOR CRITICAL EXPERIMENTS WITH MOX FUEL

Reference	Case <sup>†</sup>	MCNP4a		KENO5a	
		$k_{eff}$	EALF <sup>††</sup>	$k_{eff}$	EALF <sup>††</sup>
PNL-5803 [4A.16]	MOX Fuel - Exp. No. 21	1.0041±0.0011	0.9171	1.0046±0.0006	0.8868
	MOX Fuel - Exp. No. 43	1.0058±0.0012	0.2968	1.0036±0.0006	0.2944
	MOX Fuel - Exp. No. 13	1.0083±0.0011	0.1665	0.9989±0.0006	0.1706
	MOX Fuel - Exp. No. 32	1.0079±0.0011	0.1139	0.9966±0.0006	0.1165
WCAP-3385-54 [4A.17]	Saxton @ 0.52" pitch	0.9996±0.0011	0.8665	1.0005±0.0006	0.8417
	Saxton @ 0.56" pitch	1.0036±0.0011	0.5289	1.0047±0.0006	0.5197
	Saxton @ 0.56" pitch borated	1.0008±0.0010	0.6389	NC	NC
	Saxton @ 0.79" pitch	1.0063±0.0011	0.1520	1.0133±0.0006	0.1555

Note: NC stands for not calculated

† Arranged in order of increasing lattice spacing.

†† EALF is the energy of the average lethargy causing fission.

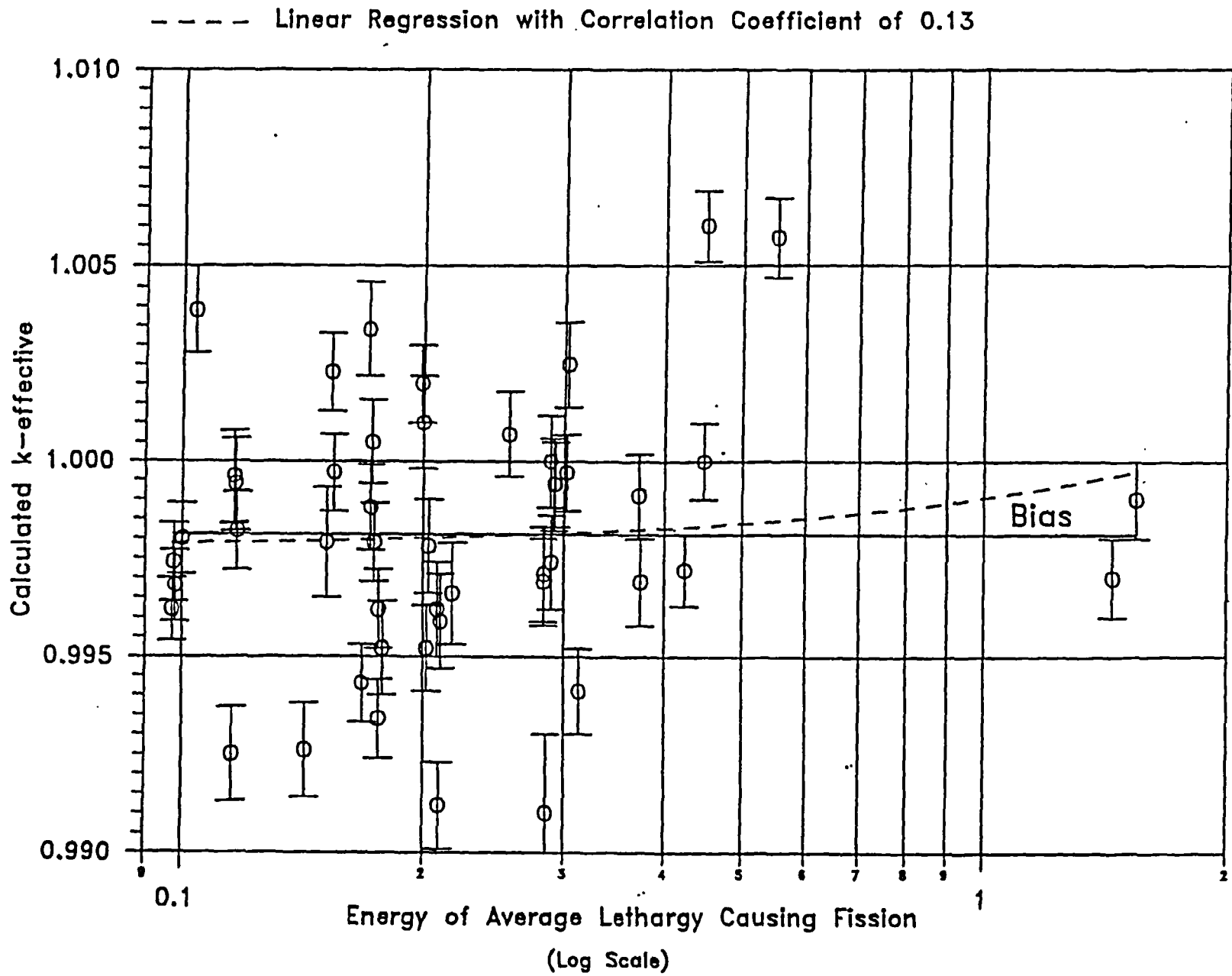


FIGURE 4A.1 MCNP CALCULATED k-eff VALUES for  
VARIOUS VALUES OF THE SPECTRAL INDEX

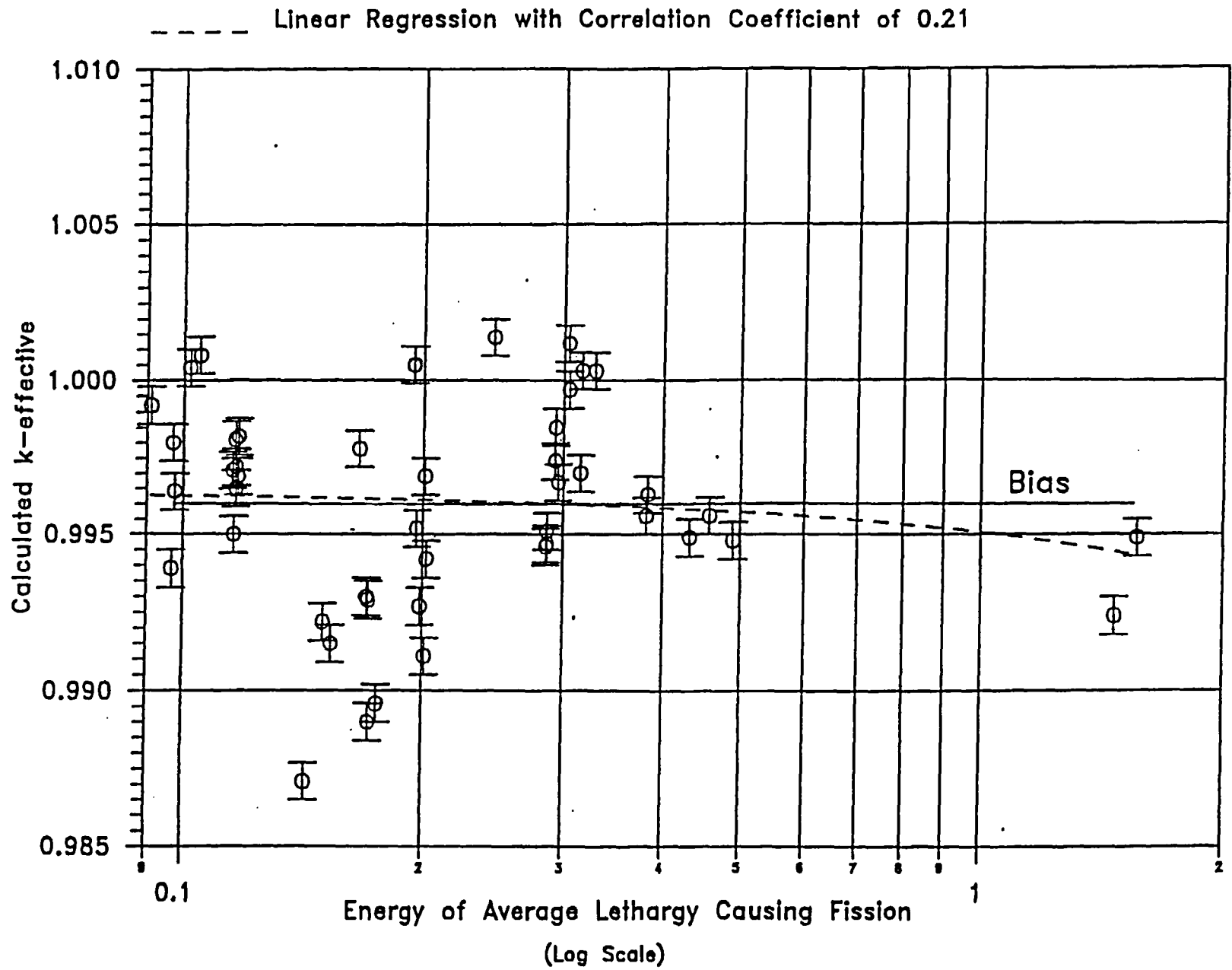


FIGURE 4A.2. KEN05a CALCULATED k-eff VALUES FOR VARIOUS VALUES OF THE SPECTRAL INDEX

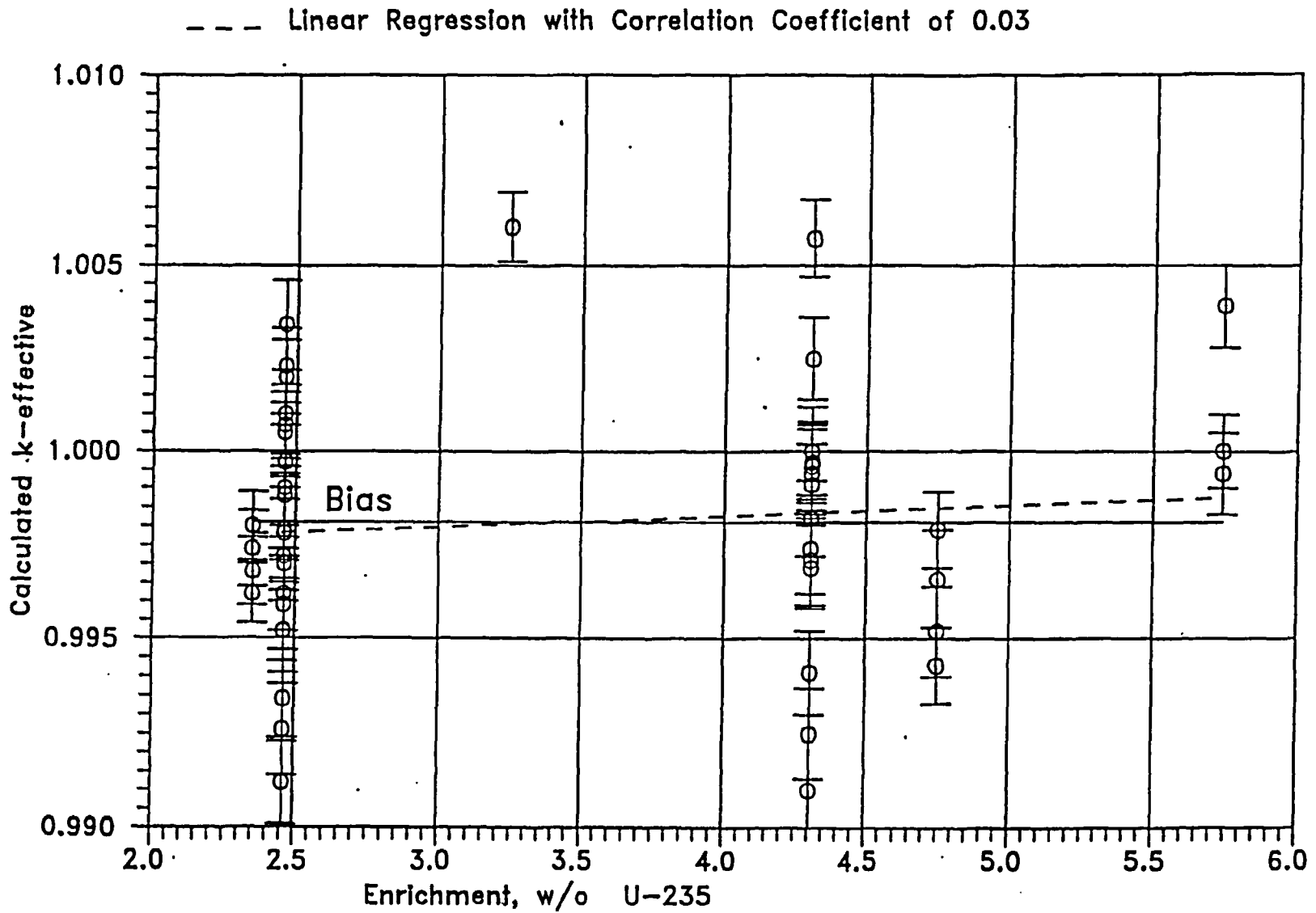


FIGURE 4A.3 MCNP CALCULATED k-eff VALUES AT VARIOUS U-235 ENRICHMENTS

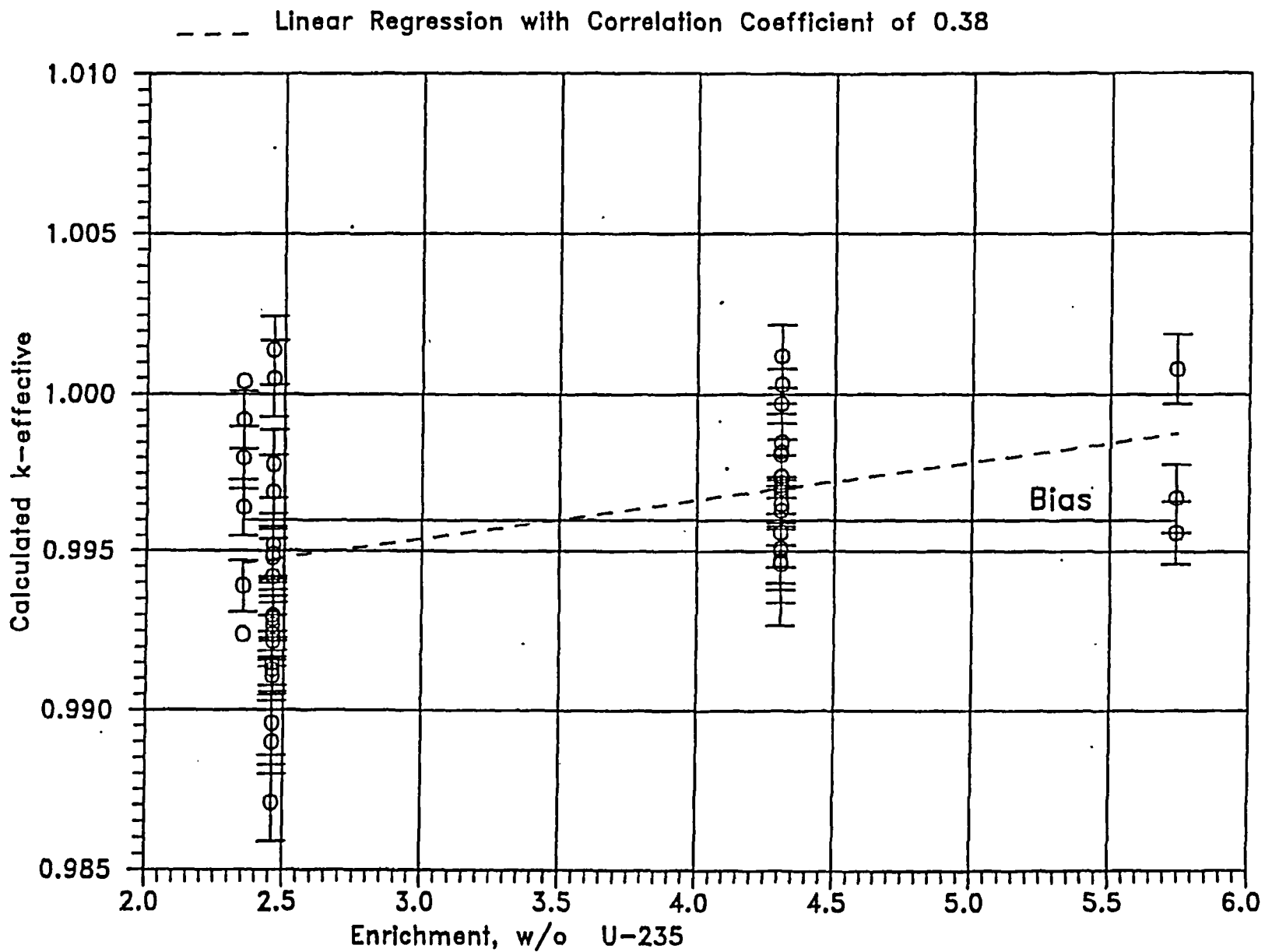


FIGURE 4A.4. KENO CALCULATED k-eff VALUES  
AT VARIOUS U-235 ENRICHMENTS

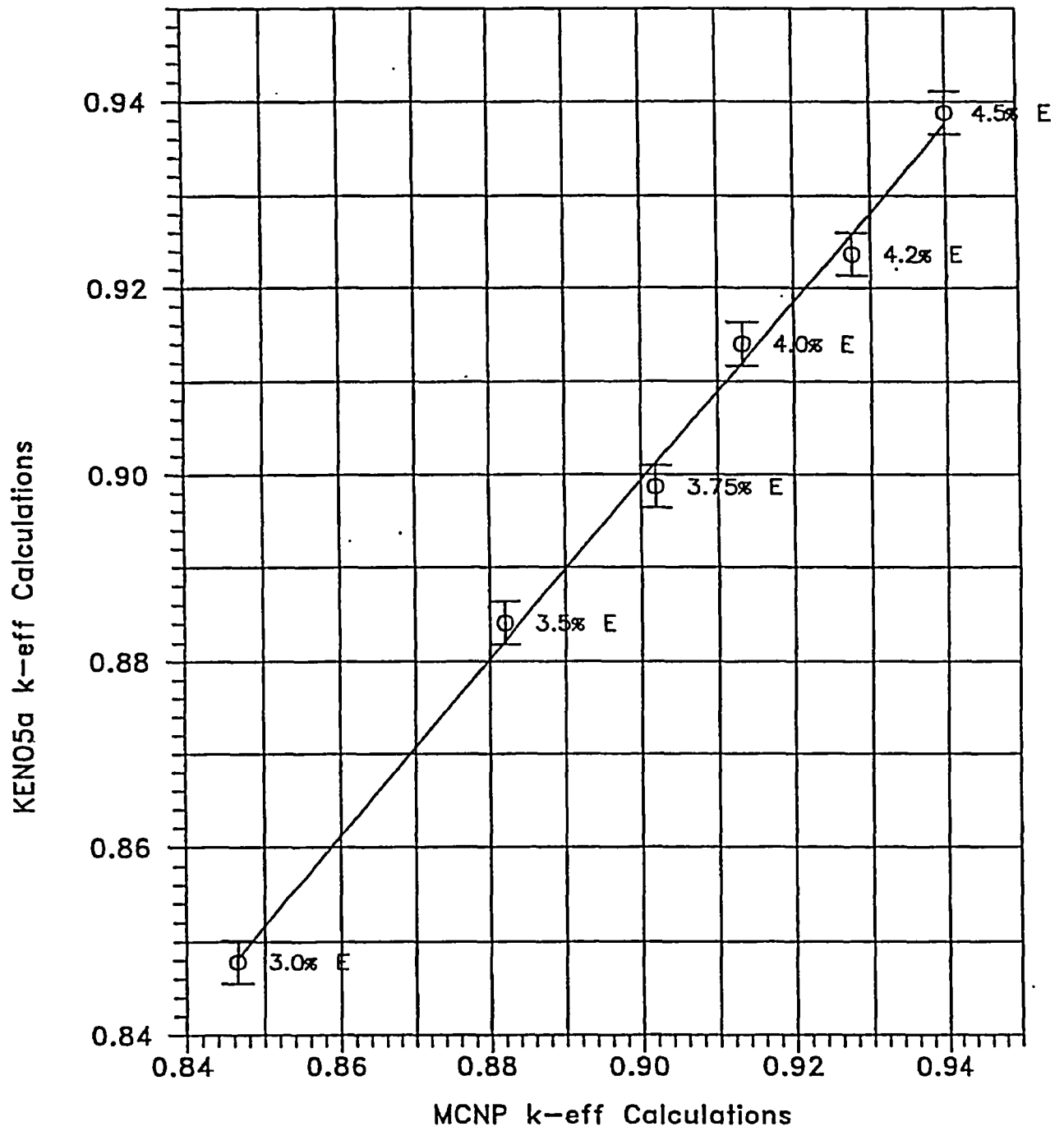


FIGURE 4A.5 COMPARISON OF MCNP AND KENO5A CALCULATIONS FOR VARIOUS FUEL ENRICHMENTS

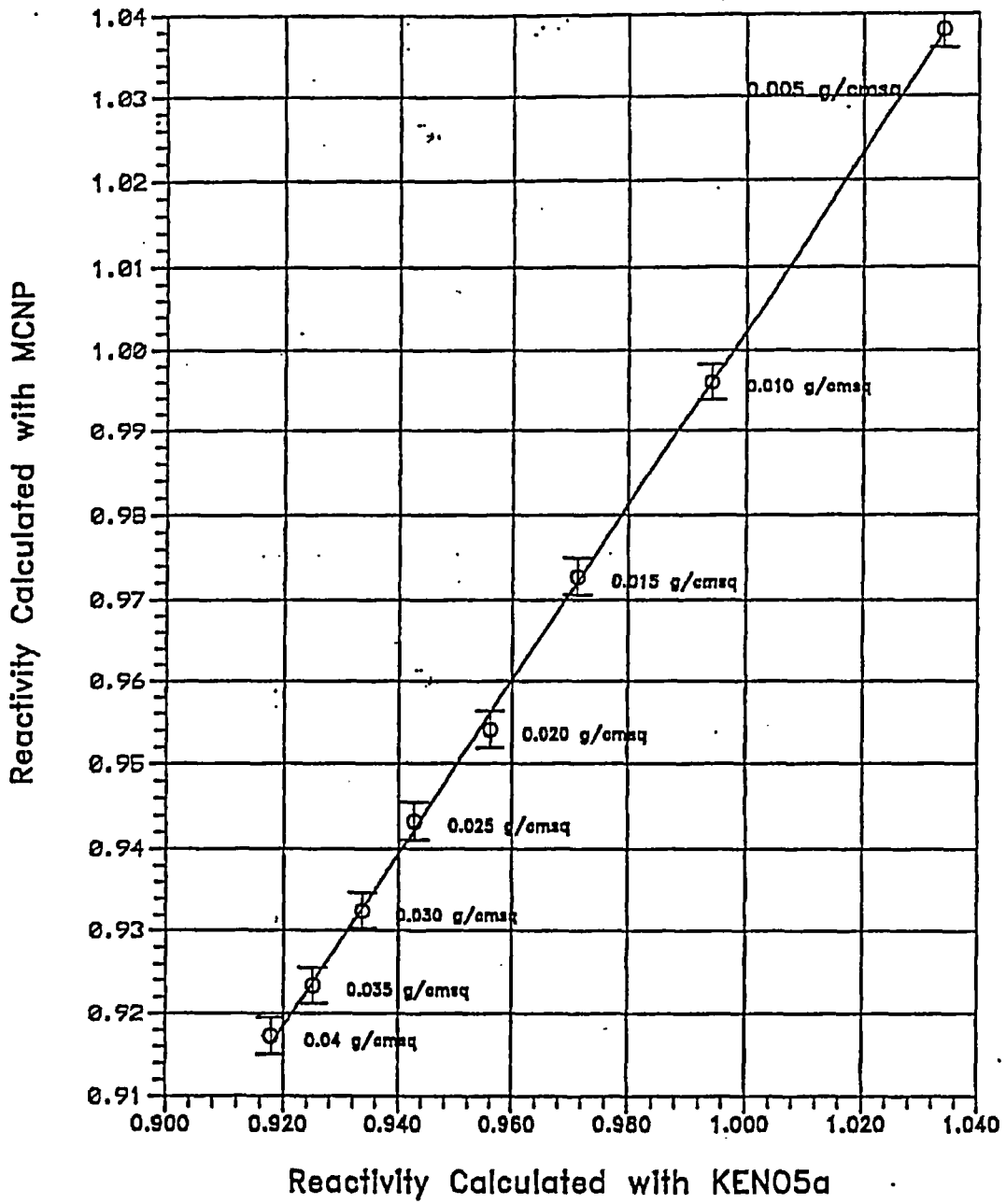


FIGURE 4A.6 : COMPARISON OF MCNP AND KENO5a CALCULATIONS FOR VARIOUS BORON-10 AREAL DENSITIES

## 5.0 THERMAL-HYDRAULIC CONSIDERATIONS

### 5.1 Introduction

This section provides a summary of the analyses performed to demonstrate the compliance of the unit spent fuel pools (SFPs) and their attendant cooling systems with the provisions of USNRC Standard Review Plan (SRP) 9.1.3 (Spent Fuel Pool Cooling and Cleanup System, Rev. 1, July 1981) and Section III of the USNRC "OT Position Paper for Review and Acceptance of Spent Fuel Storage and Handling Applications," (April 14, 1978). Similar methods of thermal-hydraulic analysis have been used in the licensing evaluations for other SFP capacity expansion projects.

The thermal-hydraulic qualification analyses for the expanded rack array may be broken down into the following categories:

- i. Evaluation of the maximum SFP bulk temperatures for the design-basis offload scenarios, to establish that maximum bulk temperature limits are not exceeded.
- ii. Evaluation of loss-of-forced cooling scenarios, to establish minimum times to boil and to perform corrective actions, and the associated makeup water requirements.
- iii. Determination of the maximum local water temperature, at the instant when the bulk temperature reaches its maximum value, to establish that localized boiling in the fuel storage racks is not possible while forced cooling is operating.
- iv. Evaluation of the maximum fuel rod cladding temperature, at the instant when the bulk temperature reaches its maximum value, to establish that nucleate boiling is not possible while forced cooling is operating.

The following sections present plant system descriptions, analysis methodologies and assumptions, a synopsis of the input data employed and summaries of the calculated results.

## 5.2 Cooling Systems Description

The SFPCS design basis for both units requires that the system must maintain the SFP bulk temperature below 150°F under the following conditions:

- During routine (non-offload) operation
- Following a normal partial core offload, with one cooling pump operating (assuming a single pump failure)
- Following a full core offload, with both cooling pumps operating (no single failure assumed)

The SFP decay heat load is greater during core offload conditions than during non-offload conditions. Therefore, the peak SFP temperature during routine operation was not evaluated, because it is bounded by the peak SFP temperatures occurring during core offload conditions.

The Unit 1 SFPCS consists of two parallel cooling pumps discharging to a single shell and tube heat exchanger. SFP water is circulated through the heat exchanger tubes and heat is transferred to component cooling water circulating through the shell side. For determining the peak SFP temperature on a partial core offload, a single pump failure is taken that reduces the SFPCS flow to one operating pump and the common heat exchanger. No pump failure is assumed for the full core offload.

The Unit 2 SFPCS consists of two parallel cooling pumps discharging to a common header which supplies two parallel heat exchangers. SFP water is circulated through the tubes and heat is transferred to component cooling water circulating through the shell side. For determining the peak SFP temperature on a partial core offload, a single pump failure is taken that reduces the SFPCS flow to one operating pump and one heat exchanger. No pump failure is assumed for the full core offload.

In addition to the three design basis conditions above, the condition of a full core offload with only one cooling pump available was also evaluated to determine the peak SFP temperature that could occur with minimum cooling. This evaluation provides a bounding value for the peak SFP temperature for a cooling condition beyond the SFPCS design basis.

The normal partial core offload condition with one operating pump is referred to as Scenario 1 in the following section. A full core offload with both cooling pumps operating is referred to as Scenario 2 and a full core offload with one cooling pump operating is referred to as Scenario 3.

### 5.3 Offload/Cooling Alignment Scenarios

Three offload scenarios are postulated for each St. Lucie unit. These scenarios are:

Scenario	Offload Type	Number of Assemblies Offloaded	Cooling System Configuration
<b>Unit 1</b>			
1	Partial Core	105	1 pump / 1 HX
2	Full Core	217	2 pumps / 1 HX
3	Full Core	217	1 pump / 1 HX
<b>Unit 2</b>			
1	Partial Core	105	1 pump / 1 HX
2	Full Core	217	2 pumps / 2 HXs
3	Full Core	217	1 pump / 1 HX

#### Scenario 1

A partial core offload is comprised of 105 assemblies offloaded into the SFP, completely filling all available storage locations. The minimum decay time of the previously offloaded fuel assemblies for this offload scenario is 18 months. A cooling alignment that includes the effects of a single active SFPCS component failure (i.e., pump failure) is considered.

### Scenario 2

A full core offload is comprised of 217 assemblies offloaded into the SFP, completely filling all available storage locations. The 217 offloaded assemblies are separated into three distinct groups: 73 assemblies with 4.5 years of irradiation at full power, 72 assemblies with 3 years of irradiation at full power and 72 assemblies with 1.5 years of irradiation at full power. The minimum decay time of the previously offloaded fuel assemblies for this scenario is 18 months. Scenario 2 assumed maximum cooling is available with flow from both pumps to all available heat exchangers (1 HX on Unit 1 and 2 HXs on Unit 2). No component failures are assumed.

### Scenario 3

Scenario 3 is identical to Scenario 2 except for the number of operating pumps (one instead of two). For both units, Scenario 3 assumes only one HX is supplied by the operating pump.

The core offload time for all scenarios on both units is 120 hours after reactor shutdown. The offload rate is assumed to be instantaneous to maximize decay heat, except for Unit 2 full core offload Scenario 3, which assumes an offload rate of 8 assemblies per hour.

Each of these offload/cooling scenarios is evaluated to determine the peak SFP bulk temperature.

One additional cooling condition was also evaluated beyond the above three scenarios, for the sole purpose of determining a worst-case decay heat load that would be imposed on the SFP and the resultant maximum bulk temperature with one cooling pump operating. This limiting cooling condition is a full core offload required 90 days after a refueling outage. The condition assumes a batch of 72 assemblies is offloaded from the reactor during refueling. After restart and 90 days at power, the full core of 217 assemblies is offloaded to the SFP starting at 72 hours after reactor shutdown, completely filling all available storage locations. One SFPCS pump is operating throughout the transient evaluation.

Tables 5.3.1 and 5.3.2 present the historic and projected offload schedules used for these analyses for Units 1 and 2, respectively.

#### 5.4 Maximum Pool Bulk Temperatures

In this section, we present the methodology for calculating the maximum SFP bulk temperatures for the scenarios presented in the preceding section.

The following conservatisms are applied in the maximum SFP bulk temperature calculations:

- The reactor thermal power level is increased by 2% to account for the plant's reactor thermal power calorimetric uncertainty.
- Appropriate parameters (i.e., burnup, batch size, assembly uranium weight and initial enrichment) are used for all projected offloads.
- The thermal performance of the SFPCS heat exchanger(s) is determined with all heat transfer surfaces fouled to their design-basis maximum levels.
- The thermal performance of the SFPCS heat exchanger(s) is determined incorporating a 5% tube plugging allowance.
- The thermal inertia (thermal capacity) of the SFP is based on the net water volume only. This conservatively neglects the considerable thermal inertia of the fuel assemblies, stainless steel racks and stainless steel SFP liners.

The transient thermal response of the SFP and the attendant cooling systems is governed by a first-order, ordinary differential equation. The governing differential equation can be written by utilizing conservation of energy as:

$$C \frac{dT}{d\tau} = Q(\tau) - Q_{HX}(T) - Q_{ENV}(T) \quad (5-1)$$

where:

C = SFP thermal capacity, Btu/°F

T = SFP bulk temperature, °F

$\tau$  = Time after reactor shutdown, hr

Q( $\tau$ ) = Time varying decay heat generation rate, Btu/hr

$Q_{HX}(T)$  = Temperature dependent SFPCS heat rejection rate, Btu/hr

$Q_{ENV}(T)$  = Temperature dependent passive heat loss to the environment, Btu/hr

$Q_{HX}(T)$  in Equation 5-1 is a function of the SFP bulk temperature and the coolant water flow rate and temperature, and can be written in terms of the temperature effectiveness ( $p$ ) as follows:

$$Q_{HX}(T) = W_t C_t p (T - t_i) \quad (5-2)$$

where:

$W_t$  = Coolant water flow rate, lb/hr

$C_t$  = Coolant water specific heat capacity, Btu/(lb-°F)

$p$  = SFPCS heat exchanger(s) temperature effectiveness

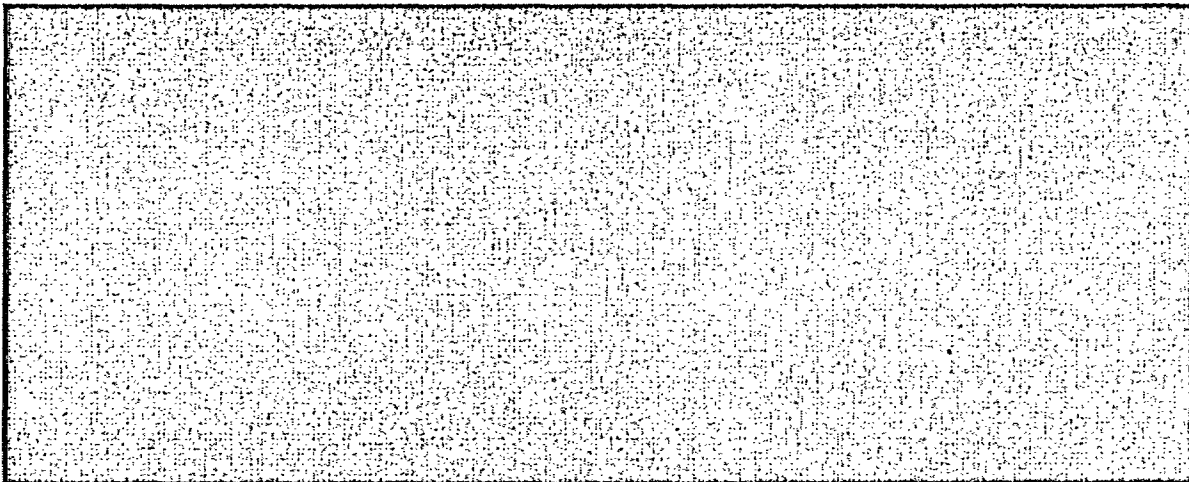
$T$  = SFP bulk water temperature, °F

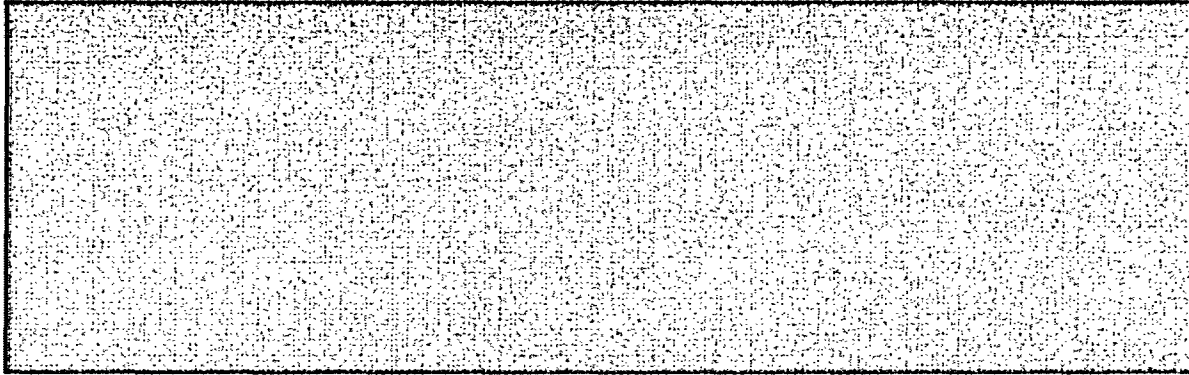
$t_i$  = Coolant water inlet temperature, °F

The temperature effectiveness, a measure of the heat transfer efficiency of the heat exchanger(s), is defined as:

$$p = \frac{t_o - t_i}{T - t_i} \quad (5-3)$$

where  $t_o$  is the coolant outlet temperature (°F) and all other terms are as defined above. The SFPCS heat exchanger(s) coolant outlet temperature ( $t_o$ ) for various SFP bulk temperatures ( $T$ ) are determined using the Holtec QA validated computer program STER [5.4.7].





The differential equation that defines the transient thermal response of the SFP (Equation 5-1) is solved numerically. The decay heat load from previously offloaded fuel assemblies is assumed to be constant and is calculated using Holtec's QA validated LONGOR computer program [5.4.3]. This program incorporates the ORIGEN2 computer code [5.4.4] to perform the decay heat calculations. The transient decay heat loads and SFP bulk temperatures are calculated using Holtec's QA validated BULKTEM computer program [5.4.5], which also incorporates the ORIGEN2 computer code. The maximum SFP bulk temperatures are extracted from the results of the transient evaluations. The major input values for these analyses are summarized in Table 5.4.1.

As the SFP temperature exceeds the building ambient temperature, both heat and moisture are rejected from the surface to the SFP into the building air. Equation 5-4 utilizes the temperature of the air directly above the SFP to calculate the heat removed from the SFP by passive mechanisms. The following enthalpy and moisture balance equations govern the interaction between heat and moisture rejection at the SFP surface and absorption by the air:

$$\begin{aligned} m_{oad} h_{oad} + m_{oaw} h_{oaw} + Q_{sens} + m_{evap} h_{evap} &= m_{bad} h_{bad} + m_{baw} h_{baw} \\ m_{oaw} + m_{evap} &= m_{baw} \end{aligned} \quad (5-5)$$

where:

- $m_{oad}$  = Mass flow rate of incoming dry air, lb/hr
- $h_{oad}$  = Enthalpy of incoming dry air, Btu/lb
- $m_{oaw}$  = Mass flow rate of incoming water vapor, lb/hr
- $h_{oaw}$  = Enthalpy of incoming water vapor, Btu/lb

$Q_{sens}$  = Sensible heat transferred from SFP, Btu/hr  
 $m_{evap}$  = Mass flow rate from surface of SFP, lb/hr  
 $h_{evap}$  = Enthalpy of evaporated pool water, Btu/lb  
 $m_{bad}$  = Mass flow rate of dry air above SFP, lb/hr  
 $h_{bad}$  = Enthalpy of dry air above SFP, Btu/lb  
 $m_{baw}$  = Mass flow rate of water vapor above SFP, lb/hr  
 $h_{baw}$  = Enthalpy of water vapor above SFP, Btu/lb

To determine bounding maximum values for the temperature of the air directly above the SFP, heat and moisture transfer rates from the surface of the SFP with SFP temperatures in excess of the expected maximum bulk temperatures are calculated using Equation 5-4. Equation 5-5 is then used to determine the enthalpies of the dry air and water vapor directly above the SFP, which are subsequently used to determine the corresponding temperature. As the SFP bulk temperatures will actually be lower than the assumed bounding temperatures, this ensures bounding maximum temperatures for the air directly above the SFP for subsequent use in solving Equation 5-1.

#### 5.5 Minimum Time-to-Boil and Maximum Boiloff Rate

In this section, we present the methodology for calculating the minimum time-to-boil and corresponding maximum boiloff rate for the scenarios presented in Section 5.3.

The following conservatisms and assumptions are applied in the time-to-boil and boiloff rate calculations:

- During the loss of forced cooling evaluations, the makeup water flow is started coincident with the onset of bulk boiling. It is assumed that the temperature of the makeup water added to the SFP is 100°F.
- The loss of forced cooling is assumed to occur coincident with the peak SFP bulk temperature. Maximizing the initial temperature will conservatively minimize the calculated time-to-boil.

- The passive heat losses from the SFP surface to the building air are evaluated assuming the relative humidity of the building air is 100%. This minimizes the evaporation driving force and reduces the resulting heat losses.
- The thermal inertia (thermal capacity) of the SFP is based on the net water volume only. This conservatively neglects the considerable thermal inertia of the fuel assemblies, stainless steel racks and stainless steel SFP liners.

The governing enthalpy balance equation for this condition, subject to these conservative assumptions, can be written as:

$$C(\tau) \frac{dT}{d\tau} = Q(\tau + \tau_0) - Q_{ENV}(T) \quad (5-6)$$

where:

$C(\tau)$  = Time-varying SFP thermal capacity

$\tau$  = Time after cooling is lost (hr)

$\tau_0$  = Loss of cooling time after shutdown (hr)

All other terms in this equation are the same as defined for Equation 5-1 in Section 5.4.

Equation 5-6 is solved using a numerical solution technique to obtain the bulk pool temperature as a function of time. The time-to-boil, boil-off rate and water depth versus time are calculated using Holtec's QA validated TBOIL program [5.4.6]. Calculations also determined the makeup water flow rate, at the onset of bulk boiling, necessary to maintain a minimum of 9' of above the stored spent fuel. The SFP decay heat loads for these analyses are extracted from the results of the BULKTEM transient evaluations. The major input values for these analyses are summarized in Table 5.5.1.

## 5.6 Maximum SFP Local Water Temperature

In this section, a summary of the methodology for evaluating the maximum local water temperatures within the fuel racks in the SFP and cask pit is presented. The results of these evaluations are maximum local water temperatures.

In order to determine an upper bound on the maximum local water temperature, a series of conservative assumptions are made. The most important of these assumptions are:

- The walls and floor of the SFP and cask pit are all modeled as adiabatic surfaces, thereby neglecting conduction heat loss through these items.
- Heat losses by thermal radiation and natural convection from the hot SFP surface to the environment are neglected.
- No downcomer flow is assumed to exist between the rack modules in the Unit 1 SFP.
- The hydraulic resistance of every fuel storage rack cell is determined based on the most hydraulically limiting (i.e., highest hydraulic resistance) fuel assembly type.
- The hydraulic resistance parameters for the rack cells, permeability and inertial resistance, are conservatively adjusted by 10%.
- The bottom plenum heights used in the model are less than the actual heights.
- The hydraulic resistance of every fuel storage rack cell is determined based on the most restrictive water inlet geometry of the cells over rack support pedestals (i.e., all baseplate holes are completely blocked). These cells have a reduced water entrance area, caused by the pedestal blocking the baseplate hole, and a correspondingly increased hydraulic resistance.
- The hydraulic resistance of every fuel storage rack cell includes the effects of blockage due to an assumed dropped fuel assembly lying horizontally on top of the racks.
- For the Unit 1 CFD model, the fuel assemblies with the highest decay heat generation rates are grouped together in the center of the model. This conservatively maximizes the distance between these highest heat fuel assemblies and the rack-to-wall downcomers, so the cooled water from the SFPCS must travel the farther along the SFP floor to cool them. Discharge of these assemblies into any rack locations that are closer to a downcomer, including the cask pit rack, is bounded by the analyzed configuration.

To demonstrate adequate cooling of hot fuel in the SFP and the cask pit, it is necessary to rigorously quantify the coupled velocity and temperature fields created by the interaction of buoyancy driven and forced water flows. A Computational Fluid Dynamics (CFD) analysis for this demonstration is required. The objective of this study is to demonstrate that the thermal-hydraulic criterion of ensuring local subcooled conditions in the SFP is met for all postulated fuel

offload/cooling alignment scenarios. The local thermal-hydraulic analysis is performed such that partial cell blockage and slight fuel assembly variations are bounded. An outline of the CFD approach is described in the following.

There are several significant geometric and thermal-hydraulic features of the St. Lucie SFPs that need to be considered for a rigorous CFD analysis. From a fluid flow modeling standpoint, there are two regions to be considered. One region is the SFP bulk region where the classical Navier-Stokes equations [5.6.1] are solved, with turbulence effects included. The other region is the fuel storage racks containing heat generating fuel assemblies, located near the bottom of the SFP. In this region, water flow is directed vertically upwards due to buoyancy forces through relatively small flow channels formed by rods of the fuel assemblies in each rack cell. This situation is modeled as a porous solid region with pressure drop in the flowing fluid governed by Darcy's Law as:

$$\frac{\partial P}{\partial X_i} = -\frac{\mu}{K(i)} V_i - C \rho |V| \frac{V_i}{2} \quad (5-7)$$

where  $\partial P/\partial X_i$  is the pressure gradient,  $K(i)$ ,  $V_i$  and  $C$  are the corresponding permeability, velocity and inertial resistance parameters and  $\mu$  is the fluid viscosity. These terms are added to the classic Navier-Stokes equations. The permeability and inertial resistance parameters for the rack cells loaded with fuel assemblies are determined based on friction factor correlations for the laminar flow conditions that would exist due to the low buoyancy induced velocities and the small size of the flow channels.

The St. Lucie SFP geometries require an adequate portrayal of both large scale and small scale features, spatially distributed heat sources in the racks and water inlet/outlet piping. Relatively cooler bulk water normally flows down between the fuel racks outline and wall liner, a clearance known as the downcomer. Near the bottom of the racks the flow turns from a vertical to horizontal direction into the bottom plenum, supplying cooling water to the rack cells. Heated water issuing out of the top of the racks mixes with the bulk water. An adequate modeling of

these features on the CFD program involves meshing the large scale bulk SFP region and small scale downcomer and bottom plenum regions with sufficient number of computational cells to capture both the global and local features of the flow field.

The distributed heat sources in the racks are modeled by identifying distinct heat generation zones considering recently offloaded fuel, bounding peaking effects, and the presence of background decay heat from previous offloads. Three heat generating zones are identified. The first consists of background fuel from previous offloads. The second and third zones consist of fuel from recently offloaded fuel assemblies. The two recent offload zones are differentiated by one zone with higher than average decay (hottest partial core offload batch of 73 assemblies) heat generation and the other with less than average decay heat generation (remainder of full core). This is a conservative model, since all of the fuel with higher than average decay heat is placed in a contiguous area. A uniformly distributed heat generation rate was applied throughout each distinct zone (i.e., there were no variations in heat generation rate within a single zone).

The CFD analysis was performed on the commercially available FLUENT [5.6.2] computational fluid dynamics program, which has been benchmarked under Holtec's QA program. The FLUENT code enables buoyancy flow and turbulence effects to be included in the CFD analysis. Buoyancy forces are included by specifying a temperature-dependent density for water and applying an appropriate gravity vector. Turbulence effects are modeled by relating time-varying Reynolds' Stresses to the mean bulk flow quantities with the standard k- $\epsilon$  turbulence model.

For Unit 1, the cask pit is actually a region within the rectangular SFP, but is separated from the SFP by a partial-height steel wall. Because the Unit 1 cask pit is not hydraulically isolated from the rest of the SFP, the entire SFP is modeled and evaluated. This model contains all of the fuel regions (i.e., hotter than average full core, cooler than average full core and background) discussed above.

For Unit 2, the cask pit is a completely separate body that is hydraulically connected to the rest of the SFP via a narrow fuel transfer slot. Because the Unit 2 cask pit is hydraulically isolated from the rest of the SFP, only the cask pit and the connecting slot are modeled with the temperature at the SFP end of the slot set equal to the SFP bulk temperature. The decay heat load in the rack in this cask pit is determined with fuel assemblies cooled for at least 18-months. Freshly discharged fuel cannot be placed in this rack.

Some of the major input values for this analysis are summarized in Table 5.6.1. Isometric views of the assembled CFD models for the St. Lucie units are presented in Figures 5.6.1 and 5.6.2.

### 5.7 Fuel Rod Cladding Temperature

In this section, the method to calculate the temperature of the fuel rod cladding is presented. As previously stated in Section 5.1, the maximum fuel rod cladding temperature is determined to establish that nucleate boiling is not possible while forced cooling is operating. This requires demonstrating that the highest fuel rod cladding temperatures are less than the local saturation temperature of the adjacent SFP water. The maximum fuel cladding superheat above the local water temperature is calculated for two different peak fuel rod heat emission rates.

A fuel rod can produce  $F_z$  times the average heat emission rate over a small length, where  $F_z$  is the axial peaking factor. The axial heat distribution in a rod is generally a maximum in the central region, and tapers off at its two extremities. Thus, peak cladding heat flux over an infinitesimal rod section is given by the equation:

$$q_c = \frac{Q \times F_z}{A_c} \quad (5-8)$$

where  $Q$  is the rod average heat emission and  $A_c$  is the total cladding external heat transfer area in the active fuel length region. The axial peaking factor is obtained by dividing the total peaking factor by the assembly peaking factor, both given in Table 5.6.1.

As described previously, the maximum local water temperature was computed. Within each fuel assembly sub-channel, water is continuously heated by the cladding as it moves axially upwards under laminar flow conditions. Rohsenow and Hartnett [5.7.1] report a Nusselt-number for laminar flow heat transfer in a heated channel. The film temperature driving force ( $\Delta T_f$ ) at the peak cladding flux location is calculated as follows:

$$\begin{aligned}\Delta T_f &= \frac{q_c}{h_f} \\ h_f &= \text{Nu} \frac{K_w}{D_h}\end{aligned}\tag{5-9}$$

where  $h_f$  is the waterside film heat transfer coefficient,  $D_h$  is the sub-channel hydraulic diameter,  $K_w$  is the water thermal conductivity and Nu is the Nusselt number for laminar flow heat transfer.

In order to introduce some additional conservatism in the analysis, we assume that the fuel cladding has a crud deposit resistance  $R_c$  (equal to  $0.0005 \text{ ft}^2\text{-hr-}^\circ\text{F/Btu}$ ) which covers the entire surface. Thus, including the temperature drop across the crud resistance, the cladding to water local temperature difference ( $\Delta T_c$ ) is given by the equation  $\Delta T_c = \Delta T_f + R_c \times q_c$ .

## 5.8 Results

This section contains results from the analyses performed for the postulated offload scenarios.

### 5.8.1 Maximum Pool Bulk Temperatures

For the offload/cooling scenarios described in Section 5.3, the maximum calculated bulk temperatures are summarized in Table 5.8.1. Given the conservatisms incorporated into the calculations, actual bulk temperatures will be lower than these calculated values. Figures 5.8.1

through 5.8.6 each present profiles of net decay heat load, passive heat losses and bulk temperature versus time for the evaluated transient scenarios.

The results presented in Table 5.8.1 demonstrate that calculated bulk temperatures for all scenarios other than Scenario 3 for each unit remain below the allowable bulk temperature limit. Table 5.8.1 provides the results of the bulk temperature evaluations for each unit. The maximum bulk temperature, the time after reactor shutdown that the maximum temperature is reached and the coincident net heat load are given for three core offload scenarios.

#### Scenarios 1 and 2:

The results presented in Table 5.8.1 demonstrate that the maximum calculated bulk temperatures for a partial core offload with one SFPCS pump (Scenario 1) and for a full core offload with two SFPCS pumps (Scenario 2) remain well below the allowable SFP bulk temperature limit of 150°F. Therefore, the SFP cooling system design basis is satisfied under maximum fuel assembly loading conditions with the new cask pit racks installed.

#### Scenario 3:

Scenario 3 is a full core offload with one SFPCS pump operating, a cooling scenario that is beyond the design basis for the SFP cooling system. For this abnormal condition, the bounding peak SFP temperature reaches approximately 161°F for Unit 1 and 166°F for Unit 2. These results demonstrate that no SFP boiling will occur under worst-case core offload conditions, provided at least one SFPCS cooling pump is available.

#### Scenario 4:

The evaluation concluded that the highest SFP bulk temperature for this “accident full core offload” scenario was 172°F on Unit 1 and 179°F on Unit 2. This demonstrates that no pool boiling will occur with one operating cooling pump for the worst-case decay heat load imposed on either unit's SFP.

### 5.8.2 Minimum Time-to-Boil and Maximum Boiloff Rate

For the offload/cooling described in Section 5.3, the calculated times-to-boil and maximum boil-off rates are summarized in Table 5.8.2. Given the conservatisms incorporated into the calculations, actual times-to-boil will be higher than these calculated values and actual boil-off rates will be lower than calculated.

### 5.8.3 Local Water and Fuel Cladding Temperatures

Consistent with our approach to make conservative assessments of temperature, the local water temperature calculations are performed for an SFP with a total decay heat generation equal to the calculated decay heat load coincident with the maximum SFP bulk temperature for Scenario 3. Thus, the local water temperature evaluation is a calculation of the temperature increment over the theoretical spatially uniform value due to local hot spots (due to the presence of highly heat emissive fuel assemblies). As described in Subsection 5.7, the peak fuel clad superheats (i.e., the maximum clad-to-local water temperature difference) are determined for two peak fuel rod heat emission levels. The resultant bounding superheat values were used to calculate bounding maximum fuel clad temperatures.

The numeric results of the maximum local water temperature and the bounding fuel cladding temperature evaluations are presented in Table 5.8.3. Figure 5.8.7 presents converged temperature contours in a vertical slice through the hot fuel region of the Unit 1 SFP. Figures 5.8.8 and 5.8.9, respectively, presents converged temperature contours and velocity vectors in a vertical slice through the center of the cask pit and slot.

The maximum local water is lower than the 240°F local boiling temperature at the top of the racks. The critical heat flux required for Departure from Nucleate Boiling (DNB) to occur is approximately  $10^6$  W/m<sup>2</sup>. However, the maximum heat flux from the hottest rod is only about

5400 W/m<sup>2</sup>. These results demonstrate that boiling, including nucleate boiling on clad surfaces, cannot occur.

## 5.9 References

- [5.4.1] "Heat Loss to the Ambient from Spent Fuel Pools: Correlation of Theory with Experiment", Holtec Report HI-90477, Revision 0, April 3, 1990.
- [5.4.2] "An Improved Correlation for Evaporation from Spent Fuel Pools", Holtec Report HI-971664, Revision 0.
- [5.4.3] "QA Documentation for LONGOR," Holtec Report HI-951390, Revision 0.
- [5.4.4] A.G. Croff, "ORIGEN2 - A Revised and Updated Version of the Oak Ridge Isotope Generation and Depletion Code," ORNL-5621, Oak Ridge National Laboratory, 1980.
- [5.4.5] "QA Documentation for BULKTEM," Holtec Report HI-951391, Revision 1.
- [5.4.6] "QA Documentation for TBOIL," Holtec Report HI-92832, Revision 5.
- [5.4.7] "QA Documentation for STER", Holtec Report HI-92776, Revision 11.
- [5.6.1] Batchelor, G.K., "An Introduction to Fluid Dynamics", Cambridge University Press, 1967.
- [5.6.2] "Validation of FLUENT Version 5.5", Holtec Report HI-2012642, Revision 0.
- [5.7.1] Rohsenow, N.M., and Hartnett, J.P., "Handbook of Heat Transfer", McGraw Hill Book Company, New York, 1973.

<b>Table 5.3.1</b>					
<b>Historic and Projected Fuel Offload Schedule – Unit 1</b>					
<b>End-of-Cycle Number</b>	<b>Offload Date</b>	<b>Number of Assemblies</b>	<b>Average Burnup (MWd/MTU)</b>	<b>Initial <sup>235</sup>U Enrichment (wt.%)</b>	<b>Assembly <sup>235</sup>U Weight (kgU)</b>
<b>Previously Discharged Assemblies</b>					
1	3/28/1978	52	13,239	1.948	396.884
2	4/1/1979	68	22,487	2.289	371.938
3	3/28/1980	88	28,111	2.703	375.866
4	9/11/1981	64	30,122	2.920	387.633
5	2/27/1983	87	32,760	2.970	380.742
6	10/23/1985	85	37,075	3.222	378.462
7	2/7/1987	84	38,253	3.552	372.521
8	7/11/1988	83	39,181	3.538	370.963
9	1/22/1990	101	35,795	3.355	373.567
10	10/18/1991	84	38,107	3.514	373.112
11	3/31/1993	84	40,374	3.615	371.897
12	10/26/1994	84	36,952	3.293	383.019
13	4/29/1996	88	38,399	3.470	397.328
14	10/20/1997	63	34,161	3.124	398.425
15	9/13/1999	89	40,136	3.668	396.868
16	4/9/2001	97	56,100	3.843	396.168
17	9/13/2002	105	56,100	4.50	380
18	3/13/2004	105	56,100	4.50	380
19	9/13/2005	105	56,100	4.50	380
20	3/13/2007	105	56,100	4.50	380
21	9/13/2008	105	56,100	4.50	380
<b>Recently Discharged Assemblies</b>					
partial core	3/13/2010	105	56,100	4.50	380
full core	3/13/2010	73	56,100	4.50	380
		72	50,490		
		72	42,075		

<b>Table 5.3.2</b>					
<b>Historic and Projected Fuel Offload Schedule – Unit 2</b>					
<b>End-of-Cycle Number</b>	<b>Offload Date</b>	<b>Number of Assemblies</b>	<b>Average Burnup (MWd/MTU)</b>	<b>Initial <sup>235</sup>U Enrichment (wt.%)</b>	<b>Assembly <sup>235</sup>U Weight (kgU)</b>
<b>Previously Discharged Assemblies</b>					
1	10/12/1984	80	12,832	1.773	387.248
2	4/5/1986	84	27,165	2.356	363.215
3	10/2/1987	72	34,035	2.977	380.255
4	1/31/1989	84	39,568	3.563	378.352
5	9/30/1990	76	40,258	3.448	380.525
6	4/26/1992	68	44,186	3.586	382.636
7	3/31/1994	80	44,977	3.905	382.946
8	10/8/1995	84	44,776	3.995	379.540
9	4/14/1997	64	46,144	3.817	379.052
10	11/9/1998	64	46,629	3.716	383.701
11	4/25/2000	77	59,160	4.189	391.774
12	05/9/2000	105	59,160	4.50	380
13	11/9/2001	105	59,160	4.50	380
14	05/9/2003	105	59,160	4.50	380
15	11/9/2004	105	59,160	4.50	380
16	05/9/2006	105	59,160	4.50	380
17	11/9/2007	105	59,160	4.50	380
18	05/9/2009	105	59,160	4.50	380
19	11/9/2010	105	59,160	4.50	380
20	05/9/2012	105	59,160	4.50	380
21	11/9/2013	105	59,160	4.50	380
<b>Recently Discharged Assemblies</b>					
partial core	15/9/2015	105	59,160	4.50	380
full core	15/9/2015	73	59,160	4.50	380
		72	53,244		
		72	44,370		

<b>TABLE 5.4.1</b>		
<b>Key Input Data for Bulk Temperature Evaluation</b>		
<b>Parameter</b>	<b>Unit 1 Value</b>	<b>Unit 2 Value</b>
Number of Storage Cells in SFP	1,849	1,809
Maximum Refueling Batch Size	105 assemblies	105
Reactor Thermal Power		
Current	2,700 MW(t)	2,700 MW(t)
Upated	2,916 MW(t)	2,916 MW(t)
Reactor Thermal Power Uncertainty	2%	2%
Reactor Core Size	217 assemblies	217 assemblies
Bounding Maximum Inlet CCW Temperature	100°F	100°F
SFPCS HX Coolant Flow Rate	2850 gpm	2850 gpm
SFP Water Flow to SFPCS HX		
One Operating Pump	2000 gpm	1746 gpm
Two Operating Pumps	3000 gpm	1368 gpm
Minimum In-Core Hold Time	120 hrs	120 hrs
Minimum Fuel Assembly Transfer Rate		
Partial Core	Instantaneous	Instantaneous
Full Core without Active Failure	Instantaneous	Instantaneous
Full Core with Single Active Failure	Instantaneous	8 per hour

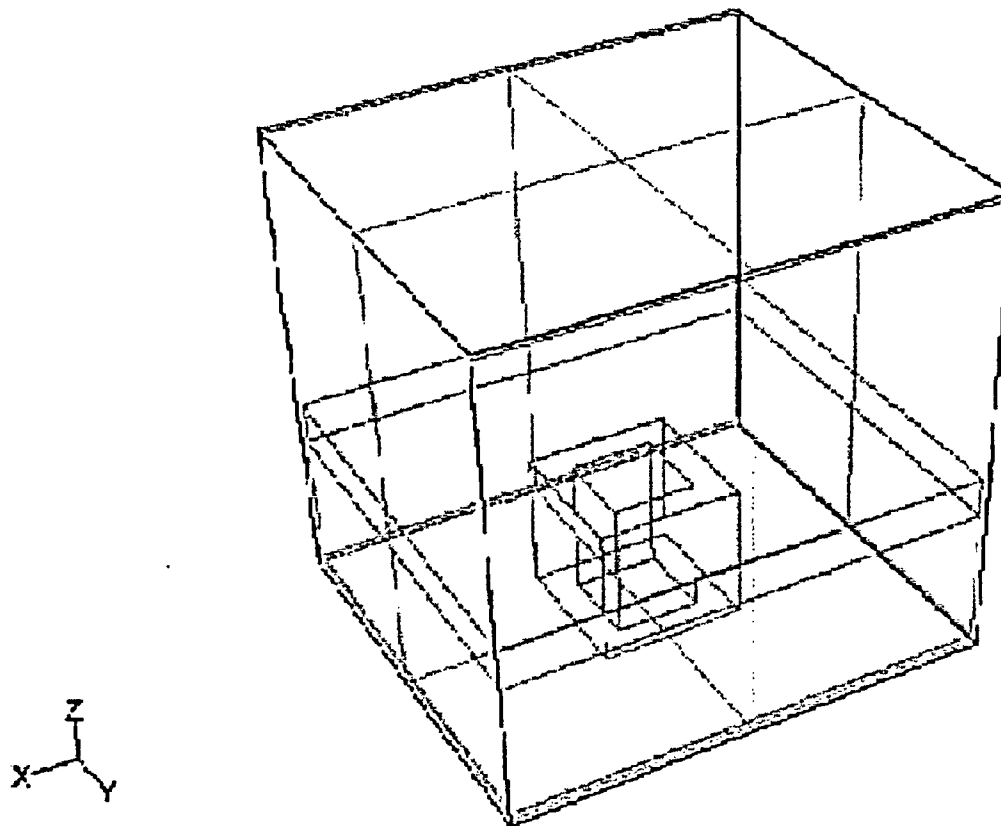
<b>Table 5.5.1</b>		
<b>Key Input Data for Time-To-Boil Evaluation</b>		
<b>Parameter</b>	<b>Unit 1 Value</b>	<b>Unit 2 Value</b>
SFP Surface Area	1221 ft <sup>2</sup>	1194 ft <sup>2</sup>
Minimum Pool Water Depth	38 feet and 4 inches	38 feet
Fuel Racks Displaced Volume	853 ft <sup>3</sup>	856 ft <sup>3</sup>
Fuel Assemblies Displaced Volume	6,257 ft <sup>3</sup>	6,121 ft <sup>3</sup>
SFP Net Water Volume	39,480 ft <sup>3</sup>	44,307 ft <sup>3</sup>

<b>Table 5.6.1</b>		
<b>Key Design Data for Local Temperature Evaluation</b>		
<b>Parameter</b>	<b>Unit 1 Value</b>	<b>Unit 2 Value</b>
Assembly Peaking Factor	1.65	1.75
Total Peaking Factor	2.80	3.09
Cooled SFP Water Flow Rate through SFPCS Heat Exchanger(s)	1×10 <sup>6</sup> lb/hr	Not Applicable
Hydraulically Limiting Fuel Assembly	Combustion Engineering 16×16	Combustion Engineering 16×16
Fuel Rod Outer Diameter	0.382 inches	0.382 inches
Active Fuel Length	134 inches	134 inches
Number of Rods per Assembly	236 rods	236 rods
Rack Cell Inner Dimension	8.58 inches	8.58 inches
Rack Cell Length	169.25 inches	172.75 inches
Modeled Bottom Plenum Height	3 inches	5 inches

<b>Table 5.8.1</b>			
<b>Result of Transient Bulk Temperature Evaluations</b>			
<b>Scenario</b>	<b>Maximum Bulk Temperature (°F)</b>	<b>Time After Reactor Shutdown (hrs)</b>	<b>Coincident Net Heat Load (Btu/hr)</b>
<b>Unit 1 Results</b>			
1 - Partial Core	134.47	137	21.31×10 <sup>6</sup>
2 - Full Core	125.01	128	39.38×10 <sup>6</sup>
3 - Full Core	161.19	137	37.17×10 <sup>6</sup>
<b>Unit 2 Results</b>			
1 - Partial Core	139.58	140	22.20×10 <sup>6</sup>
2 - Full Core	142.87	133	39.81×10 <sup>6</sup>
3 - Full Core	165.89	159	36.30×10 <sup>6</sup>

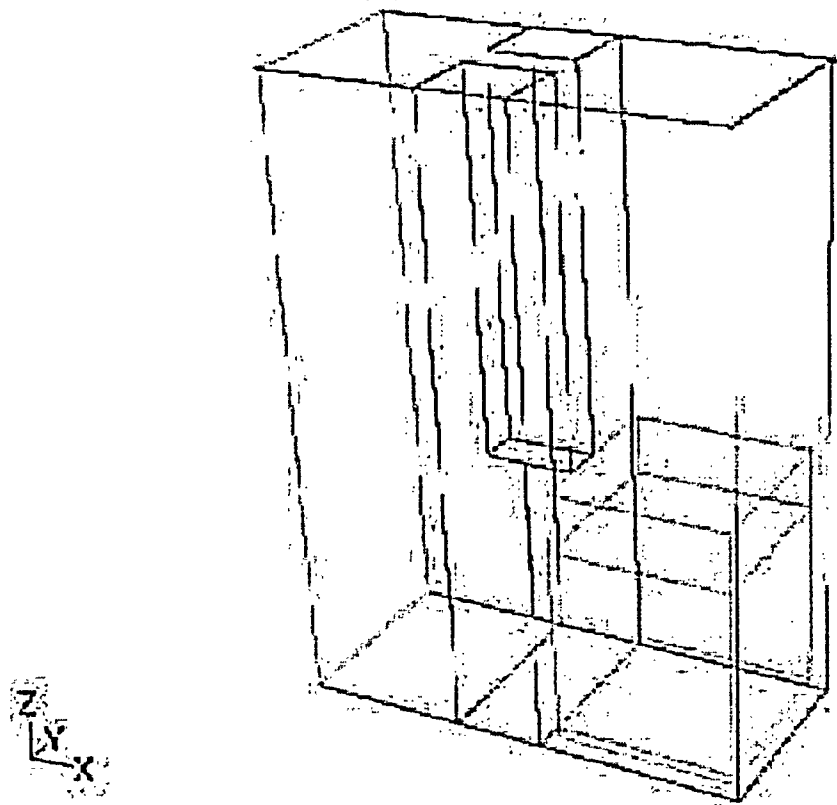
<b>Table 5.8.2</b>			
<b>Results of Loss-of-Forced Cooling Evaluations</b>			
<b>Scenario</b>	<b>Minimum Time-to-Boil</b>	<b>Maximum Boiloff Rate</b>	<b>Makeup Water Rate to Maintain 9' of Water Above Fuel</b>
<b>Unit 1 Results</b>			
Partial Core	9.39 hrs	45.98 gpm	28 gpm
Full Core	3.33 hrs	76.23 gpm	52 gpm
<b>Unit 2 Results</b>			
Partial Core	9.42 hrs	44.98 gpm	30 gpm
Full Core	3.10 hrs	84.74 gpm	54 gpm

<b>Table 5.8.3</b>			
<b>Results of Maximum Local Water and Fuel Cladding Temperature Evaluations</b>			
	<b>Maximum Local Water Temp. (°F)</b>	<b>Bounding Fuel Clad Superheat (°F)</b>	<b>Bounding Fuel Clad Temperature (°F)</b>
Unit 1	190.0	51.96	241.96
Unit 2	189.1	3.25	192.35



Grid		Jan 18, 2002 FLUENT 5.5 (3d, segregated, kb)
------	--	---

Figure 5.6.1 – Unit 1 CFD Model Isometric View



GFD Jun 27 2002  
FLUENT 5.5 (3c; segregated; ke)

Figure 5.6.2 – Unit 2 CFD Model Isometric View

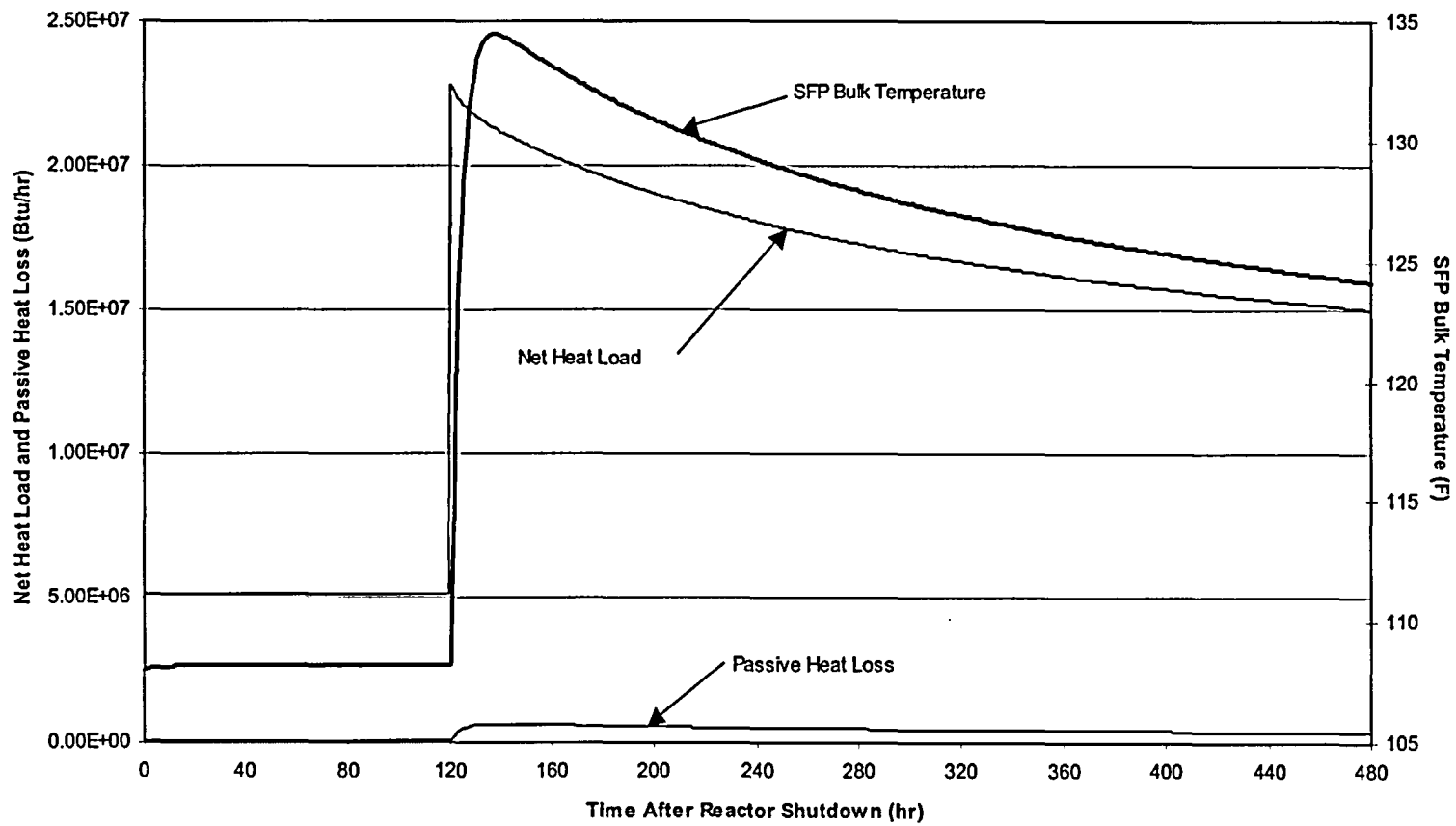


Figure 5.8.1 – Unit 1 Scenario 1 – Partial Core Discharge with Coincident Single Active Failure

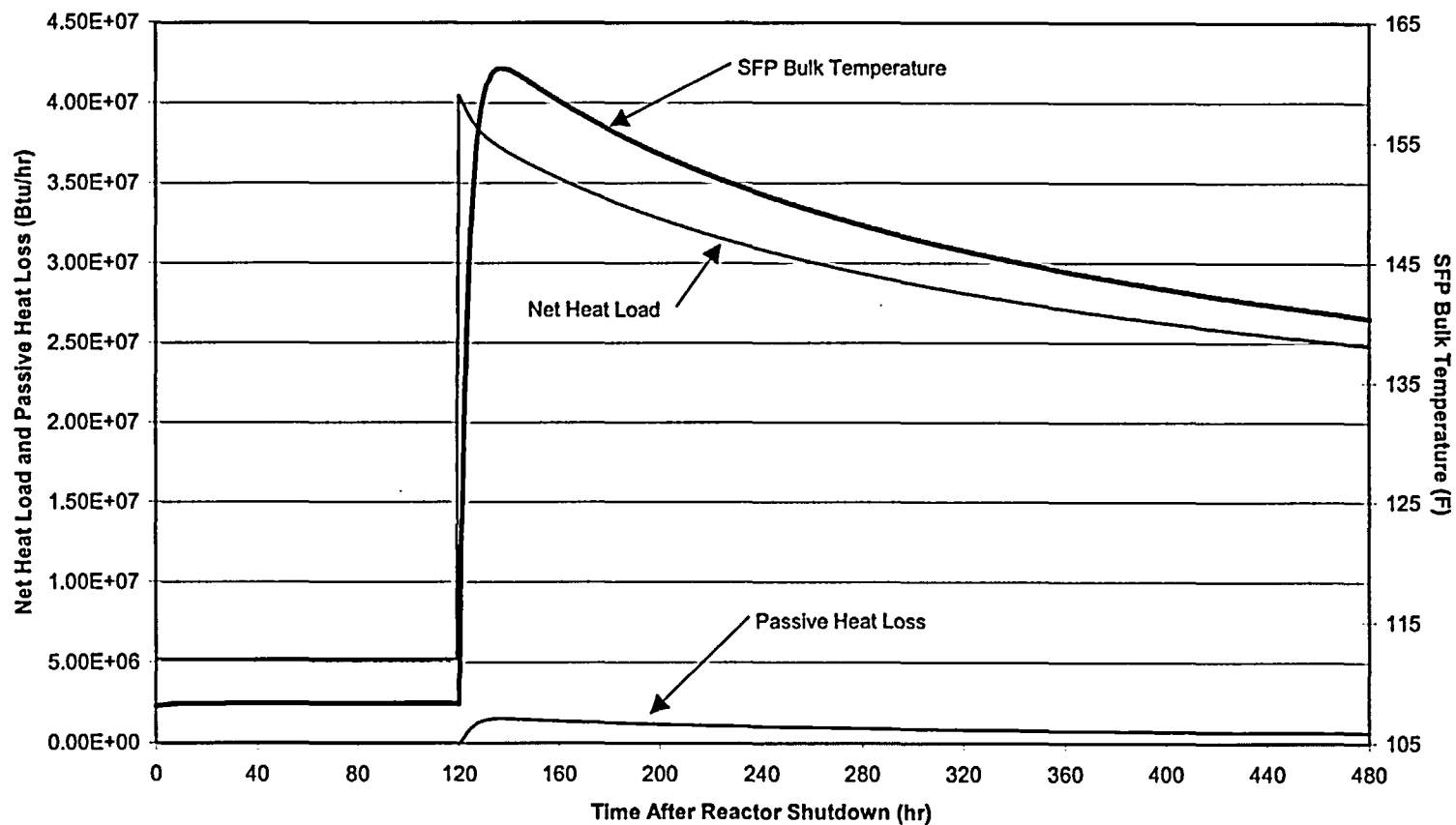


Figure 5.8.2 – Unit 1 Scenario 2a – Full Core Discharge with Coincident Single Active Failure

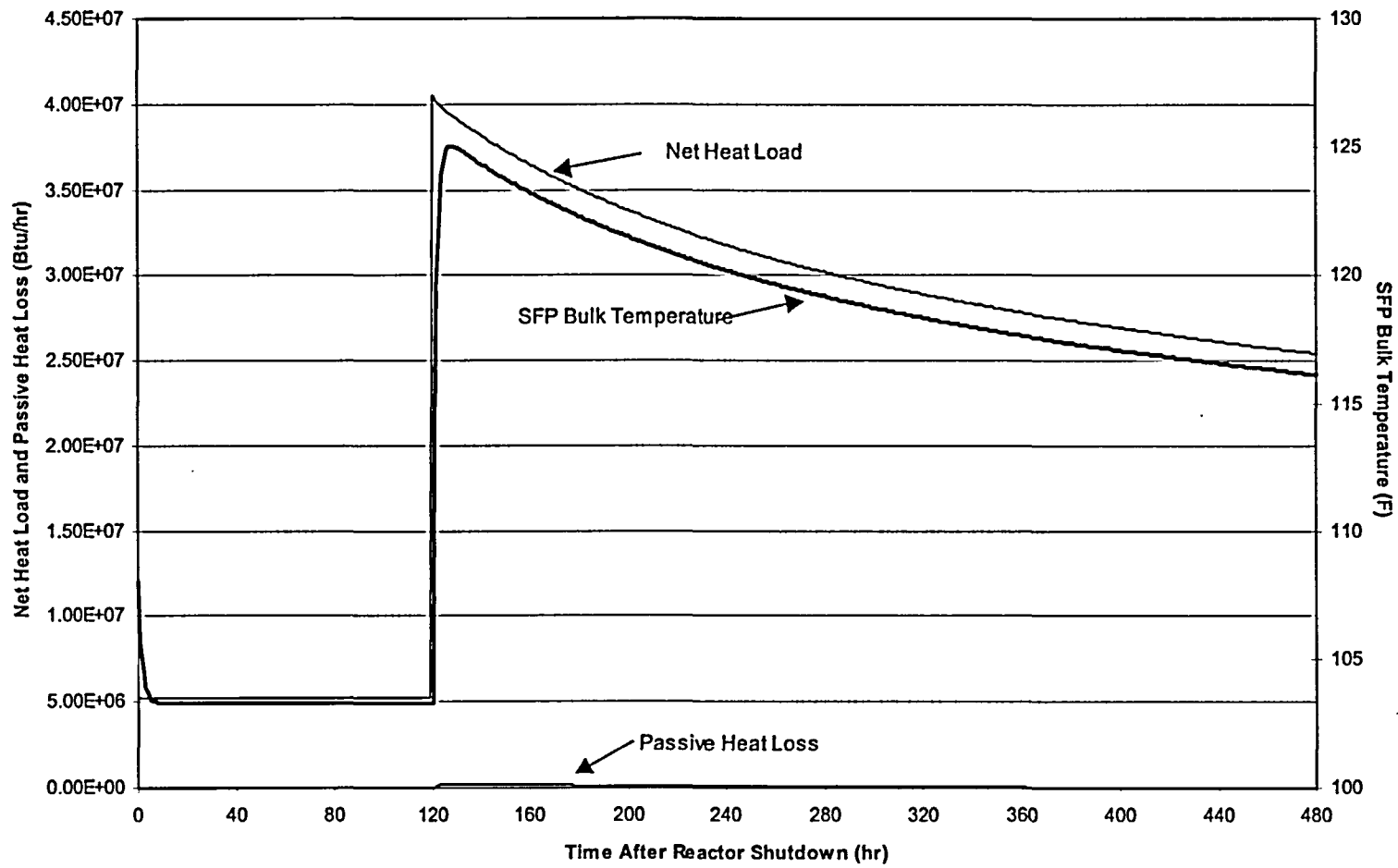


Figure 5.8.3 – Unit 1 Scenario 2b – Full Core Discharge without Coincident Single Active Failure

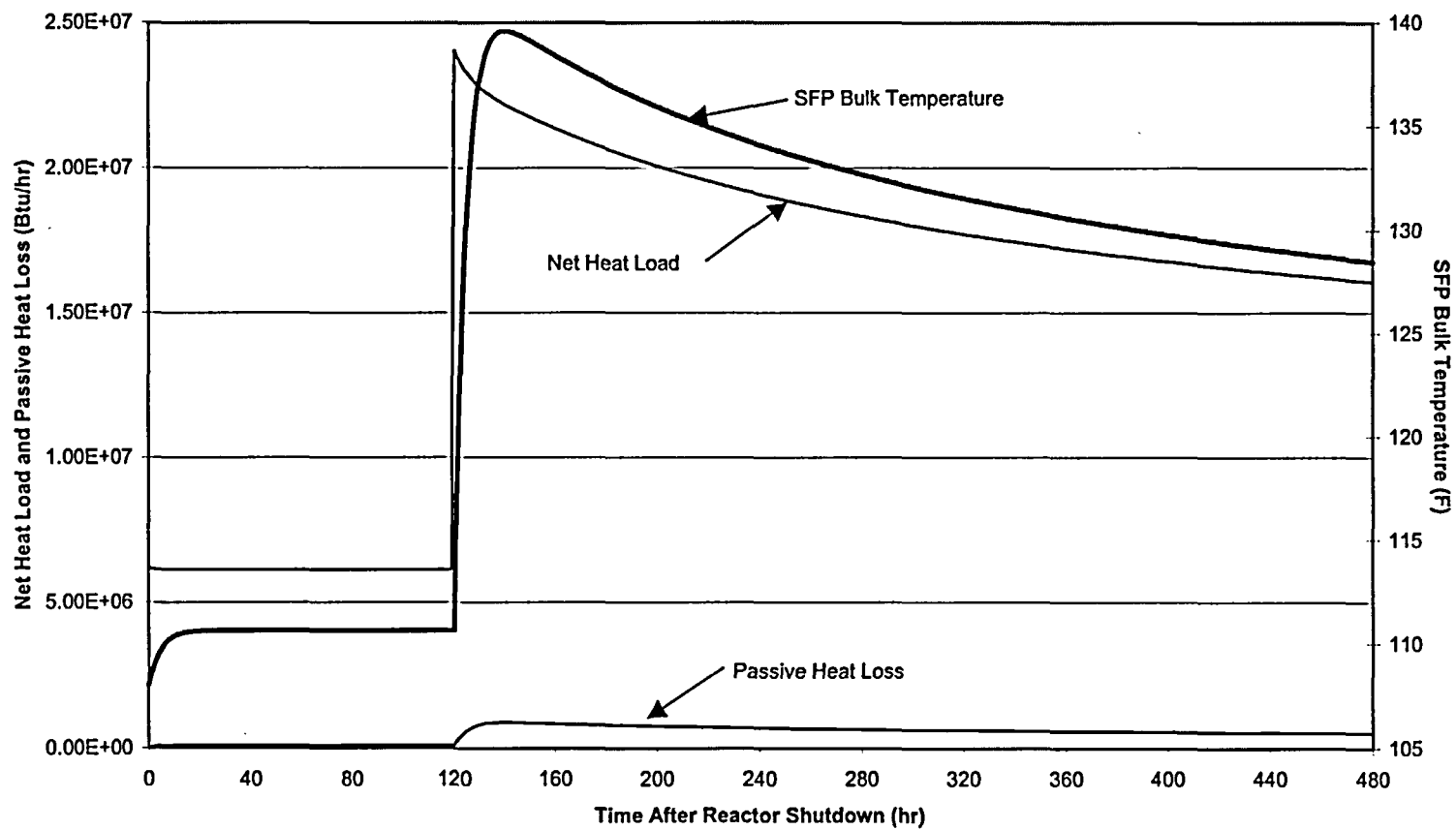


Figure 5.8.4 – Unit 2 Scenario 1 – Partial Core Discharge with Coincident Single Active Failure

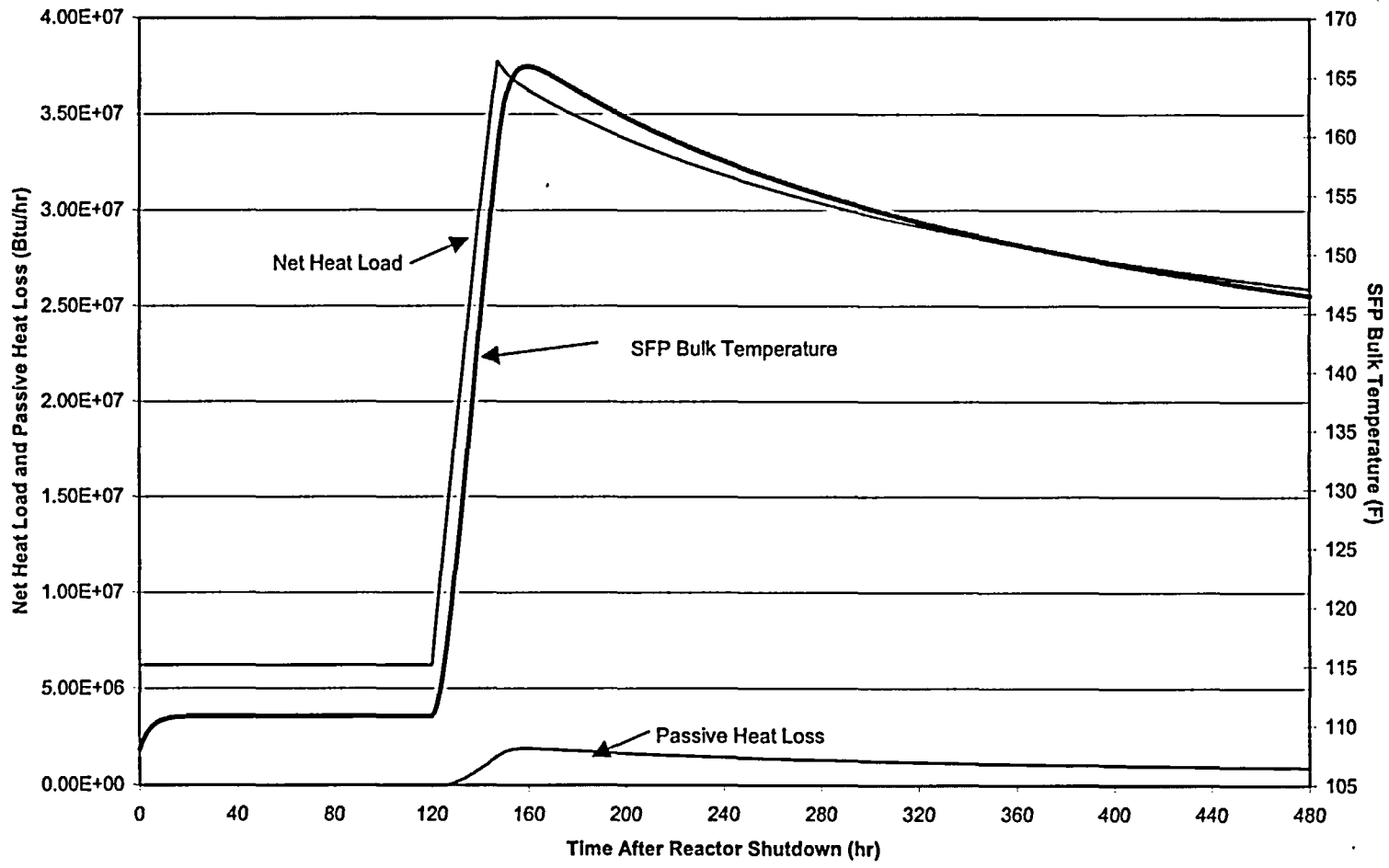


Figure 5.8.5 – Unit 2 Scenario 2a – Full Core Discharge with Coincident Single Active Failure

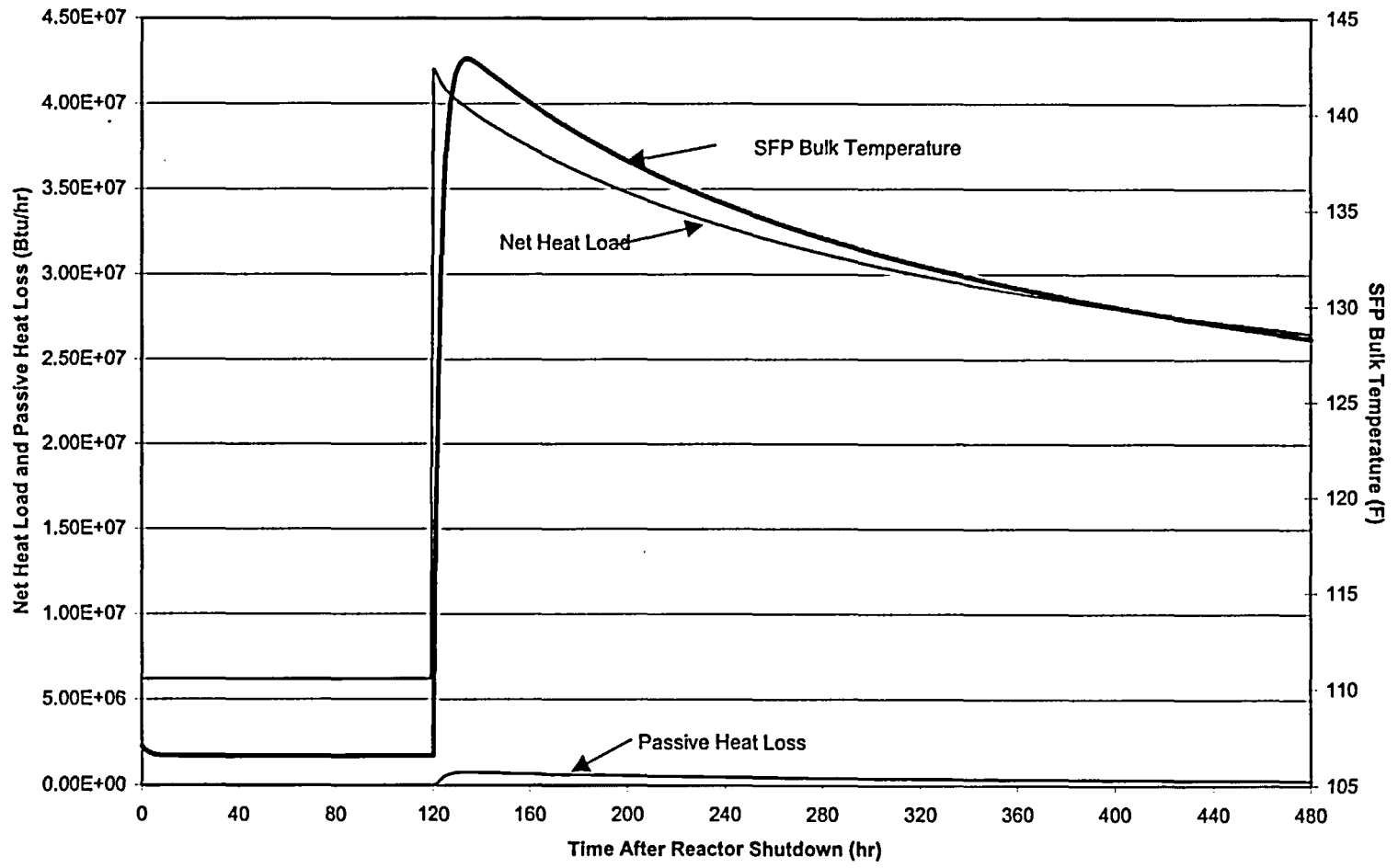


Figure 5.8.6 – Unit 2 Scenario 2b – Full Core Discharge without Coincident Single Active Failure

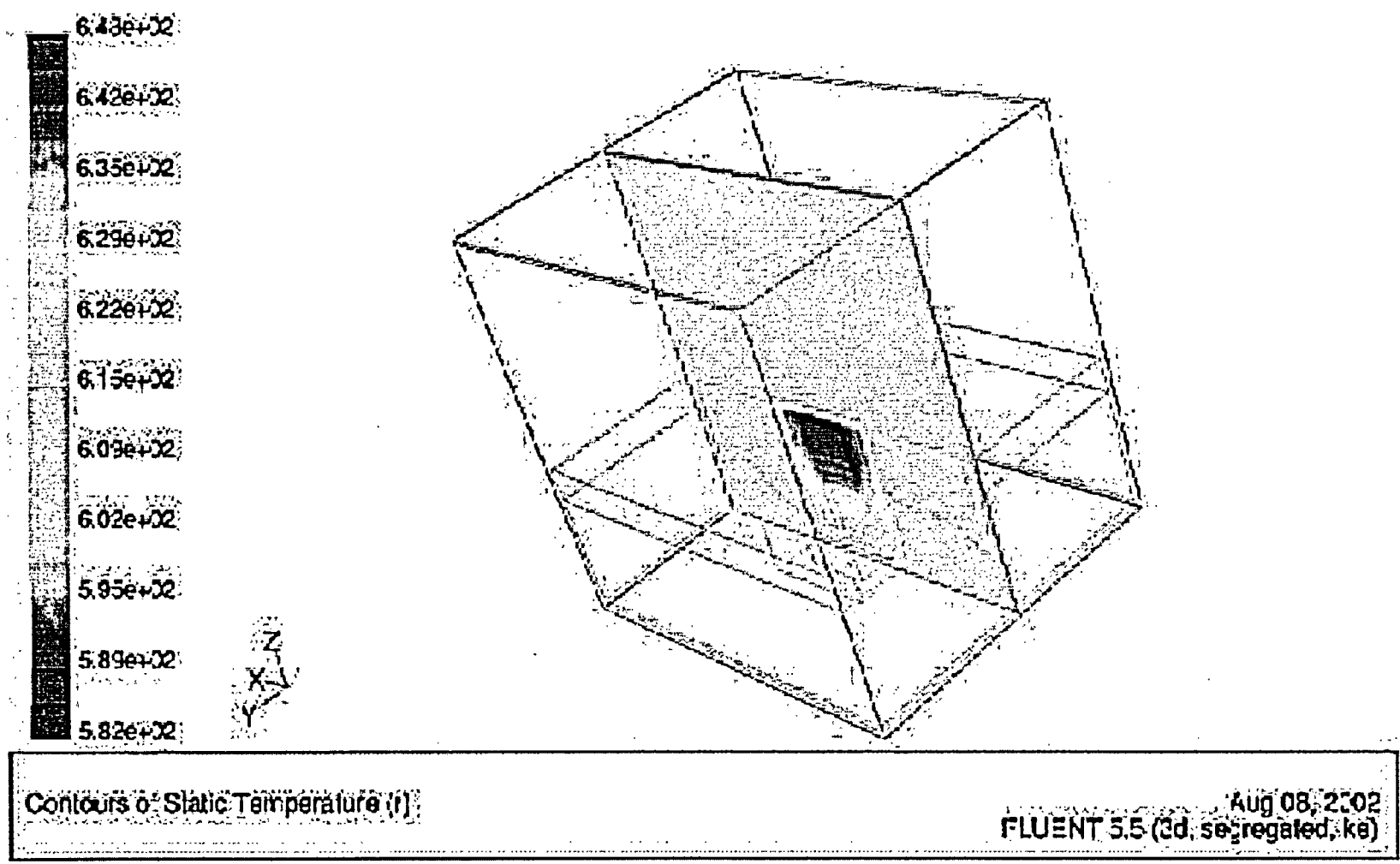


Figure 5.8.7 – Unit 1 CFD Model with Converged Temperature Contours

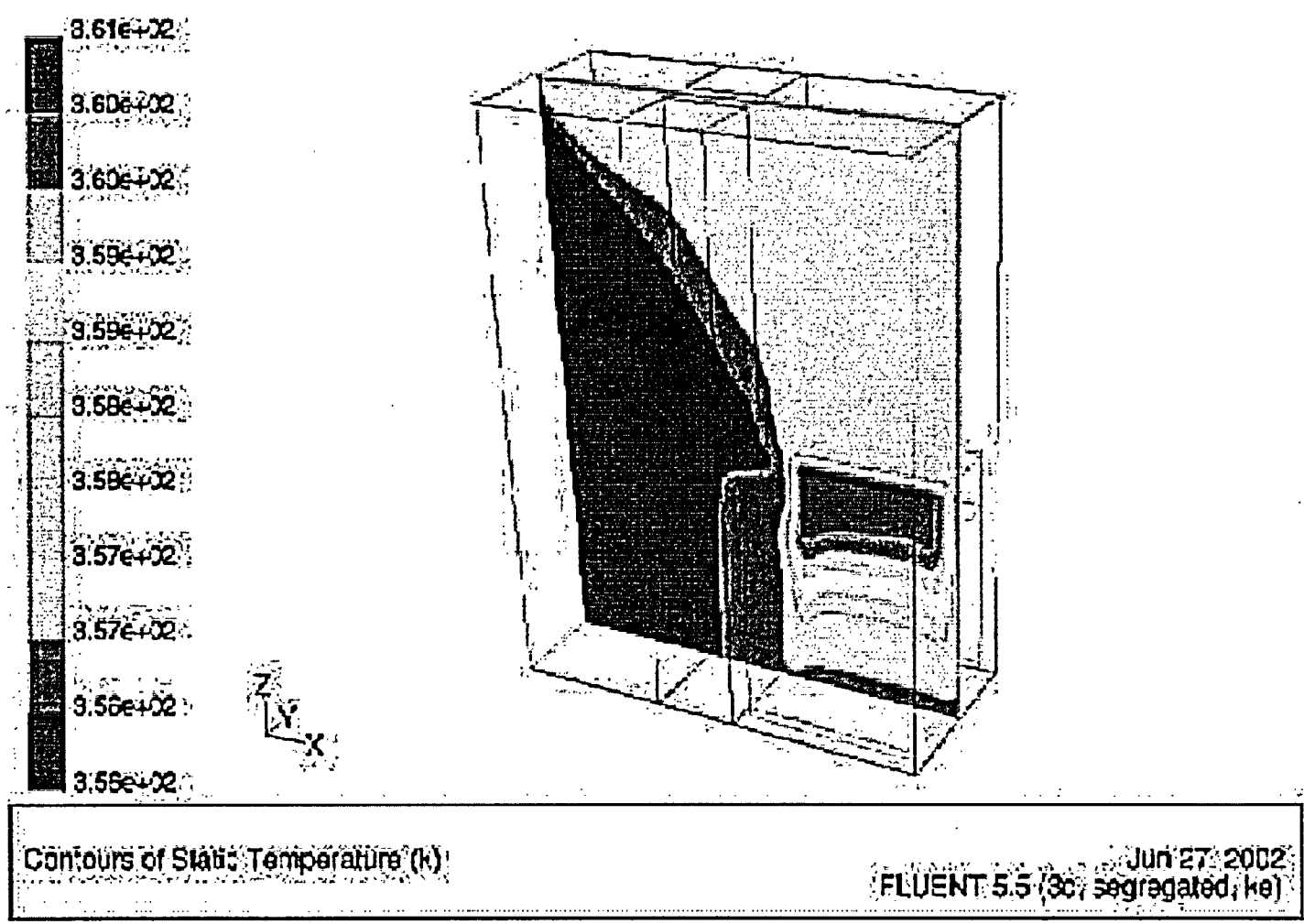


Figure 5.8.8 – Unit 2 CFD Model with Converged Temperature Contours

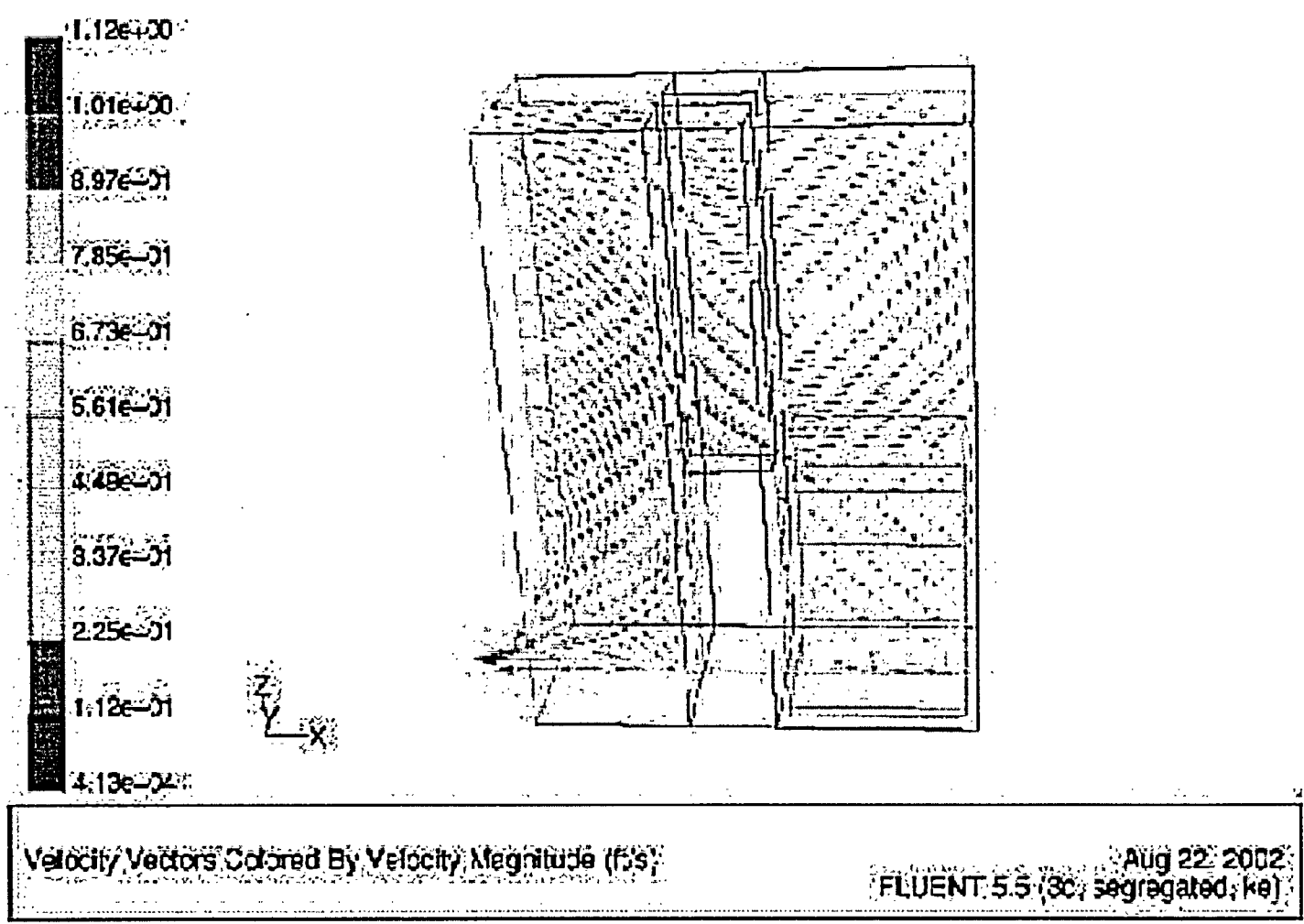


Figure 5.8.9 – Unit 2 CFD Model with Converged Velocity Vectors

## 6.0 STRUCTURAL/SEISMIC CONSIDERATIONS

### 6.1 Introduction

This section considers the structural adequacy of the new fuel racks in each of the Plant St. Lucie Cask Pit Areas under all loads postulated for normal, seismic, and accident conditions. The analyzed storage rack configurations for Unit 1 and Unit 2 are depicted in Figures 1.1.1 and 1.1.2, respectively.

The analyses undertaken to confirm the structural integrity of the racks are performed in compliance with the USNRC Standard Review Plan [6.1.1] and the OT Position Paper [6.1.2]. For each of the analyses, an abstract of the methodology, modeling assumptions, key results, and summary of parametric evaluations are presented. Delineation of the relevant criteria is discussed in the text associated with each analysis.

### 6.2 Overview of Rack Structural Analysis Methodology

The response of a free-standing rack module to seismic inputs is highly nonlinear and involves a complex combination of motions (sliding, rocking, twisting, and turning), resulting in impacts and friction effects. Some of the unique attributes of the rack dynamic behavior include a large fraction of the total structural mass in a confined rattling motion, friction support of rack pedestals against lateral motion, and large fluid coupling effects due to deep submergence and independent motion of closely spaced adjacent structures.

Linear methods, such as modal analysis and response spectrum techniques, cannot accurately simulate the structural response of such a highly nonlinear structure to seismic excitation. An accurate simulation is obtained only by direct integration of the nonlinear equations of motion with the three pool slab acceleration time-histories applied as the forcing functions acting simultaneously.

The DYNARACK solver [6.2.4] is the vehicle utilized in this project to simulate the dynamic behavior of the complex storage rack structures. The following sections provide the basis for this selection and discussion on the development of the methodology.

### 6.2.1 Background of Analysis Methodology

Reliable assessment of the stress field and kinematic behavior of the rack modules calls for a conservative dynamic model incorporating all *key attributes* of the actual structure. This means that the model must feature the ability to execute the concurrent motion forms compatible with the free-standing installation of the modules. The model must possess the capability to effect momentum transfers which occur due to rattling of fuel assemblies inside storage cells and the capability to simulate lift-off and subsequent impact of support pedestals with the rack platform. The contribution of the water mass in the interstitial spaces around the rack modules and within the storage cells must be modeled in an accurate manner, since erring in quantification of fluid coupling on either side of the actual value is no guarantee of conservatism.

The Coulomb friction coefficient at the pedestal-to-rack platform interface may lie in a rather wide range and a conservative value of friction cannot be prescribed *a priori*. In fact, a perusal of results of rack dynamic analyses in numerous docket (Table 6.2.1) indicates that an upper bound value of the coefficient of friction often maximizes the computed rack displacements as well as the equivalent elastostatic stresses.

In short, there are a large number of parameters with potential influence on the rack kinematics. The comprehensive structural evaluation must deal with all of these without sacrificing conservatism.

Briefly, the 3-D rack model dynamic simulation, involving one or more spent fuel racks, handles the array of variables as follows:

Interface Coefficient of Friction: Parametric runs are made with upper bound and lower bound values of the coefficient of friction. The limiting values are based on experimental data which have been found to be bounded by the values 0.2 and 0.8. Simulations are also performed with the array of pedestals having randomly chosen coefficients of friction in a Gaussian distribution with a mean of 0.5 and lower and upper limits of 0.2 and 0.8, respectively. In the fuel rack simulations, the Coulomb friction interface

between rack support pedestal and rack platform is simulated by piecewise linear (friction) elements. These elements function only when the pedestal is physically in contact with the platform.

Rack Beam Behavior: Rack elasticity, relative to the rack base, is included in the model by introducing linear springs to represent the elastic bending action, twisting, and extensions.

Impact Phenomena: Compression-only gap elements are used to provide for opening and closing of interfaces such as the pedestal-to-rack platform interface, and the fuel assembly-to-cell wall interface. These interface gaps are modeled using nonlinear spring elements. The term "nonlinear spring" is a generic term used to denote the mathematical representation of the condition where a restoring force is not linearly proportional to displacement.

Fuel Loading Scenarios: The fuel assemblies are conservatively assumed to rattle in unison, which obviously exaggerates the contribution of impact against the cell wall.

Fluid Coupling: Holtec International extended Fritz's classical two-body fluid coupling model to multiple bodies and utilized it to perform the first two-dimensional multi-rack analysis (Diablo Canyon, ca. 1987). Subsequently, laboratory experiments were conducted to validate fluid coupling theory. This technology was incorporated in the computer code DYNARACK [6.2.4]. This development was first utilized in Chinshan, Oyster Creek, and Shearon Harris plants [6.2.1, 6.2.3] and, subsequently, in numerous other rerack projects. Despite the fact that the analyses for this project require the simulation of only one rack, the DYNARACK code, is used for this project.

### 6.3 Description of Racks

Rack material is defined in Table 6.3.1.

As may be seen in the rack layouts provided in Figures 1.1.1 and 1.1.2, the nominal distance between the side of the Unit 1 rack and the walls is approximately 4" in the N-S direction and approximately 6" in the E-W direction, and the nominal distance between the side of the Unit 2 rack and the walls in each

direction is approximately 9". The dimensions are chosen to ensure that the rack is centered within the Cask Pit. During rack installation, these dimensions will be met to the extent possible, considering rack and wall straightness and leveling tolerances. The walls and distances separating the Cask Pit Area from the Spent Fuel Pool will effectively eliminate fluid coupling between the proposed rack in each Unit and the racks in the adjacent SFP. The excitation of the proposed racks will be primarily dependent on the motion of the floor and walls of the Cask Pit. The independence of motion of the proposed racks from the racks located in the adjacent SFP allows single rack analysis to produce accurate predictions of the rack motion during dynamic simulations.

The Cartesian coordinate system utilized within the rack dynamic model has the following nomenclature:

- x = Horizontal axis along plant East
- y = Horizontal axis along plant North
- z = Vertical axis upward from the rack base

### 6.3.1 Fuel Weights

The maximum dry weight for a Unit 1 fuel assembly is 1336 lbs. The maximum weight considering an integrally stored Control Element Assembly (CEA) is 1437 lbs. The Unit 1 dynamic rack simulations used a dry weight of 1423 lbs for every fuel assembly to account for CEAs being stored. The difference between the maximum weight with a CEA and that used in the evaluation represents a potential increase of less than 1%. The maximum dry fuel weight for Unit 2 is 1365 lbs. However, for the Unit 2 dynamic rack simulations, a higher fuel weight value of 1384 lbs is used to account for control components being stored along with fuel assemblies. The actual maximum weight of a fuel assembly plus CEA is 1452 lbs. However, this represents an increase of less than 5% over the value used in the evaluations and the analyses conservatively consider the increased weight in the assemblies at every location. Nevertheless, even if every fuel cell contained the heaviest fuel assembly type and an integrally stored CEA the weight increase would not represent a significant impact on actual loads and stresses for either rack. The conservatism discussed below in Section 6.5.1.1 (especially item c) more than compensate for the possibility of an additional 68 pounds in each cell. Given the small weight difference and large margins of safety in the design, restrictions on CEA storage are not warranted for either Unit.

#### 6.4 Synthetic Time-Histories

The synthetic time-histories in three orthogonal directions (N-S, E-W, and vertical) are generated in accordance with the provisions of SRP 3.7.1 [6.4.1]. For Unit 1 the structural damping is taken to be 2% for both OBE and SSE, and for Unit 2 the structural damping is taken to be 2% for OBE and 3% for SSE, based on the FSAR for the respective Units. The mass of the model is comprised primarily of the fuel assemblies, which rattle within the storage cells during the seismic event. This rattling behavior, and the associated friction between model components, warrants use of the damping factors associated with bolted and riveted assemblies.

*In order to prepare an acceptable set of acceleration time-histories, Holtec International's proprietary code GENEQ [6.4.2] is utilized.*

A preferred criterion for the synthetic time-histories in SRP 3.7.1 calls for both the response spectrum and the power spectral density corresponding to the generated acceleration time-history to envelope their target (design basis) counterparts with only finite enveloping inflections. The time-histories for the pools have been generated to satisfy this preferred criterion. The seismic files also satisfy the requirements of statistical independence mandated by SRP 3.7.1.

Figures 6.4.1 through 6.4.12 provide plots of the time-history accelerograms, which were generated for 20-second duration OBE and SSE events. These artificial time-histories are used in all non-linear dynamic simulations of the racks.

Results of the correlation function of the three time-histories are given in Tables 6.4.1 and 6.4.2. Absolute values of the correlation coefficients are shown to be less than 0.15, indicating that the desired statistical independence of the three data sets has been met.

## 6.5 Modeling Methodology

Recognizing that the analysis work effort must deal with both stress and displacement criteria, the sequence of model development and analysis steps that are undertaken are summarized in the following:

- a. Prepare 3-D dynamic rack models suitable for a time-history analysis. Include all fluid coupling interactions and mechanical coupling appropriate to performing an accurate non-linear simulation.
- b. Perform 3-D dynamic analyses on various physical conditions (such as coefficient of friction and extent of cells containing fuel assemblies). Archive appropriate displacement and load outputs from the dynamic model for post-processing.
- c. Perform stress analysis of high stress areas for the limiting case of all the rack dynamic analyses. Demonstrate compliance with ASME Code Section III, Subsection NF limits on stress and displacement.

### 6.5.1 Model Details for Spent Fuel Racks

The dynamic modeling of the rack structure is prepared with special consideration of all nonlinearities and parametric variations. Particulars of modeling details and assumptions for the analysis of racks are given in the following:

#### 6.5.1.1 Model Details and Assumptions

- a. The fuel rack structure motion is captured by modeling the rack as a 12 degree-of-freedom structure. Movement of the rack cross-section at any height is described by six degrees-of-freedom of the rack base and six degrees-of-freedom at the rack top. In this manner, the response of the module, relative to the baseplate, is captured in the dynamic analyses once suitable springs are introduced to couple the rack degrees-of-freedom and simulate rack stiffness.
- b. Rattling fuel assemblies within the rack are modeled by five lumped masses located at H, .75H, .5H, .25H, and at the rack base (H is the rack height measured above the baseplate). Each lumped fuel mass has two horizontal displacement degrees-of-freedom. Vertical motion of the fuel assembly mass is assumed equal to rack vertical motion at the baseplate level. The centroid of each fuel assembly mass can be located off-center, relative to the rack structure centroid at that level, to simulate a partially loaded rack.

- c. Seismic motion of a fuel rack is characterized by random rattling of fuel assemblies in their individual storage locations. All fuel assemblies are assumed to move in-phase within a rack. This exaggerates computed dynamic loading on the rack structure and, therefore, yields conservative results.
- d. Fluid coupling between rack and fuel assemblies, and between rack and wall, is simulated by appropriate inertial coupling in the system kinetic energy. Inclusion of these effects uses the methods of References [6.5.2, 6.5.3].
- e. Fluid damping and form drag are conservatively neglected.
- f. Sloshing is found to be negligible at the top of the rack and is, therefore, neglected in the analysis of the rack.
- g. Potential impacts between the cell walls of the new racks and the contained fuel assemblies are accounted for by appropriate compression-only gap elements between masses involved. The possible incidence of rack-to-wall impact is simulated by similar gap elements at the top and bottom of the rack in two horizontal directions. Bottom gap elements are located at the baseplate elevation. The initial gaps reflect the presence of baseplate extensions, and the gap element stiffnesses are chosen to simulate local structural detail.
- h. Pedestals and rack support platforms are modeled by gap elements in the vertical direction and as "rigid links" for transferring horizontal friction forces. Local pedestal vertical spring stiffness accounts for floor elasticity and for local rack elasticity just above the pedestal.
- i. Each pedestal support is linked to the supporting rack platform by two piece-wise linear friction springs. The rack platform is assumed to travel along with the pool liner during seismic events with possible slippage occurring between the support pedestal and the rack platform. The flexibility of the supporting rack platform is also addressed by the evaluation.
- j. Rattling of fuel assemblies inside the storage locations causes the gap between fuel assemblies and cell wall to change from a maximum of twice the nominal gap to a theoretical zero gap. Fluid coupling coefficients are based on the nominal gap in order to provide a conservative measure of fluid resistance to gap closure.
- k. The model for the rack is considered supported, at the base level, on four pedestals modeled as non-linear compression only gap spring elements and eight piecewise linear friction spring elements. These elements are properly located with respect to the centerline of the rack beam, and allow for arbitrary rocking and sliding motions.
- l. The nominal rack to wall dimensions shown in Figures 1.1.1 and 1.1.2 are the gaps surrounding the respective racks at the start of each dynamic simulation.

- m. The racks and support platforms are level and plumb such that the rack-to-wall dimensions are maintained over the rack vertical length).

#### 6.5.1.2 Element Details

Figure 6.5.1 shows a schematic of the dynamic model of the rack. The schematic depicts many of the characteristics of the model including all of the degrees-of-freedom and some of the spring restraint elements.

Table 6.5.1 provides a complete listing of each of the 22 degrees-of-freedom for a rack model. Six translational and six rotational degrees-of-freedom (three of each type on each end) describe the motion of the rack structure. Rattling fuel mass motions (shown at nodes 1\*, 2\*, 3\*, 4\*, and 5\* in Figure 6.5.1) are described by ten horizontal translational degrees-of-freedom (two at each of the five fuel masses). The vertical fuel mass motion is assumed (and modeled) to be the same as that of the rack baseplate. The five masses are connected to each other by an axially rigid member, which enables the fuel masses to vibrate in unison with the rack in the vertical direction. However, the connecting element has no bending or shear stiffness. Therefore, the masses vibrate independently in the horizontal direction and are driven by the inertia loads and local impact loads. The five fuel masses are connected to the rack model via impact gap elements. Impact loads between the fuel masses and the rack cell wall are obtained upon closure of this gap element. The gap dimensions are determined at each time step by establishing the independent displacements of the fuel masses and the rack geometric centerline displacement corresponding to the same elevation. Therefore, the outer boxes surrounding the fuel masses shown in Figure 6.5.1 depict the inside of the fuel cell.

The assumption of five fuel masses connected to the rack in the horizontal direction by impact gap elements is conservative in several ways. The actual fuel assembly would impact the inside of the cell walls at the rod spacer grid locations. Since there are many more than five grids, the tributary length of fuel assembly associated with each actual grid would be less than that provided by the quarter points associated with only five masses. The masses at each of the nodes of the modeled fuel is much greater than the masses associated with each length of fuel assembly centered on a spacer grid. Therefore, the

resulting dynamic impact forces would be greater. Because of the fact that the fuel masses are connected by an element that has no bending or shear stiffness, the fuel nodes come into contact with the inside of the fuel cell when the rack moves a sufficient distance to close the gap between fuel node and cell node. In other words, the rack walls actually strike and drive the fuel assembly mass during a dynamic event. The rack motion is driven by the pool floor. The inertia of the conservatively modeled masses produce a greater impact force upon closure of the gap element than the smaller inertia of the actual masses associated with each spacer grid.

Each of the five modeled fuel masses contains the mass associated with that respective elevation for every fuel assembly within the storage module. All of the fuel assemblies are modeled as one. Therefore, all of the fuel mass at each elevation behaves in unison and is free to rattle within the cell. This is conservative, since the actual fuel assemblies would rattle within each of the cells in a haphazard fashion. It is unlikely that their combined mass would travel in harmony at any one time.

The stiffness of the fuel assembly-to-cell wall impact gap elements is determined based on an evaluation of the cell wall. The fuel spacer grids are considered rigid in comparison and the flexibility of the grid and fuel rods is not included in these terms. Thus, the stiffness is overestimated and will produce conservatively higher forces. The stiffness is computed using the formula for a plate with diameter equal to the width of the cell that is loaded by uniform pressure.

Figure 6.5.2 depicts the fuel to rack impact springs (used to develop potential impact loads between the fuel assembly mass and rack cell inner walls) in a schematic isometric. Only one of the five fuel masses is shown in this figure. Four compression only springs, acting in the horizontal direction, are provided at each fuel mass.

Figure 6.5.3 provides a 2-D schematic elevation of the storage rack model, discussed in more detail in Section 6.5.3. This view shows the vertical location of the five storage masses and some of the support pedestal spring members.

Figure 6.5.4 shows the modeling technique and degrees-of-freedom associated with rack elasticity. In each bending plane a shear and bending spring simulate elastic effects [6.5.4]. Linear elastic springs coupling rack vertical and torsional degrees-of-freedom are also included in the model.

### 6.5.2 Fluid Coupling Effect

In its simplest form, the so-called "fluid coupling effect" [6.5.2, 6.5.3] can be explained by considering the proximate motion of two bodies under water. If one body (mass  $m_1$ ) vibrates adjacent to a second body (mass  $m_2$ ), and both bodies are submerged in frictionless fluid, then Newton's equations of motion for the two bodies are:

$$(m_1 + M_{11}) A_1 + M_{12} A_2 = \text{applied forces on mass } m_1 + O(X_1^2)$$

$$M_{21} A_1 + (m_2 + M_{22}) A_2 = \text{applied forces on mass } m_2 + O(X_2^2)$$

$A_1$ , and  $A_2$  denote absolute accelerations of masses  $m_1$  and  $m_2$ , respectively, and the notation  $O(X^2)$  denotes nonlinear terms.

$M_{11}$ ,  $M_{12}$ ,  $M_{21}$ , and  $M_{22}$  are fluid coupling coefficients, which depend on body shape, relative disposition, etc. Fritz [6.5.3] gives data for  $M_{ij}$  for various body shapes and arrangements. The fluid adds mass to the body ( $M_{11}$  to mass  $m_1$ ), and an inertial force proportional to acceleration of the adjacent body (mass  $m_2$ ). Thus, acceleration of one body affects the force field on another. This force field is a function of inter-body gap, reaching large values for small gaps. Lateral motion of a fuel assembly inside a storage location encounters this effect. For example, fluid coupling behavior will be experienced between nodes 2 and 2\* in Figure 6.5.1.

The derivation of the fluid coupling matrix [6.5.5] relies on the classical inviscid fluid mechanics principles, namely the principle of continuity and Kelvin's recirculation theorem. While the derivation of the fluid coupling matrix is based on no artificial construct, it has been nevertheless verified by an extensive set of shake table experiments [6.5.5].

### 6.5.3 Stiffness Element Details

Three element types are used in the rack models. Type 1 elements are linear elastic elements used to represent the beam-like behavior of the integrated rack cell matrix. Type 2 elements are the piece-wise linear friction springs used to develop the appropriate forces between the rack pedestals and the supporting rack platform. Type 3 elements are non-linear gap elements, which model gap closures and subsequent impact loadings (i.e., between fuel assemblies and the storage cell inner walls, and rack outer periphery spaces).

If the simulation model is restricted to two dimensions (one horizontal motion plus one vertical motion, for example), for the purposes of model clarification only, then Figure 6.5.3 describes the configuration. This simpler model is used to elaborate on the various stiffness modeling elements.

Type 3 gap elements modeling impacts between fuel assemblies and racks have local stiffness  $K_i$  in Figure 6.5.3. Support pedestal spring rates  $K_S$  are modeled by type 3 gap elements. Local compliance of the concrete floor is included in  $K_S$ . The type 2 friction elements are shown in Figure 6.5.3 as  $K_f$ . The spring elements depicted in Figure 6.5.4 represent type 1 elements.

Friction at support/rack platform interface is modeled by the piecewise linear friction element with a suitably large stiffness value of  $K_f$ . This friction element allows load to be increased until the limiting lateral load  $\mu N$  is reached, where  $\mu$  is the coefficient of friction and  $N$  is the current compression load at the interface between support and rack platform. At every time-step during the dynamic simulation, the current value of  $N$  (either zero, if the pedestal has lifted off the support platform, or a compressive finite value) is computed.

The gap element  $K_S$ , modeling the effective compression stiffness of the structure in the vicinity of the support, includes stiffness of the pedestal, local stiffness of the underlying pool slab, and local stiffness of the rack cellular structure above the pedestal.

The previous discussion is limited to a 2-D model solely for simplicity. Actual analyses incorporate 3-D motions.

#### 6.5.4 Coefficients of Friction

To eliminate the last significant element of uncertainty in rack dynamic analyses, multiple simulations are performed to adjust the friction coefficient ascribed to the pedestal-to-rack platform interface. These friction coefficients are chosen consistent with the two bounding extremes from Rabinowicz's data [6.5.1]. Simulations are also performed by imposing intermediate value friction coefficients developed by a random number generator with Gaussian normal distribution characteristics. The assigned values are then held constant during the entire simulation in order to obtain reproducible results. †Thus, in this manner, the analysis results are brought closer to the realistic structural conditions.

The coefficient of friction ( $\mu$ ) between the pedestal supports and the rack platform is indeterminate. According to Rabinowicz [6.5.1], results of 199 tests performed on austenitic stainless steel plates submerged in water show a mean value of  $\mu$  to be 0.503 with standard deviation of 0.125. Upper and lower bounds (based on twice standard deviation) are 0.753 and 0.253, respectively. Analyses are therefore performed for coefficient of friction values of 0.2 (lower limit) and for 0.8 (upper limit), and for random friction values clustered about a mean of 0.5. The bounding values of  $\mu = 0.2$  and 0.8 have been found to envelope the upper limit of module response in previous rerack projects.

#### 6.5.5 Governing Equations of Motion

Using the structural model discussed in the foregoing, equations of motion corresponding to each degree-of-freedom are obtained using Lagrange's Formulation [6.5.4]. The system kinetic energy includes contributions from solid structures and from trapped and surrounding fluid. The final system of equations obtained have the matrix form:

$$[M] \left[ \frac{d^2 q}{dt^2} \right] = [Q] + [G]$$

where:

---

† It is noted that DYNARACK has the capability to change the coefficient of friction at any pedestal at each instant of contact based on a random reading of the computer clock cycle. However, exercising this option would yield results that could not be reproduced. Therefore, the random choice of coefficients is made only once per run.

- [M] - total mass matrix (including structural and fluid mass contributions). The size of this matrix will be 22 x22.
- q - the nodal displacement vector relative to the pool slab displacement (the term with q indicates the second derivative with respect to time, i.e., acceleration)
- [G] - a vector dependent on the given ground acceleration
- [Q] - a vector dependent on the spring forces (linear and nonlinear) and the coupling between degrees-of-freedom

The above column vectors have a length of 22. The equations can be rewritten as follows:

$$\left[ \frac{d^2 q}{dt^2} \right] = [M]^{-1} [Q] + [M]^{-1} [G]$$

This equation set is mass uncoupled, displacement coupled at each instant in time. The numerical solution uses a central difference scheme built into the proprietary computer program DYNARACK [6.2.4].

## 6.6 Structural Evaluation of Spent Fuel Rack Design

### 6.6.1 Kinematic and Stress Acceptance Criteria

There are two sets of criteria to be satisfied by the rack modules:

#### a. Kinematic Criteria

It is not physically possible for the proposed isolated fuel rack situated in the Cask Pit Area to overturn, because of the proximity of the surrounding four walls. The rack-to-wall dimensions would not allow the rack center of gravity to be located over any pedestal(s). Rack overturning could occur only if the relative displacement between the center of gravity and the pedestals is

greater than about one-half the distance between the pedestals, since this will place the center of mass over one pair of pedestals.

According to Ref [6.1.1 and 6.1.2], the minimum required safety margins under the OBE and SSE events are 1.5 and 1.1, respectively. The maximum displacements of the rack (in the two principal axes) are obtained from a post processing of the rack time history response output. The ratio of the displacement required to produce incipient tipping in either principal plane to the actual maximum displacement in that plane from the time history solution is the margin of safety.

All ratios available for the OBE and SSE events should be greater than 1.5 and 1.1, respectively to satisfy the regulatory acceptance criteria. However, in order to be conservative, the worst case displacements from the SSE simulations must ensure a more conservative factor of safety of 1.5.

b. Stress Limit Criteria

Stress limits must not be exceeded under the postulated load combinations provided herein.

6.6.2 Stress Limit Evaluations

The stress limits presented below apply to the rack structure and are derived from the ASME Code, Section III, Subsection NF [6.6.1]. Parameters and terminology are in accordance with the ASME Code. Material properties are obtained from the ASME Code Appendices [6.6.2], and are listed in Table 6.3.1.

(i) Normal and Upset Conditions (Level A or Level B)

a. Allowable stress in tension on a net section is:

$$F_t = 0.6 S_y$$

Where,  $S_y$  = yield stress at temperature, and  $F_t$  is equivalent to primary membrane stress.

- b. Allowable stress in shear on a net section is:

$$F_v = .4 S_y$$

- c. Allowable stress in compression on a net section is given by:

$$F_a = S_y \left( .47 - \frac{k l}{444 r} \right)$$

where  $kl/r$  for the main rack body is based on the full height and cross section of the honeycomb region and does not exceed 120 for all sections.

$l$  = unsupported length of component

$k$  = length coefficient which gives influence of boundary conditions. The following values are appropriate for the described end conditions:

= 1 (simple support both ends)

= 2 (cantilever beam)

= 0.5 (clamped at both ends)

$r$  = radius of gyration of component

- d. Maximum allowable bending stress at the outermost fiber of a net section, due to flexure about one plane of symmetry is:

$$F_b = 0.60 S_y \quad (\text{equivalent to primary bending})$$

- e. Combined bending and compression on a net section satisfies:

$$\frac{f_a}{F_a} + \frac{C_{mx} f_{bx}}{D_x F_{bx}} + \frac{C_{my} f_{by}}{D_y F_{by}} < 1$$

where:

$f_a$  = Direct compressive stress in the section

$f_{bx}$  = Maximum bending stress along x-axis

$f_{by}$  = Maximum bending stress along y-axis

$C_{mx}$  = 0.85

$C_{my}$  = 0.85

$D_x$  =  $1 - (f_a/F'_{ex})$

$D_y$  =  $1 - (f_a/F'_{ey})$

$F'_{ex,ey}$  =  $(\pi^2 E)/(2.15 (kl/r)_{x,y}^2)$

$E$  = Young's Modulus

and subscripts x,y reflect the particular bending plane.

- f. Combined flexure and compression (or tension) on a net section:

$$\frac{f_a}{0.6 S_y} + \frac{f_{bx}}{F_{bx}} + \frac{f_{by}}{F_{by}} < 1.0$$

The above requirements are to be met for both direct tension or compression.

- g. Welds

Allowable maximum shear stress on the net section of a weld is given by:

$$F_w = 0.3 S_u$$

where  $S_u$  is the weld material ultimate strength at temperature. For fillet weld legs in contact with base metal, the shear stress on the gross section is limited to  $0.4S_y$ , where  $S_y$  is the base material yield strength at temperature.

(ii) Level D Service Limits

Based on Section F-1334 (ASME Section III, Appendix F) [6.6.2], the limits for the Level D condition are the minimum of  $1.2 (S_y/F_t)$  or  $(0.7S_u/F_t)$  times the corresponding limits for the Level A condition.  $S_u$  is ultimate tensile stress at the specified rack design temperature. Examination of material properties for 304L stainless demonstrates that 1.2 times the yield strength is less than the 0.7 times the ultimate strength.

Exceptions to the above general multiplier are the following:

- a) Stresses in shear shall not exceed the lesser of  $0.72S_y$  or  $0.42S_u$ . In the case of the material used here,  $0.72S_y$  governs.
- b) Axial Compression Loads shall be limited to  $2/3$  of the calculated buckling load.
- c) Combined Axial Compression and Bending - The equations for Level A conditions shall apply except that:

$F_a = 0.667 \times \text{Buckling Load} / \text{Gross Section Area}$ ,  
and the terms  $F'_{ex}$  and  $F'_{ey}$  may be increased by the factor 1.65.

- d) For welds, the Level D allowable maximum weld stress is not specified in Appendix F of the ASME Code. An appropriate limit for weld throat stress is conservatively set here as:

$$F_w = (0.3 S_u) \times \text{factor}$$

where:

$$\begin{aligned} \text{factor} &= (\text{Level D shear stress limit}) / (\text{Level A shear stress limit}) \\ &= 0.72 \times S_y / 0.4 \times S_y = 1.8 \end{aligned}$$

### 6.6.3 Dimensionless Stress Factors

For convenience, the stress results are presented in dimensionless form. Dimensionless stress factors are defined as the ratio of the actual developed stress to the specified limiting value. The limiting value of each stress factor is 1.0.

Stress factors reported are:

$R_1$  = Ratio of direct tensile or compressive stress on a net section to its allowable value (note pedestals only resist compression)

$R_2$  = Ratio of gross shear on a net section in the x-direction to its allowable value

$R_3$  = Ratio of maximum x-axis bending stress to its allowable value for the section

$R_4$  = Ratio of maximum y-axis bending stress to its allowable value for the section

$R_5$  = Combined flexure and compressive factor (as defined in the foregoing)

$R_6$  = Combined flexure and tension (or compression) factor (as defined in the foregoing)

$R_7$  = Ratio of gross shear on a net section in the y-direction to its allowable value

#### 6.6.4 Loads and Loading Combinations for Spent Fuel Racks

The applicable loads and their combinations which must be considered in the seismic analysis of rack modules is excerpted from Refs. [6.1.2] and [6.6.3]. The load combinations considered are identified below:

Loading Combination	Service Level
D + L D + L + T <sub>o</sub> D + L + T <sub>o</sub> + E	Level A
D + L + T <sub>a</sub> + E D + L + T <sub>o</sub> + P <sub>f</sub>	Level B
D + L + T <sub>a</sub> + E' D + L + T <sub>o</sub> + F <sub>d</sub>	Level D  The functional capability of the fuel racks must be demonstrated.

Where:

- D = Dead weight-induced loads (including fuel assembly weight)
- L = Live Load (not applicable for the fuel rack, since there are no moving objects in the rack load path)
- P<sub>f</sub> = Upward force on the racks caused by postulated stuck fuel assembly
- F<sub>d</sub> = Impact force from accidental drop of the heaviest load from the maximum possible height.
- E = Operating Basis Earthquake (OBE)
- E' = Design Basis Earthquake (SSE)
- T<sub>o</sub> = Differential temperature induced loads (normal operating or shutdown condition based on the most critical transient or steady state condition)
- T<sub>a</sub> = Differential temperature induced loads (the highest temperature associated with the postulated abnormal design conditions)

T<sub>a</sub> and T<sub>o</sub> produce local thermal stresses. The worst thermal stress field in a fuel rack is obtained when an isolated storage location has a fuel assembly generating heat at maximum postulated rate and

surrounding storage locations contain no fuel. Heated water makes unobstructed contact with the inside of the storage walls, thereby producing maximum possible temperature difference between adjacent cells. Secondary stresses produced are limited to the body of the rack; that is, support pedestals do not experience secondary (thermal) stresses.

### 6.7 Parametric Simulations

The following table presents a complete listing of the simulations discussed herein. Consideration of the parameters described in Section 6.5 resulted in the following runs.

<u>Run</u>	<u>Unit</u>	<u>Rack Type</u>	<u>Rack Fuel Loading Pattern</u>	<u>COF</u>	<u>Event</u>
1	1	Region 1	fully loaded	0.8	SSE
2	1	Region 1	fully loaded	0.2	SSE
3	1	Region 1	fully loaded	Random	SSE
4	1	Region 1	fully loaded	0.8	OBE
5	1	Region 1	fully loaded	0.2	OBE
6	1	Region 1	fully loaded	Random	OBE
7	1	Region 1	nearly empty rack	0.8	SSE
8	1	Region 1	half loaded (diagonally)	0.8	SSE
9	1	Region 1	Half loaded (on east side)	0.8	SSE
10	1	Region 1	half loaded (on north side)	0.8	SSE
11 *	1	Region 1	fully loaded with equipment tray	0.8	SSE
12	2	Region 2	fully loaded	0.8	SSE
13	2	Region 2	fully loaded	0.2	SSE
14	2	Region 2	fully loaded	Random	SSE
15	2	Region 2	fully loaded	0.8	OBE
16	2	Region 2	fully loaded	0.2	OBE
17	2	Region 2	fully loaded	Random	OBE
18	2	Region 2	nearly empty rack	0.8	SSE
19	2	Region 2	half loaded (diagonally)	0.8	SSE
20	2	Region 2	half loaded (one side)	0.8	SSE
21 *	2	Region 2	fully loaded with equipment tray	0.8	SSE

\* See explanatory note about runs 11 and 21 below.

where:

Random = Gaussian distribution with a mean of 0.5 Coefficient of friction (upper and lower limits of 0.8 and 0.2).

Runs 7 through 10 and 18 through 20 are performed to evaluate the rack stability against overturning. Runs were not necessary for the OBE condition, since the SSE condition will produce worse displacements and the acceptance criteria for the OBE case (margin of at least 1.5 against tipover) is applied for these simulations. The runs include various fuel loading patterns selected to place the total fuel mass centroid as far from the rack centroid as possible. These fictitious conditions were modeled to maximize horizontal displacements and the possibility of overturning. Therefore, these simulations are not concerned with rack stresses, pedestal loads, etc. and the following sections will only report the displacements for these runs.

Additionally, a review of the results for these simulations indicates that these runs do not control for rack stresses or pedestal loadings, as expected, due to the lower fuel mass considered in the simulations.

The Cask Pit Area of each Unit has historically been used for underwater storage of miscellaneous equipment. Placement of storage racks in these pits requires removal of any components in these areas and a reduction of storage space. Runs 11 and 21 are performed to consider a fictitious equipment tray (platform) weighing 2000 pounds (including all stored equipment) located 24" above the top of the storage rack and supported by the rack. These runs are prepared to address possible installation of a future miscellaneous equipment platform being placed above the storage rack. Performing these simulations for the 0.8 coefficient of friction conditions was chosen, since these conditions produced worst-case displacements and/or stress factors for fully loaded simulations performed without the fictitious storage platforms.

## 6.8 Time History Simulation Results

The results from the DYNARACK runs can be obtained from the raw data output files. However, due to the huge quantity of output data, a post-processor is used to scan for worst case conditions and develop the stress factors discussed in subsection 6.6.3. Further reduction in this bulk of information is provided

in this section by extracting the worst case values from the parameters of interest; namely displacements, support pedestal forces, impact loads, and stress factors. This section also summarizes supplemental analyses performed to develop and evaluate structural member stresses, which are not determined by the post processor.

### 6.8.1 Rack Displacements

The maximum rack displacements are obtained from the time histories of the motion of the upper and lower four corners of each rack in each of the simulations. The maximum absolute value of displacement in the two horizontal directions, relative to the pool slab, is computed for each rack, at the top and bottom corners. The maximum displacement for all simulations is 0.396" in the North-South (x) direction, which occurs in simulation 13. However, other simulations have comparable displacements in both x and y directions.

Under all of the simulations, the rack does not impact the adjacent walls at any time (i.e., the rack-to-wall gaps at every time instant during the simulation are always greater than 0.0 inches). It is noted that the minimum nominal gap between the rack and wall (3-15/16") occurs on the Unit 1 configuration.

By comparison with half the distance between the pedestals for the rack with the worst-case displacement, tipover is not a concern and the safety factor is approximately 180. The maximum displacement (0.385") for the Unit 1, region 1 rack simulations is similar, with a safety factor against tipover of 172.

### 6.8.2 Pedestal Vertical Forces

The maximum vertical pedestal force for the Unit 2 rack is 216,800 lbs, which occurs in simulation 21. The maximum vertical pedestal force for the Unit 1 rack is 136,900 lbs, which occurs in simulation 11. The Unit 2 rack pedestal loads are greater primarily due to the larger number of assemblies stored within the Region 2 style rack.

### 6.8.3 Pedestal Friction Forces

The maximum (x or y direction) shear loads are 73,400 lbs for Unit 2 (simulation 21) and 49,400 lbs for Unit 1 (simulation 3).

### 6.8.4 Rack Impact Loads

A freestanding rack, by definition, is a structure subject to potential impacts during a seismic event. Impacts arise from rattling of the fuel assemblies in the storage rack locations and, in some instances, from localized impacts between the racks and the pool wall. The following sections discuss the bounding values of these impact loads.

#### 6.8.4.1 Rack to Wall Impacts

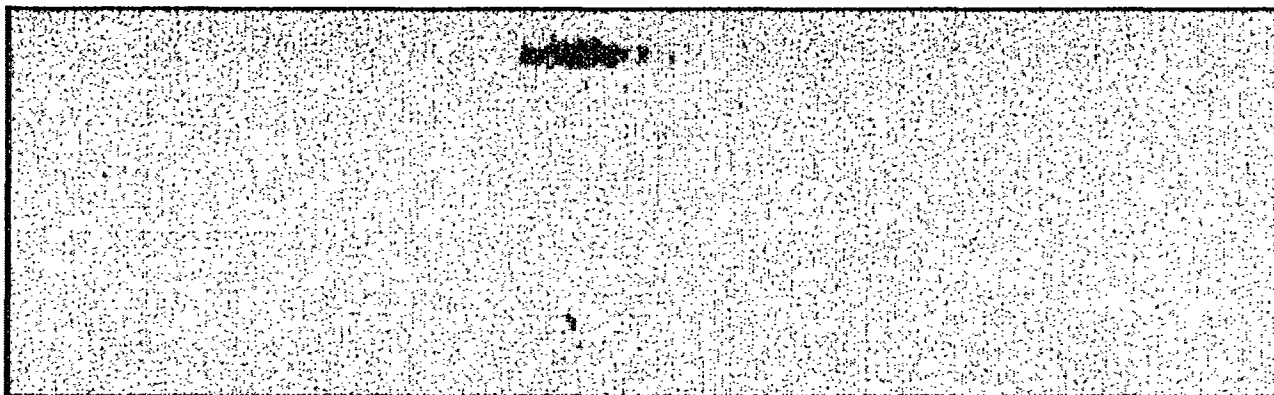
The storage racks do not impact the Cask Pit walls under any simulation. The gap between the top-of-rack and wall is several times greater than the maximum horizontal displacement.

#### 6.8.4.2 Fuel to Cell Wall Impact Loads

A review of all simulations performed allows determination of the maximum instantaneous impact load between fuel assembly and fuel cell wall at any modeled impact site. The maximum fuel/cell wall impact load value is 461 lbs, which occurs during simulation 21.

The permissible lateral load on an irradiated fuel assembly has been studied by the Lawrence Livermore National Laboratory. The LLNL report [6.8.1] states that "...for the most vulnerable fuel assembly, the axial buckling load varies from 82g's at initial storage to 95g's after 20 years storage. In a side drop, no

yielding is expected below 63g's at initial storage to 74g's after 20 years {dry} storage." The most significant load on the fuel assembly arises from rattling during the seismic event.



a = permissible lateral acceleration in g's (a=63)

Therefore, a maximum fuel assembly-to-cell wall impact load of less than 500 lbs is provided with a safety factor of about 44.

## 6.9 Rack Structural Evaluation

### 6.9.1 Rack Stress Factors

The time history results from the DYNARACK solver provide the pedestal normal and lateral interface forces, which may be converted to the limiting bending moment and shear force at the bottom baseplate-pedestal interface. In particular, maximum values for the previously defined stress factors are determined for every pedestal. With this information available, the structural integrity of the pedestal can be assessed and reported. The net section maximum (in time) bending moments and shear forces can also be determined at the bottom baseplate-rack cellular structure interface for each spent fuel rack in the pool. Using these forces and moments, the maximum stress in the limiting rack cell (box) can be evaluated.

The stress factor results for male and female pedestals, and for the entire spent fuel rack cellular cross-section just above the bottom casting have been determined. These factors are reported for every pedestal and the rack cell wall cross-section in each simulation. These locations are the most heavily loaded net sections in the structure so that satisfaction of the stress factor criteria at these locations ensures that the overall structural criteria set forth in Section 6.6 are met.

The maximum SSE condition pedestal stress factor is 0.189, which occurs under simulation 12. The maximum, OBE condition pedestal stress factor is 0.197, which occurs under simulation 16. The maximum SSE condition cell wall stress factor is 0.170, which occurs under simulation 12. The maximum, OBE condition cell wall stress factor is 0.205, which occurs under simulation 16. An evaluation of the stress factors for all of the simulations performed, leads to the conclusion that all stress factors, as defined in Section 3, are less than the mandated limit of 1.0. Therefore, the requirements of Section 3 are indeed satisfied for the load levels considered for every limiting location in the rack.

#### 6.9.2 Pedestal Thread Shear Stress

The maximum average shear stress in the engagement region under SSE conditions is 7,446 psi. This computed stress is applicable to both the male and female pedestal threads. The ultimate strength of the female part of the pedestal is 66,200 psi. The yield stress for this material is 21,300 psi.

The allowable shear stress in the female pedestal for Level B conditions is 0.4 times the yield stress, which gives 8,520 psi. The allowable shear stress for Level D conditions is the lesser of:  $0.72 S_y = 15,336$  psi or  $0.42 S_u = 27,804$  psi. Therefore, the former criteria controls. However, for conservatism the actual stress for the SSE condition may be compared against the allowable for the OBE condition. Since 7,446 psi is less than the OBE allowable of 8,520 psi, the female pedestal threads are shown to be acceptable. The allowable stress for the male pedestal threads is much larger due to the higher material strength.

### 6.9.3 Local Stresses Due to Impacts

Impact loads at the pedestal base (discussed in subsection 6.8.2) produce stresses in the pedestal for which explicit stress limits are prescribed in the Code. However, the impact loads on the cellular region of the racks, discussed in subsection 6.8.4, produce stresses, which attenuate rapidly away from the loaded region. This behavior is characteristic of secondary stresses.

Even though limits on secondary stresses are not prescribed in the Code for class 3 NF structures, evaluations must be made to ensure that the localized impacts do not lead to plastic deformations in the storage cells which affect the subcriticality of the stored fuel array.

Local cell wall integrity is conservatively estimated from peak impact loads. Plastic analysis is used to obtain the limiting impact load which would lead to gross permanent deformation. As shown in Tables 6.9.1 and 6.9.2, the limiting impact load (of 3,423 lbf, including a safety factor of 2.0) is much greater than the highest calculated impact load value (of less than 500 lbf, see subsection 6.8.4.2) obtained from any of the rack analyses. Therefore, fuel impacts do not represent a significant concern with respect to fuel rack cell deformation.

### 6.9.4 Assessment of Rack Fatigue Margin

Deeply submerged high density spent fuel storage racks arrayed in close proximity to each other in a free-standing configuration behave primarily as a nonlinear cantilevered structure when subjected to 3-D seismic excitations. In addition to the pulsations in the vertical load at each pedestal, lateral friction forces at the pedestal/ rack platform interface, which help prevent or mitigate lateral sliding of the rack, also exert a time-varying moment in the baseplate region of the rack. The friction-induced lateral forces act simultaneously in x and y directions with the requirement that their vectorial sum does not exceed  $\mu V$ , where  $\mu$  is the limiting interface coefficient of friction and V is the concomitant vertical thrust on the rack platform (at the *given* time instant). As the vertical thrust at a pedestal location changes, so does

the maximum friction force,  $F$ , that the interface can exert. In other words, the lateral force at the pedestal/ rack platform interface,  $F$ , is given by

$$F \leq \mu N(\tau)$$

where  $N$  (vertical thrust) is the time-varying function of  $\tau$ .  $F$  does not always equal  $\mu N$ ; rather,  $\mu N$  is the maximum value it can attain at any time; the actual value, of course, is determined by the dynamic equilibrium of the rack structure.

In summary, the horizontal friction force at the pedestal/ rack platform interface is a function of time; its magnitude and direction of action varies during the earthquake event.

The time-varying lateral (horizontal) and vertical forces on the extremities of the support pedestals produce stresses at the root of the pedestals in the manner of an end-loaded cantilever. The stress field in the cellular region of the rack is quite complex, with its maximum values located in the region closest to the pedestal. The maximum magnitude of the stresses depends on the severity of the pedestal end loads and on the geometry of the pedestal/rack baseplate region.

Alternating stresses in metals produce metal fatigue if the amplitude of the stress cycles is sufficiently large. In high density racks designed for sites with moderate to high postulated seismic action, the stress intensity amplitudes frequently reach values above the material endurance limit, leading to expenditure of the fatigue "usage" reserve in the material.

Because the locations of maximum stress (viz., the pedestal/rack baseplate junction) and the close placement of racks, a post-earthquake inspection of the high stressed regions in the racks is not feasible. Therefore, the racks must be engineered to withstand multiple earthquakes without reliance of nondestructive inspections for post-earthquake integrity assessment. The fatigue life evaluation of racks is an integral aspect of a sound design.

The time-history method of analysis, deployed in this report, provides the means to obtain a complete cycle history of the stress intensities in the highly stressed regions of the rack. Having determined the amplitude of the stress intensity cycles and their number, the cumulative damage factor, U, can be determined using the classical Miner's rule:

$$U = \sum \frac{n_i}{N_i}$$

where  $n_i$  is the number of stress intensity cycles of amplitude  $\sigma_i$ , and  $N_i$  is the permissible number of cycles corresponding to  $\sigma_i$  from the ASME fatigue curve for the material of construction. U must be less than or equal to 1.0.

To evaluate the cumulative damage factor, a finite element model of a portion of the spent fuel rack in the vicinity of a support pedestal is constructed in sufficient detail to provide an accurate assessment of stress intensities. The finite element solutions for unit pedestal loads in three orthogonal directions are combined to establish the maximum value of stress intensity as a function of the three unit pedestal loads. Using the archived results of the spent fuel rack dynamic analyses (pedestal load histories versus time) enables a time-history of stress intensity to be established at the most limiting location. This permits establishing a set of alternating stress intensity ranges versus cycles for an SSE and an OBE event. Following ASME Code guidelines for computing U for the Unit 2 rack, it is found that  $U = 0.196$  due to the combined effect of one SSE and twenty OBE events. This is well below the ASME Code limit of 1.0. The U value for the Unit 1 rack is much lower (less than 0.1)

### 6.9.5 Weld Stresses

Weld locations subjected to significant seismic loading are at the bottom of the rack at the baseplate-to-cell connection, at the top of the pedestal support at the baseplate connection, and at cell-to-cell connections. Bounding values of resultant loads are used to qualify the connections.

#### a. Baseplate-to-Rack Cell Welds

For Level A or B conditions, Ref. [6.6.1] permits an allowable weld stress of  $\tau = .3 S_u = 19,860$  psi. As stated in subsection 6.6.2 the allowable may be increased for Level D by some amplification factor.

Weld stresses are produced through the use of a simple conversion (ratio) factor applied to the corresponding stress factor in the adjacent rack material. The ratio is developed from the differences in material thickness and length versus weld throat dimension and length:

$$\text{RATIO} = \text{[REDACTED]}$$

The highest predicted cell to baseplate weld stress under the Unit 2 OBE simulations is conservatively calculated to be 6,436 psi. This value is less than the OBE allowable weld stress value, which is 19,860. The highest predicted cell to baseplate weld stress for the Unit 2 SSE simulation is 11,048 psi. The calculated stress value is less than the allowable weld stress value 35,748 psi. The Unit 2 rack cell-to-pedestal weld stresses control over the Unit 1 stresses. As shown in Tables 6.9.1 and 6.9.2, all weld stresses between the baseplate and cell wall base are acceptable.

b. Baseplate-to-Pedestal Welds

The weld between baseplate and support pedestal is checked using finite element analysis to determine that the maximum stress for Unit 2 is 13,780 psi under a Level D event. This calculated stress value is well below the allowable of 35,748 psi. The maximum Unit 2 weld stress under OBE conditions is 3,397 psi, which is less than the OBE allowable of 19,860 psi. The Unit 1 weld stresses are lower as shown in Table 6.9.1. Therefore, the welds are acceptable.

c. Cell-to-Cell Welds

Cell-to-cell connections are by a series of connecting welds along the cell height. Stresses in storage cell to cell welds develop due to fuel assembly impacts with the cell wall. These weld stresses are conservatively considered by assuming that fuel assemblies in adjacent cells are moving out of phase with one another so that impact loads in two adjacent cells are in opposite directions and are applied simultaneously. This load application tends to separate the two cells from each other at the weld.

Tables 6.9.1 and 6.9.2 give results for the maximum allowable load that can be transferred by these welds based on the available weld area. An upper bound on the load required to be transferred is also given in the tables and is much lower than the allowable load. This upper bound value is very conservatively obtained by applying the bounding rack-to-fuel impact load from any simulation in two orthogonal directions simultaneously, and multiplying the result by 2 to account for the simultaneous impact of two assemblies. An equilibrium analysis at the connection then yields the upper bound load to be transferred. It is seen from the results in Tables 6.9.1 and 6.9.2 that the calculated load is well below the allowable.

## 6.10 Level A Evaluation

The Level A condition is not a governing condition for spent fuel racks, since the general level of loading is far less than Level B loading and the stress allowables are the same for the two conditions. To illustrate this, the racks for each Unit are considered under the dead weight load. It is shown below that the maximum pedestal load under the deadweight condition is low and that further stress evaluations are unnecessary.

### 6.10.1 Unit 1 Cask Pit Rack

Dry Weight of Largest Holtec Rack	=	32870 lbf
Dry Weight of 143 Fuel Assemblies	=	203489 lbf
Total Dry Weight	=	236359 lbf
Total Buoyant Weight (0.87 × Total Dry Weight)	=	205632 lbf
Load per Pedestal	=	51408 lbf

The stress allowables for the normal condition is the same as for the Upset (OBE) condition, which resulted in a maximum pedestal load of 99,100 lbs. Since this load (and the corresponding stress throughout the rack members) is much greater than the 51,408 lb load calculated above, the Upset condition controls over normal (Gravity) condition. Therefore, no Level A evaluation is required to be performed.

### 6.10.2 Unit 2 Cask Pit Rack

Dry Weight of Largest Holtec Rack	=	29000 lbf
Dry Weight of 225 Fuel Assemblies	=	311400 lbf
Total Dry Weight	=	340400 lbf
Total Buoyant Weight (0.87 × Total Dry Weight)	=	296148 lbf
Load per Pedestal	=	74037 lbf

The stress allowables for the normal condition is the same as for the upset condition, which resulted in a maximum pedestal load of 130,000 lbs. Since this load (and the corresponding stress throughout the

rack members) is much greater than the 74,037 lb load calculated above, the Upset (OBE) condition controls over normal (Gravity) condition. Therefore, no Level A evaluation is required to be performed.

### 6.11 Hydrodynamic Loads on Pool Walls

The maximum hydrodynamic pressure that is developed, at any point between the fuel racks and the walls, due to fluid coupling on the Unit 1 rack is 1.05 psi. The maximum hydrodynamic pressure that is developed, at any point between the fuel racks and the walls, due to fluid coupling on the Unit 2 rack is 1.8 psi. The hydrodynamic pressure values are unsigned and, therefore, are added to or subtracted from the pool hydrostatic pressure at the depth of the tops of the racks during evaluation of the Cask Pit structure, as discussed in Section 8.0.

### 6.12 Temperature Gradient Across Rack Cell Wall

#### 6.12.1 Cell Wall Buckling

The possibility of cell wall buckling and evaluation of the cell-to-cell welded joints are examined under the loading conditions arising from thermal effects due to an isolated hot cell, in this sub-section.

The allowable local buckling stresses in the fuel cell walls are obtained by using classical plate buckling analysis. The following formula for the critical stress has been used.

$$\sigma_{cr} = \frac{\beta \pi^2 E t^2}{12 b^2 (1 - \mu^2)}$$

where  $E = 27 \times 10^6$  psi,  $\mu$  is Poison's ratio,  $t = .075$ ",  $b = 8.58$ ". The factor  $\beta$  is suggested to be 4.0 in [6.12.1] for a long panel loaded as shown in Figure 6.12.1.

For the given data  $\sigma_{cr} = 7,458$  psi

It should be noted that this calculation is based on the applied stress being uniform along the entire length of the cell wall. In the actual fuel rack, the compressive stress comes from consideration of overall bending of the rack structures during a seismic event and as such is negligible at the rack top and maximum at the rack bottom. It is conservative to apply the above equation to the rack cell wall if we compare  $\sigma_{cr}$  with the maximum compressive stress anywhere in the cell wall.

As shown in Section 6, this local buckling stress limit is not violated anywhere in the body of the rack modules, since the maximum compressive stress in the outermost cell is  $= 2*(0.6)(21,300) * R6$  (from Section 6.9.1 with  $R6 = .170$ ) = 4,350 psi < 7,458 psi. Therefore, cell wall buckling is not a concern.

#### 6.12.2 Cell-to-Cell Weld Stress Due to Hot Cell Thermal Expansion

Cell-to cell welded joints are examined under the loading conditions arising from thermal effects due to an isolated hot cell, in this sub-section. This secondary stress condition is evaluated alone and not combined with primary stresses from other load conditions.

A thermal gradient between cells will develop when an isolated storage location contains a fuel assembly emitting maximum postulated heat, while the surrounding locations are empty. We can obtain a conservative estimate of weld stresses along the length of an isolated hot cell by considering a beam strip uniformly heated by 90°F, and restrained from growth along one long edge. This thermal gradient is based on the results of the thermal-hydraulic evaluations discussed in Section 5.0, which shows that the maximum difference between the local cell maximum temperature (196°F) and the bulk pool temperature (161°F) is approximately 35°F. The configuration is shown in Figure 6.12.2.

Using shear beam theory and subjecting the strip to a uniform temperature rise  $\Delta T = 90^\circ\text{F}$ , we can calculate an estimate of the maximum value of the average shear stress in the strip. The strip is subjected to the following boundary conditions.

- a. Displacement  $U_x(x,y) = 0$  at  $x = 0$ , at  $y = H$ , all  $x$ .

- b. Average force  $M_x$ , acting on the cross section  $Ht = 0$  at  $x = l$ , all  $y$ .

The final result for wall shear stress, maximum at  $x = l$ , is found to be given as

$$\tau_{\max} = \frac{E \alpha \Delta T}{0.931}$$

where  $E = 27 \times 10^6$  psi,  $\alpha = 9.5 \times 10^{-6}$  in/in °F and  $\Delta T = 90^\circ\text{F}$ . Therefore, we obtain an estimate of maximum weld shear stress in an isolated hot cell, due to thermal gradient, as

$$\tau_{\max} = 24,796 \text{ psi}$$

Since this is a secondary thermal stress, we use the allowable shear stress criteria for faulted conditions ( $0.42 \cdot S_u = 27,804$  psi) as a guide to indicate that the maximum shear is acceptable.

### 6.13 Rack Support Platform

The floor of the Cask Pit of each Unit is at a lower elevation than the floor of the spent fuel pool. In order to ensure that the top of any spent fuel rack placed in the cask pit is at the same elevation as racks in the pool, a cask pit rack platform will be installed in each Cask Pit to raise the top of the rack to the appropriate elevation.

Figure 2.1.3 provides a schematic representation of the rack support platforms. The cask pit rack platforms consist of a frame approximately 4.0 feet tall constructed of box beam sections comprised of 1" plates with 8" diameter pipes located directly beneath each rack pedestal. The top of the platform corners are equipped with positioning rings, such that the 5" OD rack pedestals can be accurately positioned on the platform.

The evaluations for the platforms are performed using classical strength of materials formulations. Worst-case loads from the rack seismic/structural evaluation were used as the design inputs to design the platform. The platforms are designed with the same Code requirements as the supported racks. As such,

the platforms are designed as Class 3 Linear-Type component supports and must meet applicable stress levels of ASME Section III, NF-3553 [6.6.1]. The evaluations show that all required geometry checks and stress checks are satisfied for both Level A and Level D conditions and for the lifting condition. Safety factors for bearing, tearout and gross force and moment are greater than 1.0.

## 6.14 References

- [6.1.1] USNRC NUREG-0800, Standard Review Plan, June 1987.
- [6.1.2] (USNRC Office of Technology) "OT Position for Review and Acceptance of Spent Fuel Storage and Handling Applications", dated April 14, 1978, and January 18, 1979 amendment thereto.
- [6.2.1] Soler, A.I. and Singh, K.P., "Seismic Responses of Free Standing Fuel Rack Constructions to 3-D Motions", Nuclear Engineering and Design, Vol. 80, pp. 315-329 (1984).
- [6.2.2] Soler, A.I. and Singh, K.P., "Some Results from Simultaneous Seismic Simulations of All Racks in a Fuel Pool", INNEM Spent Fuel Management Seminar X, January, 1993.
- [6.2.3] Singh, K.P. and Soler, A.I., "Seismic Qualification of Free Standing Nuclear Fuel Storage Racks - the Chin Shan Experience, Nuclear Engineering International, UK (March 1991).
- [6.2.4] Holtec Proprietary Report HI-961465 - WPMR Analysis User's Manual, May, 1998.
- [6.4.1] NUREG 0800, Standard Review Plan, SRP 3.7.1, Seismic Design Parameters.
- [6.4.2] Holtec Proprietary Report HI-89364 - Verification and User's Manual for Computer Code GENEQ, January, 1990.
- [6.5.1] Rabinowicz, E., "Friction Coefficients of Water Lubricated Stainless Steels for a Spent Fuel Rack Facility," MIT, a report for Boston Edison Company, 1976.
- [6.5.2] Singh, K.P. and Soler, A.I., "Dynamic Coupling in a Closely Spaced Two-Body System Vibrating in Liquid Medium: The Case of Fuel Racks," 3rd International Conference on Nuclear Power Safety, Keswick, England, May 1982.
- [6.5.3] Fritz, R.J., "The Effects of Liquids on the Dynamic Motions of Immersed Solids," Journal of Engineering for Industry, Trans. of the ASME, February 1972, pp 167-172.
- [6.5.4] Levy, S. and Wilkinson, J.P.D., "The Component Element Method in Dynamics with Application to Earthquake and Vehicle Engineering," McGraw Hill, 1976.

- [6.5.5] Paul, B., "Fluid Coupling in Fuel Racks: Correlation of Theory and Experiment", (Proprietary), NUSCO/Holtec Report HI-88243.
- [6.6.1] ASME Boiler & Pressure Vessel Code, Section III, Subsection NF, 1989 Edition.
- [6.6.2] ASME Boiler & Pressure Vessel Code, Section III, Appendices, 1989 Edition.
- [6.6.3] USNRC Standard Review Plan, NUREG-0800 (Section 3.8.4, Rev. 2, 1989).
- [6.8.1] UCID-21246, "Dynamic Impact Effects on Spent Fuel Assemblies," Lawrence Livermore National Laboratory, dated October 20, 1987.
- [6.9.1] ACI 349-85, Code Requirements for Nuclear Safety Related Concrete Structures, American Concrete Institute, Detroit, Michigan, 1985.
- [6.9.2] ACI 318-95, Building Code Requirements for Structural Concrete, American Concrete Institute, Detroit, Michigan, 1995.
- [6.12.1] "Strength of Materials", S. P. Timoshenko, 3rd Edition, Part II, pp 194-197 (1956).

**Table 6.2.1**

**PARTIAL LISTING OF FUEL RACK APPLICATIONS USING DYNARACK**

<b>PLANT</b>	<b>DOCKET NUMBER(s)</b>	<b>YEAR</b>
Enrico Fermi Unit 2	USNRC 50-341	1980
Quad Cities 1 & 2	USNRC 50-254, 50-265	1981
Rancho Seco	USNRC 50-312	1982
Grand Gulf Unit 1	USNRC 50-416	1984
Oyster Creek	USNRC 50-219	1984
Pilgrim	USNRC 50-293	1985
V.C. Summer	USNRC 50-395	1984
Diablo Canyon Units 1 & 2	USNRC 50-275, 50-323	1986
Byron Units 1 & 2	USNRC 50-454, 50-455	1987
Braidwood Units 1 & 2	USNRC 50-456, 50-457	1987
Vogtle Unit 2	USNRC 50-425	1988
St. Lucie Unit 1	USNRC 50-335	1987
Millstone Point Unit 1	USNRC 50-245	1989
Chinshan	Taiwan Power	1988
D.C. Cook Units 1 & 2	USNRC 50-315, 50-316	1992
Indian Point Unit 2	USNRC 50-247	1990
Three Mile Island Unit 1	USNRC 50-289	1991
James A. FitzPatrick	USNRC 50-333	1990
Shearon Harris Unit 2	USNRC 50-401	1991
Hope Creek	USNRC 50-354	1990
Kuosheng Units 1 & 2	Taiwan Power Company	1990
Ulchin Unit 2	Korea Electric Power Co.	1990

**Table 6.2.1****PARTIAL LISTING OF FUEL RACK APPLICATIONS USING DYNARACK**

<b>PLANT</b>	<b>DOCKET NUMBER(s)</b>	<b>YEAR</b>
Laguna Verde Units 1 & 2	Comision Federal de Electricidad	1991
Zion Station Units 1 & 2	USNRC 50-295, 50-304	1992
Sequoyah	USNRC 50-327, 50-328	1992
LaSalle Unit 1	USNRC 50-373	1992
Duane Arnold Energy Center	USNRC 50-331	1992
Fort Calhoun	USNRC 50-285	1992
Nine Mile Point Unit 1	USNRC 50-220	1993
Beaver Valley Unit 1	USNRC 50-334	1992
Salem Units 1 & 2	USNRC 50-272, 50-311	1993
Limerick	USNRC 50-352, 50-353	1994
Ulchin Unit 1	KINS	1995
Yonggwang Units 1 & 2	KINS	1996
Kori-4	KINS	1996
Connecticut Yankee	USNRC 50-213	1996
Angra Unit 1	Brazil	1996
Sizewell B	United Kingdom	1996
Waterford 3	USNRC 50-382	1996
Vogtle	USNRC 50-424	1997
J. A. Fitzpatrick	USNRC 50-333	1997
Vermont Yankee	USNRC 50-271	1998
Callaway	USNRC 50-483	1998

**Table 6.2.1****PARTIAL LISTING OF FUEL RACK APPLICATIONS USING DYNARACK**

<b>PLANT</b>	<b>DOCKET NUMBER(s)</b>	<b>YEAR</b>
Nine Mile	USNRC 50-220	1998
Chin Shan	Taiwan Power Company	1998
Millstone 3	USNRC 50-423	1998
Byron/Braidwood	USNRC 50-454, 50-455, 50-567, 50-457	1999
Wolf Creek	USNRC 50-482	1999
Plant Hatch Units 1 & 2	USNRC 50-321, 50-366	1999
Harris Pools C and D	USNRC 50-401	1999
Davis-Besse	USNRC 50-346	1999
Enrico Fermi Unit 2	USNRC 50-341	2000
Kewaunee	USNRC 50-305	2001

<b>Table 6.3.1</b> <b>RACK MATERIAL DATA (200°F)</b> <b>(ASME - Section II, Part D)</b>			
<b>Material</b>	<b>Young's Modulus</b> <b>E</b> <b>(psi)</b>	<b>Yield Strength</b> <b>S<sub>y</sub></b> <b>(psi)</b>	<b>Ultimate Strength</b> <b>S<sub>u</sub></b> <b>(psi)</b>
SA240; 304L S.S.	27.6 x 10 <sup>6</sup>	21,300	66,200
<b>SUPPORT MATERIAL DATA (200°F)</b>			
SA240, Type 304L (upper part of support feet)	27.6 x 10 <sup>6</sup>	21,300	66,200
SA-564-630 (lower part of support feet; age hardened at 1100EF)	28.5 x 10 <sup>6</sup>	106,300	140,000

Table 6.4.1 UNIT 1 TIME-HISTORY STATISTICAL CORRELATION RESULTS	
OBE	
Data1 to Data2	-0.041
Data1 to Data3	0.032
Data2 to Data3	0.081
SSE	
Data1 to Data2	0.052
Data1 to Data3	-0.011
Data2 to Data3	-0.021

**Data1** corresponds to the time-history acceleration values along the X axis (East)

**Data2** corresponds to the time-history acceleration values along the Y axis (North)

**Data3** corresponds to the time-history acceleration values along the Z axis (Vertical)

<b>Table 6.4.2</b> <b>UNIT 2</b> <b>TIME-HISTORY STATISTICAL CORRELATION RESULTS</b>	
<b>OBE</b>	
Data1 to Data2	0.042
Data1 to Data3	0.088
Data2 to Data3	-0.025
<b>SSE</b>	
Data1 to Data2	0.006
Data1 to Data3	0.137
Data2 to Data3	-0.051

**Data1** corresponds to the time-history acceleration values along the **X** axis (North)

**Data2** corresponds to the time-history acceleration values along the **Y** axis (West)

**Data3** corresponds to the time-history acceleration values along the **Z** axis (Vertical)

Table 6.5.1 Degrees-of-freedom						
<u>LOCATION (Node)</u>	<u>DISPLACEMENT</u>			<u>ROTATION</u>		
	$U_x$	$U_y$	$U_z$	$\theta_x$	$\theta_y$	$\theta_z$
1	$p_1$	$p_2$	$p_3$	$q_4$	$q_5$	$q_6$
2	$p_7$	$p_8$	$p_9$	$q_{10}$	$q_{11}$	$q_{12}$
Node 1 is assumed to be attached to the rack at the bottom most point. Node 2 is assumed to be attached to the rack at the top most point. Refer to Figure 6.5.1 for node identification.						
2*	$p_{13}$	$p_{14}$				
3*	$p_{15}$	$p_{16}$				
4*	$p_{17}$	$p_{18}$				
5*	$p_{19}$	$p_{20}$				
1*	$p_{21}$	$p_{22}$				
where the relative displacement variables $q_i$ are defined as:  $p_i = q_i(t) + U_x(t) \quad i = 1,7,13,15,17,19,21$ $= q_i(t) + U_y(t) \quad i = 2,8,14,16,18,20,22$ $= q_i(t) + U_z(t) \quad i = 3,9$ $= q_i(t) \quad i = 4,5,6,10,11,12$ <p> <math>p_i</math> denotes absolute displacement (or rotation) with respect to inertial space  <math>q_i</math> denotes relative displacement (or rotation) with respect to the floor slab             * denotes fuel mass nodes   <math>U(t)</math> are the three known earthquake displacements         </p>						

**Table 6.9.1**  
**UNIT 1**  
**COMPARISON OF BOUNDING CALCULATED LOADS/STRESSES VS. CODE ALLOWABLES**  
**AT IMPACT LOCATIONS AND AT WELDS**

Item/Location	OBE		SSE	
	Calculated	Allowable	Calculated	Allowable
Fuel assembly/cell wall impact, lbf.	248	3,423 <sup>1</sup>	419	3,423 <sup>1</sup>
Rack/baseplate weld, psi	4,451	19,860	8,903	35,748
Baseplate/Pedestal weld, psi	2,151	19,860	6,167	35,748
Cell/cell welds, psi			1,946 <sup>2</sup>	8,520 <sup>3</sup>

1 Based on the limit load for a cell wall.

2 Cell-to-cell weld stresses, including consideration of shear.

3 Conservatively based on OBE allowable stresses.

**Table 6.9.2**

**UNIT 2**

**COMPARISON OF BOUNDING CALCULATED LOADS/STRESSES VS. CODE ALLOWABLES**

**AT IMPACT LOCATIONS AND AT WELDS**

Item/Location	OBE		SSE	
	Calculated	Allowable	Calculated	Allowable
Fuel assembly/cell wall impact, lbf.	159	3,423 <sup>1</sup>	449	3,423 <sup>1</sup>
Rack/baseplate weld, psi	6,436	19,860	11,048	35,748
Baseplate/Pedestal weld, psi	3,397	19,860	13,780	35,748
Cell/cell welds, psi			2,515 <sup>2</sup>	8,520 <sup>3</sup>

<sup>1</sup> Based on the limit load for a cell wall.

<sup>2</sup> Cell-to-cell weld stresses, including consideration of shear.

<sup>3</sup> Cell-to-cell weld stresses, including consideration of shear.

Figure 6.4.1  
Holtec Report  
HI-2022882

St. Lucie Unit 1 Elevation 21.50'  
Time History Accelerogram  
E/W Direction SSE (2% Damping)

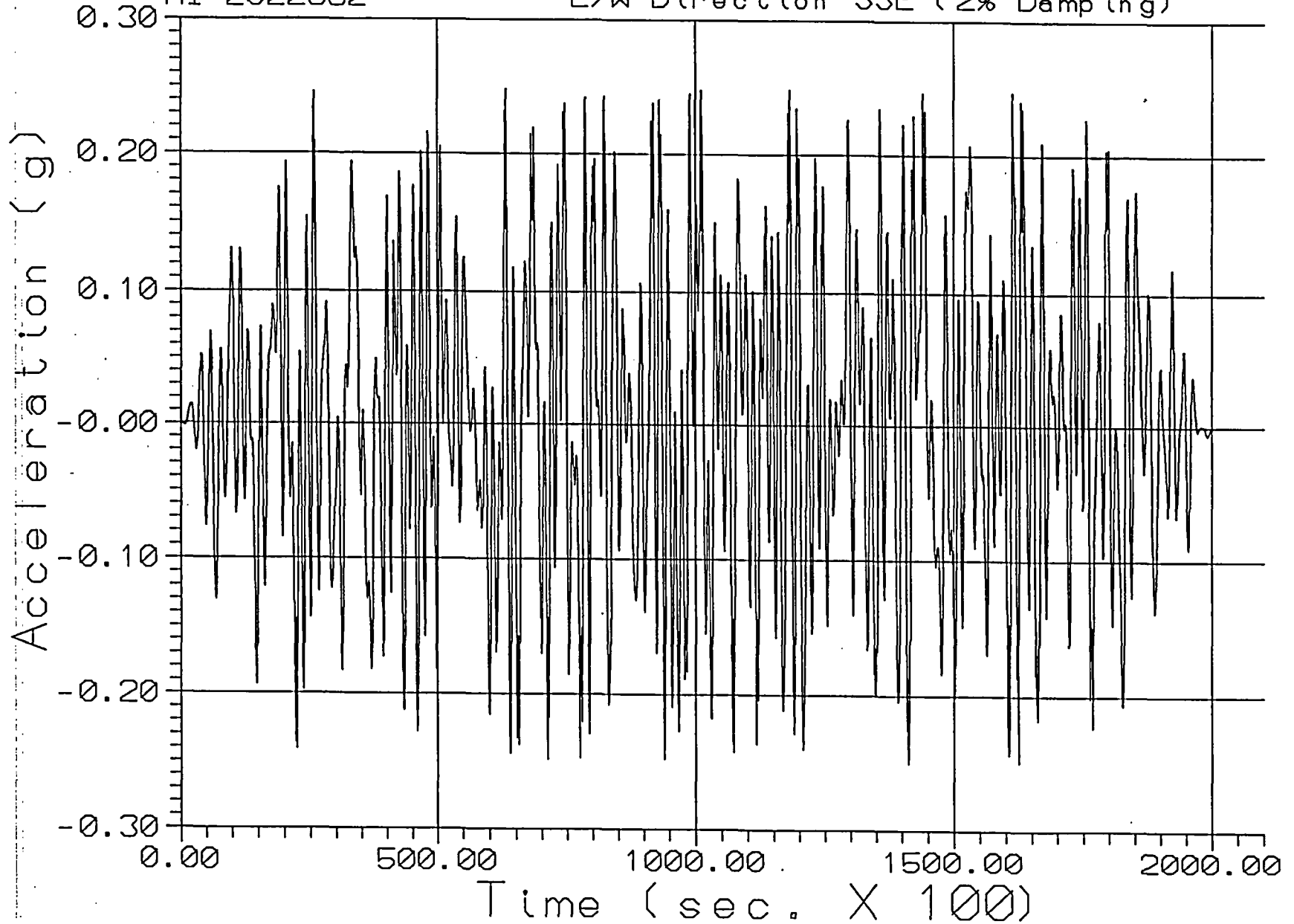


Figure 6.4.2  
Holtec Report  
HI-2022882

St. Lucie Unit 1 Elevation 21.50'  
Time History Accelerogram  
N/S Direction SSE (2% Damping)

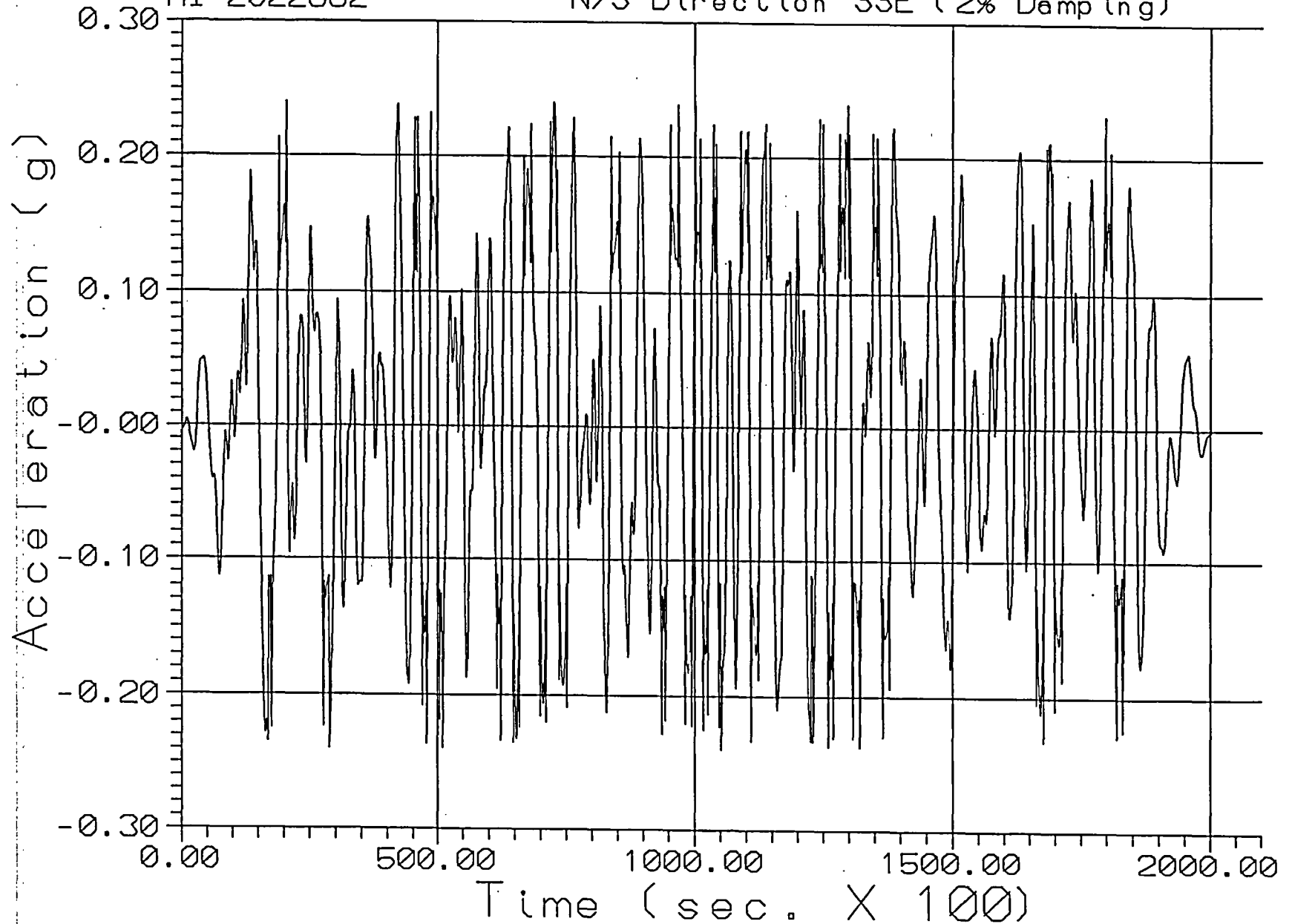


Figure 6.4.3  
Holtec Report  
HI-2022882

St. Lucie Unit 1 Elevation 21.50'  
Time History Accelerogram  
Vert SSE (2% Damping)

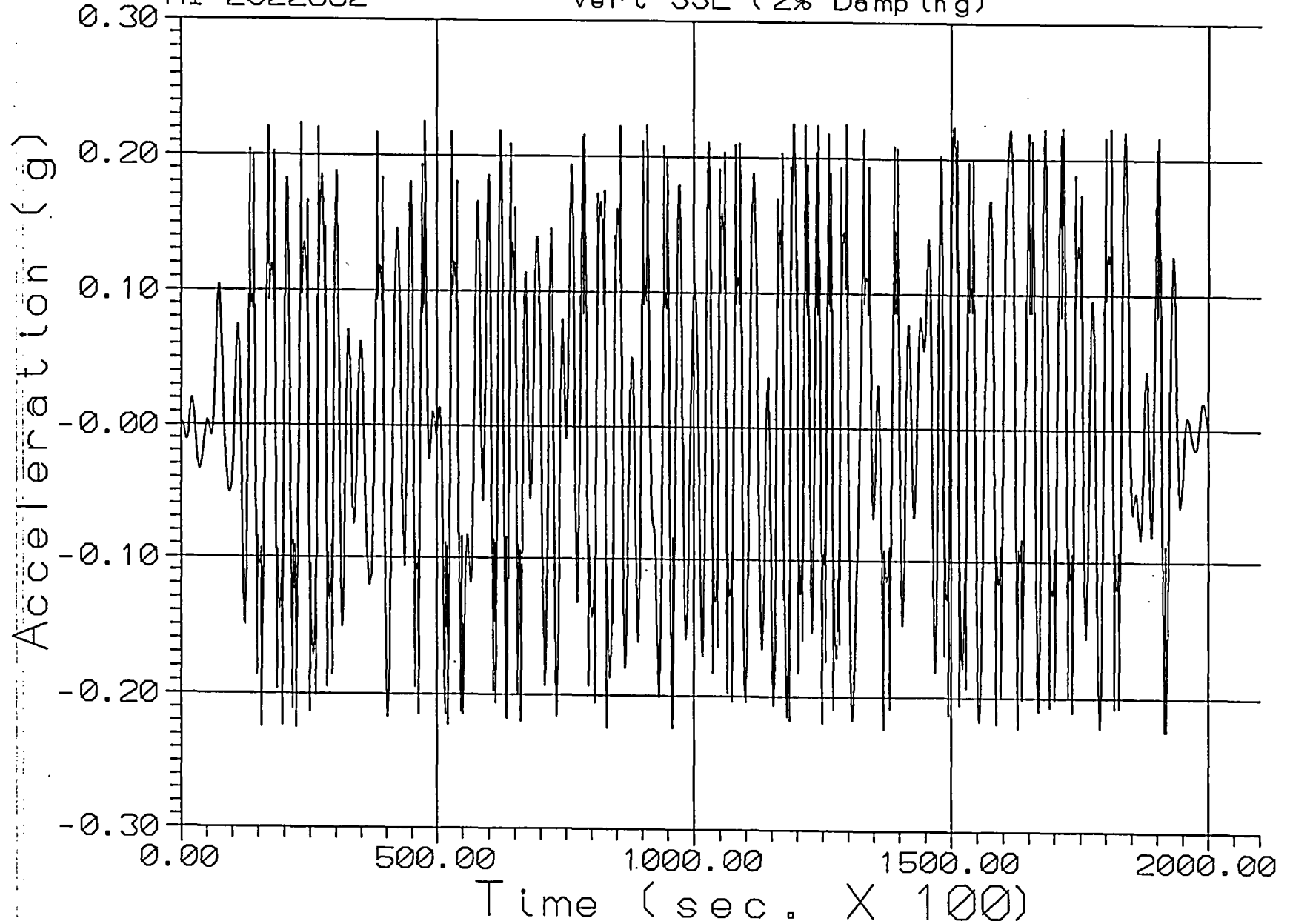


Figure 6.4.4  
Holtec Report  
HI-2022882

St. Lucie Unit 1 Elevation 21.50'  
Time History Accelerogram  
E/W Direction OBE (2% Damping)

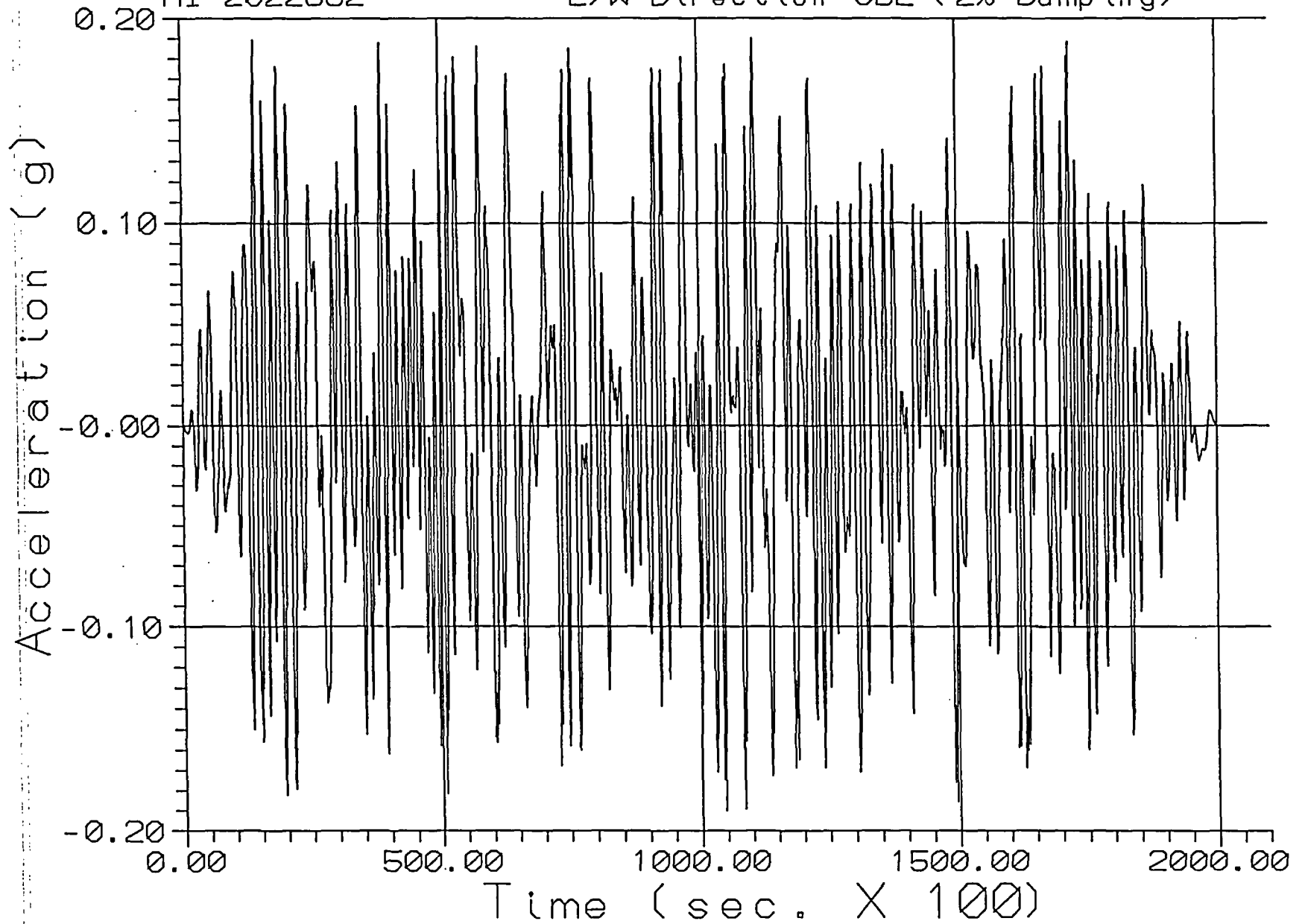


Figure 6.4.5  
Holtec Report  
HI-2022882

St. Lucie Unit 1 Elevation 21.50'  
Time History Accelerogram  
N/S Direction OBE (2% Damping)

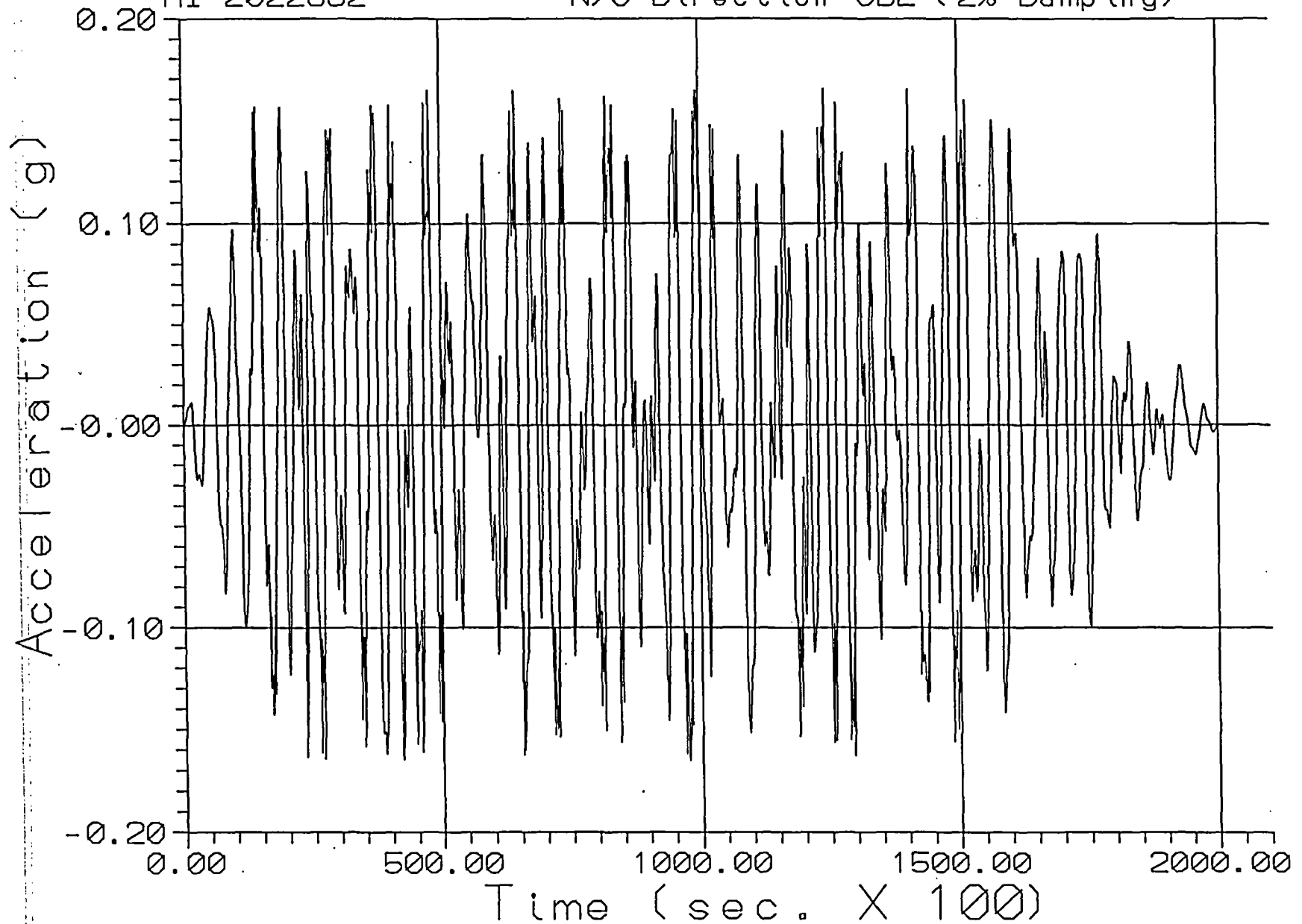
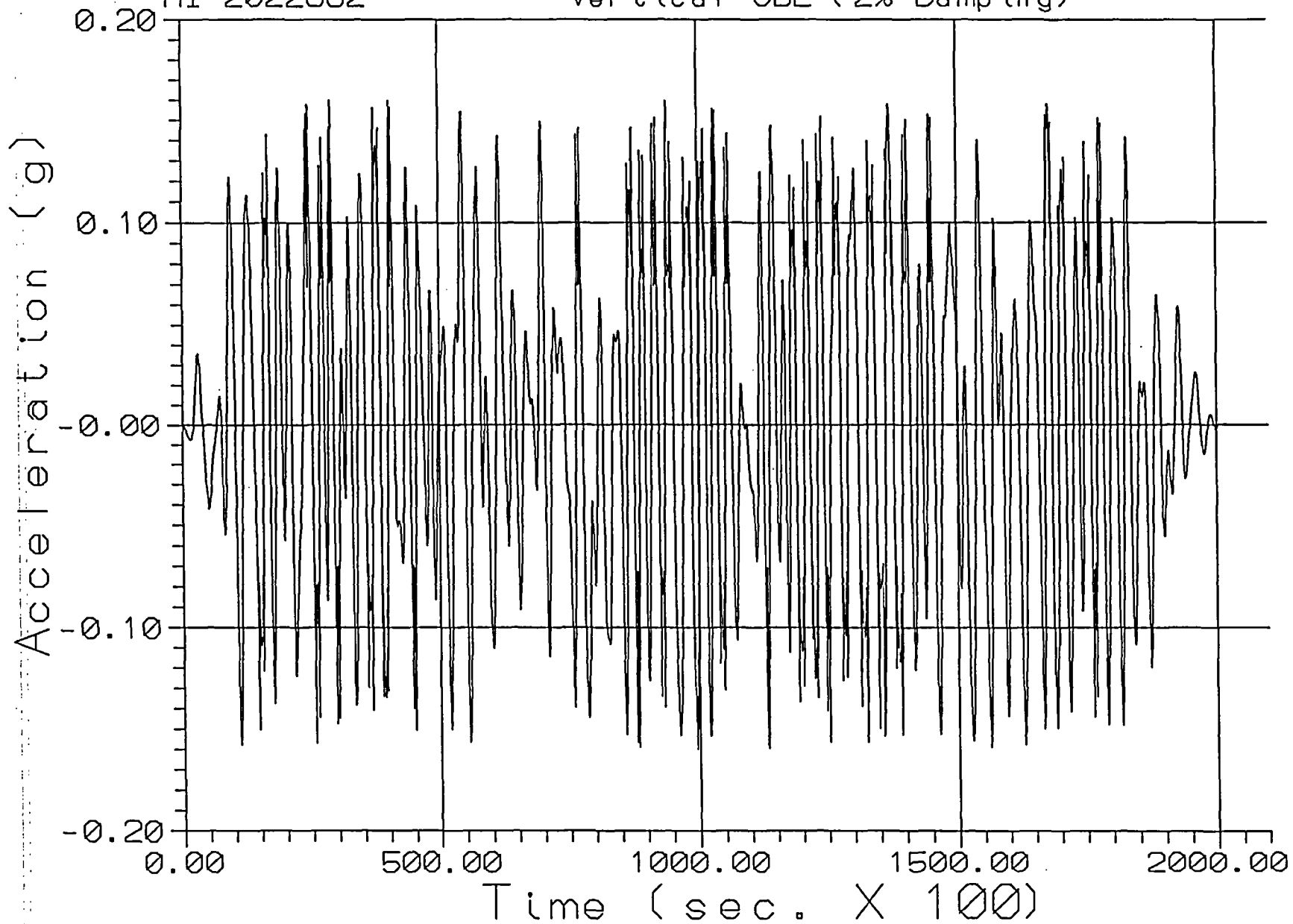


Figure 6.4.6  
Holtec Report  
HI-2022882

St. Lucie Unit 1 Elevation 21.50'  
Time History Accelerogram  
Vertical OBE (2% Damping)



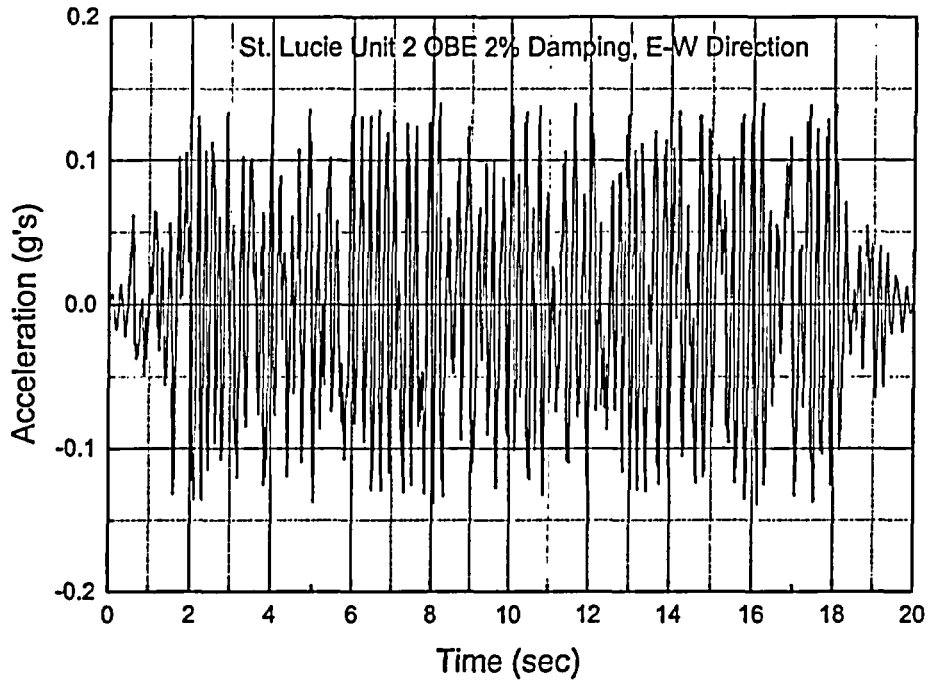


Fig. 6.4.7 OBE acceleration time history in the East-West direction

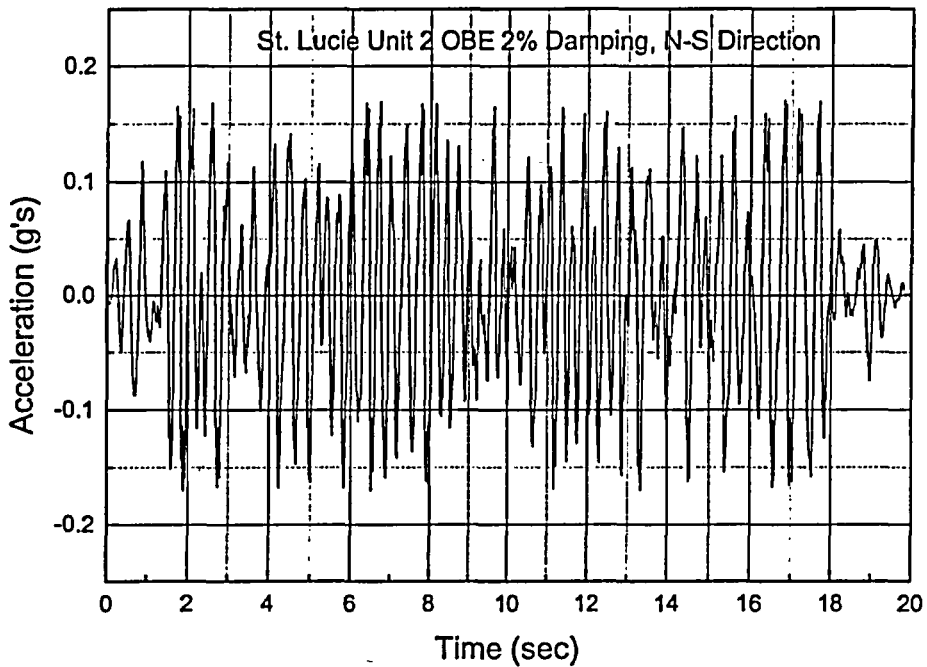


Fig. 6.4.8 OBE acceleration time history in the North-South direction

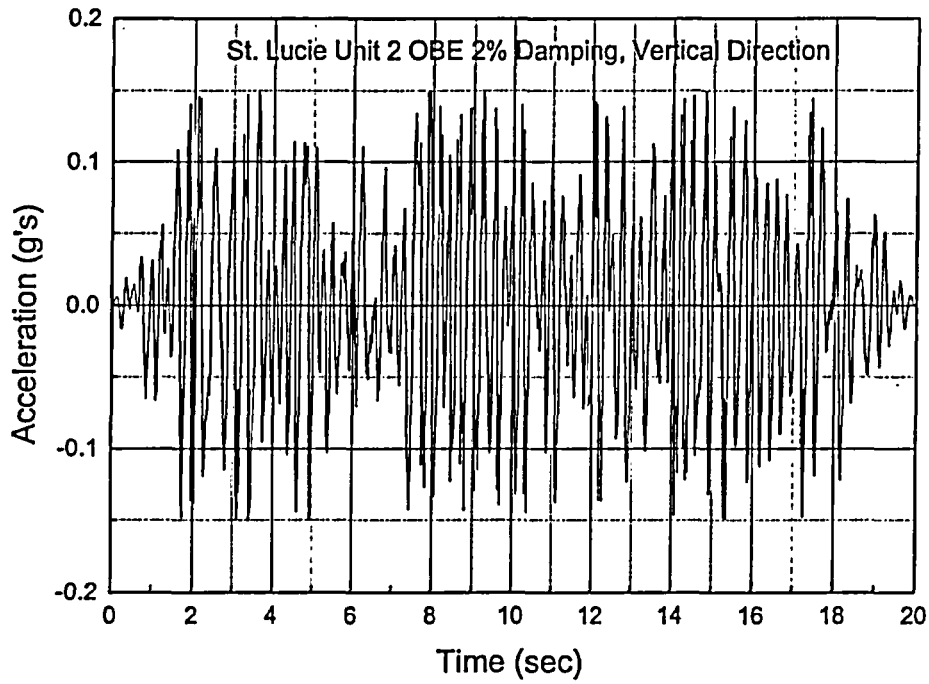


Fig. 6.4.9 OBE acceleration time history in the vertical direction

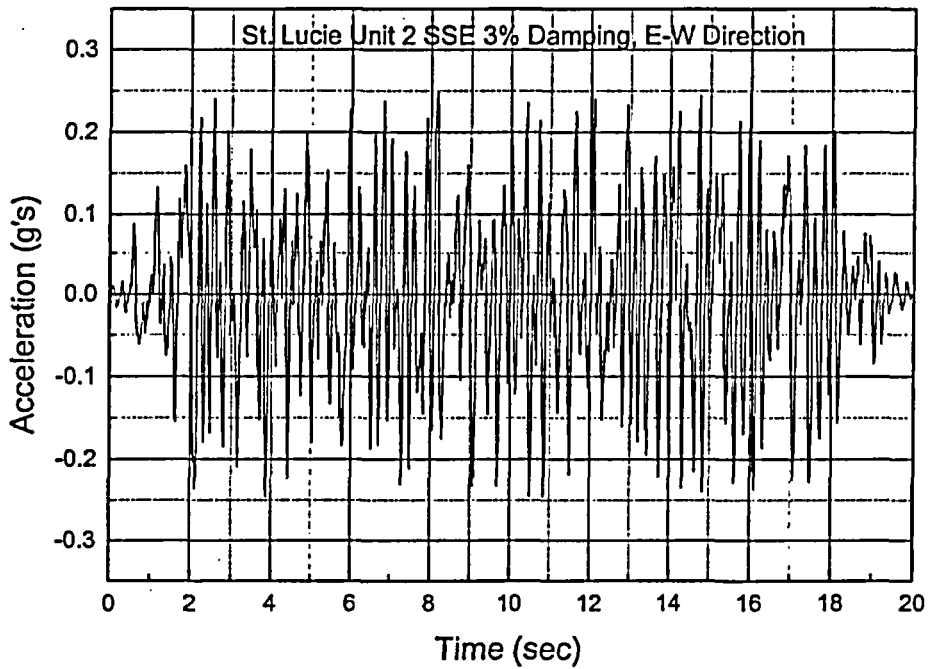


Fig. 6.4.10 SSE acceleration time history in the East-West direction

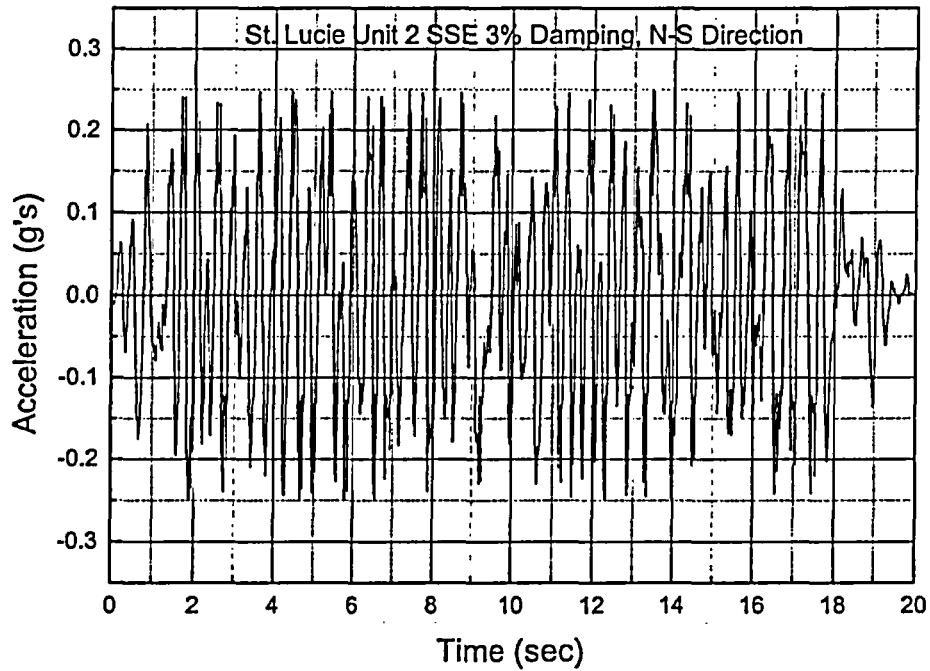


Fig. 6.4.11 SSE acceleration time history in the North-South direction

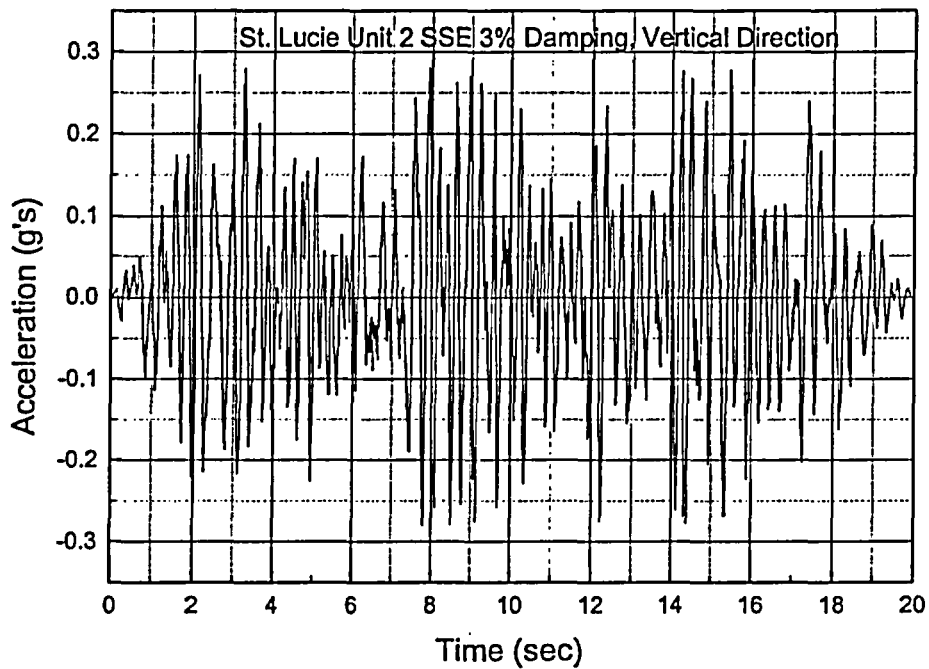


Fig. 6.4.12 SSE acceleration time history in the vertical direction

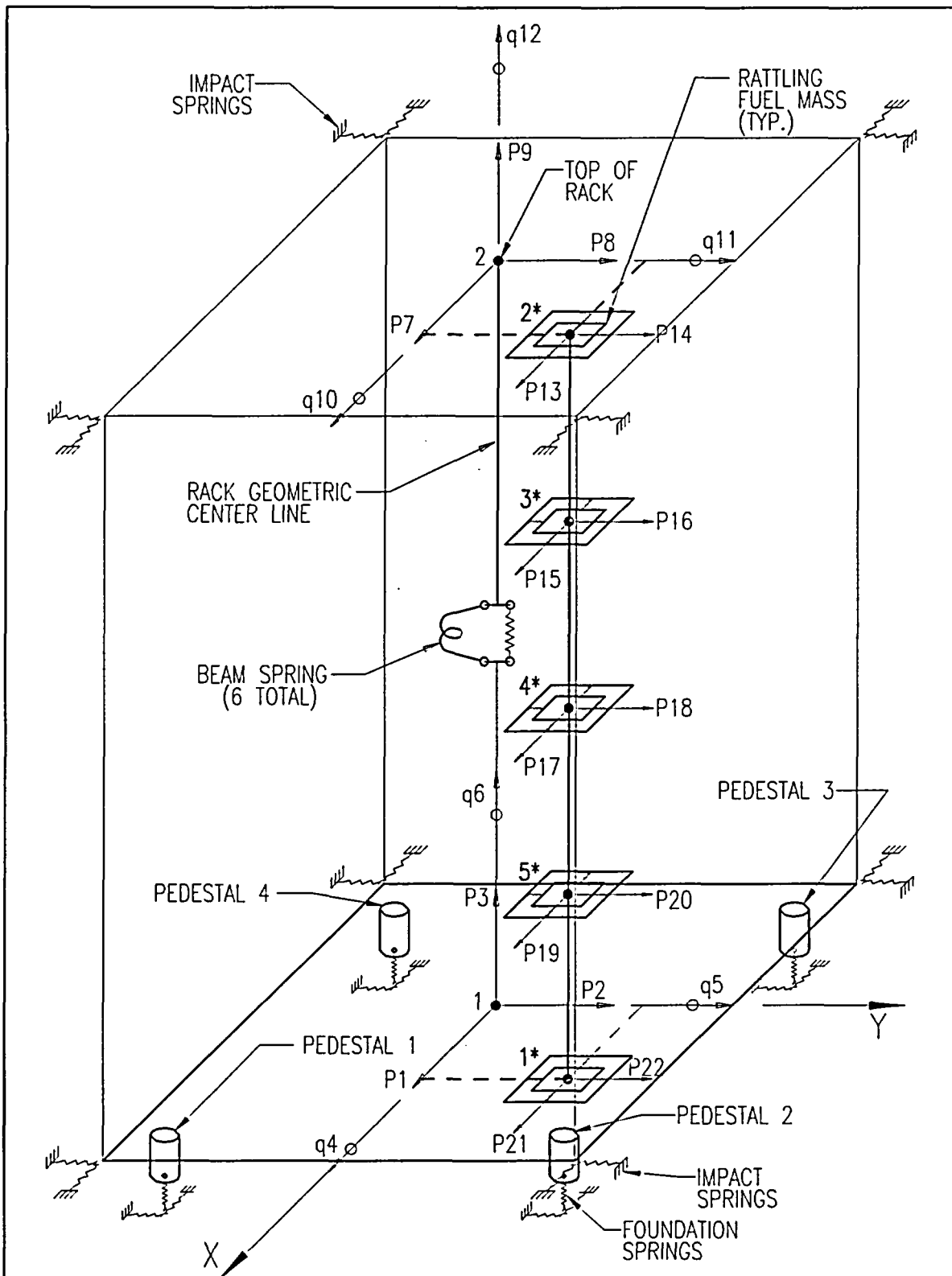


FIGURE 6.5.1; SCHEMATIC OF THE DYNAMIC MODEL OF A SINGLE RACK MODULE USED IN DYNARACK

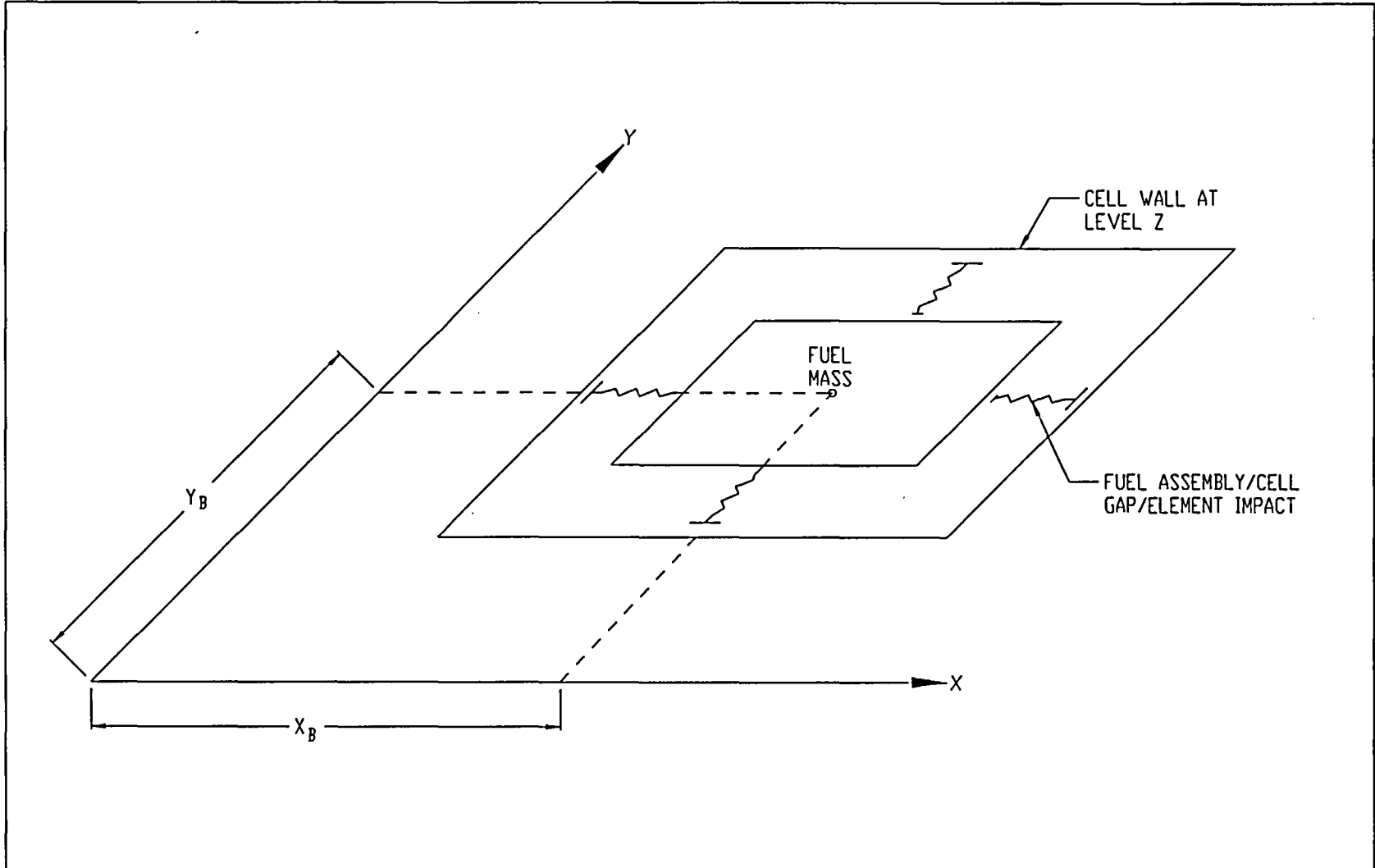


FIGURE 6.5.2; FUEL-TO-RACK GAP/IMPACT ELEMENTS AT LEVEL OF RATTLING MASS

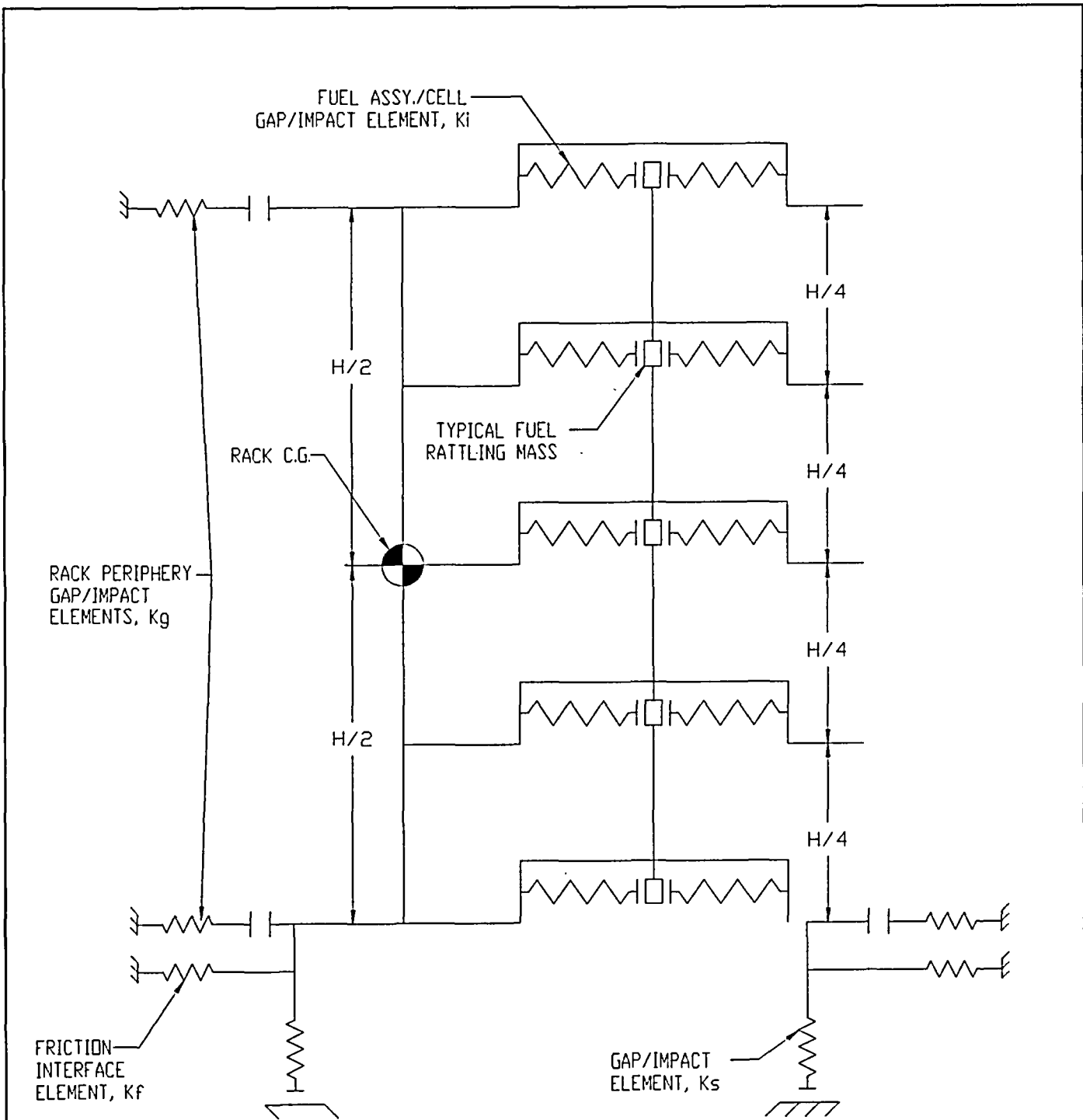
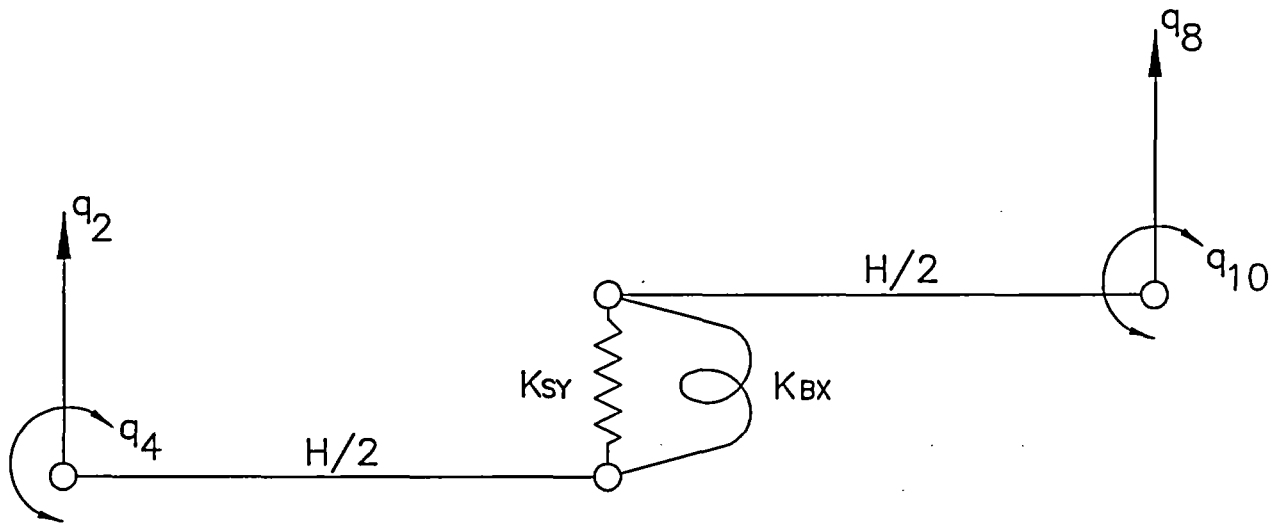
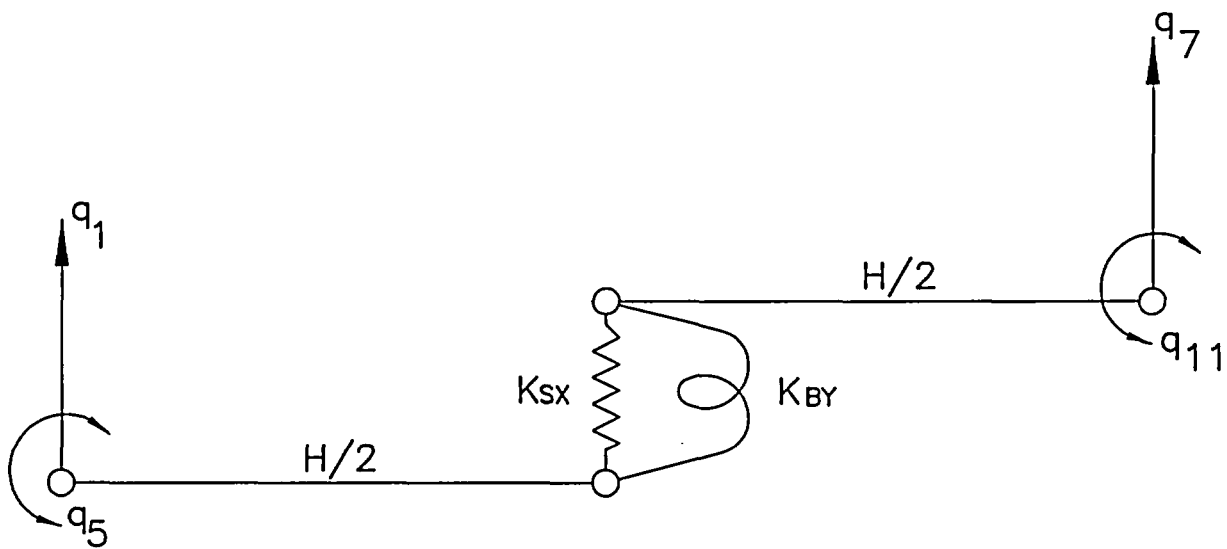


FIGURE 6.5.3; TWO DIMENSIONAL VIEW OF THE SPRING-MASS SIMULATION



FOR Y-Z PLANE BENDING



FOR X-Z PLANE BENDING

FIGURE 6.5.4; RACK DEGREES-OF-FREEDOM WITH SHEAR AND BENDING SPRINGS

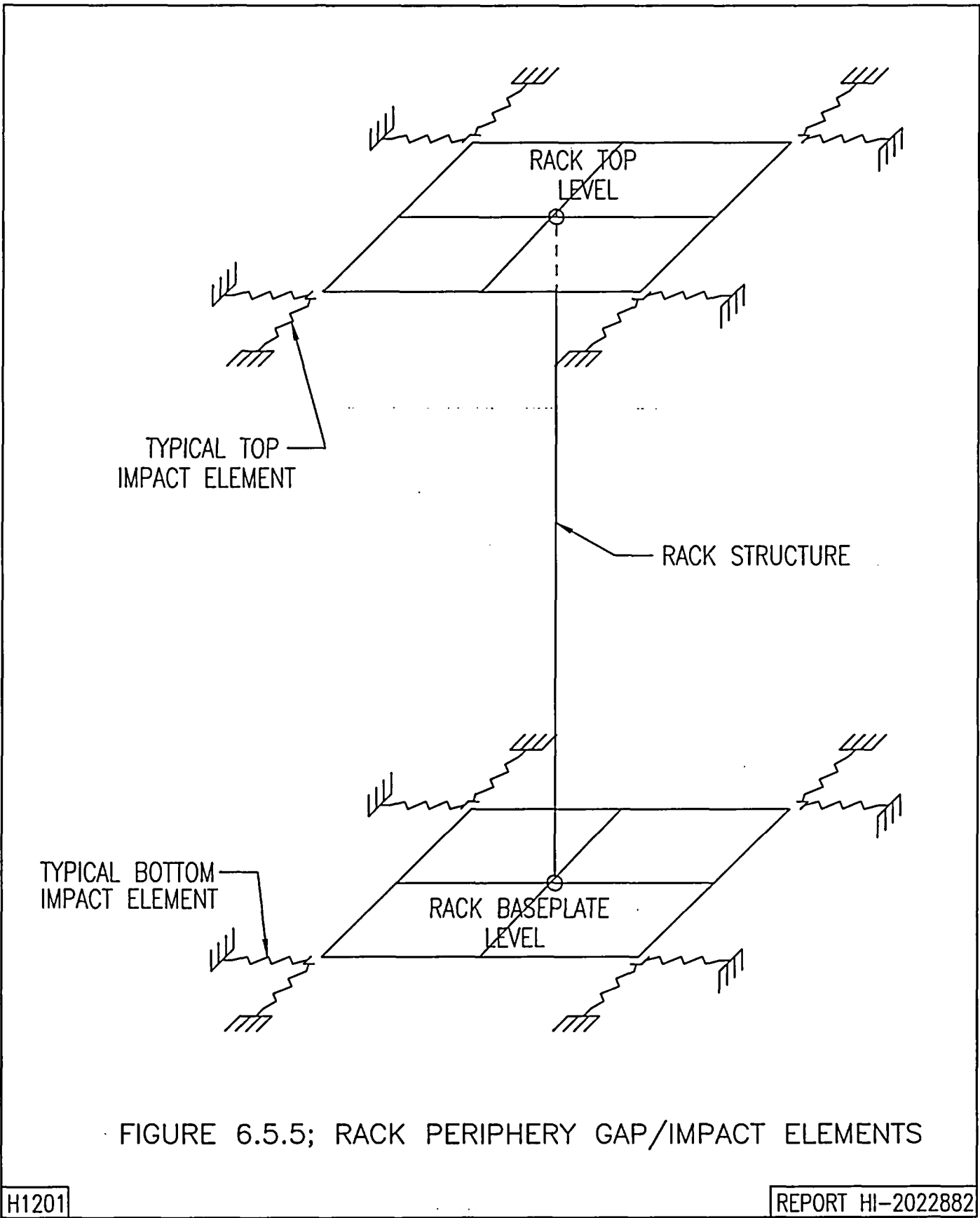


FIGURE 6.5.5; RACK PERIPHERY GAP/IMPACT ELEMENTS

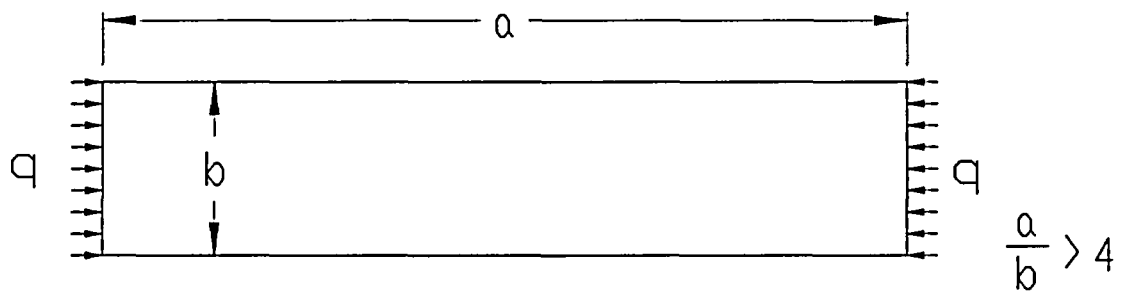


FIGURE 6.12.1; LOADING ON RACK WALL

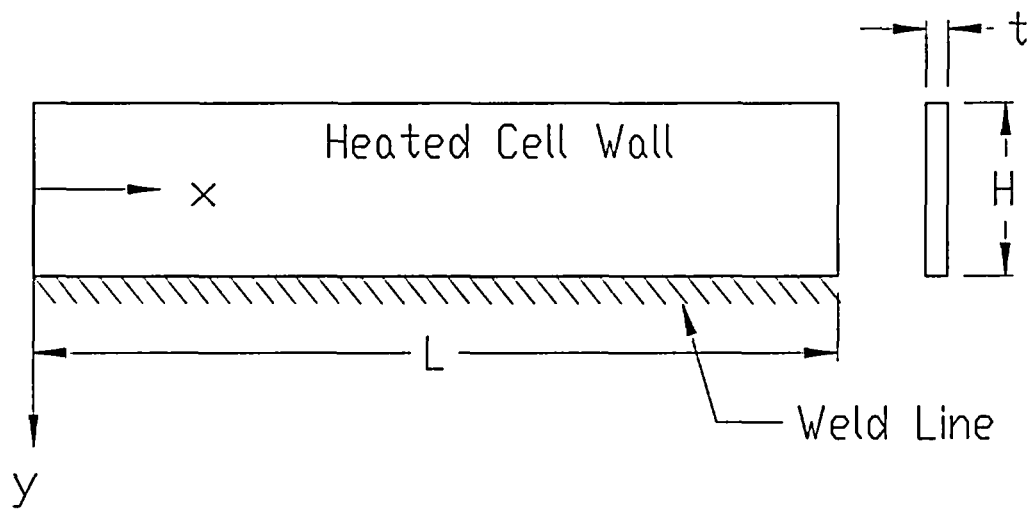


FIGURE 6.12.2; WELDED JOINT IN RACK

## 7.0 MECHANICAL ACCIDENTS

### 7.1 Introduction

The USNRC OT position paper [7.1.1] specifies that the design of the rack must ensure the functional integrity of the spent fuel racks under all credible fuel assembly drop events.

This chapter contains synopses of the analyses carried out to demonstrate the regulatory compliance of the proposed racks under postulated accidental drop events germane to the St. Lucie Plant (Unit 1 & Unit 2) cask pits; namely, that of a fuel assembly.

The proposed change does not impact assumptions in the current licensing basis on the potential fuel damage due to mechanical accidents.

### 7.2 Description of Mechanical Accidents

Analyses are performed to evaluate the racks subsequent to a fuel assembly impact under various fuel assembly drop scenarios. Two categories of accidental drop events are considered.

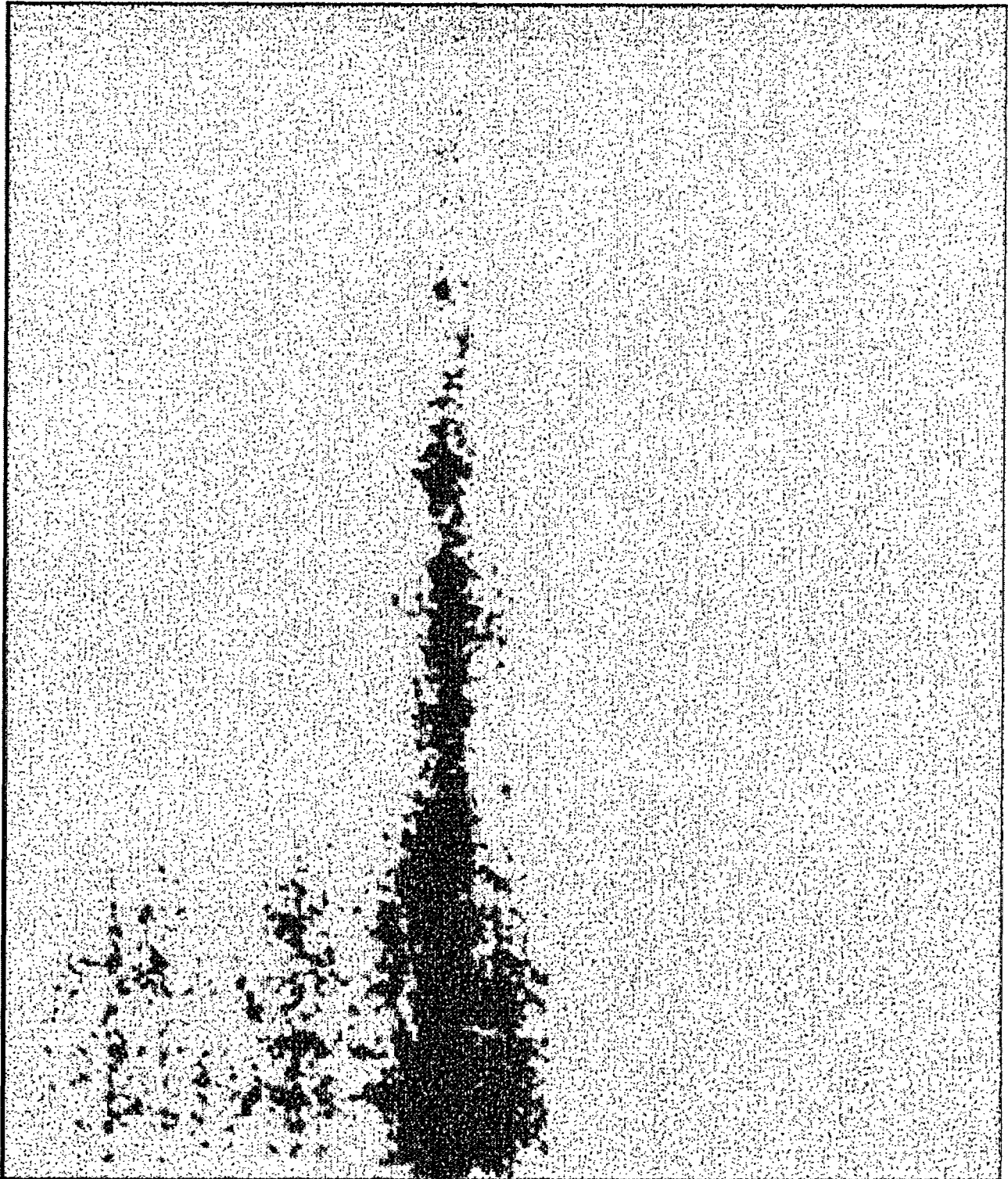
In the so-called “shallow” drop event, a fuel assembly, along with the portion of handling tool, which is severable in the case of a single element failure, is assumed to drop vertically and hit the top of the rack. Inasmuch as the new racks are of honeycomb construction, the deformation produced by the impact is expected to be confined to the region of collision. However, the “depth” of damage to the affected cell walls must be demonstrated to remain limited to the portion of the cell above the top of the “active fuel region”, which is essentially the elevation of the top of the Boral neutron absorber. Stated in quantitative terms, this criterion implies that the plastic deformation of the rack cell walls should not extend more than 26 inches (downwards) from the top for the Unit 1 rack (29.5 inches for Unit 2). In order to utilize an upper bound of kinetic energy at impact, the impactor is assumed to weigh 2,000 lbs and the free-fall height is conservatively assumed to be 36 inches.

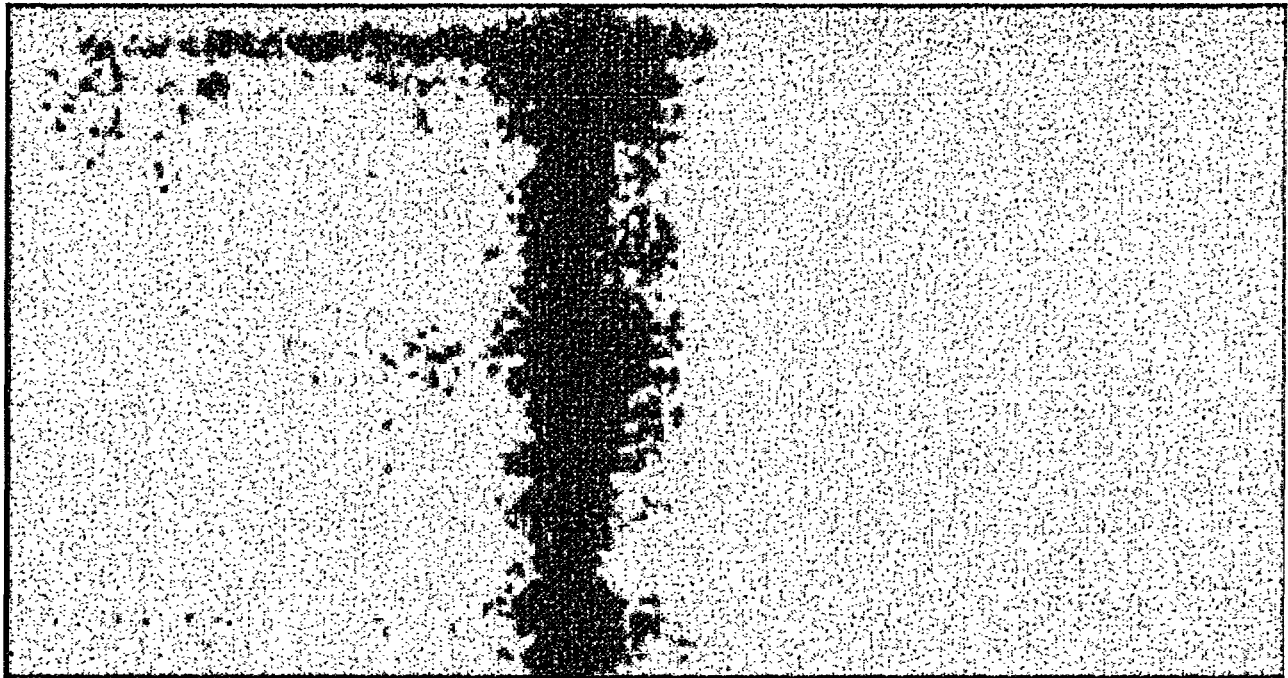
It is readily apparent from the description of the rack modules in Section 3 that the impact resistance of a rack at its periphery is considerably less than its interior. Accordingly, the limiting shallow drop scenario, which would produce maximum cell wall deformation, consists of the case where the fuel assembly impacts the peripheral cell wall, as shown in Figure 7.2.1.

The second class of fuel drop event postulates that the impactor free-falls 36 inches and then falls through an empty storage cell impacting the fuel assembly support surface (i.e., rack baseplate). This so-called “deep” drop event threatens the structural integrity of the baseplate. If the baseplate is pierced, and fuel assembly impacts the rack platform or drops onto the liner, then an abnormal condition of the enriched zone of fuel assembly outside the “poisoned” space of the fuel rack may develop. To preclude damage to the cask pit liner and to avoid the potential of an abnormal fuel storage configuration in the aftermath of a deep drop event, it is required that the baseplate remain unpierced and that the maximum lowering of the baseplate is shown to be acceptable by the criticality evaluations.

The deep drop event can be classified into two scenarios, namely, drop in an interior cell away from the support pedestal, as shown in Figure 7.2.2, and drop through cell located above a support leg, as shown in Figure 7.2.3. In deep drop scenario 1, the fuel assembly impacts the baseplate away from the support pedestal, where it is more flexible. Severing or large deflection of the baseplate leading to a secondary impact with the cask pit liner or rack platform are unacceptable results. In deep drop scenario 2, the baseplate is buttressed by the support pedestal and presents a hardened impact surface, resulting in a high load. The principal design objective is to ensure that the rack platform bottom does not tear the liner that overlays the reinforced concrete cask pit slab.

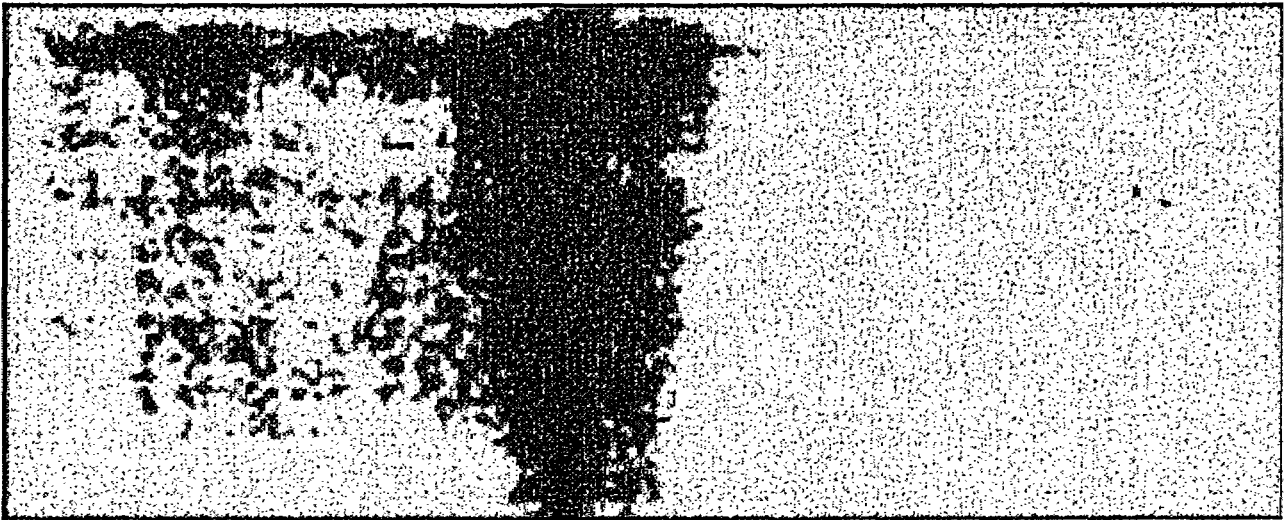
7.3 Incident Impact Velocity





#### 7.4 Mathematical Model

In the first step of the solution process, the velocity of the dropped object (impactor) is computed for the condition of underwater free fall in the manner of the formulation presented in the above section. Table 7.4.1 contains the computed velocities for the various drop events.



## 7.5 Results

### 7.5.1 Shallow Drop Event

For the shallow drop event, the dynamic analysis shows that the top of the impacted region undergoes localized plastic deformation. Figure 7.5.1 shows an isometric view of the post-impact geometry of the rack. The maximum depth of plastic deformation is limited to 12.5 inches, which is below the allowable deformation limit of 26 inches for Unit 1 and 29.5 inches for Unit 2.

### 7.5.2 Deep Drop Events

The deep drop through an interior cell does produce some deformation of the baseplate with no severing of the baseplate/cell wall welds. Figure 7.5.2 shows the deformed baseplate configuration. The fuel assembly support surface is lowered by a maximum of 1.96 inches, which is much less than the distance of 4.25 inches from the baseplate to the rack platform. The deformation of the baseplate has been determined to be acceptable with respect to lowering the fuel seating position and the resulting criticality consequences, as discussed in Chapter 4.0.

The deep drop event wherein the impact region is located directly above the support pedestal and support platform leg is found to produce a maximum stress of 3,933 psi in the liner, which is less than the yield stress of the liner material, as shown in Figure 7.5.3. Finally, the maximum compressive stress of 1,260.3 psi in the concrete slab is less than the concrete compressive strength of 3,000 psi, as shown in Figure 7.5.4. Therefore, there will be no abrupt or uncontrollable loss of water from the cask pit.

## 7.6 Conclusion

The drop events postulated for the St. Lucie Plant cask pits were analyzed and found to produce localized damage well within the design limits for the racks. The shallow drop event is found to produce some localized plastic deformation in the top of the storage cell, but the region of permanent strain is limited to the portion of the rack structure situated above the top of the active fuel region. The analysis of the deep drop event at cell locations selected to maximize baseplate deformation indicates that the downward displacement of the baseplate is limited to 1.96 inches, which ensures that unacceptable

criticality consequences would not occur. The deep drop case analyzed for the scenario to produce maximum pedestal force indicates that the pedestal axial load and corresponding load at the base of the rack platform is sufficiently small to preclude liner and concrete slab damage. Therefore, there will be no uncontrollable loss of cask pit water inventory. In conclusion, the new Holtec high-density spent fuel racks for the St. Lucie Plant cask pits possess acceptable margins of safety under the postulated mechanical accidents.

7.7 References for Chapter 7.0

[7.1.1] "OT Position for Review and Acceptance of Spent Fuel Storage and Handling Applications," dated April 14, 1978, and addendum dated 1979.

[7.4.1] NUREG/CR-6608, "Summary and Evaluation of Low-Velocity Impact Tests of Solid Steel Billet Onto Concrete Pads", dated February 1998.

Table 7.4.1

IMPACT EVENT DATA

Case	Impactor Weight (lb)	Impactor Type	Drop Height (in)	Impact Velocity (in/sec)
1. Shallow drop event	2,000	Fuel assembly & handling tools	36	150.9
2. Deep drop event scenario 1 (away from pedestal)	2,000	Fuel assembly & handling tools	216 ‡	273.7
3. Deep drop event scenario 2 (above pedestal)	2,000	Fuel assembly & handling tools	216 ‡	101.7 †

‡ The assumed drop height of 216 inches is conservative, because it exceeds 208.75 inches, which is the sum of the 36-inch free-fall height plus the largest rack cell height of 172.75 inches.

† Note that the velocity for the drop above a pedestal is much less than the condition away from the pedestal, since the hydraulic resistance is significantly increased because the pedestal blocks the baseplate flow hole.

Table 7.4.2

MATERIAL DEFINITION

Material Name	Material Type	Density (pcf)	Elastic Modulus (psi)	Stress		Strain	
				First Yield (psi)	Failure (psi)	Elastic	Failure
Stainless Steel	SA240-304L	490	2.782e+07	2.278e+04	6.772e+04	8.188e-04	3.800e-01
Stainless Steel	SA240-304	490	2.782e+07	2.700e+04	7.260e+04	9.705e-04	3.800e-01
Zircaloy	--	404	1.040e+07	8.05e+04	8.05e+04	1.000e-02	1.500e-02
Stainless Steel	SA564-630	490	2.782e+07	1.098e+05	1.400e+05	3.947e-02	3.800e-01
Concrete <sup>†</sup>	f <sub>c</sub> =3,000 psi	150	3.122e+06	--	3.000e+03	--	--

<sup>†</sup> The concrete is modeled as recommended in NUREG /CR-6608 [7.4.1].

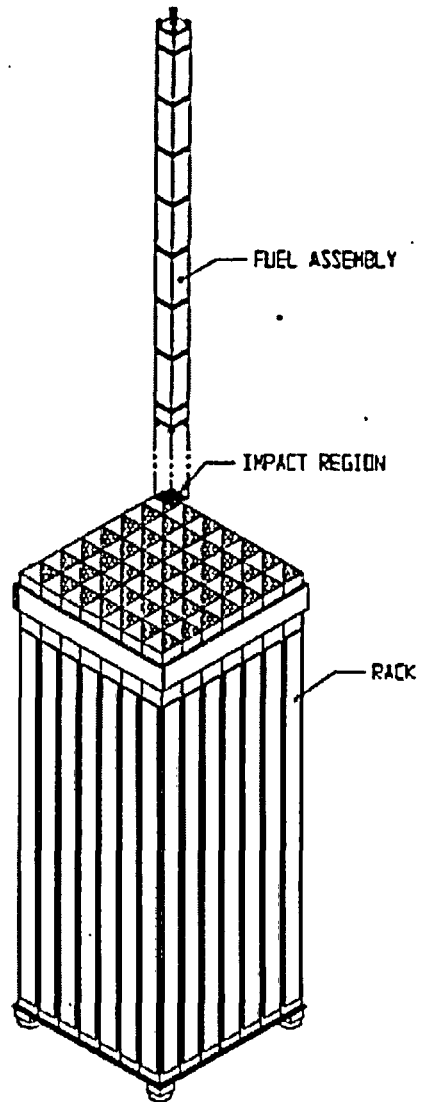


Fig. 7.2.1 Schematics of the "shallow" drop event

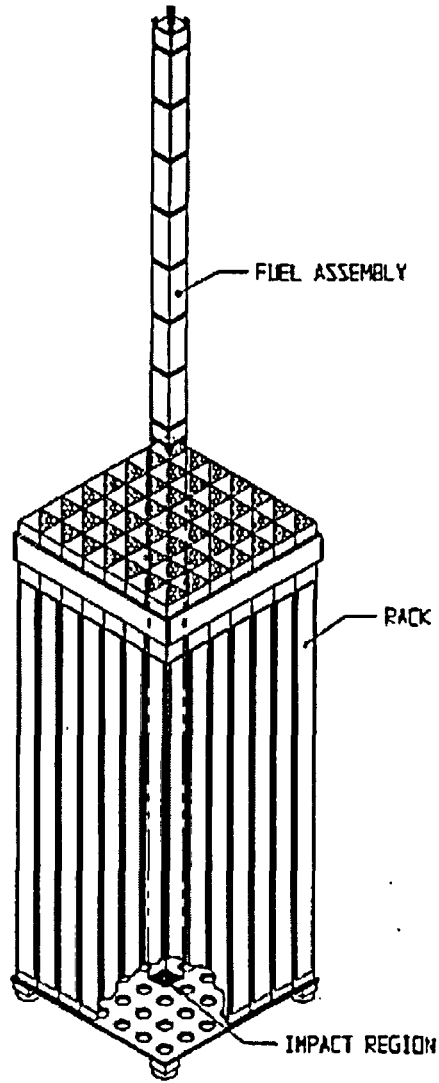


Fig. 7.2.2 Schematics of the “deep” drop scenario 1

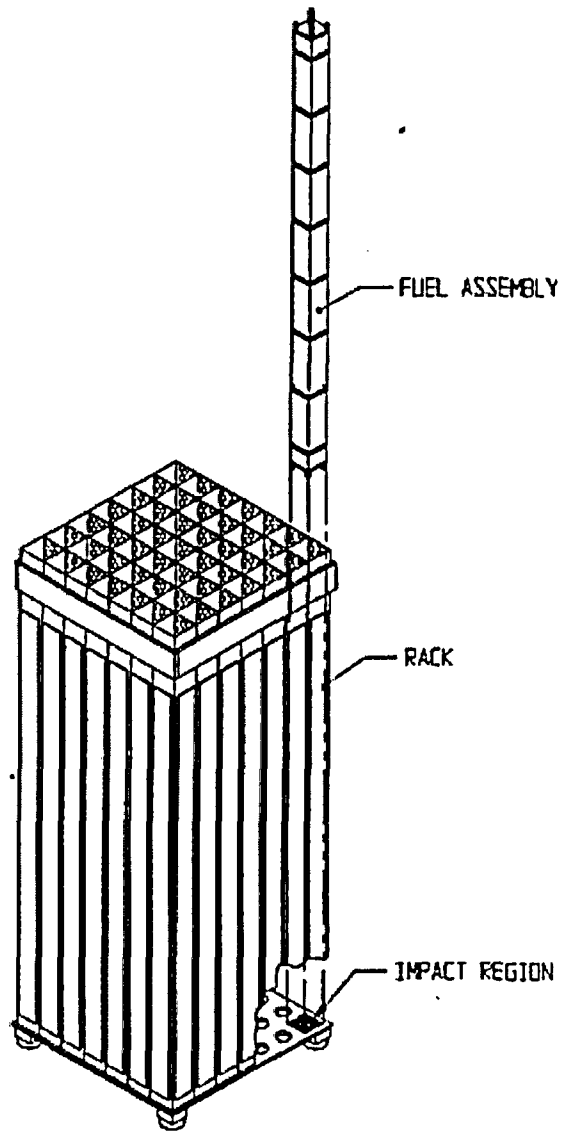


Fig. 7.2.3 Schematics of the "deep" drop scenario 2

"SHALLOW DROP" OF FUEL ASSEMBLY  
 STEP 33 TIME = 1.3000010E-001  
 PSTN(MD)

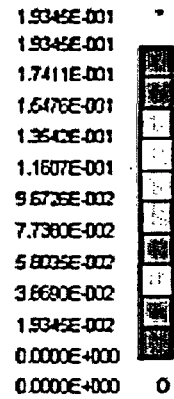
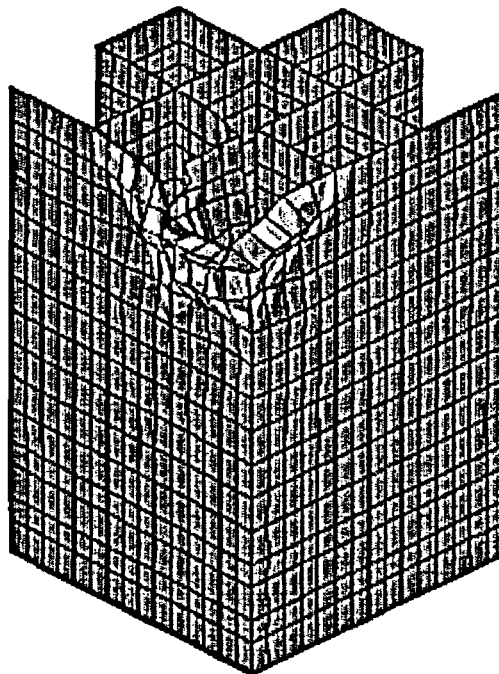


Fig. 7.5.1 "Shallow" Drop: Maximum Plastic Strain

STEP 25 TIME = 1.2499655E-002  
Z COORDINATE DISPLACEMENT

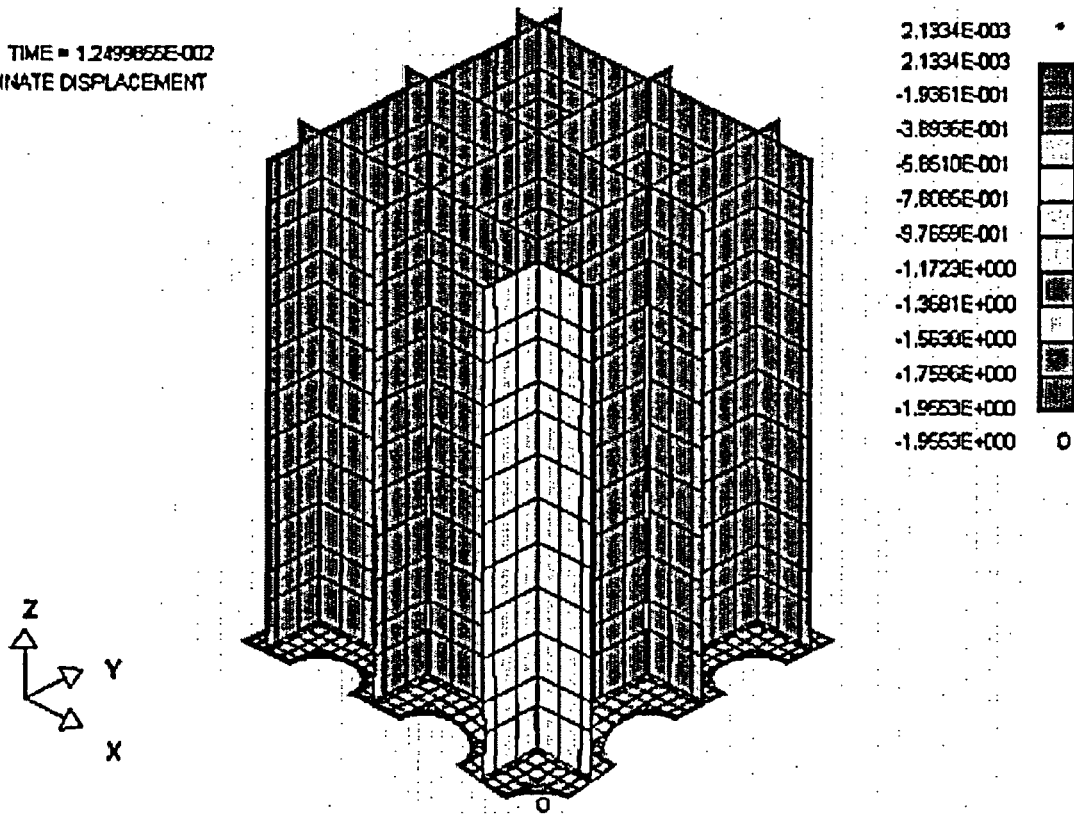


Fig. 7.5.2 "Deep" Drop Scenario 1: Maximum Vertical Displacement

FUEL ASSEMBLY "DEEP" DROP SCENARIO 2  
STEP 9 TIME = 4.499004E+003  
MAX VONMISES

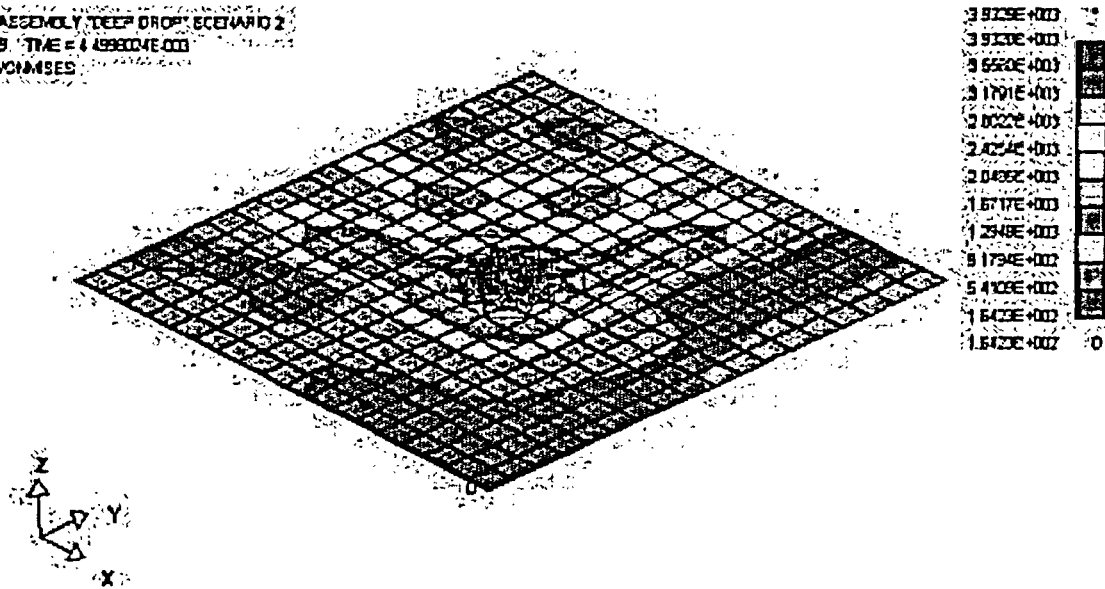


Fig. 7.5.3 "Deep" Drop Scenario 2: Maximum Von Mises Stress – Liner

FUEL ASSEMBLY DEEP DROP SCENARIO 2  
STEP 9 TIME = 4.49900E+003  
SI (M) 1000

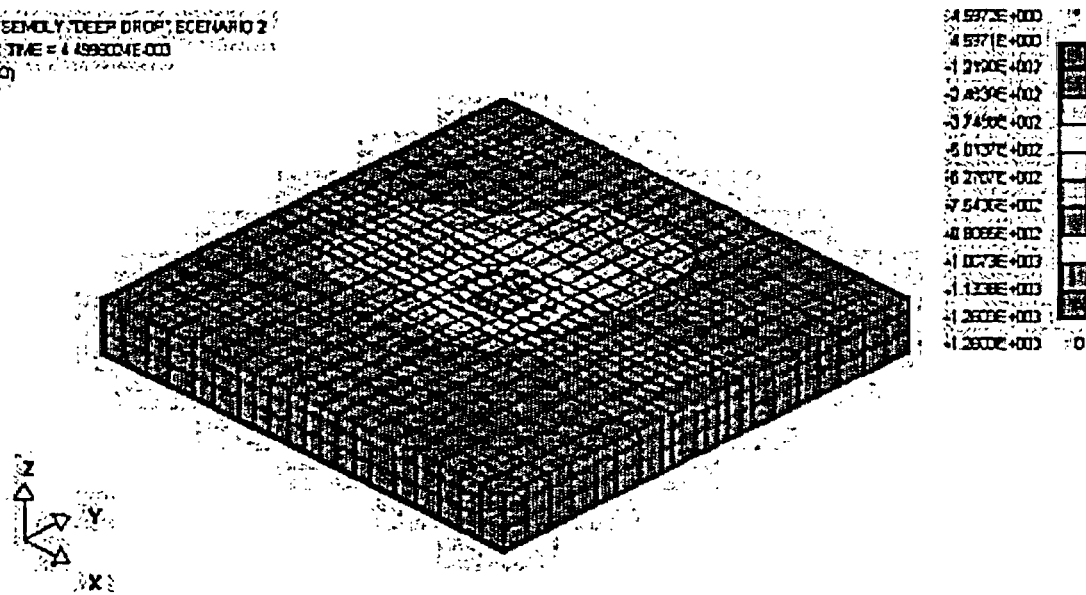


Fig. 7.5.4 "Deep" Drop Scenario 2: Maximum Compressive Stress – Concrete

## 8.0 FUEL HANDLING BUILDING STRUCTURAL INTEGRITY EVALUATIONS

Structural integrity evaluations of the regions of the reinforced concrete structure affected by the proposed capacity expansion (Cask Pit (CP) and portions of the Spent Fuel Pool (SFP) exterior walls in Units 1 and 2) are summarized in this section. For purposes of structural evaluation, the exterior walls of the SFP are also the exterior walls of the Fuel Handling Building (FHB), and the terms are used interchangeably. Since the two units have some geometric and load differences, and are governed by different structural design requirements, the evaluations are summarized in separate sub-sections.

### 8.1 Unit 1 Evaluation

#### 8.1.1 Introduction

The St. Lucie Unit 1 Cask Pit is in the northeast corner of the Fuel Handling Building (FHB), which is a safety related, Seismic Category I, reinforced concrete structure. The Cask Pit is adjacent to the SFP, and the two areas share common exterior walls on the north and east sides of the FHB. Spent fuel is to be placed within a new storage rack located in the Cask Pit. Also, the Spent Fuel Handling Crane outside the Fuel Handling Building (FHB) will be upgraded to single-failure proof, resulting in new design tornado and seismic loads on some portions of the exterior walls (mainly the east exterior wall of the FHB is affected). This section summarizes the analysis to demonstrate structural adequacy of the Cask Pit and structural adequacy of the building walls subject to the revised loadings from the fully loaded cask pit<sup>1</sup> and crane. Because the south and west walls of the SFP are unaffected by the addition of the rack in the Cask Pit or the upgraded crane loads, they are not included in this evaluation.

Figure 8.1.1 shows a horizontal section through the Unit 1 FHB above the spent fuel pool slab. The structural evaluation of the affected portion of the Unit 1 FHB is conducted using a finite element model of the north exterior wall (between row lines RAA and RAC) and the east exterior wall (between column lines FH2 and FH4) extending the width of the spent fuel pool. These are the walls affected by addition

---

<sup>1</sup> The analysis considers a fully loaded cask pit rack, with reasonable consideration for fuel inserts, and rack platform bearing on the cask pit floor (124 tons for Unit 1 and 181.6 tons for Unit 2). These weights bound those of commercially available spent fuel transfer casks such as the Holtec HI-TRAC or HI-STAR.

of the new spent fuel rack and by the increased loading from the upgraded fuel cask crane. The east exterior wall extends above the spent fuel pool operating deck at El. 62' (between column lines FH2 and FH4) to the fuel handling building roof (up to El. 94'), and this portion is also included in the evaluation since additional loads from the overhead crane are applied on this wall (at column line FH3). The column line RAC, at the juncture of the west exterior wall and the north exterior wall, is also a location where revised loadings from the building crane are imposed. These loads impart minimal bending loading to the building exterior north and west walls; the effect of these loads on the SFP walls is negligible.

Results for individual load components are combined using the factored load combinations mandated by the St. Lucie Unit 1 UFSAR [8.1.1], and are based on the "ultimate strength" design method. Bending moment capabilities are checked for appropriate sections on each wall in each direction (vertical and horizontal) for concrete structural integrity. The appropriate relationships between bending moment capacity and axial tension or compression loads are utilized in accordance with design procedures permitted by the governing ACI 318-63 Code [8.1.2]. Shear capability is evaluated along the horizontal base of the affected walls. Since the slab is founded on grade and is 5.5' thick, bending of the slab in the Cask Pit due to the addition of the new spent fuel rack is not a limiting load condition, and calculations for the slab are confined to bearing integrity and to liner stress evaluation. Load Combinations and structural capacity assessments follow requirements of the Unit 1 UFSAR [8.1.1] and the American Concrete Institute Code (ACI 318-63) [8.1.2].

The thermal loading in the reinforced concrete structure is considered in the manner specified in the applicable codes. Surface temperatures on the opposite surfaces of the pool walls are computed to reflect normal operating temperature gradients. Consistent with the standard design practices, the temperature gradient established for the pool walls is intended to subsume local thermal effects such as direct heat deposition into the concrete from the absorption of gamma radiation from the stored spent fuel.

### 8.1.2 Description of Cask Pit Structure and Exterior Building Walls

The analyzed reinforced concrete structure consists of the north exterior wall up to El. 62' (wall thickness = 6'), the east exterior wall up to El. 62' (wall thickness = 6') and the east wall above El. 62'. The east wall above El. 62' is modeled as a 2' thick wall except at the column line FH3 where the concrete thickness is increased to 3' over a 4' wide region to accommodate additional column reinforcement. The south and west pool walls are not modeled, as these receive no additional direct loading from the added cask pit rack or the revised crane loads. The Cask Pit for Unit 1 is enclosed on the west and south sides by built-up steel walls extending approximately 1/3 of the height of the SFP concrete walls. These walls are not exposed to significant loading as they are fully submerged in the pool and hydrostatic loads will be balanced across the walls. Therefore, these interior cask pit walls are conservatively not included in the finite element analysis. The finite element grid for the analysis of the Unit 1 structure is shown in Figure 8.1.2 with approximate concrete elevations used for the Unit 1 model included on the figure. Note that the Cask Pit floor at El. 17' is lower than the SFP slab at El. 20.5'. The top of the operating floor is at elevation 62'-0". Dimensions in the model are approximated to a convenient whole number to ensure a uniform element size in the analysis. Figure 8.1.3 shows the model with boundary conditions included. Connections to the south and west walls are appropriately modeled to reflect restraint of lateral displacement and rotation about the vertical axis at the respective junctions. The north and east walls are considered as planar plates fixed at the base to the supporting SFP and Cask Pit slab and to the adjacent south and east walls. The upper edge of the north wall at El. 62' is considered as a free edge; no new loadings are imposed on the upper portion of the north wall by the proposed modifications. The boundary of the east wall, above El. 62' is assumed restrained against lateral motion at column line FH4 by the adjacent wall structure.

### 8.1.3 Analysis Procedures

The reinforced concrete walls are subjected to individual "unit" load cases covering the service conditions (the structural weight of the concrete structure, the hydro-static water pressure and the temperature gradient), seismic induced loads (structural seismic loads, hydro-dynamic water loads, and rack-structure interaction dynamic loads) for OBE and SSE conditions, and tornado loads. The service

condition loads are considered as static acting loads; the seismic induced loads for both OBE and SSE seismic events are obtained from the application of bounding-two-directional acceleration spectra (vertical and one horizontal) appropriate to the base of the SFP with input seismic acceleration amplifier defined on the basis of a frequency analysis of the structure. Finally, tornado loadings are derived from applicable information on wind speeds and differential pressures given in the St. Lucie UFSAR [8.1.1]. Results from the seismic and tornado load cases are combined algebraically and then combined with the static load.

The reinforced concrete is considered elastic and isotropic. The elastic characteristics of the concrete are independent of the reinforcement contained in each structural element for the mechanical load cases when un-cracked cross-sections are assumed. This assumption is valid for all load cases with the exception of the thermal loads, where for a more realistic description of the reinforced concrete cross-section behavior the assumption of cracked concrete is used. To simulate the variation and the degree of cracking patterns, the original elastic modulus of the concrete is reduced in accordance with the methodology suggested by ACI 349 [8.1.3]. Table 8.1.1 summarizes the concrete properties employed in the structural evaluation of Unit 1.

#### 8.1.4 Definition of Loads Included in Structural Evaluation

##### 8.1.4.1 Static Loading (D = Dead Loads)

- 1) Dead weight includes the weight of the north and east walls and crane reactions
- 2) Dead weight of Cask Pit spent fuel rack fully loaded with fuel and rack platform. (this total dry weight of 124 tons only affects the Cask Pit floor slab concrete bearing evaluation).
- 3) The hydrostatic water pressure acting on the walls.

##### 8.1.4.2 Seismic (E = OBE; E' = SSE) and Tornado Induced Loads (Wt)

- 1) Vertical loads transmitted by the spent fuel rack to the slab during a seismic event (only affects the Cask Pit floor slab bearing evaluation).

- 2) Horizontal hydrodynamic inertia loads due to the contained water mass and sloshing loads in the entire SFP (considered in accordance with [8.1.4]) that arise during a seismic event.
- 3) Horizontal hydrodynamic pressures between spent fuel rack and Cask Pit walls caused by rack motions during a seismic event.
- 4) Seismic inertia force of the walls from the wall mass.
- 5) Seismic or Tornado loads from the fuel building crane acting on the east wall.
- 6) Tornado loading on the north and east exterior walls from wind force and differential pressure.

#### 8.1.4.3 Thermal Loading

The thermal load case is defined by the interior bulk temperature, the exterior air temperature, and convection heat transfer coefficients at the concrete surfaces; this data suffices to determine a temperature gradient across the wall. The normal operating pool water bulk temperature is 134.5°F. This temperature is the poolside wall temperature up to El. 62'. The east wall, above El. 62' is assumed to be exposed to a maximum inside air temperature of 106.75°F; inclusion of an appropriate free convection heat transfer coefficient results in an inside wall temperature of approximately 84.9°F where exposed to the building air. For the Fuel Handling Building structural evaluation, a suitable outdoor temperature is 41F, which represents the 99% value for West Palm Beach [8.1.5] (meaning that there would only be approximately 22 hours a year (not necessarily consecutive) at or below the temperature of 41F). Assuming still air for the purposes of computing an outside surface film coefficient, the corresponding airside (outside) wall temperature is approximately 62.8°F for the outside wall above the pool and 63.9°F for the outside walls below the pool operating floor.

#### 8.1.4.4 Load Combinations and Acceptance Criteria

No live loads are defined for the areas under consideration. Results from a suite of unit load analyses are used to form appropriate load cases and then combined in accordance with the load combinations specified in Subsection 3.8.1.5 of the St. Lucie Unit 1 UFSAR [8.1.1].

The final load combinations evaluated for structural integrity are:

For "Normal Operation and OBE Condition" the following load combinations are considered:

- Load Combination No. 1 =  $1.5 \cdot D + 1.5 \cdot T_o$

- Load Combination No. 2 =  $1.25 \cdot (D + T_o + E)$

- Load Combination No. 3 =  $1.25 \cdot (D + T_o - E)$

For the "SSE Condition", "Wind (Tornado) Condition", the load combinations are:

- Load Combination No. 4 =  $1.05 \cdot (D + T_a) + E'$

- Load Combination No. 5 =  $1.05 \cdot (D + T_a) - E'$

- Load Combination No. 6 =  $1.05 \cdot (D + T_a) + W_t$

- Load Combination No. 7 =  $1.05 \cdot (D + T_a) - W_t$

where:

D = dead loads;

T<sub>o</sub> = thermal load during normal operation;

T<sub>a</sub> = thermal load concurrent with seismic or tornado = T<sub>o</sub>

E = OBE earthquake induced loads combined in accord with the Unit 1 UFSAR;

E' = SSE earthquake induced loads combined in accord with the Unit 1 UFSAR;

W<sub>t</sub> = Tornado Loading

Note that seismic loads and tornado loads are considered to be applied in either direction and include both direct effects and loads from the overhead crane. Note also that load combinations with hurricanes (194 mph) wind are not governing as they provide surface pressure loadings that are the same order or less than the seismic pressures and/or the tornado pressures.

Moments and shears computed for each load combination are compared with their respective capacities. Consistent with the intent of the guidance provided in the ACI literature, and recognizing that there is always load re-distribution occurring in a concrete structure designed in accordance with ultimate strength methods, characteristic section widths (horizontal and vertical) are established over which moments and shears are averaged and then compared with the averaged section capacity. Similarly, the transverse shear is averaged over the same section width to define the “section shear”.

The ratios of the moment and shear capacities to their respective “section” values are referred to as the safety factor (SF). In computing the safety factor for section moments and shears in the presence of in-plane loads, the appropriate interaction relationships are employed using ACI guidance or specific formulas found in the Code.

### 8.1.5 Results of Unit 1 Reinforced Concrete Analyses

#### 8.1.5.1 Building East Wall Above Elevation 62'

The structural evaluation of the east wall above 62' is evaluated and the axial forces, the bending moments and the shear forces were computed for all load combinations. The reinforced concrete cross-sectional capacities were determined and used to obtain the safety factors of the structural elements for each load combination considered. Safety factors are defined as the allowable load divided by the computed load and continued acceptability is ensured if the safety factor exceeds 1.0. The calculated minimum safety factors for the sections of the east wall (above El. 62') for each load combination for the wall and for the intermediate vertical column FH3 strengthening the wall against lateral loads are:

East Wall Bending	Cross-section normal to vertical direction	3.86 (load case 6)
	Cross-section normal to horizontal direction	2.90 (load case 2)
East Wall Base Shear		8.31 (load case 6)
Vertical Column FH3 Bending		4.31 (load case 1)
Vertical Column FH3 Shear		1.21 (load case 6)

### 8.1.5.2 North and East SFP Walls Below Elevation 62'

The limiting safety factors from all section locations on both walls and for all load combinations are:

East and North Wall Bending	Cross-section normal to vertical direction	2.44 (load case 1)
	Cross-section normal to horizontal direction	1.17 (load case 2)
East and North Wall Base Shear		2.87 (load case 2)

### 8.1.6 Pool Liner-Cask Pit Floor Bearing Evaluation

The pool liner is subject to in-plate compressive strains due to differential thermal load arising from the different coefficient of thermal expansion ascribed to the liner and the underlying concrete in the Cask Pit. An in-plane stress is also developed in the liner to resist lateral loads arising from friction between the liner and the Cask Pit platform pedestals during a seismic event. Conservatively using a bounding 150-degree F water for this specific evaluation, the in-plane mean thermal stress in the Cask Pit slab liner, due to differential thermal expansion, is below 5200 psi. The additional in-plane stress to resist lateral forces during a seismic event is below 2300 psi. The liner will not tear or buckle under this bounding combined stress level and no tensile cracking of the concrete slab occurs from mean thermal expansion. The combined in-plane stress (7500 psi) is below the appropriate stress limit for the seismic load condition.

Concrete bearing strength requirements are satisfied by conservatively assuming the factored vertical load from the most highly loaded platform shim plate of the Cask Pit platform supporting the Cask Pit spent fuel rack and assuming that a leak chase is positioned directly below the shim plate. The allowable bearing stress for the confined concrete under the shim plate is  $2(1.9 \times 0.25)f_c'$  in accordance with ACI 318-63 limits, where  $f_c' = 5200$  psi is the slab concrete compressive strength. It is appropriate to consider the concrete as confined since the leak chase cutout is small and restricted to a 1.5" depth below the surface. The calculated safety factor (allowable strength based on confined concrete/calculated average compressive concrete stress) is:

SF(concrete bearing) = 2.42

#### 8.1.7 Conclusions for Unit 1

Regions affected by loading the Cask Pit with a new rack fully-loaded with fuel assemblies and uprated crane support loads are examined for structural integrity under bending and shearing action. It is determined that adequate safety margins exist when the factored load combinations are checked against the appropriate structural design strengths. To ensure that safety factors in excess of 1.0 were maintained in the presence of a moderate wind outside the plant, the temperature gradients were increased to reflect an outside surface heat transfer coefficient appropriate to a 9 knot steady wind. For the most limiting load combination, the minimum safety factor remained above 1.0. Finally, it is also shown that local loading on the liner does not compromise liner integrity and that concrete bearing strength limits are not exceeded.

## 8.2 Unit 2 Evaluation

### 8.2.1 Introduction

The St. Lucie Unit 2 cask pit is located in the NE corner of the Fuel Handling Building (FHB), which is a safety related, Seismic Category I, reinforced concrete structure. Spent fuel is to be placed within the new storage rack located in the cask pit. Also, the Spent Fuel Cask Handling Crane outside the Fuel Handling Building (FHB) will be replaced, resulting in new design tornado and seismic loading loads being applied on some portions of the exterior walls above the SFP and the Cask Pit. This section summarizes the analysis to demonstrate structural adequacy of the Cask Pit and the affected building walls subject to the revised loadings from the new rack and Spent Fuel Cask Handling Crane. Portions of the spent fuel pool beyond the confines of the Cask Pit are unaffected by the addition of the rack in the Cask Pit and are not reconsidered herein. Views of the Unit 2 Cask Pit area are shown in Figures 8.2.1-8.2.3.

The structural evaluation of the Cask Pit is conducted using a finite element model of the Cask Pit; additional support from the spent fuel pool structure beyond the Cask Pit is conservatively neglected. Results for individual load components are combined using the factored load combinations mandated by the St. Lucie Unit 2 UFSAR [8.2.1], and are based on the "ultimate strength" design method. The east exterior wall, above the spent fuel pool operating floor (El. 62'), is also evaluated using a separate finite element model since additional loads from the overhead crane are applied on this wall and transferred to the Cask Pit. Applicable loadings are considered and the wall evaluated in the same manner as described for the Cask Pit. Resultant loads at the base of the east exterior wall (at El. 62') are transferred to the top of the Cask Pit and included in the Cask Pit load combination evaluation.

The column line designating the juncture of the west exterior wall and the north exterior wall is also a location where revised loadings from the building crane are imposed. These loads impart minimal bending loading to the building exterior walls; the effect of these loads on the SFP walls is negligible and no analysis is required.

Moment capabilities are checked on each affected wall in each direction (vertical and horizontal) for concrete structural integrity. Moment capacities are computed including the effects of axial tension or compressive loads at the location considered and are evaluated in accord with the applicable guidance of the Unit 2 design code, ACI 318-71[8.2.2]. Shear capability is evaluated along the base of the affected components. As the slab is founded on grade and is 8.5' thick, bending of the slab in the Cask Pit is not a limiting load condition, and calculations for the slab are limited to concrete bearing integrity and to liner stress evaluation. All structural capacity calculations are made using applicable design formulas following the guidance of the applicable American Concrete Institute code.

### 8.2.2 Description of Cask Pit Structure and Exterior Building Walls

The Cask Pit reinforced concrete structure is comprised of the four full height perimeter walls of the Cask Pit and is assumed isolated from the remainder of the FHB and the SFP. The structure is conservatively considered as an independent structure. The structural evaluation focuses on the four reinforced concrete walls surrounding the Cask Pit. These four 45'-6" high reinforced concrete walls are supported at the floor elevation of 16'-6" by a massive (8'-6" thick) reinforced concrete mat, which is founded on grade. Figures 8.2.1-8.2.3 show the area of interest and the major structural dimensions of the Unit 2 Cask Pit. The top of the operating floor is at elevation 62'-0". The west wall of the Cask Pit has a 3' wide gate opening extending down to El. 36.25'. The thickness of the walls surrounding the Cask Pit are 6'-0" for the north and east exterior walls, and 5'-6" for the south and west interior walls. The floor liner covering the Cask Pit base mat is 1" thick.

The east wall of the Fuel Handling Building (from column line 2FH2 and extending to the south to column line 2FH5) is separately modeled from El. 62' up to the roof at El. 95' in order to capture the effect of the revised overhead crane loading and other environmental loads acting on the wall and on the Cask Pit structure below El. 62'. The east wall above El. 62' is 2' thick except at the column lines where the concrete thickness is increased to 3' over a 4' wide region to accommodate the additional column rebar reinforcement.

The four walls surrounding the Cask Pit are considered as planar plates connected to form a rectangular box up to the bottom of the fuel transfer gate opening at El. 36.25' and fixed at the base to the supporting mat. The remaining edge at the upper elevation is considered as a free edge (no lateral support is assumed from the adjacent operating floor at El. 62'). Figure 8.2.4 shows the finite element grid utilized for the Cask Pit analysis for Unit 2.

For the Unit 2 analysis, the wall above El. 62' is separately modeled as a plate structure. The individual plate elements making up the model have increased wall thickness at the locations of the concrete columns to properly simulate the increased stiffness at the column lines 2FH3 and 2FH4. The boundary at El. 62' is fixed as most of the wall is connected to the thicker structure below El. 62'. The remaining three sides of the plate structure are considered to support lateral load but not bending moment. Figure 8.2.5 shows the finite grid and boundary conditions utilized for the model of the east wall above El. 62'.

With a spent fuel rack in the Cask Pit, the Cask Pit will always be filled with water so that hydrostatic loads will be balanced across the two interior walls separating the Cask Pit from the main pool. Thermal gradients across these walls will be reduced or eliminated due to inter-pool water mixing through the gate opening. Thus, the addition of a spent fuel rack in the Cask Pit promotes increased safety factors on the south and west interior walls separating the pit from the main pool since there is no pressure differential from the pool water. However, the exterior north and east walls (6' thick) will be subject to dynamic water loads and thermal gradients due to the addition of the rack. Therefore, even though the four walls of the Cask Pit are modeled, the focus of the analyses is to predict the margins in the exterior walls bounding the Cask Pit and in the east wall above the spent fuel pool. The north wall above the spent fuel pool is not modeled as it is unaffected by the new loadings considered herein.

### 8.2.3 Analysis Procedures

The Cask Pit reinforced concrete walls and wall above El. 62' are modeled separately. These walls are subjected to individual "unit" load cases covering the service conditions (the structural weight of the concrete structure, the hydro-static water pressure and the temperature gradients), seismic induced loads (structural seismic loads, hydro-dynamic water loads, and rack-structure interaction dynamic loads) for

OBE and SSE conditions, and tornado loads. The service condition loads are considered as static acting loads; the seismic induced loads for both OBE and SSE seismic events are obtained from the simultaneous application of the three-directional acceleration spectra appropriate to elevation 16'-6" with input seismic acceleration amplifier defined on the basis of a frequency analysis of the structure. Finally, tornado loadings are derived from applicable information on wind speeds and differential pressures given in the UFSAR. As required by the Unit 2 UFSAR [8.2.1], results from seismic or tornado loading in each direction are first combined by the SRSS method and then added to static load results in applicable load combinations.

The reinforced concrete is considered elastic and isotropic. The elastic characteristics of the concrete are independent of the reinforcement contained in each structural element for the mechanical load cases when un-cracked cross-sections are assumed. This assumption is valid for all load cases with the exception of the thermal loads, where for a more realistic description of the reinforced concrete cross-section behavior the assumption of cracked concrete is used. To simulate the variation and the degree of cracking patterns, the original elastic modulus of the concrete is reduced in accordance with the methodology suggested by ACI 349 [8.1.3]. Table 8.2.1 summarizes the concrete properties employed in the structural evaluation of Unit 2.

#### 8.2.4 Definition of Loads

Cask Pit direct loading considered the following discrete components:

##### 8.2.4.1 Static Loading (D = Dead Loads)

- 1) Dead weight of Cask Pit structure includes the weight of the four walls constituting the Cask Pit and the weight of the north and east walls above the Cask Pit.
- 2) Dead weight of Cask Pit spent fuel rack fully loaded with fuel and rack platform (this total dry weight of 181.6 tons only affects bearing stress under the Cask Pit liner).
- 3) The hydrostatic water pressure.

#### 8.2.4.2 Seismic (E = OBE; E' = SSE) and Tornado Induced Loads (Wt)

- 1) Vertical loads transmitted by the spent fuel rack to the slab during a seismic event (only affects the Cask Pit floor slab bearing).
- 2) Hydrodynamic inertia loads due to the contained water mass and sloshing loads (considered in accordance with [8.1.4]) that arise during a seismic event.
- 3) Hydrodynamic pressures between spent fuel rack and Cask Pit walls caused by rack motion in the Cask Pit during a seismic event.
- 4) Seismic inertia force of the walls from the wall mass.
- 5) Seismic or Tornado loads from the fuel building crane acting on the east walls.
- 6) Tornado loading on the north and east exterior wall of the Cask Pit up to El. 62'.
- 7) Seismic or tornado loads transferred from the east exterior wall above the Cask Pit

#### 8.2.4.3 Thermal Loading

With the addition of a rack in the Cask Pit, the Cask Pit concrete walls are subject to a thermal gradient plus a mean temperature rise above the assembly temperature. The gradient through the exterior north and east walls is the difference between the bulk temperature of the water in the Cask Pit and the exterior air temperature. The normal and accident operating condition (in the presence of a seismic or tornado event) conservatively considers the bulk Cask Pit temperature  $T_o$  to be 150°F (which exceeds the computed bulk pool temperature). The ambient temperature outside of the structure is considered to be 41°F (per discussion in Sub-section 8.1.4.3). The thermal gradient across the interior walls is assumed to be 10°F since both sides of the interior walls are subject to essentially the same bulk temperature corresponding to the water in the pit and the water in the main spent fuel pool. These temperatures and the computed thermal gradients are chosen to represent bounding conditions or conservative extremes.

Loadings applied to the separately modeled exterior east wall (from El. 62' to El. 95') above the Cask Pit are:

#### 8.2.4.4 Static Loading (D = Dead Loads)

- 1) Dead weight of wall

#### 8.2.4.5 Seismic (E or E') or Tornado Induced Loads (Wt)

- 1) Vertical and Lateral seismic inertia loads acting on the wall
- 2) Tornado pressure load
- 3) Seismic and tornado loading from the overhead crane transferred at the crane support.

#### 8.2.4.6 Thermal Loading Above Elevation 62'

The east wall, above El. 62' is exposed to a maximum inside air temperature of 108°F; the inside wall temperature is approximately 78°F. This is combined with the outside air temperature of 41°F and a conservatively computed surface heat transfer coefficient to establish a lower bound outside wall temperature of 45°F.

#### 8.2.4.7 Load Combinations

Results from a suite of unit load analyses are used to form appropriate load cases and then combined in accordance with the load combinations specified in Subsection 3.8.4.3.2.1 of the St. Lucie Unit 2 UFSAR [8.2.1].

The final load combinations evaluated for structural integrity are:

For "Normal and Severe Environmental Conditions" the following load combinations are:

- Load Combination No. 1 =  $1.4 * D + 1.3 * T_o$
- Load Combination No. 2 =  $1.4 * D + 1.3 * T_o + 1.9 * E$

- Load Combination No. 3 =  $1.4 \cdot D + 1.3 \cdot T_o - 1.9 \cdot E$

- Load Combination No. 4 =  $1.2 \cdot D + 1.9 \cdot E$

- Load Combination No. 5 =  $1.2 \cdot D - 1.9 \cdot E$

For "Extreme Environmental and Abnormal/Severe Load Conditions" the load combinations are:

- Load Combination No. 6 =  $D + T_a + E'$

- Load Combination No. 7 =  $D + T_a - E'$

- Load Combination No. 8 =  $D + T_a + W_t$

- Load Combination No. 9 =  $D + T_a - W_t$

- Load Combination No. 10 =  $D + T_a + 1.25 \cdot E$

- Load Combination No. 11 =  $D + T_a - 1.25 \cdot E$

where:

D = dead loads;

T<sub>o</sub> = thermal load during normal operation;

T<sub>a</sub> = thermal load concurrent with seismic or tornado event = T<sub>o</sub>;

E = OBE earthquake induced loads;

E' = SSE earthquake induced loads.

W<sub>t</sub> = Tornado Loading

L = Live loads; no live loads are considered applicable for this analysis

Note that seismic loads and tornado loads are considered to be applied in either direction and include both direct effects and loads from the overhead crane and wall above the Cask Pit that are transferred into the Cask Pit at El. 62'. Note also that load combinations with hurricanes (194 mph) wind are not governing in any factored load combination as they provide surface pressure loadings that are the same order or less than the seismic pressures and/or the tornado pressures.

The same load combinations are applied to the separate east wall model (above El. 62') except that thermal gradient loading is based on the maximum interior air temperature above the spent fuel pool, and no loads are imposed from fuel racks.

The ACI Code sets limits for representative section widths of a wall. The determination of the appropriate section width follows the same rationale discussed in Subsection 8.1.4.4 for the Unit 1 analysis. Safety factors are defined as the allowable load divided by the computed load and continued acceptability is ensured if the safety factor exceeds 1.0 for the characteristic width associated with the wall section. Safety factors for horizontal sections in the cask pit walls and the upper east wall are computed based on a section width of 12', which is the span between opposite cask pit walls. Safety factors for the column (in the east wall above El. 62') are conservatively based on averaging over the 4' column width. Vertical sections of the cask pit walls are evaluated at limiting sections in the lower 20' width (below the gate in the west wall).

## 8.2.5 Results of Unit 2 Reinforced Concrete Analyses

### 8.2.5.1 Building Wall Above Elevation 62'

The structural evaluation of the east wall above 62' was performed and the axial forces, the bending moments and the shear forces were computed for all load combinations. The reinforced concrete cross-sectional capacities, including the effects of axial load at the particular location were determined and used to obtain the safety factors of the appropriate wall sections for each load combination considered. The calculated minimum safety factors for the limiting sections of the east wall (above El. 62') for all evaluated load combinations for the wall and for the intermediate vertical column 2FH3 strengthening the wall against lateral loads are:

East Wall Bending	Cross-section normal to vertical direction	1.30 (Load Combination 2)
	Cross-section normal to horizontal direction	1.66 (Load Combination 2)
East Wall Base Shear		2.76 (Load Combination 9)

Vertical Column Bending	1.42 (Load Combination 8)
Vertical Column Shear	1.16 (Load Combination 8)

#### 8.2.5.2 Cask Pit

The structural evaluation focused on the four reinforced concrete walls pertaining to the Cask Pit. The axial forces, bending moments and shear forces were computed for each load combination and included the effects of the factored load combinations from the portion of the east wall above El. 62'. The reinforced concrete cross-sectional capacities including axial force effects were determined and used to obtain the safety factors for the limiting section widths in each wall of the pit. The calculated minimum safety factors for all load combinations considered are:

North Wall Bending	Cross-section normal to vertical direction	2.12 (Load Combination 2)
	Cross-section normal to horizontal direction	2.0 (Load Combination 2)
North Wall Averaged Shear		3.05 (Load Combination 4)
East Wall Bending	Cross-section normal to vertical direction	1.76 (Load Combination 6)
	Cross-section normal to horizontal direction	1.68 (Load Combination 2)
East Wall Averaged Shear		4.7 (Load Combination 2)
South Wall Bending	Cross-section normal to vertical direction	2.33 (Load Combination 2)
	Cross-section normal to horizontal direction	3.09 (Load Combination 2)
South Wall Averaged Shear		2.4 (Load Combination 1)
West Wall Bending	Cross-section normal to vertical direction	1.44 (Load Combination 2)
	Cross-section normal to horizontal direction	1.4 (Load Combination 2)
West Wall Averaged Shear		2.13 (Load Combination 2)

### 8.2.6 Pool Liner-Cask Pit Floor Bearing Evaluation

The pool liner is subject to in-plate compressive strains due to differential thermal load arising from the different coefficient of thermal expansion ascribed to the liner and the underlying concrete in the Cask Pit. An in-plane stress is also developed in the liner to resist lateral loads arising from friction between the liner and the Cask Pit platform shim plates during a seismic event. Assuming a conservative 150-degree F water temperature in the Cask Pit, the in-plane mean thermal stress in the liner due to the differential thermal expansion is below 6000 psi. The additional in-plane stress to resist lateral forces during a seismic event is below 3250 psi. The liner will not tear or buckle under this stress level. The combined in-plane stress level (9250 psi) is below the appropriate stress limit for the seismic load condition.

Bearing strength requirements are satisfied by conservatively assuming the factored vertical load from the most highly loaded shim plate of the Cask Pit platform supporting the Cask Pit spent fuel rack and assuming that a leak chase is directly below the shim plate. The allowable bearing stress for the confined concrete under the pedestal is  $2(0.85)(0.7)f_c$ , where  $f_c=5000$  psi is the slab concrete compressive strength per the UFSAR [8.2.1]. The small depth of the leak chase (1.5") does not alter the assumption of confinement of the concrete under bearing action. The computed safety factor (allowable strength/calculated average compressive concrete stress) is:

$$SF(\text{concrete bearing})=1.88$$

### 8.2.7 Conclusions for Unit 2

Regions affected by loading the Cask Pit with a high-density rack loaded with fuel assemblies and additional crane support loads are examined for structural integrity under bending and shearing action. It is determined that adequate safety margins exist when the factored load combinations are checked against the appropriate structural design strengths. It is also shown that local loading on the liner does not compromise liner integrity and that concrete bearing strength limits are not exceeded.

### 8.3 References

[8.1.1] St. Lucie Nuclear Plant, UFSAR (Unit 1).

[8.1.2] ACI 318-63, Building Code Requirements for Reinforced Concrete, American Concrete Institute, Detroit, Michigan.

[8.1.3] ACI 349-85, Code Requirements for Nuclear Safety Related Concrete Structures, American Concrete Institute, Detroit, Michigan.

[8.1.4] "Nuclear Reactors and Earthquakes, U.S. Department of Commerce, National Bureau of Standards, National Technical Information Service, Springfield, Virginia (TID 7024).

[8.1.5] ASHREA Handbook, Fundamentals, Chap. 24, Table 1, 1989.

[8.2.1] St. Lucie Nuclear Plant, UFSAR (Unit 2).

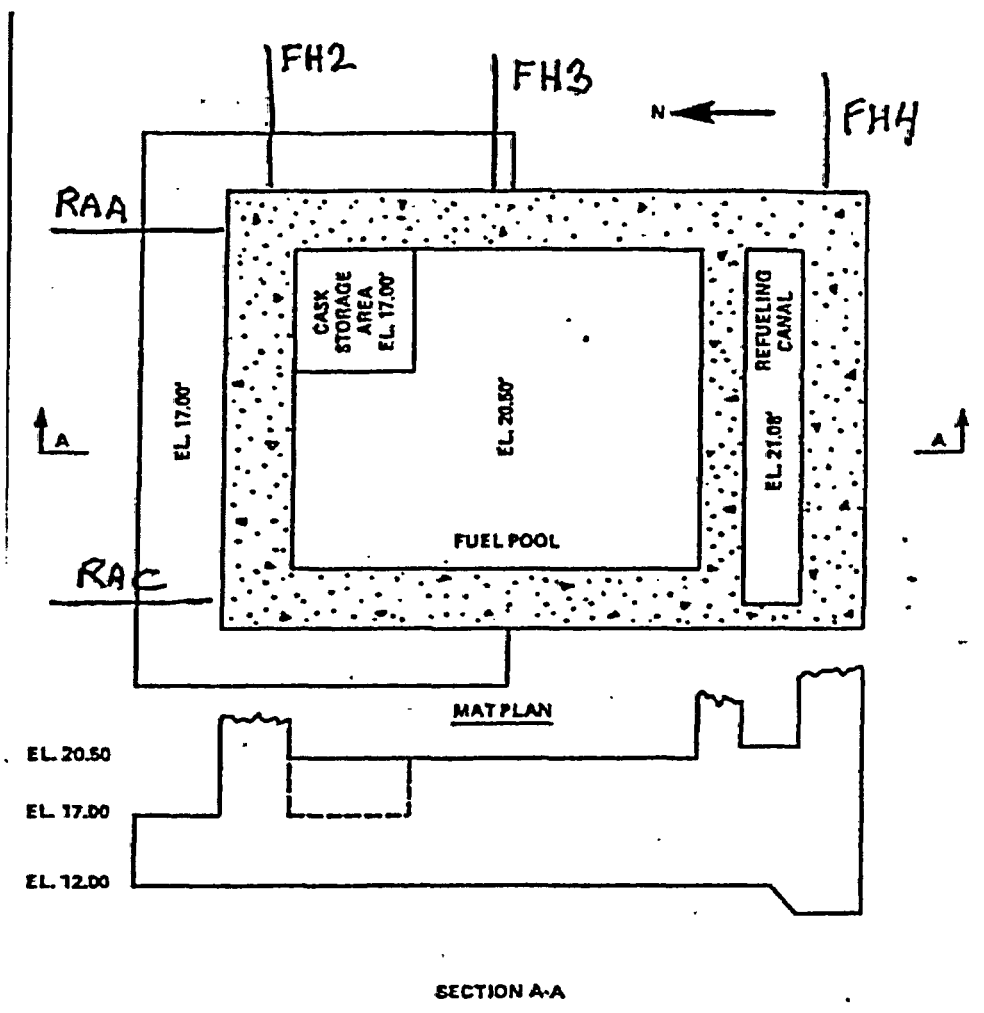
[8.2.2] ACI 318-71, Building Code Requirements for Reinforced Concrete, American Concrete Institute, Detroit, Michigan.

**Table 8.1.1 Unit 1 Concrete and Rebar Properties**

Parameter	Value
Concrete Compressive Strength (psi)	5.200E+03
Un-Cracked Concrete Elastic Modulus (psi)	4.110E+06
Concrete Poisson's Ratio	0.16
Concrete Weight Density (lb/ft <sup>3</sup> )	150.0
Concrete Thermal Expansion Coefficient (in./in.-degree F)	5.500E-06
Reinforcement Yield Strength (psi)	4.000E+04
Reinforcement Elastic Modulus (psi)	2.900E+07

Table No. 8.2.1 Unit 2 Concrete and Rebar Properties

Parameter	Value
Concrete Compressive Strength (psi)	4.000E+03
Un-Cracked Concrete Elastic Modulus (psi)	3.605E+06
Concrete Poisson's Ratio	0.16
Concrete Weight Density (lb/ft <sup>3</sup> )	150.0
Concrete Thermal Expansion Coefficient (in./(in.-degree F))	5.500E-06
Reinforcement Yield Strength (psi)	6.000E+04
Reinforcement Elastic Modulus (psi)	2.900E+07



FLORIDA POWER & LIGHT COMPANY  
 ST. LUCIE PLANT UNIT 1  
 MAT PLAN AND SECTION

Note that Elevations refer to concrete. Liner plate floor elevations are typically one foot higher due to grout and liner plate thickness.

Figure 8.1.1 Plan View of Unit 1 FHB

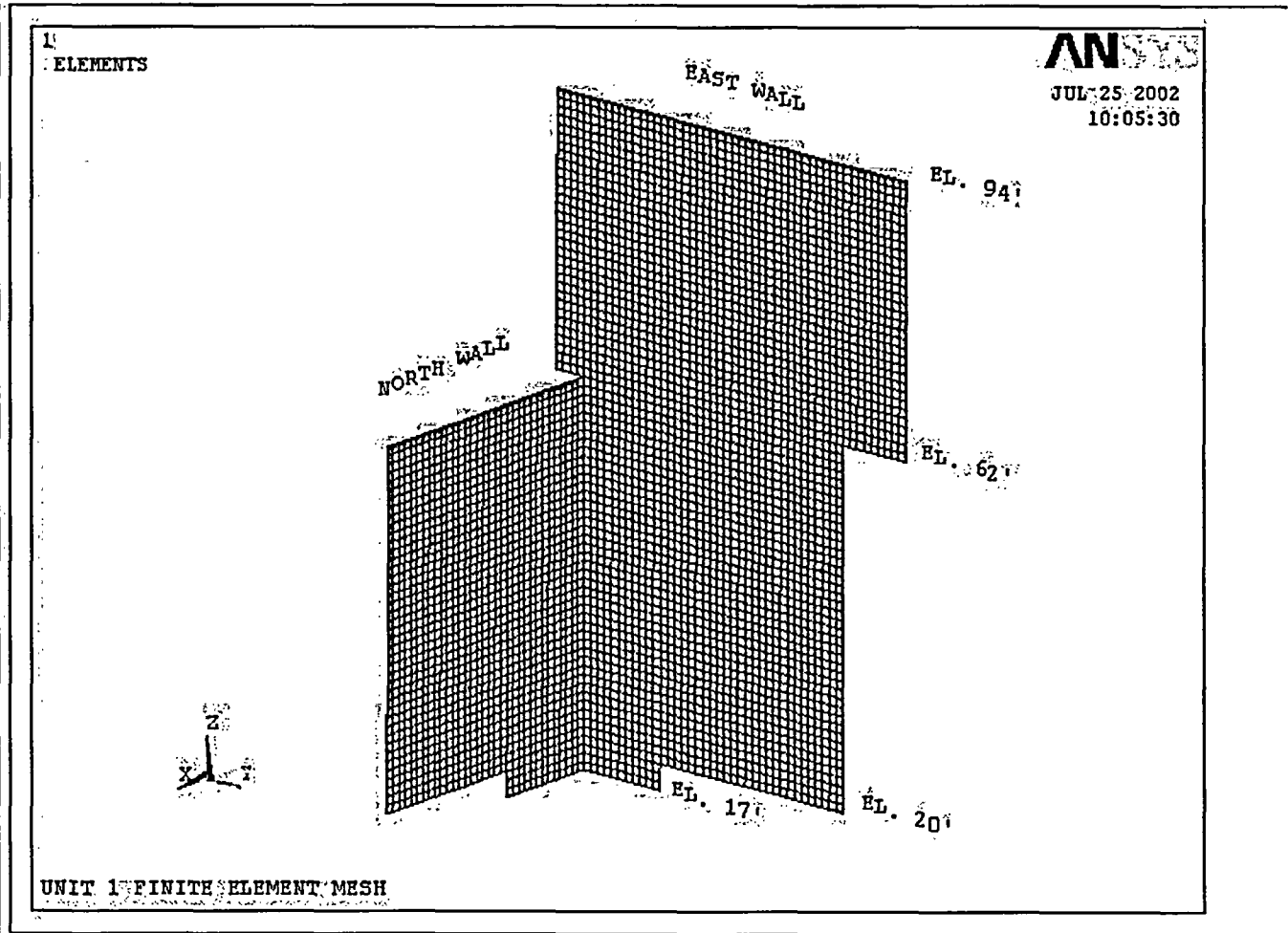


Figure 8.1.2- Unit 1 Finite Element Mesh

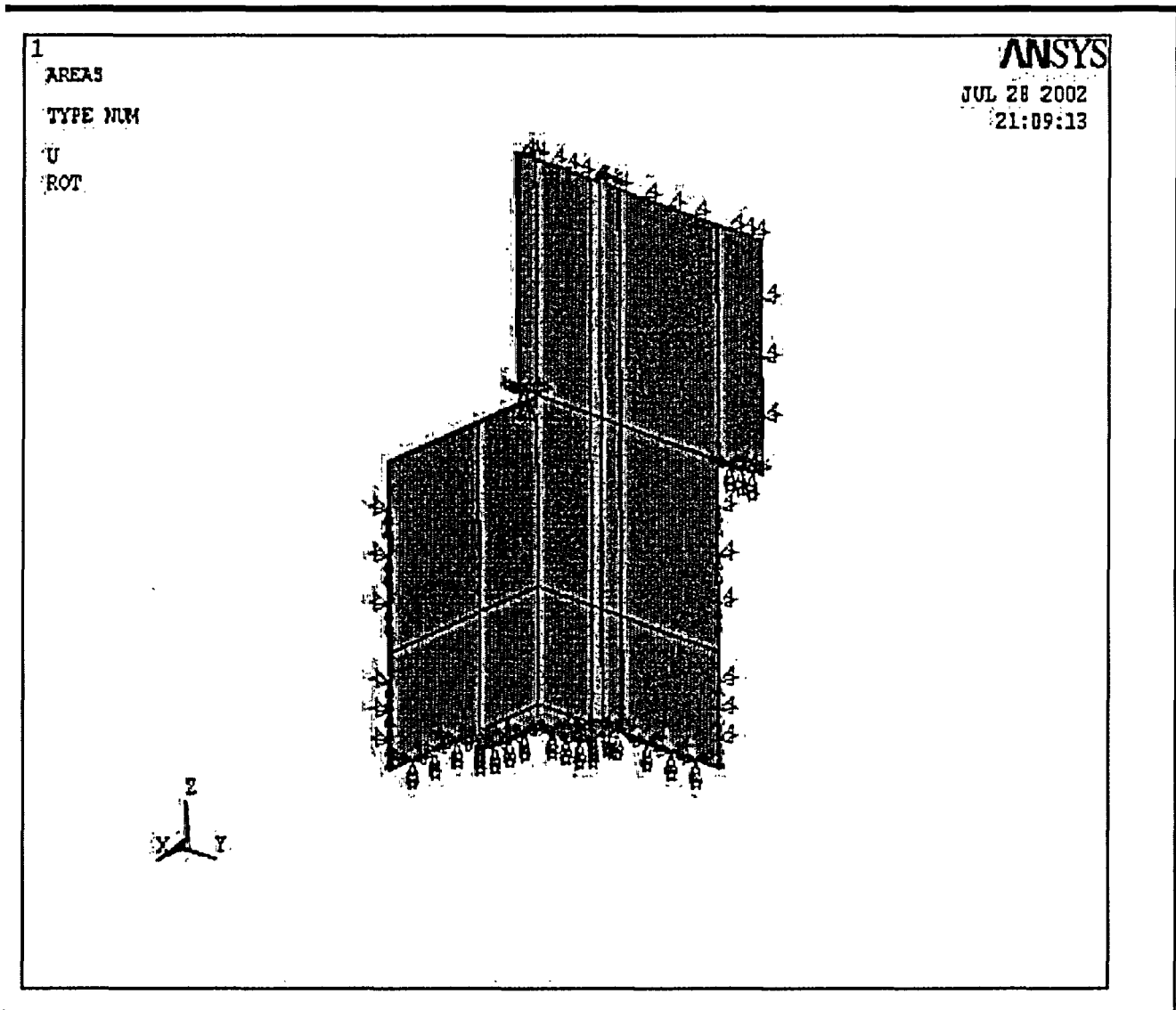
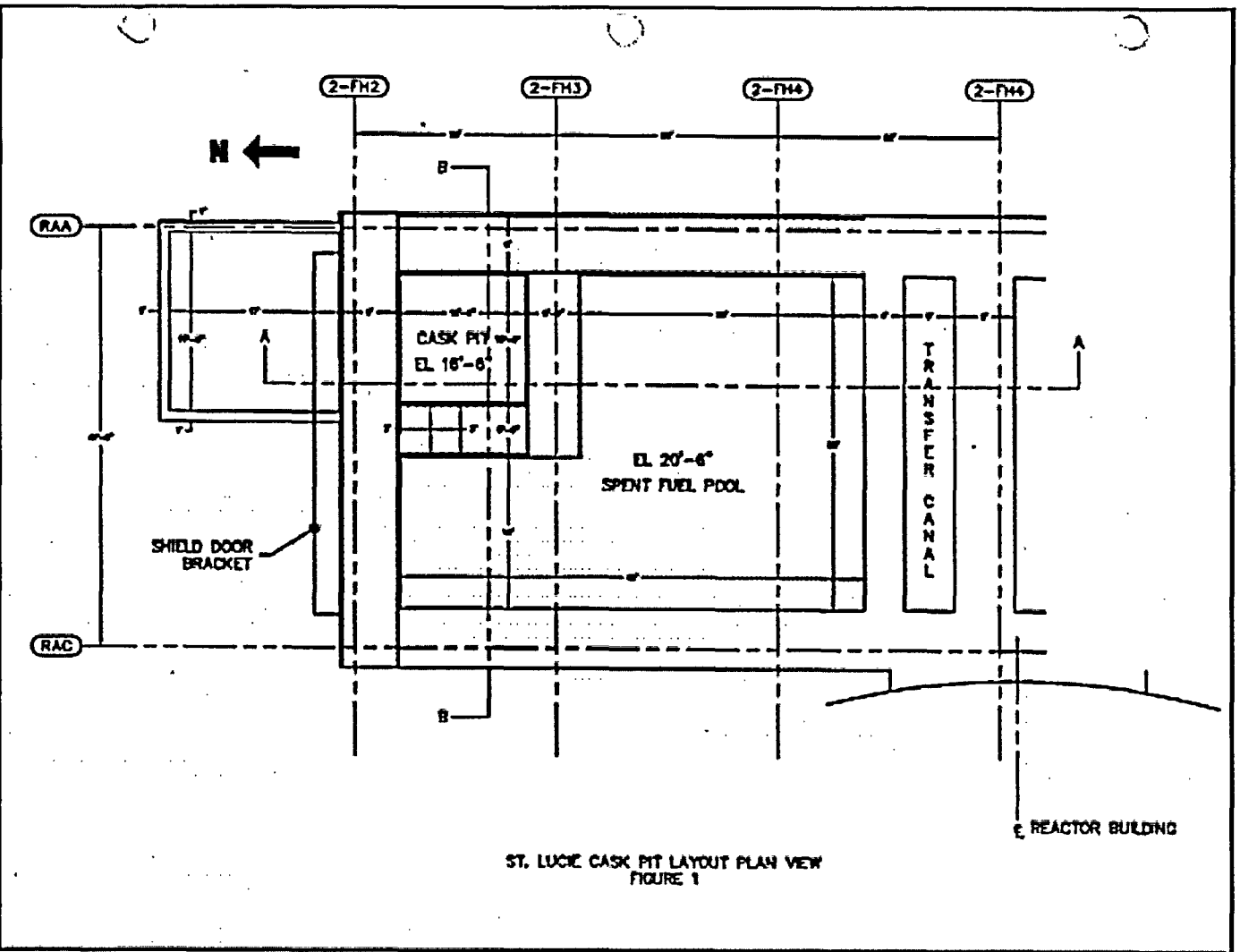


Figure 8.1.3 Unit 1 Finite Element Boundary Conditions



ST. LUCIE CASK PIT LAYOUT PLAN VIEW  
FIGURE 1

Note that Elevations refer to concrete. Liner plate floor elevations are typically one foot higher due to grout and liner plate thickness.

Figure 8.2.1 Plan View of Unit 2 FHB

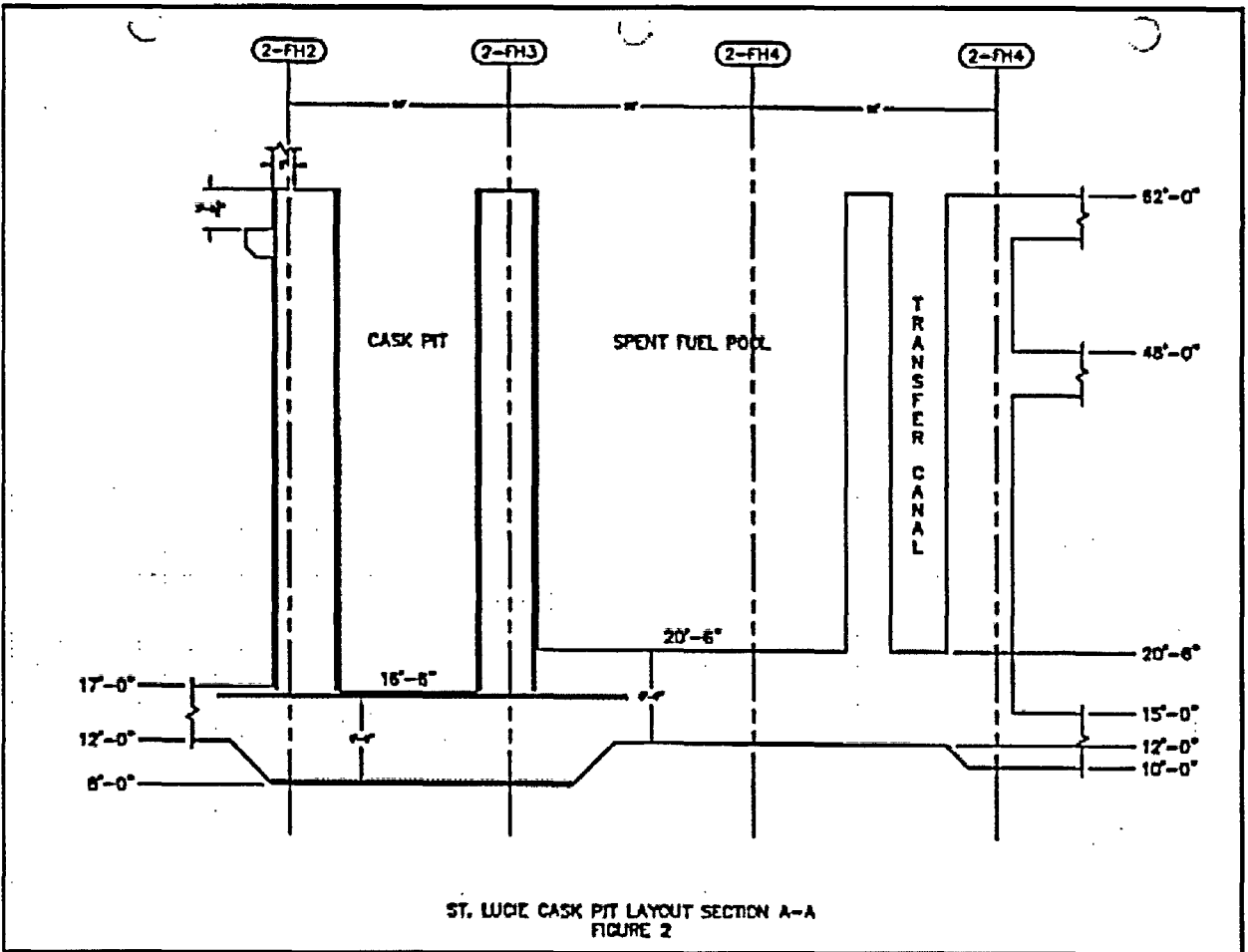
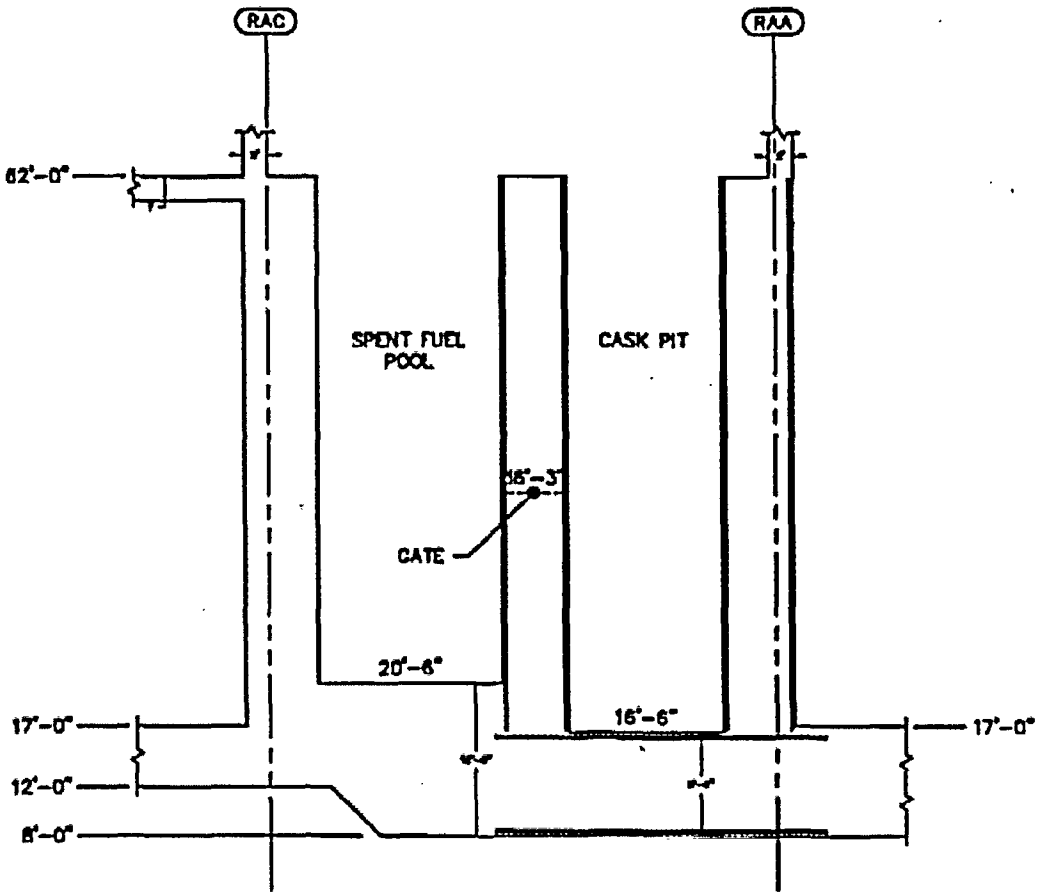


Figure 8.2.2 View Through Section A-A



ST. LUCIE CASK PIT LAYOUT SECTION B-B  
FIGURE 3

Figure 8.2.3 View Through Section B-B

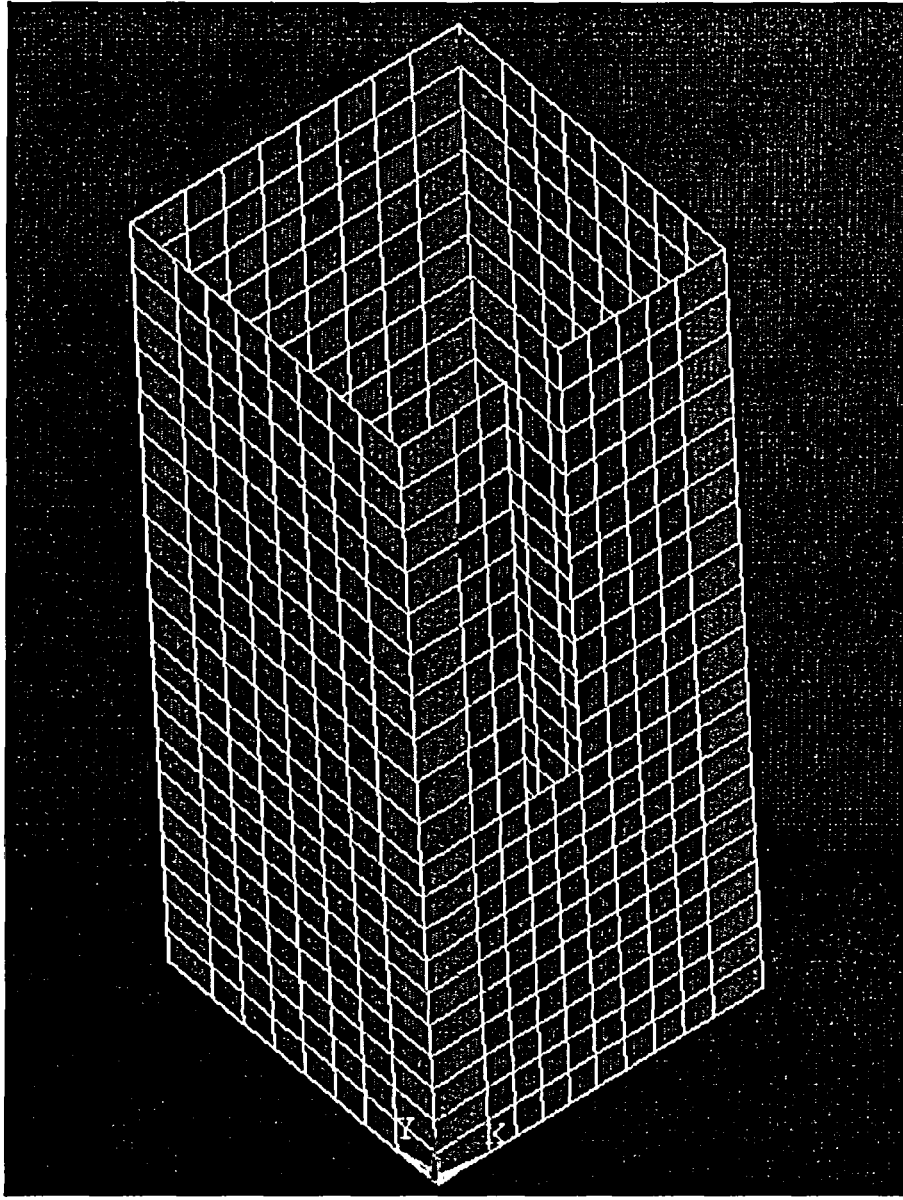


Figure 8.2.4 Unit 2 Cask Pit Finite Element Grid

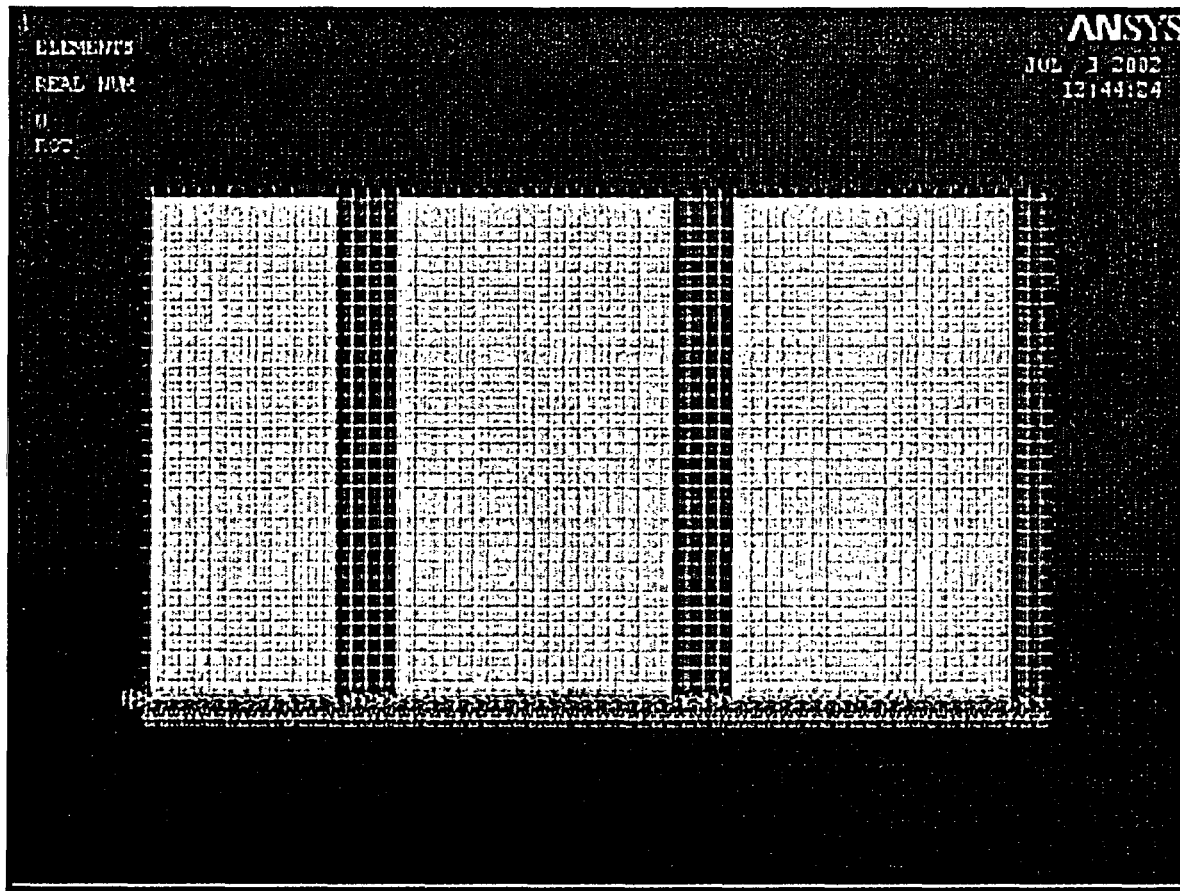


Figure 8.2.5 East Wall Above El. 62' (Between Column Lines 2FH2 and 2FH5) Finite Element Grid and Boundary Conditions

## 9.0 RADIOLOGICAL EVALUATION

### 9.1 Fuel Handling Accident

The installation of a fuel storage rack (module) in the cask pit of St. Lucie Unit 1 or St. Lucie Unit 2 will not result in a change in the previously-analyzed fuel handling accident or its consequences. The new rack installed in each unit will simply provide increased fuel storage capacity for that unit.

### 9.2 Solid Radwaste

The necessity for resin replacement is determined primarily by the requirement for water clarity, and the resin is normally changed about once a year. No significant increase in the volume of solid radioactive waste from either unit is expected to result from the expanded fuel storage capacities in the units.

### 9.3 Gaseous Releases

Gaseous releases from the fuel storage area in each unit are combined with other exhausts from that unit. Normally, the contributions from the fuel storage areas are negligible compared to the other releases and no significant increases are expected in either unit as a result of the expanded storage capacity.

### 9.4 Personnel Exposures

Personnel exposures in the vicinity of the fuel storage facility at each unit result principally from radionuclides in the pool water and from fuel in transit. The radionuclides in the water derive generally from: 1) the mixing of primary system water with the pool water and 2) the spalling of crud deposits from the spent fuel assemblies as they are moved in the storage pool during refueling operations. Although the overall capacity of each pool is being increased, the movement of fuel during refueling is independent of storage capacity. Similarly, the dose rate from fuel in transit does not increase with increased storage capacity. However, the use of the cask pit rack will require fuel transits in the vicinity of the northeast corner of each spent fuel pool, similar to transit paths that would be used during cask loading. These transit

paths will not increase the dose rate beyond that already experienced at either the north or east walls during placement of fuel into racks adjacent to those walls. Similarly, the dose rate from fuel stored in the cask pit racks is expected to be comparable to the dose rate from fuel stored in the spent fuel pool racks adjacent to the north and east walls, because the exterior wall thickness surrounding the cask pit is the same as the wall thickness surrounding the pool.

Operating experience has shown that there have been negligible concentrations of airborne radioactivity, and no increases are expected as a result of the expanded storage capacities. However, area monitors for airborne radioactivity are available in the immediate vicinity of the fuel storage facility in each unit.

No increase in radiation exposure to operating personnel of either unit is expected; therefore, neither the current health physics programs nor the area monitoring systems need to be modified.

9.5 Anticipated Exposure During Rack Installation

All operations involved in installing a cask pit rack in Unit 1 and a cask pit rack in Unit 2 will utilize detailed procedures prepared with full consideration of ALARA principles. Similar (but more complex) operations have been performed in a number of facilities in the past, and there is every reason to believe that the relatively-simple task of installing these single rack modules in locations not previously occupied by other rack modules can be accomplished with minimum radiation exposure to personnel. Diving operations are not expected to be required based on a physical survey of the existing Cask Pit configuration.

The occupational exposure for installing the rack in Unit 1 and the rack in Unit 2 is estimated to be a total of approximately 0.3 person-rem. This estimated dose is based on the following.

<u>OPERATION</u>	<u>NUMBER OF PERSONNEL</u>	<u>HOURS EACH</u>	<u>ESTIMATED PERSON-REM EXPOSURE</u>
Clean and Vacuum Pits	4	8	0.1
Install New Racks	4	16	0.2

For the cleaning and vacuuming operations, a conservative dose rate of approximately 2.5 mrem/hr is estimated, while the rack installation operations are based on the radiation-zone maximum dose rate of 2.5 mrem/hr. The cleaning and vacuuming exposure is rounded down, while the installation exposure is rounded up in the preceding table.

The existing radiation protection programs at Units 1 and 2 are adequate for the rack-installation operations. Radiation Work Permit(s) will govern activities, and personnel monitoring equipment will be issued to each individual. As a minimum, this will include thermoluminescent dosimeters and pocket dosimeters. Work, personnel traffic, and the movement of equipment will be monitored and controlled to assure that exposures are maintained ALARA.

#### 9.6 Rack Removal and Storage during Cask Handling Operations

The cask pit racks must be unloaded and removed from their respective cask pit in preparation for future dry cask storage loading operations. Based on projected storage improvements for St. Lucie (i.e., Unit 2 reracking) and DOE performance by 2015, FPL expects to perform this rack removal process only once or twice in the next 20 years. Thereafter, the storage rack may be disposed, stored for temporary use, or permanently stored until decommissioning.

Based on Holtec experience with rack module removal and decontamination projects, the removal and storage process will not create significant radiological waste or personnel exposure. The removal and decontamination process should not result in more than 200 mrem based on a pool surface dose rate of 2.5 mrem/hr, an estimated rack contact surface dose rate of 20 mrem/hr and a job estimate of 80 manhours. Typically, the surfaces of a rack module can be decontaminated to a level that would allow free release; however, the inaccessible areas of the rack may prohibit storage as such. Accordingly, appropriate radiologically-controlled storage on-site will be provided as required.

Rack contamination and the risk of environmental release during removal and storage will be minimized by the following practices:

1. Prior to cask pit rack platform installation, the cask pit will be vacuumed and visually inspected for debris.
2. During rack installation, the cask pit rack will be wetted with deionized water.
3. During storage operations, only select non-failed fuel will be stored in the racks
4. Prior to removal from the cask pit, the racks will be visually inspected to ensure fuel and all debris are removed.
5. During rack removal (over the cask pit), the racks will be rinsed with deionized water, leaving most loose contamination in the spent fuel pool
6. During rack removal (over the cask pit), the racks will be drained of pool water and rinsed with water through holes in each cell
7. During rack removal (over the cask pit), after the racks are drained and drip-dried, the external surfaces will be wiped down
8. Prior to removal from the Fuel Handling Building, a "diaper" and plastic liner will be attached to absorb any subsequent liquid
9. After removal from the Fuel Handling Building, the racks will be placed in a [good integrity container] capable of protecting the rack from the elements and containing any reasonably-postulated leakage.
10. The storage container will be radiologically-controlled and stored in a secure building or otherwise secured within the protected area, similar to practices used for high-integrity containers (HICs) and other temporary radiological storage containers.
12. During storage, the storage facility will be routinely monitored for leakage.
13. FPL ALARA practices will be applied to every step of removal and storage.

Rack contamination and activation will be minimized by a fuel-loading process, which is careful to select non-failed spent fuel with good inspection records and operating history. Furthermore, the Unit 1 cask pit rack contamination will be minimized because that rack will be dedicated to temporary storage of fresh, unburned fuel and once-burned fuel.

## 10.0 INSTALLATION

### 10.1 Introduction

The installation phase of the St. Lucie Cask Pit Area fuel storage rack project will be executed by Holtec International's Field Services Division. Holtec, serving as the installer, is responsible for performance of specialized services, such as underwater diving and welding operations, as necessary. All installation work at St. Lucie is performed in compliance with NUREG-0612 (refer to Section 3.0), Holtec Quality Assurance Procedure 19.2, St. Lucie project specific procedures, and applicable St. Lucie procedures.

Crane and fuel bridge operators are trained in the operation of overhead cranes per the requirements of ANSI/ASME B30.2, and the plant's specific training program. Consistent with the installer's past practices, a videotape aided training session is presented to the installation team, all of whom are required to successfully complete a written examination prior to the commencement of work. Fuel handling bridge operations are performed by St. Lucie personnel, who are trained in accordance with St. Lucie procedures.

A rack lifting device is required. This lifting device is designed to engage and disengage on lift points at the bottom of the racks. The lifting device complies with the provisions of ANSI N14.6-1978 and NUREG-0612, including compliance with the design stress criteria, load testing at a multiplier of maximum working load, and nondestructive examination of critical welds.

A surveillance and inspection program shall be maintained as part of the installation of the racks. A set of inspection points, which have been proven to eliminate any incidence of rework or erroneous installation in previous rack projects, is implemented by the installer.

Underwater diving operations are not required for this project.

Holtec International developed procedures, to be used in conjunction with the St. Lucie procedures, which cover the scope of activities for the rack installation effort. Similar procedures have been utilized and successfully implemented by Holtec on previous rack installation projects. These procedures are

written to include ALARA practices and provide requirements to assure equipment, personnel, and plant safety. These procedures are reviewed and approved in accordance with St. Lucie administrative procedures prior to use on site. The following is a list of the Holtec procedures, used in addition to the St. Lucie procedures to implement the installation phase of the project.

A. Installation/Handling Procedure:

This procedure provides direction for the handling/installation of the new storage rack modules in the Cask Pit. This procedure delineates the steps necessary to receive the new maximum density racks on site, the proper method for unloading and uprighting the racks, staging the racks prior to installation, and installation of the racks. The procedure provides for the installation of cask support platforms, adjustment of the rack pedestals and verification of the as-built field configuration to ensure compliance with design documents.

B. Receipt Inspection Procedure:

This procedure delineates the steps necessary to perform a thorough receipt inspection of a new rack module after its arrival on site. The receipt inspection includes dimensional measurements, cleanliness inspection, visual weld examination, and verticality measurements.

C. Cleaning Procedure:

This procedure provides for the cleaning of a new rack module, if required. The modules are to meet the requirements of ANSI N45.2.1, Level B, prior to placement in the Cask Pit. Methods and limitations on cleaning materials to be utilized are provided.

D. Pre- and Post-Installation Drag Test Procedure:

These two procedures stipulate the requirements for performing a functional test on a new rack module prior to and following installation. The procedures provide direction for inserting and withdrawing an insertion gage into designated cell locations, and establishes an acceptance criteria in terms of maximum drag force.

E. ALARA Procedure:

Consistent with Holtec International's ALARA Program, this procedure provides guidance to minimize the total man-rem received during the rack installation project, by accounting for time, distance, and shielding. This procedure will be used in conjunction with the St. Lucie ALARA program.

F. Liner Inspection Procedure:

In the event that a visual inspection of any submerged portion of the pool liner is deemed necessary, this procedure describes the method to perform such an inspection using an underwater camera and describes the requirements for documenting any observations.

G. Leak Detection Procedure:

This procedure describes the method to test the pool liner for potential leakage using a vacuum box. This procedure may be applied to any suspect area of the liner.

H. Liner Repair and Underwater Welding Procedure:

In the event of a positive leak test result, underwater welding procedures may be implemented which provide for a weld repair, or placement of a stainless steel repair patch, over the area in question. The procedures contain appropriate qualification records documenting relevant variables, parameters, and

limiting conditions. The weld procedure is qualified in accordance with ASME Section XI , or may be qualified to an alternate code accepted by Florida Power & Light and Holtec International.

## 10.2 Rack Arrangement

The rack installation process will not require any fuel shuffling. The final rack arrangement allows for an 11 by 13 cell Region I style rack installed in the Unit 1 Cask Pit Area and a 15 by 15 cell region II style storage rack installed in the Unit 2 Cask Pit Area. Schematic plan views depicting Cask Pit Area storage rack configurations are shown in Figures 1.1.1 and 1.1.2.

## 10.3 Rack Interferences

A survey was conducted to identify any objects which would interfere with rack installation or prevent usage of any storage locations. This section discusses existing pool items that would physically interfere with placing the racks into the SFP, present interferences subsequent to reracking, or were considered during the design of the racks. There are no permanently installed components interfering with the installation of the racks in the Cask Pit Areas. Existing miscellaneous equipment that is temporarily stored within these areas will be removed followed by vacuuming prior to installation of the racks.

## 10.4 SFP Cooling

The pool cooling system shall be operated in order to maintain the pool water temperature at an acceptable level. It is anticipated that activities, such as rack platform placement, may require the temporary shutdown of the Spent Fuel Pool cooling system.

Prior to any shutdown of the Spent Fuel Pool cooling system, the estimated time after shutdown to increase the pool bulk coolant temperature to a selected value of  $\leq 120$  °F will be determined. A temperature of  $\leq 120$  °F is chosen with enough margin such that cooling may be restored to ensure the pool bulk temperature will not exceed 150 °F.

## 10.5 Installation of New Racks

Installation of the new high density racks, supplied by Holtec International, involves the following activities. The racks are delivered in the horizontal position. A new rack module is removed from the shipping trailer using a suitably rated crane, while maintaining the horizontal configuration. The rack is placed on the up-ender and secured. Using two independent overhead hooks, or a single overhead hook and a spreader beam, the module is up-righted into a vertical position.

The new rack lifting device is engaged in the lift points at the bottom of the rack. The rack is then transported to a pre-leveled surface where, after leveling the rack, the appropriate quality control receipt inspection is performed. (See 10.1B & D.)

The Cask Pit Area floor is inspected and any debris, which may inhibit the installation of platforms, is removed. New rack platforms are lowered by the Cask Handling Crane into position on the floor and leveled before the rack module is lowered into the Cask Pit Area. The new rack module is lifted with the Cask Handling Crane and transported along the pre-established safe load path. The rack module is carefully lowered into the Cask Pit Area.

Elevation readings are taken to confirm that the module is level. In addition, rack-to-wall off-set distances are also measured. Adjustments are made as necessary to ensure compliance with design documents. The lifting device is then disengaged and removed from the Cask Pit Area under Health Physics direction. As directed by procedure, post-installation free path verification is performed using an inspection gage.

## 10.6 Safety, Health Physics, and ALARA Methods

### 10.6.1 Safety

During the installation phase of the Cask Pit Area fuel storage rack project, personnel safety is of paramount importance. All work shall be carried out in compliance with applicable approved procedures.

### 10.6.2 Health Physics

Health Physics is carried out per the requirements of the St. Lucie Radiation Protection Program.

### 10.6.3 ALARA

The key factors in maintaining project dose As Low As Reasonably Achievable (ALARA) are time, distance, and shielding. These factors are addressed by utilizing many mechanisms with respect to project planning and execution.

#### Time

Each member of the project team is trained and provided appropriate education and understanding of critical evolutions. Additionally, daily pre-job briefings are employed to acquaint each team member with the scope of work to be performed and the proper means of executing such tasks. Such pre-planning devices reduce worker time within the radiological controlled area and, therefore, project dose.

#### Distance

Remote tooling such as lift fixtures, pneumatic grippers, a support leveling device and a lift rod disengagement device have been developed to execute numerous activities from the SFP surface, where dose rates are relatively low.

## Shielding

During the course of the Cask Pit Area fuel storage rack project, primary shielding is provided by the water in the Spent Fuel Pool. The amount of water between an individual at the surface (or a diver in the pool) and an irradiated fuel assembly is an essential shield that reduces dose. Additionally, other shielding may be employed to mitigate dose when work is performed around high dose rate sources. If necessary, additional shielding may be utilized to meet ALARA principles.

### 10.7 Radwaste Material Control

Radioactive waste generated from the rack installation will be controlled in accordance with established St. Lucie procedures.

## 11.0 ENVIRONMENTAL COST / BENEFIT ASSESSMENT

### 11.1 Introduction

Article V of the USNRC OT Position Paper [11.1] requires the submittal of a cost/benefit analysis for a fuel storage capacity enhancement. This section provides justification for selecting installation of additional racks in the St. Lucie Cask Pit Area as the most cost effective alternative.

### 11.2 Imperative for Additional Spent Fuel Storage Capacity

The specific need to increase the limited existing storage capacity of the St. Lucie Spent Fuel Pool is based on the continually increasing inventory in the pool, the prudent requirement to maintain full-core offload capability, and a lack of viable economic alternatives.

St. Lucie Unit 1 is projected to lose full core reserve (FCR) in its Spent Fuel Pool (SFP) following Cycle 19, which ends in 2005. St. Lucie Unit 2 is projected to lose full core reserve (FCR) in its Spent Fuel Pool (SFP) following Cycle 17, which ends in 2007. The projected loss of storage capacity in the pool would affect the owner's ability to operate the reactor.

### 11.3 Appraisal of Alternative Options

Adding fuel storage space to the St. Lucie SFP is the most viable option for increasing spent fuel storage capacity.

The key considerations in evaluating the alternative options included:

- Safety: Minimize the risk to the public.
- Economy: Minimize capital and O&M expenditures.
- Security: Protection from potential saboteurs, natural phenomena.
- Non-intrusiveness: Minimize required modifications to existing plant systems.

- Maturity: Extent of industry experience with the technology.
- ALARA: Minimize cumulative dose.
- Schedule: Minimize time to implement a plan which will maintain full-core offload capability for the distant future.
- Risk Management: Maximize probability of completing the expansion to support fuel storage needs.

### Rod Consolidation Option

Rod consolidation has been shown to be a potentially feasible technology. Rod consolidation involves disassembly of a fuel assembly and the disposal of the fuel assembly skeleton outside of the pool (this is considered a 2:1 compaction ratio). The rods are stored in a stainless steel can that has the outer dimensions of a fuel assembly. The can is stored in the spent fuel racks. The top of the can has an end fixture that matches up with the spent fuel handling tool. This permits moving the cans in an easy fashion.

Rod consolidation pilot project campaigns in the past have consisted of underwater tooling that is manipulated by an overhead crane and operated by a maintenance worker. This is a very slow and repetitive process.

The industry experience with rod consolidation has been mixed thus far. The principal advantages of this technology are: the ability to modularize, moderate cost, no need of additional land and no additional required surveillance. The disadvantages are: potential gap activity release due to rod breakage, potential for increased fuel cladding corrosion due to some of the protective oxide layer being scraped off, potential interference of the (prolonged) consolidation activity which might interfere with ongoing plant operation, and lack of sufficient industry experience. The drawbacks associated with consolidation are expected to diminish in time. However, it is FPL's view that rod consolidation technology has not matured sufficiently to make this a viable option for the present St. Lucie SFP limitations.

### On-Site Dry Cask Storage Option

Dry cask storage is a method of storing spent nuclear fuel in a high capacity container. The cask provides radiation shielding and passive heat dissipation. Typical capacities for PWR fuel range from 21 to 37 assemblies that have been removed from the reactor for at least five years. The casks, once loaded, dried, and sealed are then stored outdoors on a seismically qualified concrete pad.

The casks, as presently licensed, are limited to 20-year storage service life. Once the 20 years has expired the cask manufacturer or the utility must recertify the cask or the utility must remove the spent fuel from the container. In the interim, the U.S. DOE has embraced the concept of multi-purpose canisters obsolescing all existing licensed cask designs. Work is also continuing by several companies, including Holtec International, to provide an MPC system that will be capable of long storage, transport, and final disposal in a repository. It is noted that a cask system makes substantial demands on the resources of a plant. For example, the plant must provide for a decontamination facility where the outgoing cask can be decontaminated for release.

Several plant modifications may be required to support cask use, including: (1) tap-ins must be made to the gaseous waste system, (2) chilled water to support vacuum drying of the spent fuel, and (3) piping must be installed to return cask water back to the Spent Fuel Pool/Cask Loading Pit. A seismic concrete pad would be needed to store the loaded casks. This pad would require a security fence, surveillance protection, a diesel generator for emergency power and video surveillance for the duration of fuel storage, which may extend beyond the life of the adjacent plant.

### Other Storage Options

Other options such as Modular Vault Dry Storage and a new Fuel Storage Pool are overly expensive as compared to placing new racks in the Cask Pit. Due to the complexity of implementation, these options could not meet the required schedule for extending full-core offload capability.

### 11.3.1 Alternative Option Cost Summary

An estimate of relative costs in 2001 dollars for the aforementioned options is provided in the following:

Cask Pit Area Rack Installation:	\$3-4 million
Rod consolidation:	\$25 million
Dry Storage Horizontal Silo:	\$35-45 million
Dry Storage Modular vault:	\$56 million
Dry Storage Metal cask (MPC):	\$68-100 million
New fuel pool:	\$150 million

The above estimates are consistent with estimates by EPRI and others [11.2, 11.3].

To summarize, based on the required short time schedule, the status of the dry spent fuel storage industry, and the storage expansion costs, the most acceptable alternative for increasing the on-site spent fuel storage capacity at St. Lucie is expansion of the wet storage capacity. First, there are no commercial independent spent fuel storage facilities operating in the United States. Second, the adoption of the Nuclear Waste Policy Act (NWPA) created a de facto nuclear fuel cycle requiring disposal. Since the cost of spent fuel reprocessing is not offset by the salvage value of the residual uranium, reprocessing represents an added cost for the nuclear fuel cycle which already includes the NWPA Nuclear Waste Fund fees. In any event, there are no domestic reprocessing facilities. Third, at over \$½ million per day replacement power cost, shutting down St. Lucie is many times more expensive than addition of high density racks to the existing Cask Pit.

### 11.4 Cost Estimate

The plant modification proposed for the St. Lucie fuel storage expansion utilizes a freestanding, high density, poisoned spent fuel rack in the Cask Pit for each Unit.

The total capital cost is estimated to be approximately \$3 ½ million as detailed below.

Engineering, design, project management:	\$1-1/4 million
Rack fabrication:	\$2 million
Rack installation:	\$½ million

As described in the preceding section, other fuel storage expansion technologies were evaluated prior to deciding on the use of SFP racks. Storage rack capacity expansion provides a cost advantage over other technologies.

### 11.5 Resource Commitment

The expansion of the St. Lucie spent fuel storage capacity via augmentation of the racks in the SFP is expected to require the following primary resources per Unit:

Stainless steel:	20 tons
Boral neutron absorber:	2 tons, of which 1 ton is Boron Carbide powder and 1.5 tons are aluminum.

The requirements for stainless steel and aluminum represent a small fraction of total world output of these metals (less than 0.001%). Although the fraction of world production of Boron Carbide required for the fabrication is somewhat higher than that of stainless steel or aluminum, it is unlikely that the commitment of Boron Carbide to this project will affect other alternatives. Experience has shown that the production of Boron Carbide is highly variable, depends upon need, and can easily be expanded to accommodate worldwide needs.

### 11.6 Environmental Considerations

The proposed rack installation results in an additional heat load burden to the Spent Fuel Pool Cooling and Cleanup System due to increased spent fuel pool inventory, as discussed in Section 5.0. The maximum bulk pool temperature will be limited to less than 150°F under normal refueling scenarios.

The peak heat load from the spent fuel pool is less than 40 million Btu/hr, which is a minuscule fraction of the total operating plant heat loss to the environment and is well within the capability of the SFP cooling system. Consequently, the short duration of increased heat loading during an outage is not expected to have any significant impact on the environment.

The increased peak bulk pool temperature during a refueling results in a slightly higher increased pool water evaporation rate for a short period of time. This increase is within the Fuel Handling Building HVAC system capacity and does not necessitate any hardware modifications for the HVAC system. Therefore, the environmental impact resulting from the increased heat loss and water vapor generation at the pool surface is negligible.

11.7        References

- [11.1] OT Position Paper for Review and Acceptance of Spent Fuel Storage and Handling Applications, USNRC (April 1978).
- [11.2] Electric Power Research Institute, Report No. NF-3580, May 1984.
- [11.3] "Spent Fuel Storage Options: A Critical Appraisal", Power Generation Technology, Sterling Publishers, pp. 137-140, U.K. (November 1990).

L-2004-029  
Enclosure 2  
Page 1 of 3

**St. Lucie Unit 2 Proposed  
Mark-Up and Word-Processed  
Technical Specification Changes**

DESIGN FEATURES

VOLUME

5.4.2 The total water and steam volume of the reactor coolant system is  $10,931 \pm 275$  cubic feet at a nominal  $T_{avg}$  of  $572^\circ\text{F}$ .

5.5 METEOROLOGICAL TOWER LOCATION

5.5.1 The meteorological tower shall be located as shown on Figure 5.1-1.

5.6 FUEL STORAGE

CRITICALITY

5.6.1 a. The spent fuel pool and spent fuel storage racks <sup>are designed and</sup> shall be maintained with:

1. A  $k_{eff}$  equivalent to less than 1.0 when flooded with unborated water, including a conservative allowance for biases and uncertainties as described in Section 9.1 of the Updated Final Safety Analysis Report.
2. A  $k_{eff}$  equivalent to less than or equal to 0.95 when flooded with water containing 520 ppm boron, including a conservative allowance for biases and uncertainties as described in Section 9.1 of the Updated Final Safety Analysis Report.

and a nominal 8.80 inch center-to-center distance between fuel assemblies placed in the cask pit storage rack.

A nominal 8.96 inch center-to-center distance between fuel assemblies placed in the <sup>spent fuel pool</sup> storage racks.

b. Fuel placed in Region I of the spent fuel storage racks shall be stored in a configuration that will assure compliance with 5.6.1 a.1 and 5.6.1 a.2, above, with the following considerations:

1. Fresh fuel shall have a nominal average U-235 enrichment of less than or equal to 4.5 weight percent.
2. The reactivity effect of CEAs placed in fuel assemblies may be considered.
3. The reactivity equivalencing effects of burnable absorbers may be considered.
4. The reactivity effects of fuel assembly burnup and decay time may be considered as specified in Figures 5.6-1c through 5.6-1e.

4. The cask pit storage rack shall contain neutron absorbing material (Boral) between stored fuel assemblies when installed in the spent fuel pool

c. Fuel placed in Region II of the spent fuel storage racks shall be placed in a configuration that will assure compliance with 5.6.1 a.1 and 5.6.1 a.2, above, with the following considerations:

1. Fuel placed in <sup>the</sup> Region II shall meet the burnup and decay time requirements specified in Figure 5.6-1a or 5.6-1b.
2. The reactivity effect of CEAs placed in fuel assemblies may be considered.
3. The reactivity equivalencing effects of burnable absorbers may be considered.

Fuel placed in the Region II cask pit storage rack shall meet the burnup requirements specified in Figure 5.6-1f.

**DESIGN FEATURES**

**VOLUME**

5.4.2 The total water and steam volume of the reactor coolant system is  $10,931 \pm 275$  cubic feet at a nominal  $T_{avg}$  of 572°F.

**5.5 METEOROLOGICAL TOWER LOCATION**

5.5.1 The meteorological tower shall be located as shown on Figure 5.1-1.

**5.6 FUEL STORAGE**

**CRITICALITY**

- 5.6.1 a. The spent fuel storage racks are designed and shall be maintained with:
1. A  $k_{eff}$  equivalent to less than 1.0 when flooded with unborated water, including a conservative allowance for biases and uncertainties as described in Section 9.1 of the Updated Final Safety Analysis Report.
  2. A  $k_{eff}$  equivalent to less than or equal to 0.95 when flooded with water containing 520 ppm boron, including a conservative allowance for biases and uncertainties as described in Section 9.1 of the Updated Final Safety Analysis Report.
  3. A nominal 8.96 inch center-to-center distance between fuel assemblies placed in the spent fuel pool storage racks and a nominal 8.80 inch center-to-center distance between fuel assemblies placed in the cask pit storage rack.
  4. The cask pit storage rack shall contain neutron absorbing material (Boral) between stored fuel assemblies when installed in the spent fuel pool.
- b. Fuel placed in Region I of the spent fuel storage racks shall be stored in a configuration that will assure compliance with 5.6.1 a.1 and 5.6.1 a.2, above, with the following considerations:
1. Fresh fuel shall have a nominal average U-235 enrichment of less than or equal to 4.5 weight percent.
  2. The reactivity effect of CEAs placed in fuel assemblies may be considered.
  3. The reactivity equivalencing effects of burnable absorbers may be considered.
  4. The reactivity effects of fuel assembly burnup and decay time may be considered as specified in Figures 5.6-1c through 5.6-1e.
- c. Fuel placed in Region II of the spent fuel storage racks shall be placed in a configuration that will assure compliance with 5.6.1 a.1 and 5.6.1 a.2, above, with the following considerations:
1. Fuel placed in the Region II spent fuel pool storage racks shall meet the burnup and decay time requirements specified in Figure 5.6-1a or 5.6-1b. Fuel placed in the Region II cask pit storage rack shall meet the burnup requirements specified in Figure 5.6-1f.
  2. The reactivity effect of CEAs placed in fuel assemblies may be considered.
  3. The reactivity equivalencing effects of burnable absorbers may be considered.